Pyrometallurgical refining of high grade PGM leach residues prior to precious metals separation

by

Gert Adrian Bezuidenhout

Dissertation presented for the degree

of

Doctor of Philosophy

(Extractive Metallurgical Engineering)

in the Faculty of Engineering

at Stellenbosch University

Supervisors

Professor Steven M Bradshaw

Professor Guven Akdogan

Professor Jacques J Eksteen

December 2014

Declaration

By submitting this dissertation electronically, I declare that the entirety of the work contained therein is my own, original work, that I am the sole author thereof (save to the extent explicitly otherwise stated), that reproduction and publication thereof by Stellenbosch University will not infringe any third party rights and that I have not previously in its entirety or in part submitted it for obtaining any qualification.

G.A. Bezuidenhout Date: 9 June 2014

Abstract

Primary platinum mining companies use a complex multistage recovery and refining process. The removal of base metals in the base metal refinery (BMR) leaves a residue that requires a number of hazardous and expensive unit operations to prepare the platinum group metal (PGM) concentrate for final separation and refining. In the PGM industry, hydrometallurgy is used almost exclusively to refine material with a PGM content of more than a couple of per cent. This thesis proposes and investigates an alternative pyrometallurgical refining method to remove contaminants from a high grade PGM residue (e.g. residue from a BMR after the bulk of the base metals has been removed), whilst minimising aqueous wastes and potential PGM losses. The hypothesis behind the use of a pyrometallurgical process was the effective separation of a number of elements from the PGMs through the use of only a few processing steps. The noble nature of PGMs, i.e. their resistance to oxidation and low vapour pressure at high temperature, allows for effective separation.

The theoretical feasibility of the concept was explored using thermochemical modelling. Modelling suggested that the use of a controlled atmosphere roasting step, followed by smelting and atomisation, could lead to a technically feasible process to separate PGMs from other metals. Throughout this thesis, thermochemical modelling was shown to be a useful tool to interpret and understand elemental behaviour across the roasting and smelting steps.

It was experimentally illustrated that roasting of PGM residues in an oxidising environment at low temperatures (700 °C - 900 °C range) will selectively vaporise the volatile oxides of S, Se, Te and As (to varying degrees), that would otherwise be quite stable in the alloy or matte phase during a melt at low oxygen partial pressure. Arsenic volatilisation proceeded only partially (30 wt% to 60 wt%), probably due to the formation of a temperature stable species of arsenate. Osmium volatilisation was not properly described by modelling and proceeded only partially (30 wt% to 70 wt%), possibly due to the presence of Osmium in a solid solution phase that depresses the activity and correspondingly the fugacity. Although a number of the PGMs oxidise in the roasting temperature range, their vapour pressures do not allow measurable losses to the gas phase (apart from Osmium that is not recovered in most precious metal refineries). Almost all the PGMs reported to two separate solid solution phases during roasting.

The smelting step allows the PGMs to dissociate from oxygen, alloy and melt, without the addition of a collector. The liquidus temperature was shown to be strongly influenced by the concentrations of impurities (S, Se, Te, As, Fe, Ni and Cu) in the feed to the melt and ranged between 1 235 °C and 1 510 °C. The most important variable necessary to avoid non-PGM elements (especially As, Pb, Fe and Ni) from joining the alloy phase is control of the partial oxygen pressure in the melt. Au losses due to volatilisation of species such as AuS, AuSe and AuTe were shown possible at higher temperatures, with 21% recovery loss measured at 1 700 °C in the presence of 6% Se, Te and S. Ru losses (ranging from 9% to 39%) across the smelting step were shown to be sensitive to the combined Fe, Ni and Cu content of the feed, the melting temperature and the partial oxygen pressure across the melt. With Cu addition (to achieve Cu content in the alloy phase >60% by weight), melting temperatures as low as 1 200 °C is sufficient to collect PGMs and separate them from the slag phase. However, Ru is insoluble in the Cu-rich alloy and varying Ru recoveries were

measured, pointing to a possible loss mechanism. After casting and solidification of the melt, the alloy phase can be separated from the slag phase by mechanical means.

Atomisation is necessary to break the alloy phase into fine particulate that allows improved leaching kinetics. From experimental test work and literature studies, it appears that fine particulate sizing (D_{50} of 20 µm) can be achieved at high pressure requirements (in excess of 400 bar). The necessity of re-melting the alloy phase before atomisation allows the opportunity for a high temperature treatment step. It was experimentally shown that near complete volatilisation of Pb and Bi can be achieved if the alloy is kept at 1 700 °C for 30 minutes in an inert environment. Significant Ag losses to the vapour phase were also measured across this high temperature treatment step.

This study fundamentally and practically illustrated that it is possible to use pyrometallurgy to separate PGMs from a large number of metals/oxides/amphoterics present in leach residues. By effectively using a combination of roasting and smelting, it is possible to upgrade the PGM content of a pressure leach residue from low forty per cent to high eighty per cent, with low PGM losses. The proposed roasting, smelting and atomisation processes were able to remove the bulk of S, Se, Te, Bi, Pb, oxides (such as SiO_2 and Cr_2O_3) and partially remove Os, As, Fe, Ni and Cu. It was experimentally shown that the PGM containing alloy is amenable to leaching in a chlorine environment as used in a precious metal refinery, but more work is necessary to achieve near complete dissolution.

This investigation spanned a number of processing steps and measured the associated impact of each on multiple elements, and in that regard it does not follow a classical or typical doctoral thesis approach. However, a field of research has been studied that enjoys very little publication, apart from specialist alloys or specialist characteristics. This is in part due to the proprietary nature of PGM refining. This study contributes to the existing scientific knowledge base, but also to the process engineering knowledge base of the behaviour of high grade PGM residues at high temperatures.

Opsomming

Primêre platinum mynbou maatskappye gebruik 'n komplekse multi herwinning en raffinerings proses. Die verwydering van basismetale in die BMR laat 'n oorskot wat 'n aantal gevaarlike en duur eenheid bedrywighede vereis om die PGM te konsentreer en voor te berei vir die finale PGM skeiding en raffinering. In die PGM-industrie word hidrometallurgie byna uitsluitlik gebruik om materiaal met 'n PGM inhoud van meer as 'n paar persent te raffineer. Hierdie tesis ondersoek 'n alternatiewe pirometallurgiese raffinerings metode om onsuiwerhede vanuit 'n hoë graad PGM oorskot (bv. oorskot van 'n BMR na die grootste deel van die basismetale verwyder is) te verwyder, terwyl waterige afval en potensiële PGM verliese verminder word. Die hipotese agter die gebruik van 'n pirometallurgiese proses was die effektiewe skeiding van 'n aantal elemente van die PGM'e deur die gebruik van slegs 'n paar verwerking stappe. Die edele aard van PGM'e, dws hul weerstand teen oksidasie en lae dampdruk by hoë temperature, maak voorsiening vir doeltreffende skeiding.

Die teoretiese haalbaarheid van die konsep is ondersoek met behulp van termochemiese modelle. Modellering het voorgestel dat die gebruik van 'n beheerde atmosfeer rooster stap, gevolg deur smelting en atomisasie, kan lei tot 'n tegnies uitvoerbare proses om PGM'e te skei van ander metale. Dwarsoor hierdie tesis, is gewys dat termochemiese modelle 'n nuttige instrument is om elementele gedrag oor die rooster en smelt stappe te interpreteer en verstaan.

Dit is eksperimenteel aangetoon dat die roostering van PGM oorskot in 'n oksiderende omgewing by lae temperature (700 °C - 900 °C), selektiewe verdamping van die vlugtige oksiede van S, Se, Te en As (met wisselende effektiwiteit) tot gevolg sal hê, wat andersins baie stabiel sal wees in die allooi of mat fase tydens 'n smelt stap teen 'n lae suurstof parsiële druk. Arseen vervlugtiging het slegs gedeeltelik voortgegaan (30 wt% tot 60 wt%), waarskynlik as gevolg van die vorming van 'n stabiele temperatuur spesie van arsenaat. Osmium vervlugtiging was nie behoorlik beskryf deur modellering nie en het slegs gedeeltelik voortgegaan (30 wt% tot 70 wt%), moontlik te danke aan die teenwoordigheid van Osmium in 'n vaste oplossing fase wat die aktiwiteit onderdruk en dienooreenkomstig die fugasiteit. Hoewel 'n aantal van die PGM’e oksideer in die rooster temperatuur bereik, laat hul dampdrukke nie meetbaar verliese na die gas fase toe nie (afgesien van Osmium, wat nie in die meeste edel metaal raffinaderye verhaal word nie). Byna al die PGM'e het gerapporteer aan twee afsonderlike vaste oplossing fases tydens die rooster stap.

Tydens die smelt stap kan die PGM'e dissosieer van suurstof, legeer en smelt, sonder die toevoeging van 'n versamelaar. Die liquidus temperatuur word sterk beïnvloed deur die konsentrasies van onsuiwerhede (S, Se, Te, As, Fe, Ni en Cu) in die voer na die smelt en het gewissel tussen 1 235 °C en 1 510 °C. Die belangrikste veranderlike wat nodig is om nie-PGM elemente (veral, Pb, Fe en Ni) te verhoed dat hulle by die allooi fase aansluit, is die beheer van die parsiële suurstofdruk in die smelt. Au verliese as gevolg van vervlugtiging van spesies soos AuS, AuSe en AuTe is moontlik getoon by hoër temperature, met 21% verliese gemeet teen 1 700 °C in die teenwoordigheid van 6% Se, Te en S. Ru verliese (wat wissel van 9% tot 39%) oor die smelt stap is getoon om sensitief te wees vir die gekombineerde Fe, Ni en Cu inhoud van die voer, die smelt temperatuur en die parsiële suurstofdruk oor die smelt. Met Cu toevoeging (Cu-inhoud in die allooi fase >60% van die gewig) is smelt temperature so laag as 1 200 °C voldoende om PGM'e te versamel en hulle te skei van die slak fase. Ru is egter onoplosbaar in die Cu-ryk allooi en wisselende Ru herwinnings is gemeet, wat dui op 'n

moontlike verlies meganisme. Na gieting en stolling van die smelt, kan die allooi fase van die slak fase geskei word op 'n meganiese wyse.

Atomisering is nodig om die allooi fase in fyn partikels te breek wat verbeterde loging kinetika toelaat. Vanuit eksperimentele toetswerk en literatuur studies, blyk dit dat klein partikel groottes (D_{50} van 20 µm) bereik kan word teen hoë druk vereiste (meer as 400 bar). Die noodsaaklikheid om die allooi fase te her-smelt voor atomisering, laat die geleentheid toe vir 'n hoë temperatuur behandeling stap. Dit is eksperimenteel getoon dat naby volledige vervlugtiging van Pb en Bi bereik kan word indien die allooi by 1 700 °C gehou kan word vir 30 minute in 'n inerte omgewing. Beduidende Ag verliese na die dampfase is ook gemeet oor hierdie hoë temperatuur behandeling stap.

Hierdie studie het fundamenteel en prakties geïllustreer dat dit moontlik is pirometallurgie te gebruik om PGM'e te skei van 'n groot aantal metale / oksiedes / amphoteriese elemente wat teenwoordig is in loog oorskot. Deur effektief gebruik te maak van 'n kombinasie van roostering en smelting, is dit moontlik om die PGM inhoud van 'n drukloog oorskot op te gradeer van lae veertig persent na hoë tagtig persent met lae PGM verliese. Die voorgestelde rooster, smelt en atomisering proses was in staat om die grootste deel te verwyder van S, Se, Te, Bi, Pb, oksiedes (soos SiO_2 en Cr_2O_3) en om Os, As, Fe, Ni en Cu gedeelteliks te verwyder. Dit is eksperimenteel aangetoon dat die PGM allooi vatbaar is vir loging in 'n PMR chloried omgewing, maar meer werk is nodig om naby volledige oplosbaarheid te bereik.

Hierdie ondersoek het 'n aantal verwerking stappe en die gepaardgaande impak van elk op verskeie elemente beslaan, en in dié opsig volg dit nie die klassieke of tipiese doktorale proefskrif benadering na nie. Maar, dit het 'n gebied van navorsing bestudeer wat baie min publikasie geniet, afgesien van spesialis legerings of spesialis eienskappe. Dit is deels te danke aan die geheimhoudelike aard van PGM raffinering. Hierdie studie dra nie net by tot die bestaande wetenskaplike kennis nie, maar dra ook by tot die proses-ingenieurswese kennis van die gedrag van hoë graad PGM loog oorskot teen hoë temperature.

Acknowledgements

A number of people contributed to this study. Their assistance and guidance is much appreciated. They are thanked and acknowledged below:

Ali Brey and Francois Koeslag, from Hot Platinum: Smelting, atomisation and high temperature treatment test work took a number of years and a lot of effort, hours and, frankly, heartache. Thank you for the assistance, dedication and guidance during the test work.

Professor Johan de Villiers, from the University of Pretoria: Most of the SEM and XRD work was managed by Johan. He also assisted with the first set of roasting work in the stationary bed. Thank you for the assistance and guidance and quick response during the study.

Yolandi Fourie studied the alloy particles and conducted the test work on the leaching of concentrate and alloy in the HCl/Cl_2 environment. She did the test work as her final year project at the University of Stellenbosch. Her assistance and commitment is much appreciated.

Gerhard and Ewout Overbeek from Golden Pond: Leaching test work on third stage residue and roasted calcine were done by Golden Pond. Two of the smelting tests with Cu addition were also done at Golden Pond. Golden Pond was also used as one of three laboratories for assaying work. Thank you for the assistance and guidance provided during the study.

Outotec in Frankfurt conducted the roasting test work in the fluidised bed. Jochen Guentner managed most of the test work and provided guidance.

My thanks to Jacques Eksteen for supervision: Although Jacques is a formal supervisor in this thesis and would not require further acknowledgement, special appreciation needs to be expressed. Jacques assisted with the concept of a pyrometallurgical process to remove contaminants and provided guidance throughout the study. The effort and dedication is deeply appreciated.

Table of Contents

List of Figures

List of Tables

Nomenclature

Abbreviation	Explanation
BMR	Base Metal Refinery
6E	Total of 6 precious metals (for the purposes of this paper comprising Pt, Pd, Rh, Ru, Ir and Au)
atm	atmosphere
Eh/ pH	Pourbaix diagram, also known as a potential/pH diagram. Eh/pH diagrams map out possible stable (equilibrium) phases of an aqueous electrochemical system
FCC	Face Centred Cubic crystal structure
HCP	Hexagonal Close Packed crystal structure
Liquidus temperature	Temperature at which the last solid in a substance being heated melts into the liquid phase
M	Molar concentration or Molarity (mol/L)
OPM	Other Precious Metals (Rh, Ru and Ir)
ORP	Oxidation Reduction Potential. This means the same as redox.
PGM	Platinum Group Metals (for the purposes of this paper comprising Pt, Pd, Rh, Ru, Ir and Au)
PM	Precious Metals – term used to describe the grouping of Pt, Pd and Au
PMR	Precious Metal Refinery
pO_2	Partial pressure of oxygen
ppmv	Parts per million by volume
redox	Reduction-Oxidation potential. The meaning is the same as ORP.
Solidus temperature	Temperature at which the first liquid phase appears in a substance being heated
wt%	Weight percentage

Chapter 1: Introduction

1.1 Background to PGM refining

More than 80% of the global platinum supply is mined and processed to final metal in South Africa (Jones, 2005). The Platinum Group Metals (PGMs) are contained in a large ultramafic intrusive formation, called the Bushveld Igneous Complex. Ores that contain platinum also contain other precious metals and base metals that are co-processed to generate revenue. The platinum group metals (PGMs) comprise six metals, being Pt, Pd, Rh, Ru, Ir and Os. However, Au often co-occurs with the PGM ores and Au is often refined, while Os is not recovered, due to a very small market for Os. The notation for PGM in this document will refer to Pt, Pd, Rh, Ru, Ir and Au (instead of Os). These 6 metals are sometimes noted as 6E in literature and in the analytical environment. The primary production of PGMs in South Africa is mostly done by four major players, each having their own processing plants. These are Anglo American Platinum Ltd, Impala Platinum Ltd, Lonmin Plc and Northam Platinum Ltd. All these plants operate similar processes (or variants thereof) up until the point where the PGMs are separated from each other in the precious metals refinery (PMR).

A typical beneficiation sequence to recover PGMs from ores contained in the Bushveld Igneous Complex would entail:

- Open-pit or underground mining of ores, stratified as distinct reefs. The reef types most often mined for PGM recovery are the Merensky, UG2 and Platreef types.
- Flotation of ore to produce a concentrate (PGM head grade is upgraded from around 3-5 g/tonne to 100-240 g/tonne).
- Electrical smelting to separate the remaining oxide/gangue phases from the matte (PGM content upgraded from 100-240 g/tonne to around 600-1 500 g/tonne). PGMs are collected in a base metal sulphide phase, called a matte.
- Converting to remove iron sulphides from the matte phase (PGM content upgraded from around 600-1 500 g/tonne to 2 500-6 000 g/tonne).
- Base metal refining to remove Ni and Cu sulphides from the matte phase and leave behind a PGM rich residue (PGM content upgraded from 2 500-6 000 g/tonne to around 50-65% content). Cu and Ni are recovered as by-products. Cu is electrowon as cathode, while Ni is refined to nickel sulphate crystals, Ni cathode or Ni briquettes. In some cases Co is also recovered as a by-product.
- Precious metal refining to separate the 6 individual PGM metals (Pt, Pd, Rh, Ru, Ir and Au) to over 99.9% purity.

The concentrate from the BMR process is referred to as PGM concentrate and contains around 55%-65% PGMs by weight (not to be confused with conventional flotation concentrate). The remaining content of the PGM concentrate contains impurities that reduce efficiency in the subsequent PMR process. The list below shows the impurities that are present in the Lonmin feed material. A description of the maximum concentration and impact on the Lonmin PMR is also provided. It must be noted that different precious metal refining technologies will have different tolerances towards impurities and the impact of the impurity on the process will be different.

- SiO_2 or silica containing minerals. Feed total to the PMR is typically less than 4.5%. In the PMR, SiO_2 can partly hydrolyse under the highly oxidising conditions of primary dissolution,

making the particles gelatinous. These gel-like particles then blind filter cloths during filtration in several filtration steps across the plant.

- Residual Base Metal (mostly Cu) sulphides. Feed total to the PMR is typically less than 3.5%. Residual base metals mostly consume expensive reagents and lengthen processing steps, due to their participation (oxidation and reduction) in several of the refining process steps. In the PMR, most of the base metals and Fe are precipitated out with a pH adjustment. If there are large quantities of base metals, PGMs can be entrained with this precipitate.
- Oxides such as Al_2O_3, Cr_2O_3, MgO and CaO. Feed total to the PMR is typically less than 3.5%. Oxides of Ni and Fe are often present as spinel ($(M1^{2+})$, $(M2^{3+})_2)O_4$ type oxides and their content is typically less than 8.5%. The oxides originate from imperfect slag separation during converter matte granulation. This is especially true for the denser spinel type oxides that will tend to settle between the slag and the matte phase (in both the furnace and the converter). Fe and Ni go into solution across the primary dissolve and will react similar to Cu described above.
- Amphoteric elements (Se, Te, Bi, Sb, As, S). Feed total to the PMR is typically less than 4.0%. These elements are called amphoteric because they can occur in both the anionic and cationic state. The amphoteric elements are often associated with PGM minerals in the ore. They are poorly removed during the smelter process, and to a varying degree by the BMR process. Se and Te cause Pt and Pd to co-precipitate with Au during hydrazine reduction, forcing a Pt and Pd removal step from the Au sponge. Overall, the amphoteric elements end up in several streams across the plant and they contribute to effluent production, residue formation, pipeline times and reagent cost during refining.
- Pb (with varying and unsure speciation, but probably a combination of sulphates/ oxy-sulphates/ oxides/ sulphides). Feed total to the PMR is typically less than 3.5%. Pb is largely removed (around 90% removal) across the smelter, in both slag and off-gas. However, Pb is inert in the Lonmin BMR process, with negligible removal achieved. This inertness is mostly explained by the formation (and possibly surface passivation) of $PbSO_4$, which is almost insoluble and very stable in the BMR environment. In the PMR, Pb precipitates together with Rh and Ir in the hydrolysis step, operated at pH 5. Pb complicates Ir and Rh separation and causes excessive effluent generation, lower Rh and Ir recoveries and higher reagent consumption by necessitating several re-dissolution and precipitation steps.
- Os and Ag. Feed total to the PMR is typically less than 3.0%. These elements are often not recovered as products in a typical BMR/ PMR flow sheet and their removal and control often complicate the existing flow sheet. Os and Ru are distilled together. Os then needs to be separated from Ru by addition of hydrogen peroxide in order to oxidize Os back to volatile OsO_4. The Os then needs to be reduced with hydrochloric acid in a scrubbing column.

The aim of this thesis was to investigate the addition of a processing step in between the BMR and PMR processes to remove contaminants from a PMR feed, with minimal PGM losses. It was hypothesised that a pyrometallurgical refining step could be used to remove the contaminants from leach residues with reduced base metal contents, in order to simplify the remaining PMR process Initial modelling was performed with FactSage® (Bale *et al.*, 2001), which showed that it is thermodynamically possible to remove almost all of the contaminants from the PMR feed and produce a final alloy with a PGM content of >90 wt%. The positive modelling results served as an incentive to explore the practical technical viability of such a novel process. Thermodynamically it is

possible to produce an alloy of >90 wt% without any PGM losses, and with the use of just two processing steps: roasting followed by smelting. The evaluation of this concept through modelling and experimental test work forms the subject matter of the thesis. Section 2.2 contains a list of the objectives and hypotheses that were set for this study.

1.2 Description of the Lonmin BMR and PMR process

In order to provide context regarding the origin of the high grade PGM residue samples studied in this thesis and the objectives that were set, the Lonmin BMR and PMR processes are briefly described. Lonmin funded the project, supplied samples and registered a patent of the process (Bezuidenhout *et al.*, 2012) based on the study findings.

The BMR process starts with milling of converter matte, followed by an atmospheric oxidative leach to dissolve Ni sulphides, primarily Heazlewoodite (Ni_3S_2), Millerite (NiS) and Ni alloy (Van Schalkwyk *et al.*, 2011). Impure $NiSO_4.6H_2O$ crystals, containing some $CoSO_4$ and $FeSO_4$, serve as the outlet stream of Ni and S (and also of Fe and Co) from the Lonmin BMR process. The atmospheric leach is followed by a two step pressure leach to bring Cu sulphides, primarily covellite (CuS), chalcocite (Cu_2S) and cuprite (Cu_2O) into solution (Dorfling *et al.*, 2011). The residue product from the final pressure leach contains between 45% and 50% PGM material (referred to as third stage leach residue). This residue is then processed using a high pressure caustic leach to partially remove Se, Te, S, Cr, Os and As from the residue and finally, through a combined formic acid/ sulphuric acid leach, to dissolve complex Fe and Ni oxides before being dried and dispatched to the PMR. Se and Te that went into solution during the high pressure (second and third stage) leach are precipitated with sulphurous acid as Cu_2Se and Cu_2Te (referred to as Se/Te precipitate). Se and Te are leached from this precipitate with a caustic solution at atmospheric pressure (referred to as the low pressure caustic leach). Figure 1 shows the existing BMR flow sheet and the position at which the third stage leach residue and the Se/Te precipitate were taken for test work.

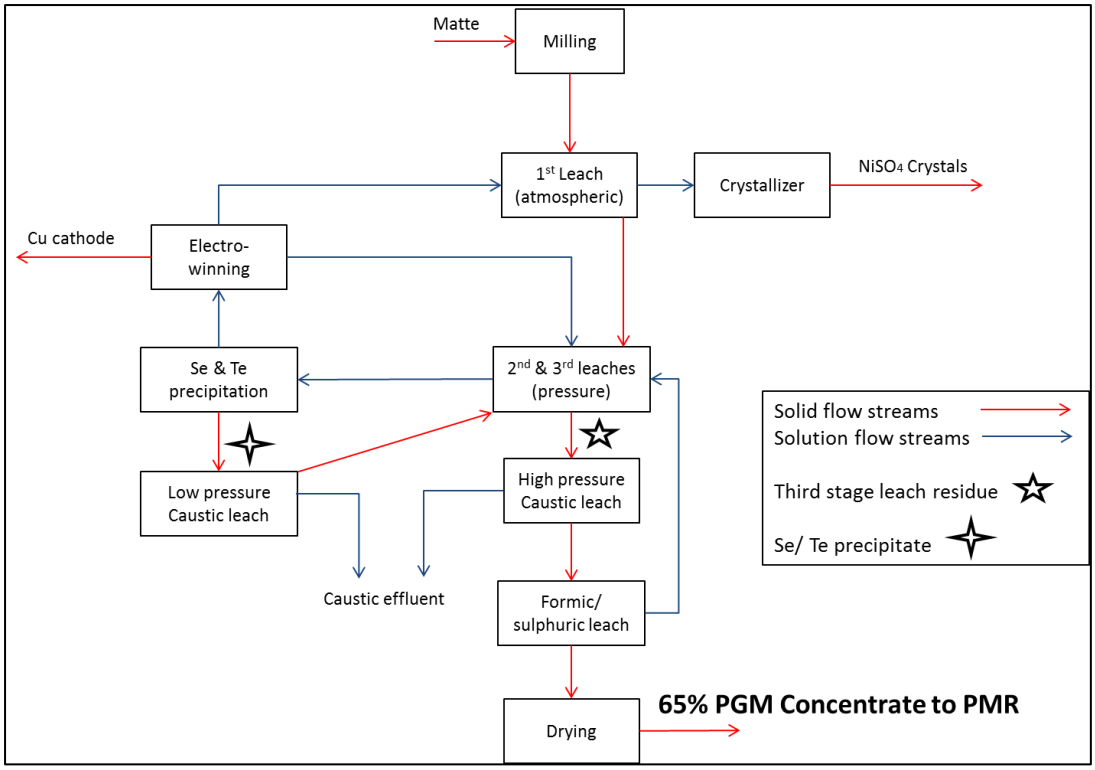

Figure 1: Block flow diagram of the current Lonmin BMR process. The position where samples were collected in the BMR process is also shown

The proposed pyrometallurgical refining process would remove the metals which are currently targeted in the existing caustic and formic leach processes. For this reason, the test work was performed on residue coming from the final pressure Cu leach (known as the third stage leach residue in the Lonmin context). The atmospheric leach is known as the first stage leach, with the first high pressure Cu leach being known as the second stage leach and the second high pressure Cu leach known as the third stage leach). The PGM content of third stage leach residue is typically in the 45% to 50% range. Cutting out the batch leaches from the BMR would lower the PGM losses to caustic effluent and would reduce the cost of the BMR process.

The Se/Te precipitate was also studied to understand its behaviour during roasting (the results are reported in Appendix C). The objectives set for the study, which are provided in Section 2.2, included the elimination of PGM-containing caustic effluent production in the BMR. The proposed flow sheet that was studied is shown in Figure 3. From Figure 3 it can be seen that a roasting step was intended to replace the low pressure caustic leach.

Since the two caustic leach processes used in the BMR and the combined formic/sulphuric leach could be replaced with the proposed pyrometallurgical process, it is important to review what these leaches are currently achieving in the existing flow sheet as a bleed stream for contaminants. McCulloch (2012) studied the deportment of elements from these streams from actual plant data with a mass balance.

- The low pressure caustic leach acts as the main bleed of Te out of the BMR. Roughly 60 wt% of the Te entering the BMR leaves the process via this effluent. The other 40 wt% ends up in

final concentrate. Te in the third stage residue goes into solution across the high pressure caustic leach as Te^{4+} (Na_2TeO_3), but then oxidises further and re-precipitates as Te^{6+} (Na_2TeO_4). Around 14% of the Se entering the BMR circuit is also removed via the low pressure caustic leach.

- The high pressure caustic leach acts as main bleed for Se from the BMR circuit. Around 77 wt% of Se leaves the BMR process via the high pressure caustic effluent. About 14 wt% of the Se leaves the circuit through the low pressure caustic effluent. Only around 5 wt% of the Se ends up in the final concentrate. Arsenic is also partially removed by the high pressure caustic leach. Around 27 wt% of the As entering the BMR circuit leaves via the high pressure caustic effluent and around 4 wt% via the low pressure caustic effluent. About 36 wt% As leaches in the first stage and is lost with Ni sulphate crystals and about 33 wt% of the As entering the BMR circuit ends up in the final concentrate.
- The formic/sulphuric acid leach really targets only Ni and Fe removal, by reducing the Fe^{3+} in stable spinels (like trevorite and magnetite) to the Fe^{2+} state, thereby leaving the Ni and Fe from the spinel amenable to leaching in an acidic environment. This is discussed in more detail in Appendix A. Approximately 45 wt% Fe removal, and 50 wt% Ni removal, are achieved across the formic/sulphuric acid leach. Some Ir (around 7 wt% to 10 wt%) also leaches in the formic/sulphuric acid leach.

Both the low pressure caustic leach on Se/Te precipitate and the high pressure caustic leach on third stage residue dissolve some PGMs (about 0.2% of total PGMs across both leaches). The caustic solution is sent for toll refining as an effluent of the BMR process. The two caustic leaches result in about 30 m^3 of aqueous effluent per month, which contains a number of mobile toxic species (including Cr^{6+}) as well as PGMs. In addition, caustic soda is an expensive reagent (compared to acids).

The Lonmin PMR process was implemented in 1974 and is based on the classical chemistry of dissolution and precipitation through control of pH, redox potential, ionic strength and ligand-complex chemistry. This technology is sometimes referred to as 1st generation processes. The majority of platinum producing companies nowadays make use of newer technologies to refine the PGMs by second generation (Solvent Extraction) and third generation (Ion Exchange and Molecular Recognition Technology) processes (Crundwell *et al.*, 2011). In the Lonmin dissolution and precipitation circuit, the impurities contribute significantly to the formation of residues and effluents that must be reprocessed or tolled to recover PGMs. This leads to poor first pass metal recoveries and extends the duration of the production pipeline for efficient recovery. The impact on recoveries and pipeline affect especially the Other Precious Metals (OPMs) circuits. OPM is a term used to describe the metals Ru, Rh and Ir. Figure 2 below shows the existing Lonmin PMR flow sheet (Crundwell, 2011). The multiple purification steps after the primary separation are clearly illustrated by the flow sheet.

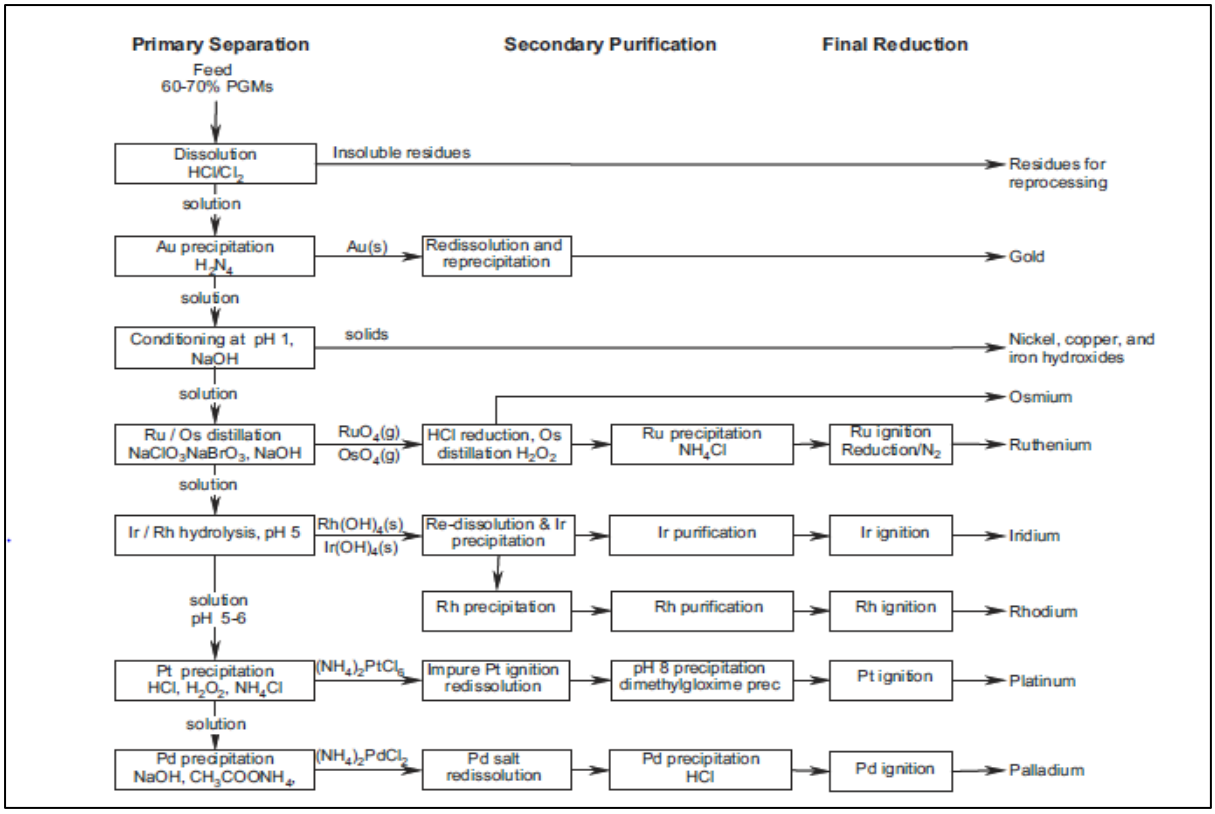

Figure 2: Block flow diagram of multiple re-dissolution and precipitation steps for refining at Lonmin PMR (adopted from Crundwell et al., 2011)

1.3 Proposed pyrometallurgical refining process

From the initial thermochemical modelling that was performed (described in Chapter 2), a conceptual flow sheet was drawn up. Figure 3 below shows the conceptual flow sheet that was studied in this thesis.

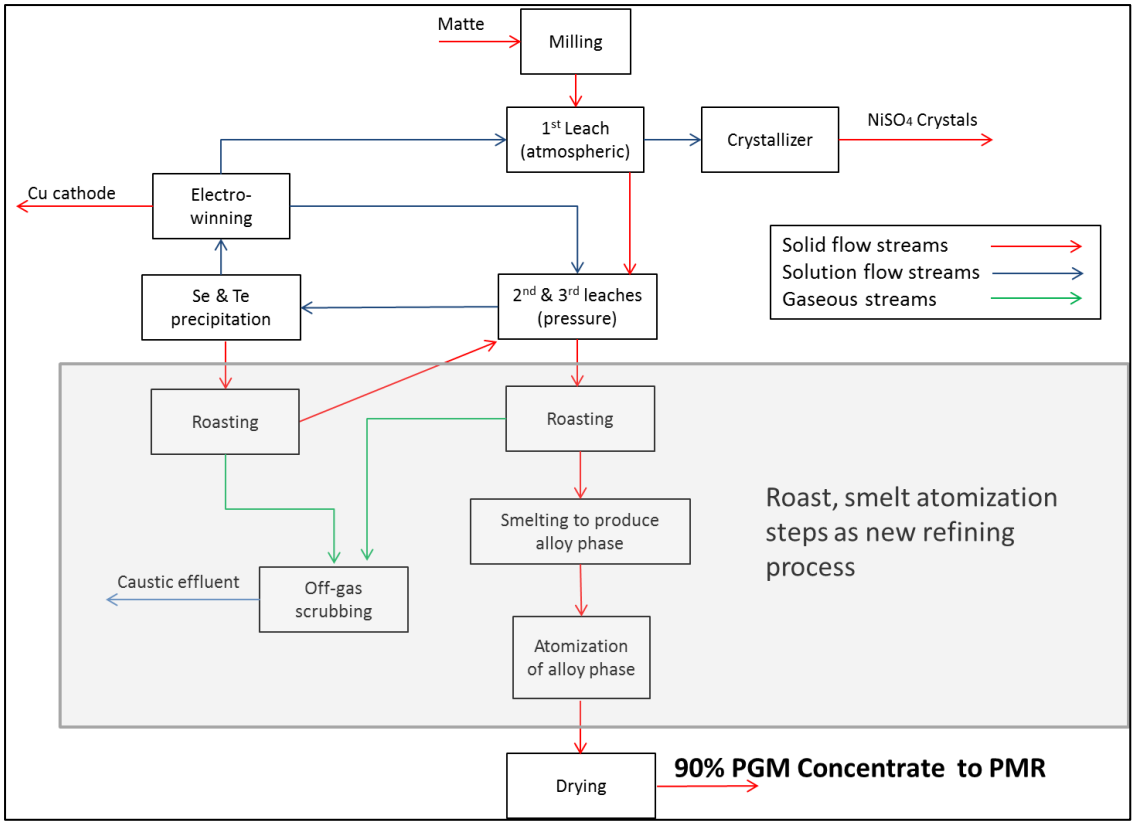

Figure 3: Block flow diagram of the proposed pyrometallurgical process that could be implemented between the BMR and PMR processes in order to remove contaminants from the PMR feed

The proposed process starts with a roasting step on both the third stage leach residue and the Se/Te precipitate. FactSage® modelling showed that some of the contaminant elements can be readily removed through roasting, due to the formation of oxide species that show volatile behaviour at low temperatures. These elements include S, Se, Te, As and Os. These same elements show high stability when an alloy and/or matte phase is allowed to form during smelting, making their removal possible only in well controlled oxygen partial pressure environments during the melt. Since the roasting process was foreseen to be oxidative, it needed to precede the smelting step. The final alloy that is sent forward to the PMR needed to be metallised, otherwise poor dissolution of especially the OPMs was expected in the primary HCl/Cl_2 dissolve.

The roasting step should be followed by a smelting step, since all the stable oxides that recrystallised during the roasting step would be dissolved or broken down in the smelting step. The high temperatures of a smelting step allow the PGMs to dissociate from oxygen, to alloy and form an alloy phase. The alloy phase will settle and separate from the slag phase. Modelling showed that very good selectivity could be achieved, leaving most of the oxides from the roasting step in the slag phase. An alloy phase with a PGM content >90% by mass was modelled, with negligible losses of PGMs to the slag or gas phase. It should be noted at this point that the loss mechanism of PGMs due to suspension (incomplete settling from the slag or particulate losses to the gas phase) was not modelled.

Separation of the slag and alloy phases can be achieved either by tapping the 2 phases on different elevations or by casting, allowing the two phases to cool, followed by separation. Alloys are often very hard, or not very brittle, making comminution difficult. Atomisation is widely used to break alloys into fine particulate, increasing the reactivity and general kinetics in a leaching step. Atomisation was foreseen and studied as the preferred method to produce a metallic powder for dissolution in the PMR. In order to atomise the solidified alloy (after separation from slag), it is necessary to heat the alloy to between 50 °C to 120 °C above the liquidus temperature. Some experiments were performed by maintaining the alloy at high temperatures (1 700 °C studied) in an inert environment, and it was shown that this heating step could serve as a control step for Pb and Bi (with high removal efficiencies measured) prior to atomisation.

The atomised alloy finally becomes the PMR feed. An investigation was done to determine the leaching behaviour of the PGM alloy in a typical HCl/Cl_2 leach in the PMR. This investigation is reported in Appendix B. However, the impact of feeding a higher grade PGM alloy to the PMR was not investigated and remains unquantified. Nevertheless, the foreseen advantages of the proposed pyrometallurgical process are discussed next.

1.3.1 Advantages of the pyrometallurgical refining process

The advantages gained by implementation of the proposed process will vary according to different feed materials and companies. However, some of the generic advantages of the process should include one or more of the items listed below:

- Optimisation of the existing BMR flow sheet, leading to lower PGM losses and lower effluent production rates. In the case of Lonmin this means removal of the two caustic leaches and possibly the formic/sulphuric acid leach.
- A less variable feed to the PMR and therefore more predictable operation in the PMR. In the case of Lonmin the advantage is primarily seen in SiO_2 and Pb, where rather limited control steps are currently included in the existing flow sheets.
- Lower effluent and residue production rates in the PMR process. This will lead to lower disposal cost, lower tolling charges and shorter pipelines on the PGMs in this stream.
- A shorter pipeline for PGMs can be achieved by higher first pass recoveries, since PGMs would not be locked up in the residue stream.
- It is possible to apply the learning from the proposed pyrometallurgical process to the treatment of low grade residues (such as the residues generated in BMR and PMR processes), since the basic processing steps will be similar (roasting, smelting and atomisation).

1.4 Thesis layout

The thesis document is structured in the following manner:

- Chapter 1 is an introduction explaining the context of where the proposed pyrometallurgical refining process will fit into the current processes and why it is relevant.
- Chapter 2 is a thermochemical overview of the process and the objectives that were set for the study.

- Chapter 3 describes the methodology that was followed for the analytical work, sampling, modelling and the experimental plan.
- Chapter 4 describes the materials that were used and produced during the study.
- Chapters 5 through 7 discuss the experimental results and the evaluation of the three different processing steps.
    - Chapter 5: Roasting.
    - Chapter 6: Smelting.
    - Chapter 7: Atomisation and high temperature treatment.
- Chapter 8 contains the overall process evaluation, including self-critique of the process.
- Chapter 9 contains the conclusion.

Over and above the investigation of the primary steps of roasting, smelting and atomisation, additional work was done to meet the objectives set for the study. These results are included as Appendices. The studies included in the Appendices are summarised below:

- Appendix A: Leaching of Fe, Ni, Cu, As and Pb. Experimental results showed that these elements were not removed across the smelting step to the extent predicted by modelling (mostly due to a non-optimal experimental smelting design). Additional test work was performed to see whether these elements could be leached from third stage residue or roasted third stage residue.
- Appendix B: Dissolution of atomised alloy in HCl/Cl_2. One of the important objectives that had been set for the study was to produce an alloy that would be amenable to leaching in the HCl/Cl_2 dissolve typically utilised by PMR processes.
- Appendix C: Roasting test work on Se/Te precipitate. This is reported in an appendix, since it was an important objective set for the study (removal of both caustic leaches from the BMR circuit). However, it is not fundamentally related to the main study of the high grade PGM leach residue.
- Appendix D: Additional detail around the roasting, smelting and high temperature tests that were performed. All the test work and conditions are summarized in tables.
- Appendix E: Additional flow sheet suggestion for Lonmin. The evaluation for the new process was done within the Lonmin context, but is applicable to most of the refiners that utilise the smelting-BMR-PMR route. Within the Lonmin context, some learning from the studied process can be applied outside of the roasting, smelting and atomisation flow sheet. Two flow sheets are proposed: 1) A flow sheet is suggested where only roasting is done, to replace the caustic leaches currently performed in the BMR. 2) The basic steps of roasting, smelting and atomisation can be applied to many PGM containing residues. A flow sheet is suggested for Lonmin to handle the residues that they generate internally from the BMR and PMR.

1.5 Modelling and experimental approach limitations

The concept of removing contaminants from a high grade PGM residue by the use of a pyrometallurgical process was studied by means of modelling to establish technical feasibility. The high level modelling investigation is reported in Chapter 2. Over and above establishing feasibility, modelling had the important function of defining a narrow set of experimental conditions that

needed to be studied. The number of experiments that could be performed was restricted for a number of reasons: The

- value of the residue, due to PGM content. With a PGM content of around 50%, the value of the samples become restrictive
- broad nature of the investigation and the number of processing steps that needed to be studied. These steps included roasting, smelting and atomisation
- nature of pyrometallurgical experiments (especially smelting experiments), which are often insufficiently representative if they are too small. Poor representation by small experiments can be caused by a number of factors for example, interaction with the crucible, lack of stirring/settling and difficulty of obtaining a representative sample from the melt. The roasting experiments could be performed with smaller lots of around 50 g, but the smelting tests needed a minimum quantity of around 350 g per smelt in order to obtain a decent alloy button that could be sampled
- cost of equipment and access to equipment for the experimental work.

This limitation on the number of experiments led to a less than optimal experimental design, with few variables and with the variables defined in a narrow band. Few repeats were also performed, leading to poor statistical evaluation of results.

The major challenge for the experimental smelting tests was to obtain a representative sample of the alloy, together with an accurate and precise assay result. The best conceivable method of sampling the alloy is described in section 3.2. ICP-OES and ICP-MS are normally employed in PGM assaying, and were used throughout the study. However, a total of three different laboratories had to be used for analytical work according to availability. The use of different standards, etc. led to varying assay results (shown in section 4.5). In an effort to keep the results free from analytical bias (specific to a laboratory), as-reported values were always used to determine recoveries and the same lab was always used to assay the feed and product from any given test. The contribution of sampling and analytical error on recovery could not be quantified, leaving the interpretation of data statistically inconclusive at times. Therefore, modelling was often used to assist in the interpretation of results.

1.5.1 Justification for the use of different feed materials to the smelting and high temperature treatment step

Smelting test work was not limited to the roasted third stage product, although this was the envisaged processing route. Section 6.1 contains a detailed discussion of the different materials that were studied in the smelting and high temperature treatment steps. Three different feed materials were used for both the smelting step and the high temperature treatment step, being:

- Roasted third stage leach residue
- Unroasted third stage leach residue
- Roasted third stage leach residue with base metal leaching prior to roasting

The smelting test work also investigated the addition of Cu as a melt modifier, leaving a total of four different systems that were studied across the smelting step. The justification for investigating different feed systems across the smelting step is given below:

- To understand the removal of Se, Te, S, As and Os across the smelting step when roasting was not performed.
- To understand the effect of feed concentration of Se, Te and S on Au losses.
- To understand the effect of lower Fe, Ni and Cu loadings on the liquidus temperature and the partial oxygen pressure control.
- To understand the effect of Cu addition on the partial oxygen pressure control and melting temperature.

Chapter 2: Thermochemical overview and objectives and hypotheses set for thesis

This chapter will illustrate the basic concept behind the proposed pyrometallurgical process to treat high grade PGM leach residues by means of a thermodynamic modelling example, as the concept can be most clearly illustrated by modelling. Since the process was novel, thermodynamic modelling was used to explore the concept, develop the process steps and to set the hypothesis and objectives for the study, which were then studied experimentally. Modelling was also used to develop the experimental plan by defining the most important variables and setting the experimental ranges for variables during the experimental work. Lastly, modelling was used to assist with interpretation of results. Database development and validation was not set as an objective of the modelling activity, although differences between modelling predictions and experimental results are highlighted and discussed in chapters 5 through 7.

The illustration of the capability of the concept by the use of modelling leads to the setting of objectives and hypotheses at the end of the chapter. Interpretation of the thermodynamic modelling and comparison with experimental results are not done in this chapter, but are discussed in chapters 5 through 7.

2.1 Modelling illustration

Thermodynamic modelling was done with FactSage® version 6.2, as the databases for high PGM containing materials were available within this commercial software modelling package. The use of FactSage databases and the calculation modules are discussed in section 3.3. This chapter will therefore not contain any discussion on the modelling methodology.

2.1.1 Roasting

The impact of a single variable (temperature) will be illustrated in a modelling run. The other major variables, i.e. the oxidation/reduction potential of the gaseous atmosphere and the gas quantity in contact with the system (equivalent to gas flow rate and roasting time), will not be discussed. These variables were optimised based on separate modelling runs.

Modelling was performed on third stage leach residue (composition provided in Table 3) in contact with air (21% oxygen and 79% nitrogen by volume) in a temperature range of 600 °C to 1000 °C. The Open equilibrium system, which simulates periodic removal of gaseous components, was used to perform the calculations (see Section 3.3). For every 100 g initial third stage residue, 10 g air per step was allowed to be in contact with the system for a total of 14 steps. The air requirements were based on the expected flushing rate that would be used in the experimental set-up. Table 1 below shows the elemental removal (in wt%) to the gas phase that can be achieved at different temperatures.

Table 1: Modelling result of the weight percentage removal to the gas phase (Only the volatile elements of interest are listed)

Element	600 °C	650 °C	700 °C	750 °C	800 °C	850 °C	900 °C	950 °C	1000 °C
Ru	0.0%	0.0%	0.0%	0.0%	0.0%	0.0%	0.1%	0.2%	0.4%
Ir	0.0%	0.0%	0.0%	0.0%	0.0%	0.1%	0.3%	0.9%	1.6%
Os	100.0%	100.0%	100.0%	100.0%	100.0%	100.0%	100.0%	100.0%	100.0%
Pb	0.0%	0.1%	0.4%	1.8%	6.0%	17.3%	38.5%	73.5%	99.2%
Te	0.3%	2.0%	11.1%	53.9%	100.0%	100.0%	100.0%	100.0%	100.0%
Ag	0.0%	0.0%	0.0%	0.0%	0.0%	0.0%	0.0%	0.0%	0.1%
Se	89.4%	100.0%	100.0%	100.0%	100.0%	100.0%	100.0%	100.0%	100.0%
As	100.0%	99.4%	93.7%	93.7%	93.7%	93.7%	93.7%	100.0%	100.0%
S	90.5%	91.5%	95.0%	96.8%	97.5%	100.0%	100.0%	100.0%	100.0%

Sections 3.3.1 and 5.3.3 contain a more detailed discussion on elemental behaviour. Some problem areas are highlighted below:

- The increased removal of S with increasing temperature is due to the formation/dissociation of stable sulphate species.
- Arsenic removal shows a decreased efficiency for the temperature range roughly between 700 °C and 900 °C. This behaviour is due to the stability temperature range for the mineral $Ca_3(AsO_4)_2$.
- The prediction of Pb removal is due to the formation of PbSe and PbTe species. The formation of these species is highly unlikely in the roasting conditions. Other Pb species do not show volatile behaviour in the temperature range studied.
- Ir and Ru are the only two PGM elements (apart from Os) that can show volatile behaviour in the atmosphere and temperature range modelled. Below 900 °C, the losses appear insignificant.

A roast at 850 °C was used to illustrate the process capabilities shown in Table 4. This temperature was chosen due to the perceived benefits of complete S removal with minimal Ir losses (0.1%).

2.1.2 Smelting

The impact of a single variable (temperature) will be illustrated in a modelling run. The other major variables, ie the oxygen partial pressure achieved in the melt, pressure, slag type, slag addition rate and the gas quantity in contact with the system (equivalent to gas flow rate and smelting time), will not be discussed. These variables were optimised based on separate modelling runs.

Due to high oxygen content of roasted product feed (estimated by FactSage® at around 11.5%), some Ru losses (up to 15% by mass) were predicted during the initial melting. In order to avoid Ru losses, reductant (in the form of sugar or $C_{12}H_{11}O_{22}$) was added to the initial melt in the ratio of 7 g of sugar to 100 g of roasted product feed. Slag (CaO-SiO_2-Al_2O_3-Na_2O type, as described in section 4.4) was added to the melt in a ratio of 50 g slag addition to 100 g of roasted product feed. Nitrogen gas (in the ratio of 100 g per 100 g roasted product feed) was allowed to be in contact with the system. The inert gas ratio was based on the flushing gas that would be used in the experimental set-up.

Table 2 below shows the elemental recovery that can be achieved across the smelting step per temperature interval.

Table 2: Modelling result of the recovery to the alloy phase across the smelting step (Only the elements of interest are show)

Element	1300 °C	1350 °C	1400 °C	1450 °C	1500 °C	1550 °C	1600 °C	1650 °C	1700 °C
Pt	100.0%	100.0%	100.0%	100.0%	100.0%	100.0%	100.0%	100.0%	100.0%
Pd	100.0%	99.9%	99.9%	99.8%	99.6%	99.4%	99.1%	98.7%	98.1%
Rh	100.0%	100.0%	100.0%	100.0%	100.0%	100.0%	100.0%	100.0%	100.0%
Ru	100.0%	100.0%	100.0%	100.0%	100.0%	99.9%	99.9%	99.9%	99.9%
Ir	100.0%	100.0%	100.0%	100.0%	100.0%	100.0%	100.0%	100.0%	100.0%
Au	100.0%	100.0%	100.0%	100.0%	99.9%	99.8%	99.7%	99.5%	99.2%
Ag	97.3%	95.3%	92.2%	87.6%	81.3%	73.4%	64.0%	54.0%	44.0%
Pb	57.7%	44.2%	31.6%	21.7%	16.3%	12.6%	9.8%	7.6%	6.0%
Cu	95.7%	94.3%	92.0%	87.6%	85.2%	84.1%	83.5%	83.1%	82.6%
Ni	49.5%	52.2%	55.1%	58.2%	60.8%	63.2%	65.7%	68.2%	70.8%
Co	14.5%	16.7%	19.1%	21.9%	25.6%	29.7%	33.8%	38.0%	42.4%
Fe	0.9%	1.1%	1.4%	1.8%	2.3%	3.1%	4.1%	5.5%	7.1%

Sections 3.3.2 and Chapter 6 contain a more detailed discussion on elemental behaviour. Some problem areas are highlighted below:

- The lower recovery of especially Ag and Pb reflects the increased vapour pressures of these elements at higher temperatures.
- The volatility of Pd is predicted as the gaseous species PdOH (with the H coming from the hydrocarbon reductant addition). If this species is not allowed, Pd losses reduce by a factor of > 100.
- Fe, Ni and Co partitioning increases to the alloy phase at higher temperatures, while Cu partitioning to slag phase increases with temperature. Since Cu is the single biggest contaminant that remains in the alloy (according to modelling), the overall effect of temperature on the final grade of PGM achieved in the alloy is almost negligible.

A smelt at 1 500 °C was used to illustrate the process capabilities shown in Table 4. This temperature was perceived to be necessary due to preliminary test work that showed melting temperature requirements of at least 1 400 °C.

2.1.3 Summary of process capability according to modelling

Table 3 shows the upgrading that can be done across the roasting and smelting steps according to elemental analyses. From modelling, it appears possible to produce an alloy with a PGM content of 88% in a simple two step process.

Table 3: Elemental composition of feed material and product after the roasting and smelting steps, reflecting the degree of upgrading achieved

Element	Third stage feed	Roasted product	Alloy after smelting
Pt	24.5%	31.4%	44.5%
Pd	11.7%	15.0%	21.2%
Ru	6.2%	7.9%	11.2%
Rh	4.0%	5.2%	7.3%
Ir	1.5%	1.9%	2.7%
Au	0.6%	0.8%	1.1%
6E	**48.6%**	**62.2%**	**88.0%**
Os	4.0%	0.0%	0.0%
Ag	0.7%	0.9%	1.1%
As	2.0%	0.2%	0.2%
Se	3.4%	0.0%	0.0%
Te	0.5%	0.0%	0.0%
Pb	4.2%	4.4%	1.0%
S	8.5%	0.0%	0.0%
Fe	4.9%	6.2%	0.2%
Co	0.1%	0.1%	0.0%
Ni	2.9%	3.7%	3.2%
Cu	4.1%	5.2%	6.3%
Mg	0.3%	0.4%	0.0%
Al	0.2%	0.3%	0.0%
Si	1.9%	2.4%	0.0%
Cr	0.3%	0.3%	0.0%
Ca	0.1%	0.1%	0.0%
Total	86.6%	86.5%	100.0%

Table 4 shows the recovery that can be achieved across each step, together with the total recovery. For all the PGMs, the recovery approximates 100%. However, Ag losses are a concern for refineries that recover Ag. Ni and Cu removal is not very good across the circuit. Chapter 6 discusses the sensitivity of the recovery of the base metals to the partial oxygen pressure (pO_2) that were achieved during the melt. A higher rate of removal of the base metals could be achieved with better control over the pO_2 in the melt. Removal of the oxides (Si, Ca, Cr, Mg and Al) was complete. Removal of the volatile species of S, As, Pb, Os, Se and Te also ranged from high to complete.

Table 4: Summary of total recovery modelled across the roasting and smelting steps in the envisaged process

Element	Recovery across roasting step	Recovery across smelting step	Total Recovery
Pt	100.0%	100.0%	100.0%
Pd	100.0%	99.6%	99.6%
Ru	100.0%	100.0%	100.0%
Rh	100.0%	100.0%	100.0%
Ir	99.9%	100.0%	99.9%
Au	99.9%	99.9%	99.8%
Os	0.0%	0.0%	0.0%
Ag	100.0%	81.3%	81.3%
As	6.3%	99.0%	6.3%
Se	0.0%	0.0%	0.0%
Te	0.0%	0.0%	0.0%
Pb	82.7%	16.3%	13.5%
S	0.0%	0.0%	0.0%
Fe	100.0%	2.3%	2.3%
Co	100.0%	25.6%	25.6%
Ni	100.0%	60.8%	60.8%
Cu	100.0%	85.2%	85.2%
Mg	100.0%	0.0%	0.0%
Al	100.0%	0.0%	0.0%
Si	100.0%	0.0%	0.0%
Cr	100.0%	0.0%	0.0%
Ca	100.0%	0.0%	0.0%

Based on the modelling results that were achieved for the proposed process, a number of objectives were set for the study. Furthermore, based on the understanding of each processing step from modelling, hypotheses were set for each processing step.

2.2 Objectives of the study and hypothesis per processing step

A number of primary objectives were identified as success criteria at the beginning of the study. These are listed below.

Objectives

- Practically illustrate the use of roasting, smelting and atomisation steps for refining of high grade PGM residue.
- Removal of PGM-containing caustic effluent production from the BMR.
- Production of a PGM alloy that is at least as amenable to leaching in the PMR as the existing BMR concentrate.
- Production of an alloy with ~ 90% PGM content by weight, with negligible PGM losses.

- Achievement of 90 wt% Pb removal across the process.

Hypotheses

The hypotheses set for each processing step are given below:

Roasting

- Roasting in an oxidising environment between 600 °C and 1 000 °C will allow > 90% removal of S, Se, Te, As and Os without any associated PGM losses to vapour.
- Air is a sufficiently oxidising medium able to rapidly oxidise impurities to their respective volatile compounds, while at the same time providing the transport volume of gas (in the form of nitrogen) necessary to remove volatile oxides.
- Mass transfer will proceed sufficiently fast that stationary bed roasting will give similar results to agitated or fluidised bed roasting, thereby simplifying the design of the roaster to avoid particulate loss to the gas phase.

Smelting

- At sufficient temperature, PGMs will dissociate from oxygen and alloy and collect in an alloy phase without the addition of a collector.
- It is possible to selectively partition the PGMs to the alloy phase without losses to the slag or gas phase.
- Liquidus temperature of the smelting system will be between 1 300 °C and 1 400 °C.
- There will be minimal effect on the smelting temperature requirement and PGM grade produced whether unroasted or roasted material, or roasted material with prior base metal leaching, is used as feed material.
- A Borate based slag will perform best, due to the low melting temperature and high solubility of spinel phases produced in the roasting step.
- Partial oxygen pressure of the melt can be controlled by the addition of reducing and oxidising agents.
- The melt needs to start with the addition of a reducing agent to remove excess oxygen from the system and avoid PGM losses as oxide vapours.
- The melt needs to end with the addition of an oxidising agent to partition Fe, Ni and some Cu to the slag phase.
- As, Pb Fe, Cu and Ni deportment control is possible through partial oxygen pressure control.
- The alloy phase and slag phase will separate completely to facilitate phase separation with almost negligible losses of alloy to the slag phase.
- Stable oxides (such as Cr_2O_3, CaO, SiO_2, Al_2O_3 and MgO) will join the slag phase and be completely removed from the alloy phase.

Atomisation

- The cast alloy will not be amenable to crushing and milling.
- Atomisation will be able to break up the alloy phase to produce particulate with a D_{50} of 20 μm with acceptable pressure (<250 bar) requirements.

- Atomisation can proceed in ambient air conditions, without any measurable PGM oxidation or volatilisation resulting from rapid heating and quenching.
- The atomised alloy will be very reactive and should dissolve completely in HCl or Cl_2.
- The effect of elements that reduce surface tension (such as S, Se and Te) will reduce the pressure requirements for a set particulate size.
- The presence of S, Se and Te could lead to losses of Au as a vapour during high temperature treatment.

Chapter 3: Methods

This chapter summarises the methodology followed for analytical work, sampling, thermodynamic modelling and the experimental set-up. The sampling and analytical errors are quantified at the end of the chapter.

3.1 Analytical characterisation methodology

Below follows a description of the analytical techniques that were employed.

SEM EDS to identify phases and analyse elemental composition of phases

Sample preparation consisted of mounting polished sections of the sample in resin and coating them with a layer of carbon (in the case of non-conductive samples).

The samples were analysed using a Quanta 600 scanning electron microscope (SEM), fitted with energy dispersive spectroscopy (EDS) detectors. The backscatter resolution allows mineral phase boundaries to be identified on density differences only. Chemical (EDS) resolution is much more difficult, depending on the relationship between the individual grain size (often around a micron or less) and the electron beam diameter (typically 3 micron).

MLA/SEM EDS to determine mineral phase composition and associations

Sample preparation consisted of mounting polished sections of the sample in resin and coating them with a layer of carbon (in the case of non-conductive samples).

The mineral/phase quantification was carried out by the Mineral Liberation Analyser (MLA®) software, to determine the mineral speciation of PGMs and associations with gangue components. The X-Ray Back-Scatter Electron (XBSE) technique was used in conjunction with MLA to determine the bulk mineralogy of the samples. This technique uses back-scattered electron (BSE) images to define phase boundaries and X-ray spectra to estimate the mineralogy of each phase.

XRD bulk mineral phase quantification

The samples were all micronised in a McCrone micronising mill before mounting in standard 15 mm sample holders using a standard back-loading technique. Analysis time was 10 minutes per sample with an angular range of 5° to 90° (2θ). X-Ray Diffraction (XRD) analyses were performed with a PANalytical X'Pert Pro powder diffractometer with X'Celerator detector and variable divergence and receiving slits with Fe filtered Co-Kα radiation. Phases were identified using X'Pert Highscore plus software. Rietveld refinement software (Kleeberg *et al.*, 2002) was used for the modal analysis of the minerals. Rietveld refinement has its constraints, being a peak-curve-fitting routine, particularly for amorphous, near amorphous or poorly crystallised phases.

Chemical analyses

A suite of analytical methods was used to determine different elemental abundances in the samples. These methods are summarised below:

- Inductively Coupled Plasma-Optical Emission Spectrometry (ICP-OES) for Pt, Pd, Au, Rh, Ru, Ir, Ag, Al, Co, Cr, Cu, Fe, Mg, Mn, Pb and Zn. Sample preparation was done with sodium peroxide fusion, followed by dissolution in concentrated hydrochloric acid.
- Inductively Coupled Plasma- Mass Spectrometry (ICP-MS) for all low level determinations of the toxic elements (As, Se, Te, Sb, Sn, and Bi). Initial solid samples were prepared by either acid digestion (nitric, perchloric and hydrofluoric acids) or fusion (dependant on concentration). Os was also determined with ICP-MS. ICP-MS makes use of isotopes identified in the plasma phase. Where multiple isotopes exist, the redundancy in data allows the elimination of plasma-isotope combinations that may lead to false spectral analyses. Single isotopes may sometimes give rise to false combinations of lighter elements with the plasma gases. Silicon (as colloidal silica) may lead to inaccurate results when the silicon has not been completely dissolved, as particles may spend insufficient time in the plasma to volatilise.
- A LECO CS200 C/S analyser was used to determine total S content. Analysis is based on infrared absorption of the liberated SO_2 and CO_2 gases upon sample combustion. Samples were pulverised and weighed out prior to combusting them in the crucibles.
- X-Ray fluorescence (XRF) analyses were used for the full set of chemical element analyses. The XRF analyses proved to be an accurate indication of elemental removal efficiencies across the roasting step. Constraints such as sample homogeneity and matrix interference effect should always be taken into consideration when interpreting the results. XRF was used for the major oxide composition of the slag phase. The samples were prepared as pressed powder briquettes.

Thermo-Gravimetric analyses

About 50 mg of pulverised sample were loaded in the crucible. Thermo-Gravimetric Analysis (TGA) and Differential Thermal Analyses (DTA) were performed on the third stage leach residue and Se/ Te precipitate to understand the thermal behaviour and mass loss of the material. The samples were analysed with a Mettler Toledo 851STARe simultaneous DTA/TGA analyser. The temperatures where weight loss occurs indicate important transition points. The DTA component allows the quantification of the reaction heats and latent heats of phase changes.

3.2 Sampling methodology

This section will describe the sampling methods that were followed for the different materials.

Sampling of residue and roasted calcine

Sampling of the fine particulate (powder) samples, like the Se/Te precipitate, third stage residue and roasted calcine, proceeded by riffle splitting and sub-splitting in order to obtain a representative sample for analytical work.

Sampling of the alloy phase (after melting and after a high temperature treatment step)

Sampling of alloy buttons produced during the smelting test work and the high temperature test work was performed by drilling two holes through the alloy (5 mm each) adjacent to each other and just off-centre, as shown in Figure 4. The shavings from this drill sample were sent for full dissolution and wet chemical analyses.

Figure 4: Photograph of sampling method that was used on the alloy button. Two holes were drilled and the shavings from the drilling were submitted for assaying

The system poses a number of difficulties, such as the high monetary value of the alloy and the need to perform subsequent tests (high temperature treatment or atomisation), which require samples that are as representative as possible. However, the alloy complexity invariably leads to melt heterogeneity, particularly upon cooling. Although this sampling technique is clearly not ideal and contributed to sampling error, no other technique could be conceived that would eliminate sampling error on the alloy button. The recovery values calculated in the smelting and high temperature treatment step are obviously impossible or incorrect at times. A decision was taken not to manipulate the values (for instance to limit recovery to 100% across a system that cannot release inventory), so that the shortcomings of the sampling technique would allow transparency of the limitations of the data set. As already discussed in the Introduction, sample heterogeneity and assaying inconsistency causes errors in the smelting and high temperature treatment results, and makes statistical evaluation of significant deviations very difficult.

Sampling of the slag phase

All of the slag phase was gathered from selected melts after separation from the alloy button. The slag phase was then crushed and milled before splitting. Splitting proceeded in the same manner as with the other fine particulate material described above.

Sampling of the atomised alloy phase

Sampling of the atomised alloy proceeded by representative riffle splitting of the fully atomised batch after dewatering.

3.3 Thermodynamic modelling methodology

Thermodynamic equilibrium modelling was performed with a commercial software package, FactSage®, version 6.2 (Bale *et al.*, 2001).

Background to FactSage®

According to Bale *et al.* (2008), FactSage® was introduced in 2001 as the fusion of the F*A*C*T/FACT-Win and ChemSage thermochemical packages. The FactSage® package runs on a PC operating under Microsoft Windows® and consists of a series of information, database, calculation and manipulation modules that enable one to access and manipulate pure substances and solution databases. It is used worldwide at approximately 400 installations in universities, governmental and non-governmental research laboratories and in industry (2008 data). The original F*A*C*T package was designed to simulate the thermochemistry of pyrometallurgical processing. With the migration to the Windows-based FACT-Win and then to FactSage® the applications have been expanded to include hydrometallurgy, electrometallurgy, corrosion, glass technology, combustion, ceramics, geology, environmental studies, etc.

Databases description used in the thesis

The FACT databases are the largest set of evaluated and optimised thermodynamic databases for inorganic systems in the world and have been under development for over 30 years. Data is added by consortium projects receiving funding from industry and research councils.

Below follows a summary of the main databases that were used in this thesis for equilibrium calculations.

ELEM - This compound database contains standard state data for all the elements, taken from the FACT53 compound database. The modules EQUILIB and PHASE DIAGRAM always require standard state data for the elements, even elements that may not be involved in the calculation.

FACT53 – This database contains data on most compounds (4 549 compounds) in their liquid, solid and gaseous states. The compounds will not be listed here.

FToxid - oxide database for slags, glasses, minerals, ceramics, refractories, etc., which contains data for stoichiometric oxides and oxide solutions of the following compounds: Al_2O_3, As_2O_3, B_2O_3, CaO, CoO, CrO, Cr_2O_3, Cu_2O, FeO, Fe_2O_3, GeO_2, K_2O, MgO, MnO, Na_2O, NiO, PbO, SiO_2, SnO, TiO_2, Ti_2O_3, ZnO and ZrO_2. Not all binary, ternary and higher-order sub-systems have been evaluated and optimised, nor are all composition ranges covered. However, the system Al_2O_3-CaO-FeO-Fe_2O_3-MgO-SiO_2 has been fully optimised from 25 °C to above the liquidus temperatures at all compositions and oxygen partial pressures.

FTmisc - miscellaneous databases for copper, nickel, lead, zinc, etc. sulphides. The following systems are included: the S-Fe-Ni-Co-Cu-Cr-Mn system; the matte smelting system S-Cu-Fe-Ni-Co-Pb-Zn-As.

SGTE (2007) - database includes 78 elements: Ag, Al, Am, As, Au, B, Ba, Be, Bi, C, Ca, Cd, Ce, Co, Cr, Cs, Cu, Dy, Er, Eu, Fe, Ga, Gd, Ge, Hf, Hg, Ho, In, Ir, K, La, Li, Lu, Mg, Mn, Mo, N, Na, Nb, Nd, Ni, Np, O,

Os, P, Pa, Pb, Pd, Pr, Pt, Pu, Rb, Re, Rh, Ru, S, Sb, Sc, Se, Si, Sm, Sn, Sr, Ta, Tb, Tc, Te, Th, Ti, Tl, Tm, U, V, W, Y, Yb, Zn, Zr. From among these elements, there are some 350 completely assessed binary alloy systems, of which over 40 are newly assessed systems while many others have been revised or amended on the basis of newly published experimental information. The database also includes about 120 ternary and higher-order systems for which assessed parameters are available for phases of practical relevance. The systems now incorporate approximately 180 different solution phases and 600 stoichiometric intermetallic compound phases.

SGnobl (2010) - noble metal database contains evaluated thermodynamic parameters for alloys of Ag, Au, Ir, Os, Pd, Pt, Rh, Ru alloyed amongst themselves and also in alloys with the metals: Al, As, Bi, C, Co, Cr, Cu, Fe, Ge, In, Mg, Ni, Pb, Sb, Si, Sn, Ta, Te, Ti, Tl, Zn, Zr.

The calculation module

Equilib employs the Gibbs energy minimisation algorithm for treating complex heterogeneous equilibrium using compound and solution databases. The Equilib module is the Gibbs energy minimisation workhorse of FactSage®. It calculates the concentrations of chemical species when specified elements or compounds react or partially react to reach a state of chemical equilibrium. Phases from the compound and solution databases are retrieved and offered as possible products. The products may include pure substances (liquid, solid), ideal solutions (gas, liquid, solid, aqueous) and non-ideal solutions (real gases, slags, spinels, molten salts, mattes, ceramics, alloys, dilute solutions, aqueous solutions, solid solutions, etc.) retrieved from the activated databases. The Equilib module can handle up to 48 reactants consisting of up to 32 different components.

Within the Equilib module, it is possible to calculate equilibrium according to a Normal and Open system. The Normal system calculates equilibrium products of the entire input feed streams (gaseous, liquid and solid). The Open system allows the gaseous atmosphere to be removed in a number of steps. Equilibrium is calculated for a gaseous atmosphere, after which it is removed from the system and a new gas addition is done upon which equilibrium is calculated again. The equilibrium products (apart from gas) are seen as the feed to the next step. The number of repetitive steps can be specified, together with the gas addition per step. Equilibrium data can be retrieved per step. The Open system can be more accurate in calculating equilibrium across systems where the gaseous atmosphere is periodically (or continuously) removed and replaced by a specified gaseous stream.

In Sections 3.3.1-3.3.3 both the choice of database and calculation mode are assessed by means of preliminary case studies.

3.3.1 Roasting

The basic model set-up is summarised below. :

- Feed streams. The feed streams included third stage leach residue (described in section 4.1) and gas addition. The gas addition was either inert (N_2 or Ar), oxidising (air or oxygen enriched air) or reducing (CO and H_2).

- Products: According to both the SGTE and SGNoble databases, the only solid solution phase that formed was the Face Centred Cubic (FCC) phase. Neither the FToxid nor the FACT Spinel databases predicted that any PGMs or volatile components (Os, As, Se, Te, Ag) would enter the spinel phase in the temperature range studied. For this reason only the ideal gas phase, pure solids phases and the SGNoble FCC solid solution phase were activated during the modelling runs. It is important to understand the limitations of the selected databases. As an example, the solution model might not be regressed and calibrated to allow Ru and Rh to enter the FToxid solid solution phase.
- Variables: Gaseous addition rate (0 to 200 g gas addition per 100 g of third stage residue feed), Gaseous type (see Feed streams above), Temperature (600 °C to 1 000 °C).
  Module: The Equilib module was used to calculate equilibrium products from complex feed streams. The Open and the Normal calculation methods were compared.

Preliminary database and calculation mode assessment

A comparison was done between the SGTE and SGNoble databases with regard to their prediction of the FCC solid solution phase. This comparison was done with the Normal calculation method in Factsage® with excess oxygen available in the system to ensure oxidation (140 g air allowed per 100 g third stage residue). The results from this comparison are shown in Table 5. The SGNoble database was optimised for most of the binary element combinations below, while the SGTE database has limited data on the PGMs. A decision was taken to use the SGNoble database for modelling, as an understanding of the PGM behaviour was of first importance. It must be highlighted that Cu shows the greatest deviation between the two databases, with the SGNoble databases showing almost complete dissolution of Cu into the FCC phase above 850 °C. However, actual experimental results did not reveal Cu in the FCC solid solution phase.

Table 5: Comparative modelling result of the weight percentage reporting to the FCC solid solution phase with the SGNoble and SGTE databases at 140 g air per 100 g of third stage residue feed

	Databasis	600 °C	650 °C	700 °C	750 °C	800 °C	850 °C	900 °C	950 °C	1 000 °C
Ir	SGNoble	0%	0%	0%	1%	3%	8%	25%	85%	99%
	SGTE	0%	0%	1%	7%	26%	91%	100%	100%	100%
Ag	SGNoble	1%	3%	13%	100%	100%	100%	100%	100%	100%
	SGTE	10%	29%	94%	100%	100%	100%	100%	100%	100%
Pd	SGNoble	1%	6%	29%	100%	100%	100%	100%	100%	100%
	SGTE	3%	11%	51%	100%	100%	100%	100%	100%	100%
Rh	SGNoble	0%	0%	1%	2%	6%	11%	27%	49%	67%
	SGTE	0%	0%	1%	3%	8%	22%	58%	100%	100%
Ru	SGNoble	0%	0%	0%	0%	0%	0%	0%	0%	0%
	SGTE	0%	0%	0%	0%	0%	0%	0%	0%	0%
Cu	SGNoble	0%	4%	20%	32%	38%	80%	100%	100%	100%
	SGTE	0%	0%	0%	1%	1%	3%	6%	13%	24%

A comparison was also done between the Normal calculation option and the Open calculation option in FactSage®. The Open method is more appropriate, since gas was continuously added and removed from the roasting test work. In both calculation methods a total of 140 g of air was allowed per 100 g of third stage leach residue. In the Open method, the air was added in steps of 10 g for each of 14 steps. Table 6 below shows a comparison of the deportment to the gas phase and the FCC solid solution for both the Normal and Open systems.

Table 6: Comparison between the Normal and Open calculation methods of the overall wt% deportment to the gas phase and FCC solid solution phase, using FactSage®

Element	Phase	System	600 °C	650 °C	700 °C	750 °C	800 °C	850 °C	900 °C	950 °C	1 000 °C
Pb	Gas	Normal	0%	0%	0%	0%	0%	0%	0%	0%	4%
		Open	0%	0%	0%	2%	6%	17%	38%	73%	99%
S	Gas	Normal	28%	43%	59%	70%	74%	89%	91%	91%	93%
		Open	90%	91%	95%	97%	98%	100%	100%	100%	100%
As	Gas	Normal	9%	100%	100%	100%	100%	100%	100%	100%	94%
		Open	100%	99%	94%	94%	94%	94%	94%	100%	100%
Cu	FCC	Normal	0%	4%	20%	32%	38%	80%	100%	100%	100%
		Open	7%	12%	22%	38%	48%	67%	89%	100%	100%
Rh	FCC	Normal	0%	0%	1%	2%	6%	11%	27%	49%	67%
		Open	0%	0%	0%	1%	3%	8%	17%	40%	55%

The results from Table 6 will be discussed in more detail in Chapter 5. In summary, the main difference between the two methods is related to the lower oxidation potential in the Open system when equilibrium is calculated in the first steps with low air addition. Due to incomplete oxidation of most elements, Pb is lost in volatile species such as PbSe, PbTe and PbS, while S is lost in volatile species such as SO_2. In the case of S, the Open system more favourably compares to actual

experimental results, rather than the Normal system, where complete oxidation occurs and stable sulphates form. However, in the case of Pb, where the actual experiments did not show any Pb loss to the gas phase, the formation of the volatile Pb species such as PbTe and PbSe probably does not happen, as Se and Te potentially oxidise during the heating cycle of the furnace.

The Open system better models the elemental deportment to the FCC solid solution phase, by being closer to actual experiments' results. FactSage® modelling results from the Open system were used to interpret actual results in the Discussion section, except in the case of Pb, where the Normal system better describes the measured results.

3.3.2 Smelting

The basic model set-up is summarised below. :

- Feed streams. The feed streams included roasted third stage leach residue (described in section 4.3.1), slag addition (described in section 4.4), oxidation and reduction agent addition (described in section 4.3.2) and gas addition (as air or N_2).
- Products: FT Oxid Spin (single phase), FT Oxid SlagA (single phase), Pure solids (limited) and Ideal gas phase. The SGNobl-LIQ1 and SGTE-LIQU were used to model the alloy phase that formed.
- Variables: Temperature, gas addition rate, gas type, oxidant and reductant addition rates, pressure, slag type and slag addition rate.
  Module: The Equilib module was used to calculate equilibrium products from complex feed streams. The Open and the Normal calculation methods were compared.

Preliminary database and calculation mode assessment

A comparison between the SGTE and SGNoble databases showed significant differences in the recovery of especially As, Pb, Ag and Fe to the alloy phase. In the case of the SGNoble database, the list of optimised systems included most of the PGMs with each other, and also the PGMs with As, Pb, Ag and Fe, while the SGTE database had limited optimised systems of the PGMs with each other or other significant elements in the system. It was decided to use the SGNobl-LIQ1 database throughout to model the alloy phase (as the PGMs constituted the bulk of the alloy content).

The Normal system was used for evaluation of the smelting tests. This was done in order to run sets of conditions and to back-calculate the pO_2 achieved in the melt. The Open system would be slightly more representative (due to gas flushing across the melt). However, the Normal and Open system compared closely and the Normal system was used, due to the ease of running pO_2 range calculations.

An evaluation was also done on the ability of FactSage® to predict the smelting range of the systems studied (Direct Smelt, Roast-Smelt, Leach-Roast-Smelt). PGM alloys are known to form high temperature solid solution phases. SGNobl-HCP1 (HCP stands for Hexagonal Close Packed phase structure) and SGNobl-FCC phases were activated. The SGNoble database predicted that large proportions of the PGMs would be contained in solid solution phases at temperatures well above the observed melting temperature. Without the solid solution phases activated, FactSage® predicted

liquid formation far below the point where liquid phases were observed (discussed on section 5.3). For all systems studied, the observed melting temperature fell between the temperatures predicted by FactSage®, with and without the solid solution phase activated. This was to be expected, due to heating rates in the experimental set-up that did not allow the solid solutions phases to diffuse/change composition, resulting in compositions with lower melting point. The melting temperatures predicted by FactSage® and those observed in the smelting tests are provided in Section 4.4.

In alloys with a Cu content greater than approximately 9%, SGNoble predicts that Ru will form a pure solid (if solid solution phases are not active), due to the complete insolubility of Cu and Ru (Cu-Ru optimised system for SGNoble database). The SGTE database does not predict pure Ru, probably because the Cu-Ru system was not optimised. SEM work on the actual alloys produced could confirm the presence of a primary Ru solid phase that remained solid at the melting temperature, once again pointing out that the use of the SGNoble database was most appropriate. This is discussed in more detail in sections 4.3.2 and 6.2.5.

3.3.3 Atomisation and high temperature treatment

FactSage® modelling was used to evaluate volatile behaviour across the high temperature treatment step, and gas solubility into the alloy at different temperatures.

Nitrogen purging gas was added in steps of 20 g per 100 g alloy feed. 10 steps were allowed for each model. The Nitrogen purging gas was set to contain 1 000 ppmv (parts per million by volume) of O_2. Although this was not measured, some oxygen would come into contact with the melt because the chamber was left open. The oxygen content of industrial nitrogen gas is specified to be below 10 ppm (without contamination by air).

The ideal gas, SGnobl-LIQ1 phase and the FToxid-SLAGA phase were activated. Pure solids were deactivated, as phases like solid CaS would otherwise be predicted. The slag phase was allowed, as it constituted a very small part of the melt (<5% of the weight of the alloy). With FactSage®, if the slag phase was not activated while oxygen was allowed into the melt, Si and Cr, for example, would artificially be removed to the gas phase. In reality, however, the presence of the reducing graphite crucible (both reducing the melt and preferentially reacting with oxygen in the gas) would ensure that a slag phase would not form and that metals like Si and Cr would dissolve in the alloy. SEM work confirmed that no slag inclusions were apparent in the alloy.

The basic model set-up is summarised below. :

- Feed streams. Alloy (described in section 4.3.1) and gas addition (N_2 or Ar with some oxygen allowed into the system at times).
- Products: Ideal gas, SGNobl-LIQ1 and FT Oxid SlagA (single phase).
- Variables: Temperature, gas addition rate, gas type and pressure.
- Module: The Equilib module was used to calculate equilibrium products from complex feed streams. The Open system was used, because it was more representative; gas was constantly removed and fresh Nitrogen was purged across the melt. The Open system also

predicted losses of Au better, as the amphoteric elements (that might otherwise result in losses) are removed to the gas phase, and therefore from the model, in each step.

3.4 Experimental set-up

This section will describe the experimental set-up that was used to study the roasting, smelting and atomisation processes. Appendix D contains a summary of all the test conditions that were used during roasting, smelting and high temperature experimental test work.

3.4.1 Roasting

A number of roasting campaigns were performed to study the major variables of temperature, time, gas type, flow rate and the redox environment.

Based on the thermodynamic modelling and the thermo-Gravimetric results, a first round of stationary bed roasting test work was done in a simple muffle furnace under normal atmospheric pressure and oxygen partial pressure conditions using 30 g of material for each test. The roasting temperature was varied between 600 °C and 1 000 °C in 100 °C intervals. Roasting time for all the tests were set at 2 hours. A small air flow was allowed into the muffle furnace by leaving the door slightly open (10 mm). The air draft through the furnace was done with a small fan that maintained slight suction in the furnace and bubbled the off-gas through a water scavenger to condense and absorb soluble species. From this work it became clear that most of the elements behaved according to the thermodynamic equilibrium conditions predicted by FactSage®, but that specifically Te, As and Os failed to be extracted to the extent predicted. The reason for the poor removal is discussed in Chapter 5.

It was decided to investigate roasting with a fluidised bed to see whether the removal of Te, As and Os could be improved through better gas-solid contact and possibly more uniform temperature control. A vertical type fluidised bed reactor with an inner diameter of 50 mm was used for roasting tests on the third stage leach residue. Some muffle furnace tests were also performed in order to compare stationary bed results with fluid bed results. Figure 5 shows a schematic of the fluid bed tube that was used for the test work.

The reactor was constructed of stainless steel and could be used for temperatures up to 1 100 °C. The tube diameter for fluidisation was 50 mm. Different gas mixtures (Air, N_2, H_2, CO_2, CO, or any combination of these) could be used for fluidisation in the reactor. Temperature set-point was achieved via an electrical heating system. The temperature of the fluid bed was measured with a thermocouple located in the centre of the reactor. The fluidisation gas was fed to the reactor via a steel pipe through the grate. The stainless steel tube was sealed with a glass lid on top and the off-gas left the reactor via a pipe through the glass lid. A bag filter was used to collect very fine particulate carry-over from the gas.

The gas flow rate was set at 1.2 Nm^3/hr. 80 g of material was charged per test. At the end of each test all the material remaining in the reactor was collected, weighed, sampled and submitted for assaying. Pt was used as tie element to determine recoveries, since a closed mass balance could not be achieved. The fine particulate that was carried over with the gas phase and collected in the bag

filter was also weighed and submitted for assaying. Typical carry-over with the off-gas was less than 3% of the feed weight.

The controlled gas atmosphere in the experimental conditions varied from ambient air, oxygen enriched air (40% volume basis oxygen), inert gas (N_2) and reducing gas (20% CO and 80% N_2 per volume). Combinations of gas atmospheres (for instance oxidative following reductive and vice versa) were also tested. The test campaign had the following objectives: To

- optimise Te, As and Os removal.
- compare different solid-gas contacting configurations, such as fluid bed roasting and stationary roasting (in a muffle furnace).

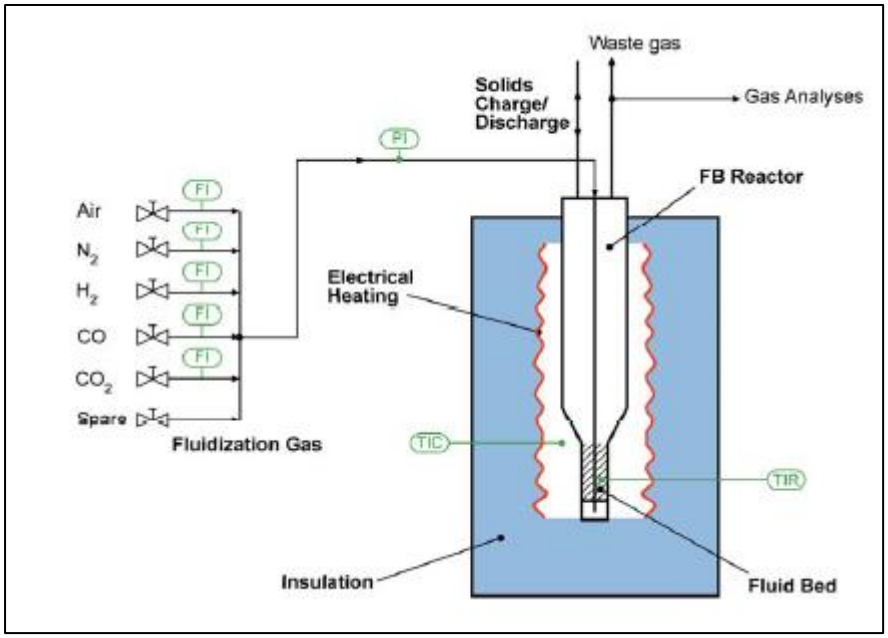

Figure 5: Schematic drawing of the fluid bed reactor that was used for the roasting test work

Table 74 in Appendix D contains a summary of all the roasting test work that was performed on PGM residue.

3.4.2 Smelting and high temperature treatment

Appendix D contains additional information about the smelting test campaigns that were carried out.

General induction smelting set-up

Most smelting tests were performed using a purpose-built induction furnace. Induction heating was chosen in order to allow for a large temperature range, pressure control in the furnace and the ability to add collector/fluxing/oxidising/reducing agents during the melt with relative ease. Typical ranges for the major smelting variables are provided below:

- Temperature range 1 200 °C to 1 700 °C.
- Pressure control between 1 and 0.3 atmosphere absolute.
- Reducing agent (table sugar or sucrose) addition rate between 0 g and 7 g per 100 g residue feed material.
- Oxidising agent ($NaNO_3$) addition rate between 0 g and 15 g per 100 g residue feed material.
- Total slag (flux) addition rate between 20 g and 100 g per 100 g residue feed material.
- Cu (in the form of Cu, CuO or $CuSO_4$) addition between 0 and 150 g per 100 g residue feed material.

The induction furnace could not achieve direct coupling to the feed material. This meant that heating of the melt needed to proceed through indirect heating of the crucible and subsequent heat transfer to the melt from the crucible walls. In order for the generated field to heat the crucible, the crucible needed to be constructed from conductive material able to act as receptor for the electrical field. Silicon carbide (SiC) and various different graphite crucibles were used in the smelting campaigns. Above 1 400 ˚C, SiC crucibles show high rates of wear; they start breaking down and their electrical conductivity changes, making it difficult to control heat input to the melt through the receptor crucible. For experiments above 1 400 °C only graphite was used. However, the deportment of base metals (Cu and Ni) and Fe to the alloy phase pointed to the crucible surface participating in the melt by allowing locally reducing environments. An attempt was made to move away from the reducing receptor crucibles (SiC and graphite). Different ceramic crucibles (high magnesia, high purity alumina, alumina silicate and zirconia crucibles) were tested by inserting them in a graphite crucible that still acted as the receptor, but slag and alloy penetration into the ceramic crucible was noted in all the materials tested, skewing and disqualifying this experimental set-up. The penetration of the slag and alloy into the ceramic phase was most probably due to the heat transfer proceeding through the crucible to the melt. The insulating nature of the ceramic crucibles led to a strong temperature gradient over the crucible and therefore high local temperature conditions at the crucible wall, allowing rapid reaction or penetration. Figure 6 shows a picture of a typical graphite crucible (glowing red hot) in the open chamber used to control pressure. The thermocouple in the sleeve is seen next to the crucible. A second picture of the larger set-up can also be seen with the generator box feeding power to the stainless steel chamber and a flexible extraction duct located close to the chamber.

Figure 6: Photographs of the induction furnace used in the experimental setup. On the left the heated crucible is visible in the open vacuum chamber. The thermocouple in the graphite sleeve is visible next to the crucible

Temperature measurements of the melt for tests up to 1 600 °C were done by immersed thermocouple. A Type S thermocouple with 90% Pt and 10% Rh composition and a maximum temperature range up to 1 600 °C was used. The thermocouple was protected from the melt by a graphite sleeve and the graphite sleeve was allowed to rest on the centre of the bottom of the crucible. Temperature measurement for the high temperature treatment tests at 1 700 °C were performed with an optical pyrometer (Raytek Marathon Mr series: two-colour optical pyrometer with temperature range from 800 °C to 2 500 °C). In order to clearly see the surface of the slag, inert gas flushing was done onto the slag surface and the chamber had to be opened, which meant that air ingress could occur. The choice of induction heating has the disadvantage that temperature control is not as precise as with other furnaces (such as tube furnaces) and it is possible that there might be a thermal gradient in the melt if the crucible is not evenly heated by the induction coil.

In the first set of smelting tests, the slag and alloy was cast by tilting the work head of the induction furnace into a pre-heated steel mould to solidify. The casting process caused agitation and suspended alloy prills into the solidifying slag. The low thermal mass of the melt meant that the slag and alloy solidified quickly and some small alloy prills were noted in the slag after solidification. For the first set of smelting tests, Pt was used as a tie element to express recoveries, as the losses to the slag were an artefact of the small scale experimental set-up (suspension). A decision was made to rather simply switch off the furnace and allow the entire system to cool in ambient conditions. The solidified slag and alloy was in most cases easily removed from the crucible by tilting. The slag was in most cases separated from the alloy with a simple knock of a hammer. Allowing the entire melt to cool in the furnace allowed recoveries to be determined by mass balance.

An inert atmosphere was maintained above the melt by sealing the chamber hood and continuously flushing with N_2 gas above the melt. This was done both to avoid oxidation of the graphite or SiC crucible, as well as to limit atmospheric interaction with the melt.

Reducing and oxidising agents

Rh, Ru and Ir are left in an oxide state after the roasting step. Thermodynamic modelling showed that the oxides of Ru have vapour pressures sufficiently high to constitute losses of up to 1.4% to the gas phase as the temperature is increased in the melt and before the Ru dissociates from oxygen to join the alloy phase. To limit reduction of Cu, Ni and Fe to their metallic states during the melt, a mild reducing agent (carbohydrate as table sugar or sucrose with the composition $C_{12}H_{22}O_{11}$) was chosen and only added to stoichiometrically remove oxygen associated with PGMs and some oxides in the spinel phase. An addition of 7 g sugar per 100 g roasted third stage feed was used. In two control experiments, 7 g sugar was added with the feed and compared to the result when no reducing agent addition was done.

It is thermodynamically possible to oxidise most of the Fe, a significant amount of Ni and limited Cu from the alloy phase before Ru oxidation (the first PGM to oxidise from the alloy) should proceed and cause Ru losses to the gas phase (mostly as RuO_3). As Fe, Cu and Ni were present in the alloy phase, it was decided to trial the effect of an oxidising agent addition near the end of the melt, in order to preferentially oxidise Fe, Cu and Ni from the alloy to the slag phase. $NaNO_3$ was chosen as the oxidising agent and it was added to the melt by simply decanting a set weight onto the molten slag surface. Addition rates of $NaNO_3$ were varied from 0 g to 15 g per 100 g of roasted third leach residue.

Smelt sequencing

Most of the melts were divided into distinct steps, being 1) premixing and charging into the crucible 2) heating and initial melt of the material in reducing, inert or oxidising conditions, 3) central part of the melt that either drew a vacuum or remained at ambient pressure, 4) addition of an oxidising agent to force some Fe, Ni and Cu to the slag phase, or no oxidising agent addition, 5) cooling by casting or allowing solidification in the crucible. The time of each individual step also varied between 10 minutes and 60 minutes.

Pressure control over the smelting step

Results of the first smelting tests indicated that Pb removal was not achieved to the required extent (recovery of around 40% to the alloy phase was measured, while 10% recovery to the alloy phase was set as target). A number of variables could improve Pb recovery to the gas and slag phases, these being higher temperature, lower pressure, more oxidising conditions and different slag chemistry. As all the other options had some restriction on practicality or recovery of PGMs to the alloy phase, it was decided to investigate the effect of the system pressure on Pb recovery. A sealed chamber was constructed that could enclose the induction furnace and a vacuum pump maintained a set pressure down to 0.3 bar absolute. The melt was contained in the partial vacuum for only 30 minutes.

Melts with Cu addition in muffle furnace

Two melts were performed in a muffle furnace to study the system of Roast-Smelt feed with Cu addition. A muffle furnace was used that could control up to 1 300 °C. The furnace seal was not perfectly air tight, so neither the gas atmosphere nor the temperature control would have been very

good. The material was well mixed and added to the alumina-silica crucible and placed in the melt. No addition was made to the melts at temperature. After the melts had been completed, the power to the furnace was cut and the melt was left to cool. The idea was to study the system and see whether it held promise regarding improved redox control when compared to the induction furnace arrangement with crucible interaction.

High temperature treatment test work

A total of four tests were performed. A single test was done on each of three different alloy systems, these being Direct Melt, Roast-Smelt and Leach-Roast-Smelt of third stage residue. The Leach-Roast-Smelt system was repeated, but the Roast-Smelt with Cu addition was not studied. It was decided to use a single temperature and time (30 minutes at 1 700 °C) in order to prove the concept only. After the melt was completed, power to the system was cut while inert gas flushing continued. The alloy was left to solidify in the crucible, and upon cooling, was removed from the crucible by simply knocking it out.

3.4.3 Atomisation

Figure 7 shows a simplified schematic of the atomisation process. An induction heating furnace melts the alloy to above the liquidus temperature. This molten alloy is then tilted into an induction heated tundish. The tundish serves to queue and direct the molten alloy stream into the high pressure water jets that break up the alloy into fine particulate.

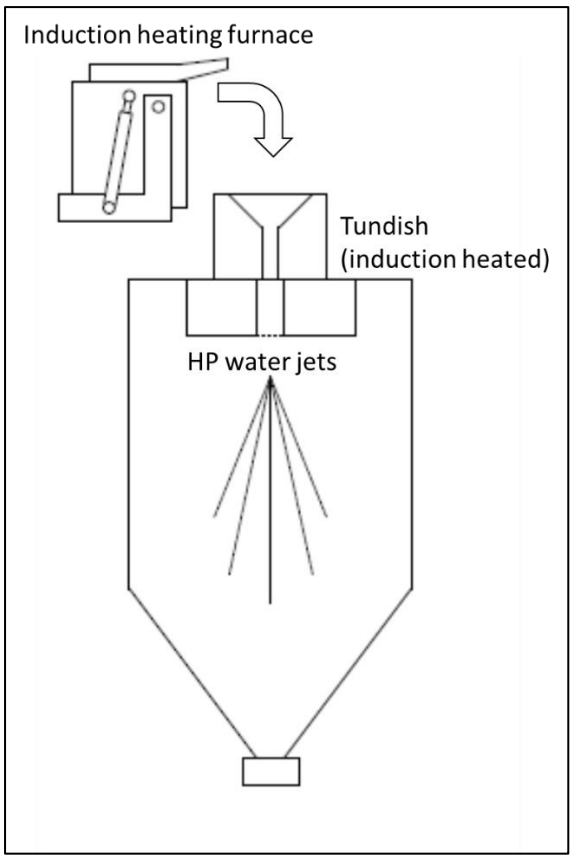

Figure 7: Simple illustration of the atomisation process, showing the main components: the induction heating furnace, the tundish and the high pressure water jets that break up the liquid alloy stream

A total of 15 atomisation test runs were performed on alloys produced by the smelting test work on the Direct-Smelt and Roast-Smelt systems. Budget and schedule restrictions did not allow the study of the Leach-Roast-Smelt system and the Roast-Smelt system with Cu addition. The atomisation of Cu alloys is well documented (Neikov, 2009) and small particle sizes can be achieved. The high Cu alloy (60%-70% Cu content) should therefore also atomise easily with the proper design. It is uncertain how the alloy from the Leach-Roast-Smelt system would react, as this alloy was not studied.

Figure 8 shows a picture of the small atomiser that was built for the test work. Below follows a description of the main parts:

- Induction heated primary crucible: As direct coupling to the alloy could be done, a high purity alumina crucible was used. Temperature control was done with a pyrometer. Inert gas purging was done on top of the crucible to minimise oxygen interaction during the melt. Since heat could be added by direct coupling to the alloy phase, heating took place extremely quickly, with the final temperature achieved within two to three minutes after power was supplied to the coil. Melting behaviour of the alloy was visually monitored. The temperature at which the entire surface was molten could be used as a crude indication of the liquidus temperature. The temperature was lifted to 50 °C above the 'all molten'

temperature and the crucible was tilted into the tundish. For the experiments performed, the final temperature before casting varied between 1 400 °C and 1 550 °C.

- Induction heated tundish: The tundish crucible was inductively heated and was made of graphite in order to enable it to receive the induction current without liquid alloy inside it. A top mounted pyrometer was used to control the temperature of the tundish at 1 400 °C. Inert gas (N_2) flushing was done at the top of the crucible to prevent it from rapid oxidation.
- Water jets: The jets were located inside the collection chamber, just beneath the top plate of the chamber.Three water jets were positioned 120^o from each other. They sprayed towards the centre at an angle to ensure overlap. The water jets were mounted at a 45^o angle downwards from the horizontal. A water pressure of 30 bar was measured just behind the water jets.
- Collection chamber: The chamber in which the jets were mounted and where the atomisation took place was constructed in such a way that the collection of slurry was done of the bottom of the same vessel via a conical section. The stainless steel vessel was sealed, but had an opening to allow steam and gases from the atomisation process to escape. A single drain valve allowed to contents of the chamber to be drained after the atomisation run was completed. Dewatering of the alloy was done by manually filtering the alloy.

Figure 8: Picture of the atomiser built for the test work

3.5 Sampling and analytical error and repeatability

The results from the experimental test work showed a number of measured recoveries higher than 100%. This is not possible for a system that cannot release inventory. This section contains a high level statistical evaluation of the errors for the roasting and smelting test work. It is included in order to appreciate the accuracy limits of results interpretation, and also to instill confidence in trends that were observed from experimental data. The discussion does not distinguish the relative contribution of sampling error, assaying error, random vs. systematic error, etc. as sufficient data were not gathered to asses this.

Due to the high value and complex nature of high PGM containing materials, understanding assaying error remains a priority for PGM companies. In order to illustrate the typical assaying error for high PGM content materials, a short discussion of round robin results from the industry is included. Assaying for high grade PGM containing materials is difficult, as standards are not readily available (for alloys, standards do not exist, unless they are custom prepared from pure metal). Most laboratories partake in routine round robin tests in order to evaluate their own results for metal accounting purposes. Lonmin performs monthly round robin assays on BMR concentrate and eight laboratories partake in this process. A total of 18 months (18 data points per laboratory) for each of the six PGM metals were evaluated in order to understand assaying variance that can be expected. The mean deviation per laboratory can be calculated from the mean assay (from all eight laboratories) per month. It is also possible to calculate the standard deviation for this difference to the mean across the 18 data points. By dividing the standard deviation to the mean content, a relative standard deviation can be calculated. (This relative standard deviation is useful as it gives an indication of the percentage from the original content and is an indication of the assay reliability). Table 7 shows a summary of the findings. It can be seen that standard deviation is in almost all cases larger than the mean difference, pointing to variance between assay results. The relative standard deviation for most laboratories is larger for the OPMs (Rh, Ru and Ir) than for the PMs. According to these round robin results, relative standard deviation of between 1% and 8% can be expected for the PMs, while relative standard deviation of between 4% and 10% can be expected for OPMs.

Table 7: Summary of round robin results performed on PGM concentrate between 8 laboratories.

		Pt	Pd	Au	Rh	Ru	Ir
	Mean content of PGM rich residue	35,3	16,6	0,9	5,1	8,1	1,7
Lab A	Mean difference from mean assay	-0,2	-0,3	0,0	0,1	0,4	0,0
	Standard deviation	0,4	0,3	0,0	0,2	0,5	0,1
	Relative Standard deviation	1,2	1,9	2,0	4,7	5,7	7,0
Lab B	Mean difference from mean assay	-0,3	0,0	0,0	-0,1	-0,4	-0,1
	Standard deviation	0,4	0,5	0,0	0,3	0,6	0,2
	Relative Standard deviation	1,2	2,9	2,2	6,1	7,4	10,6
Lab C	Mean difference from mean assay	0,4	0,1	0,0	0,2	0,8	0,1
	Standard deviation	0,8	0,5	0,0	0,4	0,6	0,2
	Relative Standard deviation	2,3	2,8	3,5	6,9	7,3	11,0
Lab D	Mean difference from mean assay	-0,5	-0,6	-0,1	0,1	0,2	0,1
	Standard deviation	0,7	0,7	0,1	0,2	0,3	0,1
	Relative Standard deviation	2,0	4,0	9,2	4,0	3,6	4,8
Lab E	Mean difference from mean assay	0,5	0,1	0,0	0,2	0,4	0,1
	Standard deviation	1,6	0,8	0,0	0,5	0,8	0,1
	Relative Standard deviation	4,6	4,8	4,7	9,1	9,9	5,7
Lab F	Mean difference from mean assay	0,6	0,8	0,0	0,3	0,4	0,1
	Standard deviation	1,6	1,4	0,1	0,4	0,7	0,1
	Relative Standard deviation	4,5	8,3	10,3	8,4	8,4	8,4
Lab G	Mean difference from mean assay	-0,5	0,1	0,0	-0,7	-2,0	-0,4
	Standard deviation	1,6	0,7	0,0	1,3	2,9	0,7
	Relative Standard deviation	4,5	4,2	5,0	24,5	35,5	42,4
Lab H	Mean difference from mean assay	0,1	-0,3	0,0	0,1	0,6	0,2
	Standard deviation	1,2	1,6	0,0	0,4	0,5	0,1
	Relative Standard deviation	3,3	9,4	4,5	8,6	6,6	5,8

3.5.1 Statistical evaluation of sampling/ assaying error for roasting

A statistical evaluation was done in order to quantify the sampling and analytical error contributing to the roasting results. Thirteen trials were taken from the fluidized bed roasting test work and all performed under oxidative roasting conditions. Since no PGM recovery loss or gain was expected across the roasting test, the deviation on recovery of the PGMs was used to calculate the probability of producing a result with a recovery difference of +/- 5% and +/- 10% respectively. The PGM recoveries should be able to provide an indication of the total sampling and analytical error.

Table 8 shows the recovery data per PGM element. The probability calculation for set limits (+/- 5% and+/- 10%) is also shown. The data distribution for the 13 tests was shown to be normally distributed and the standard Z test method was therefore used. For the average PGM, there is a 65% probability that a value of +/- 5% recovery change will be measured across a roasting test and there is a 96% probability that a value of +/- 10% recovery change will be measured across a roasting test. From these results it is clear that poor accuracy exist for the results, and small deviations should be ignored (not taken as real) and ascribed to sampling/ analytical error.

Table 8: Recovery for PGMs across 13 roasting tests. Calculation of probability within limits (+/- 5% and 10%) is also shown.

Description	Au	Ir	Pd	Rh	Ru	Average PGM
Recovery results						
% Recovery change measured across test	6.5	7.4	4.3	4.4	4.7	
	-4.4	-3.1	3.1	6.5	9.7	
	-3.9	8.1	4.0	8.9	6.9	
	-1.3	5.4	2.4	5.4	4.9	
	-2.4	6.8	-0.3	5.0	2.0	
	-1.6	4.1	1.0	1.6	3.4	
	-2.5	4.9	1.4	1.9	4.7	
	-3.5	5.3	2.4	6.6	2.4	
	-3.5	3.9	-0.3	2.3	1.6	
	2.8	4.6	2.8	2.8	1.1	
	2.4	6.7	1.0	3.7	1.5	
	-9.0	10.0	-0.7	4.1	4.7	
	0.4	-8.0	10.9	17.3	3.1	
Mean	**-1.5**	**4.3**	**2.5**	**5.4**	**3.9**	**3.5**
stdev	**3.9**	**4.8**	**3.0**	**4.1**	**2.4**	**3.7**
Probability of +/- 5% result						
Upper spec limit USL	**5**	**5**	**5**	**5**	**5**	**5**
Lower spec limit LSL	**-5**	**-5**	**-5**	**-5**	**-5**	**-5**
Z LSL	0.8871	1.9397	2.4761	2.5279	3.6556	2.3329
Z USL	1.6754	0.1409	0.8418	-0.1014	0.4528	0.4027
Value from Z table LSL	0.8125	0.9738	0.9934	0.9943	0.999	0.9902
Value from Z table USL	0.9531	0.5560	0.8000	0.4596	0.6747	0.6564
Probability	77%	53%	79%	45%	67%	65%
Probability of +/- 5% result						
Upper spec limit USL	**10**	**10**	**10**	**10**	**10**	**10**
Lower spec limit LSL	**-10**	**-10**	**-10**	**-10**	**-10**	**-10**
Z LSL	2.1683	2.9801	4.1350	3.7412	5.7098	3.7007
Z USL	2.9567	1.1813	2.5008	1.1119	2.5070	1.77051
Value from Z table LSL	0.9849	0.9999	0.9999	0.9999	0.9999	0.9999
Value from Z table USL	0.9999	0.8813	0.9938	0.8669	0.9939	0.9617
Probability	98%	88%	99%	87%	99%	96%

Equations 1 and 2 are involved in the calculation of the cumulative area under the standard normal distribution (equal to the probability). Equation 1 shows the calculation of the error function and equation 2 shows the calculation of the cumulative distribution function, where μ is the mean, σ is the standard deviation, and erf is the error function.

$$\operatorname{erf}(x) = \frac{2}{\sqrt{\pi}} \int_0^x e^{-t^2} dt. \quad (1)$$

$$F(x; \mu, \sigma^2) = \frac{1}{2} \left[1 + \operatorname{erf} \left(\frac{x - \mu}{\sigma \sqrt{2}} \right) \right], \quad (2)$$

3.5.2 Statistical evaluation of sampling/ analytical error for smelting

A total of 3 repeat test sets was performed across the smelting trials. For the repeat tests, the same laboratory was always used to eliminate external error between laboratories. Table 9 shows the mean and the standard deviation for some of the most important elements. In most cases the standard deviation is below 5 (expressed as the standard deviation for the recovery across the melt). Pd, as an example, is the second most abundant element (after Pt) and has a small standard deviation (highest 3.7). A less abundant PGM like Ir shows higher standard deviation (highest 14). Elements that are sensitive to small changes in the melt (like As and Pb) also shows higher standard deviations. For As and Pb, the standard deviations become more significant, given that the recovery values are not necessarily close to 100%.

The repeatability results below impart some confidence in the experimental, sampling and analytical method employed. However, some outliers were still noticed in results (example is Au recovery of 186% in Table 41, etc.). These values were left as measured throughout the thesis.

Table 9: The recovery (in mass %) for three sets of repeat tests during smelting. The mean and standard deviation is also shown per repeat test set.

Number	Au	Ir	Pd	Rh	Ru	Os	Ag	Fe	As	Cr_2O_3	Ni	Pb
Repeat set 1												
1	79.2	98.7	94.7	98.4	102.7		57.4	86.7	26.8	54.6	91.1	44.3
1	83.8	98.0	96.3	97.1	102.1		51.9	82.2	35.0	56.7	89.5	43.6
Mean	**81.5**	**98.3**	**95.5**	**97.8**	**102.4**		**54.6**	**84.5**	**30.9**	**55.6**	**90.3**	**44.0**
Standard Deviation	**3.2**	**0.5**	**1.1**	**0.9**	**0.4**		**3.9**	**3.2**	**5.7**	**1.5**	**1.1**	**0.6**
Repeat set 2												
2	85.8	106.1	99.6	96.3	94.3	96.6	81.0	93.3	82.0	43.9	103.4	44.5
2	84.6	103.8	98.1	100.5	101.6	72.8	88.5	87.6	80.9	22.9	106.9	57.9
2	88.9	114.6	101.1	104.9	110.6	62.9	84.3	91.3	80.7	39.3	104.3	46.8
Mean	**86.4**	**108.2**	**99.6**	**100.6**	**102.2**	**77.5**	**84.6**	**90.8**	**81.2**	**35.4**	**104.9**	**49.7**
Standard Deviation	**2.2**	**5.7**	**1.5**	**4.3**	**8.2**	**17.3**	**3.7**	**2.9**	**0.7**	**11.1**	**1.8**	**7.2**
Repeat set 3												
3	100.4	118.9	106.5	97.9	111.5	115.7	92.7	70.4	90.6	25.4	115.8	53.6
3	96.4	93.1	109.3	101.6	91.2	83.2	91.9	81.4	79.8	21.5	96.9	46.2
3	93.7	96.6	101.9	102.1	95.5	49.5	90.2	90.1	87.6	31.9	111.6	62.8
Mean	**96.8**	**102.9**	**105.9**	**100.5**	**99.4**	**82.8**	**91.6**	**80.6**	**86.0**	**26.3**	**108.1**	**54.2**
Standard Deviation	**3.4**	**14.0**	**3.7**	**2.3**	**10.7**	**33.1**	**1.3**	**9.9**	**5.6**	**5.3**	**9.9**	**8.3**

Table 10 shows an analyses of variance for Pd (as a representative example) between the three sets of repeats. The analyses of variance allows a comparison for the variation contribution within the group (a single set of repeats) and between groups (between repeat sets). From this analyses it can be seen that there is a clear distinction between variance caused by repeatability (within group) and variance caused by changing smelting conditions (between groups). Despite uncertainty around sampling and assaying error, deviations caused by changing smelting conditions remains significant and can be distinguished.

Table 10: The analyses of variance for Pd for the repeats performed during smelting. The comparison includes for data within a repeat set and for the data between repeat sets.

Source of Variation	*SS*	*df*	*MS*	*F*	*P-value*	*F crit*
Between Groups	0.028217	3	0.009406	12.69419	0.005226	4.757063
Within Groups	0.004446	6	0.000741			

It is also possible to use the same approach as was used for roasting probability evaluation in section 3.5.1. It is possible to use Pd and Rh as indicators of metals that should have recoveries close to 100%. When recoveries are reported with Pt as a tie element, the distribution for Pd and Rh recoveries are normal. The data for nine tests in phase 2 were used for the evaluation (as the same lab was used for these tests). Table 11 shows that there is a 95.9% probability that a recovery value

between 90% and 110% will be recorded across a smelting test. The capability is therefore very similar to that of the roasting test work and small deviations in recovery values should not be viewed as real.

Table 11: Recovery for Rh and Pd across 9 smelting tests. Probability within limits (+/- 5% and 10%) is also shown.

	Pd	Rh	PGM
Recovery measured across test	111,1	100,0	
	104,7	108,6	
	101,4	105,1	
	99,6	96,3	
	98,1	100,5	
	106,5	97,9	
	101,1	104,9	
	109,3	101,6	
	101,9	102,1	
Mean	**103,74**	**101,89**	**102,82**
Stdev	**4,44**	**3,81**	**4,12**
Probability for value between 95% and 105%	58,7%	75,8%	67,3%
Probability for value between 90% and 110%	82,7%	98,3%	95,9%

3.5.3 Statistical evaluation of sampling/ analytical error for high temperature treatment

A single repeat test set was performed across the high temperature treatment trials. Table 12 shows the mean and the standard deviation for some of the most important elements. The repeatability for PGM recovery seems to be acceptable, with standard deviations being small (< 3.3). However, for the minor elements standard deviations are larger and several elements/ oxides report recoveries well above 100% (Fe, Cr_2O_3 and Cu).

Table 12: The recovery (in mass %) for a repeat test during high temperature treatment. The mean and standard deviation is also shown for the repeat test set.

Number	Au	Ir	Pd	Rh	Ru	Ag	Fe	As	Cr_2O_3	Cu	Ni	Pb
1	68.3	89.8	89.1	92.4	95.5	4.7	131.5	27.0	101.2	120.1	88.1	1.9
2	72.1	90.8	93.7	93.9	96.8	5.6	115.7	46.8	117.1	101.4	95.7	2.9
Mean	**70.2**	**90.3**	**91.4**	**93.1**	**96.1**	**5.1**	**123.6**	**36.9**	**109.1**	**110.7**	**91.9**	**2.4**
Standard Deviation	**2.7**	**0.7**	**3.3**	**1.0**	**0.9**	**0.6**	**11.2**	**14.0**	**11.3**	**13.2**	**5.4**	**0.7**

Chapter 4: Materials

This chapter will describe the material used in the study. This includes all materials used as feed and the products that were generated.

4.1 Characterising residue after pressure leaching

The residue after the pressure leaching step in the BMR was used as feed material for the pyrometallurgical refining process of roasting, smelting and atomisation. This residue is known as the third stage leach residue in the Lonmin context.

Chemical Composition of pressure leach residue

A typical composition of the third stage leach residue is provided in Table 13 below. The PGM content was 48.5%.

Table 13: Typical chemical composition of Lonmin BMR third stage residue, expressed as species that were used for thermodynamic modelling

Species	Pt	Pd	Au	Rh	Ru	Ir	6E	SiO_2	Al_2O_3	CaO	Cr_2O_3	MgO
Weight %	24.5	11.7	0.6	4.0	6.2	1.5	48.5	4.0	0.5	0.1	0.4	0.5

Species	NiO	CuS	Co_3O_4	Fe_3O_4	Se	Te	As	$PbSO_4$	S	Os	Ag	Total
Weight %	3.7	6.1	0.1	6.7	3.4	0.5	2.0	6.1	5.6	4.6	0.7	93.5

The chemical composition provided in Table 13 reflects the feed speciation used for FactSage® modelling. Although the oxides of Ni, Fe and Co may form a range of mixed oxide spinel minerals, this does not significantly influence the thermodynamic modelling outcomes (mineral speciation will influence the energy balance of the system, but the mass balance is insensitive to the chosen feed speciation). The total adds up to 93.5% and the remaining 6.5% is probably acid-stable hydroxi-oxides or sulphates (such as jarosite).

Particle size distribution of pressure leach residue

Figure 9 below reflects a typical particle size distribution of the third stage leach residue. During the process of roasting and even drying at 100 °C, the particles tend to form agglomerates that are quite stable and the particle size changes, as can be seen in the graph in Figure 9. In the wet product from the filter directly after the pressure leach step, 74% of the sample weight has a particle size smaller than 10 micron (as measured by a Malvern Mastersizer 2000 laser diffraction particle size analyser), while the dried/roasted product contains the bulk of the mass in the particle size range between 500 µm and 2 000 µm (measured by sieve analyses). After roasting, fine particles were separated from coarser particles by sieving and separate elemental analyses were performed on the two samples. No measurable difference in concentration of volatiles (or other elements) was noted.

The effect that the larger particle size (agglomerates) had on the removal of volatile compounds was therefore found to be negligible.

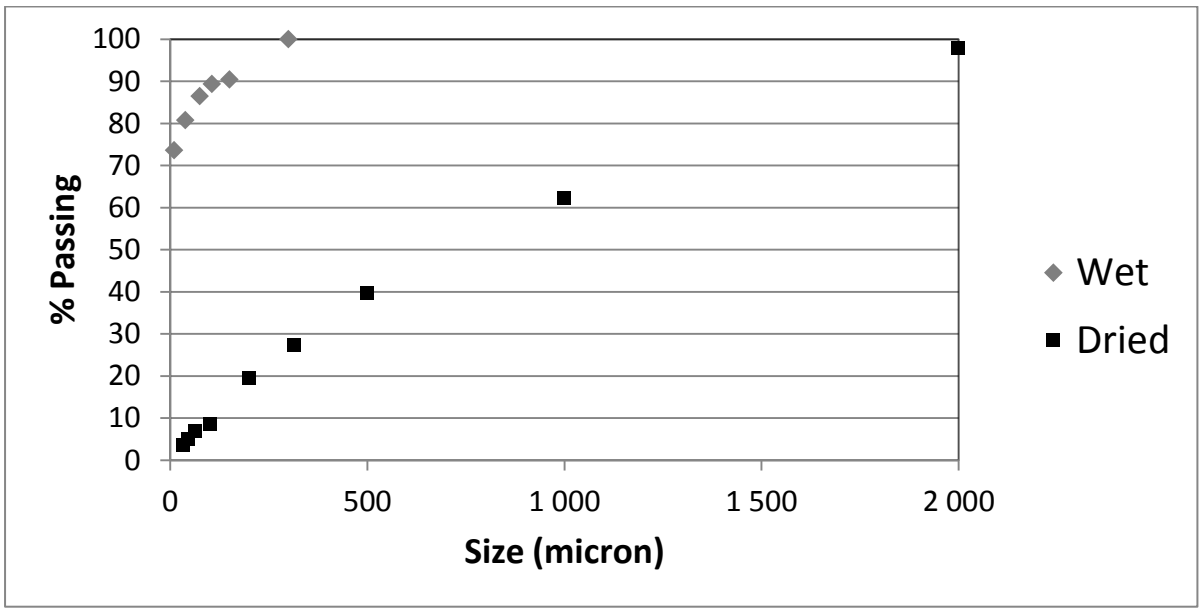

Figure 9: Cumulative percentage passing as a function of the particle size. The wet sample was measured by a Malvern analyser and the dried sample by multiple sieve sizes

SEM MLA characterisation of pressure leach residue

To interpret the behaviour of volatile elements, an understanding of the minerals at grain level is necessary. However, it became clear that the residue from the pressure leach in the BMR is extremely fine grained and amorphous (lacking a definable crystalline form), resulting in varying compositions, which could not be assigned stoichiometric compositions.

The bulk of the third stage leach residue sample consisted of oxidised particles composed of Pt-Pd-Rh-Ru-Se-As-S-O, with various other PtPd phases making up the remainder of the sample. 8% (of surface area) was present as silicates. The material tended to be porous particles, containing inclusions consisting of trevorite ($NiFe_2O_4$) and other spinel minerals, villamaninite of varying compositions ((Cu, Ni, Co, Fe)S_2) and silicate gangue (feldspar type). These may have provided nuclei for the growth of the Pt-Pd-Rh-Ru-Se-As-S-O phases. At higher magnification brighter phases, enriched in Pt, Pd, Rh, Ru and in some cases Os, were observed, with most of the particles at the micron or sub-micron level. In some cases, PGE enriched phases appeared to be growing on the surfaces of the silicate gangue and in other places the PGE enriched phases could have been secondary growth from the Pt-Pd-Rh-Ru-Se-As-S-O matrix.

The modal abundance data for third stage leach residue are presented in Table 14. Since the densities of most of the phases are unknown, the data have been expressed as area percentage rather than weight percentage. No stereological correction was applied to the results. Latti *et al.* (2001) found that the stereological bias might not be a very important factor for multiphase natural ore systems. Due to the amorphous nature and inherent variability of mineral phases, the compositions measured are approximations of the compositions of the bulk samples. Due to the

small grain size (most of the grains smaller than 3 µm), the electron beam might interact with adjacent grains and this will contribute to variability of elemental distribution that is used by the MLA software to make up the phase composition (Lloyd, 1985).

Table 14: Average modal abundance in third stage leach residue (Area%) as determined by MLA

Mineral abundance, as defined by MLA processing with EDS elemental distribution	Surface area abundance (%)
PGM Alloys	0.4
PtPdRuSeS	7.2
PtPdRuSeS2	0.3
PtPdSRuFeO	2.2
PtPdRuSeSFeCrPb	4.2
PtPdRhRuSSeSi	6.9
PtPdRuRhSeAsSO	4.1
PtPdRhRuSeAsSO	48.1
PtRuPdSe_SiPbCO	2.0
PtPdRuAsSeSO	9.3
PdCuTeSe_RuNiSO	0.1
OsPtPdSSe_CO	0.8
NiS_Fe	0.7
Pyrite	0.4
Quartz	1.6
Other silicates	6.6
Trevorite	3.9
Other	1.4
Total	100.0

Figure 10 shows a micrograph of the third stage leach residue and illustrates the fineness of grains contained in the larger particles, as well as the intermixed and varying nature of the residue. Some grain inclusions are visible at this magnification. Grain M (PtPdRuSeS) could be secondary nucleation and growth within the matrix. Grain J is a chromite type grain ($FeCr_2O_4$). Grain K is a type of feldspar (alumina silicate) inclusion. Grain L (OsPtPdSSe_CO) shows enrichment in Os (about 20 weight %) and some traces of C (due to contamination). The point indicated as I is rich in Pb, Se and S.

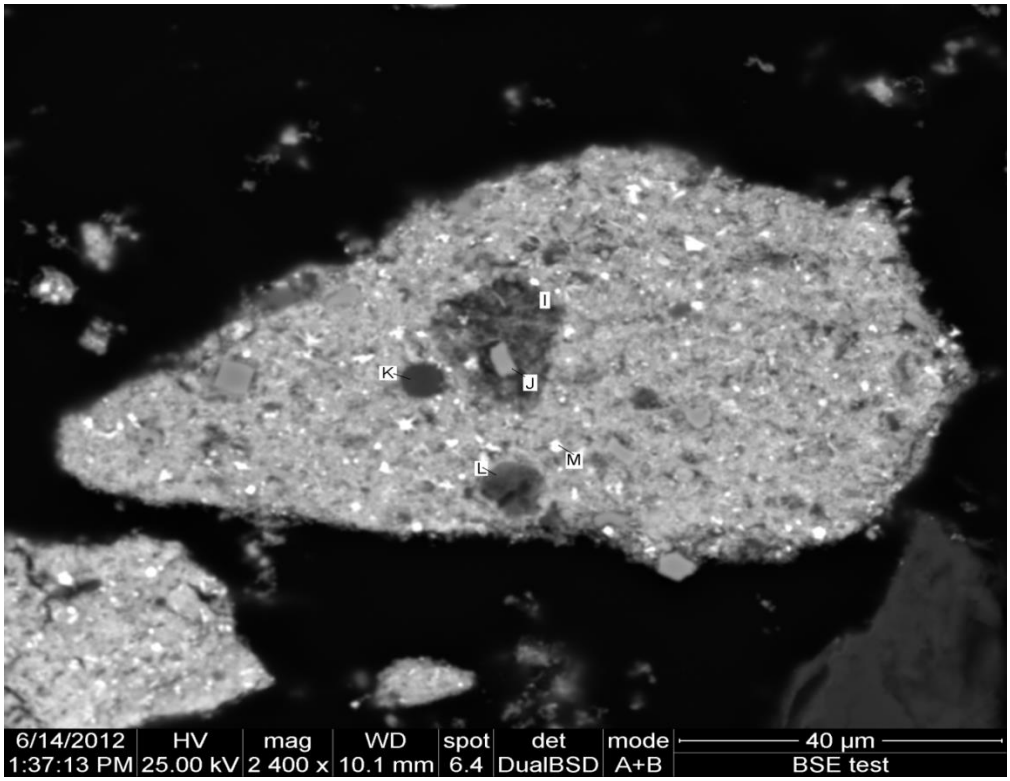

Figure 10: Photo micrograph of a particle from the third stage leach residue

DTA/TGA/ SDTA Investigation of pressure leach residue

Figure 11 shows the TGA/DTA/SDTA curves as generated from third stage leach residue, with the top block of the figure representing the TGA curve, the middle section representing the DTA curve and the lower section representing the SDTA curve.

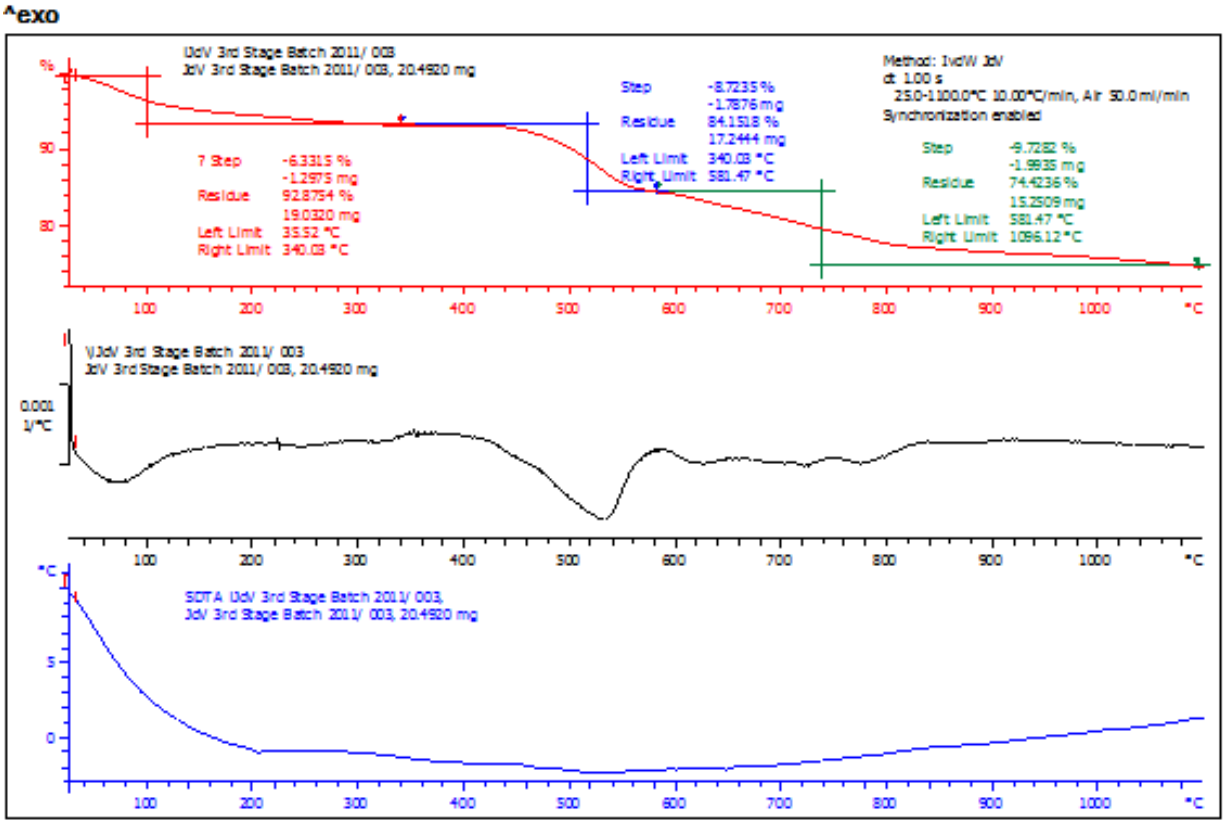

Figure 11: Combined TGA, DTA and STDA analysis of the BMR 3rd stage leach residue, TGA, DTA and STDA, from top to bottom, respectively

Thermo-gravimetric analysis (TGA) measures the change in weight as a function of the temperature. The TGA curve shows essentially a continuous mass loss with increasing temperature, with an accelerated mass loss between 450 °C and 550 °C. The increased mass loss and endothermic range between 450 °C and 550 °C probably corresponds to the loss of water of crystallisation. The presence of a number of ferri (amongst others ions) oxides/ hydroxides/ oxyhydroxides/ sulphates make definite evaluation of thermal decomposition temperatures difficult. According to Mitov et al. (2002) and Frosta et al. (2007) temperature ranges of thermal decomposition and water of hydration loss can span a large temperature range between 130°C and 600°C for iron oxyhydroxides, depending on the composition, mineral and degree of oxidation. Further heating once again shows continuous mass loss till 1 200 °C (maximum temperature of TGA test). Total mass loss is around 25% at 1 000 °C (starting from a product that was dried at 100 °C).

DTA compares a material as it undergoes heating relative to an inert reference. By comparing it to an inert sample, any endothermic or exothermic reactions can be measured as a function of temperature. Differential Thermal analysis (DTA) showed an endothermic range of around 400 °C to 550 °C. This corresponds to the oxidation temperature range of primarily the sulphides, selenides and tellurides. No other significant reactions took place in the 600 °C to 1 000 °C temperature range.

Simultaneous Differential Thermal analyses (SDTA) is the application of TGA and DTA to the same sample at the same time. The complimentary information (to TGA and DTA) obtained from SDTA allows differentiation between endothermic and exothermic events which have no associated

weight loss (for example melting and crystallisation) and those which involve weight loss (for example degradation). The SDTA curve confirms that no melting has taken place below 1 000 °C.

Table 15 shows that the actual mass loss from roasted samples at different temperatures compared very closely to the TGA curves.

Table 15: Mass loss comparison between TGA, roasting test work and FactSage® prediction

	600 °C	700 °C	800 °C	900 °C	1 000 °C
TGA measurement	15%	17%	20%	22%	24%
Roasting test work measurement	19%	22%	24%	24%	25%
FactSage predictions	9%	11%	17%	20%	24%

At higher temperatures (above 800 °C), the FactSage® predictions on mass loss are comparable to measured values from TGA and the roasting tests. The variation of the FactSage® prediction from actual measurements at 600 °C and 700 °C is probably due to the kinetic effects relative to the equilibrium calculation. Under equilibrium conditions FactSage® predicts the full oxidation of all the PGMs (apart from Pt and Au) and Base Metals to their respective stable oxides at 600 °C, while the XRD analysis in Table 16 confirms the presence of unoxidised Pd. Other PGMs and the base metals probably did not oxidise to the extent predicted by FactSage®.

4.2 Characterising roasted product (calcine)

Chemical composition of roasted product

The chemical composition of the roasted product is provided in section 4.3.1 in Table 17 as third stage leach residue after roasting.

XRD Analysis of roasted product

Samples from the stationary bed roasting test work were subjected to bulk XRD analysis. Combined XRD patterns are shown in Figure 12 below. They show the changes in the major peaks as the roasting temperature is raised. Apparent is the change in the crystallinity of the phases with increase in roasting temperature. At 25 °C the crystallite sizes of the phases are so small (mostly less than 3 µm) that the peaks are excessively broadened. At higher temperatures the peaks are sharpened due to recrystallisation and annealing. The trevorite or spinel peak intensity increases with increasing temperature.

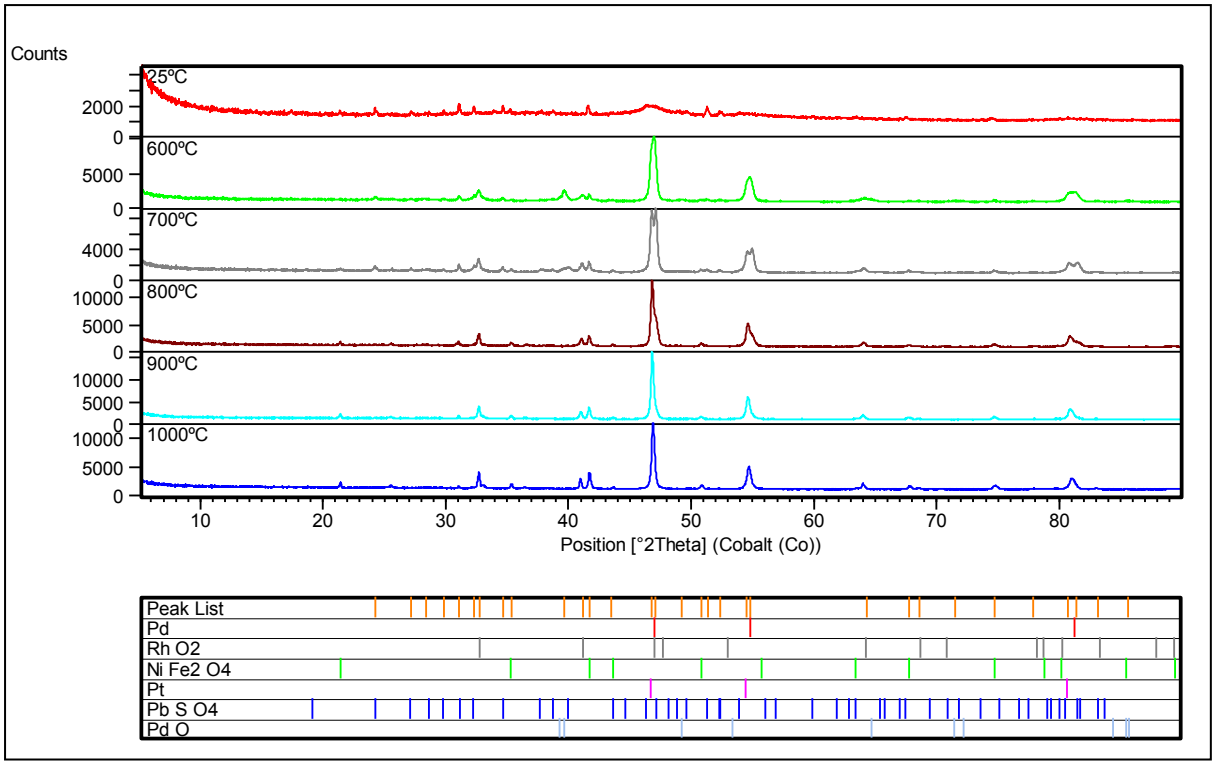

Figure 12: Comparative XRD data of the BMR third stage leach residue as received and roasted at the indicated temperatures

Qualitative analysis of the 25 °C data indicates the presence of very fine-grained platinum and palladium, together with trevorite ($NiFe_2O_4$) and anglesite ($PbSO_4$). The metallic peaks are broadened, indicative of less crystallinity and/or smaller grain size, whereas the other two phases have sharp peaks. There is only one unaccounted minor peak present.

The 600 °C data show sharp peaks of the metals platinum and palladium, RhO_2 and PdO, as well as $NiFe_2O_4$ and $PbSO_4$. All the peaks are accounted for. The pattern for RuO_2 is very similar to that of RhO_2 and the pattern probably represents a mixture of the two phases.

The 1 000 °C data is characterised by the disappearance of the PdO and anglesite ($PbSO_4$) phases. This is discussed in more detail in section 5.3. The XRD pattern represents the phases of platinum, palladium, RuO_2, together with trevorite, quartz and cristobalite. In this case RuO_2 is a better fit than RhO_2, but the same argument as before is relevant, i.e. that the peaks represent a mixture of the two.

Quantified results of the BMR 3rd stage leach residue roasted at different temperatures are shown in Table 16. The increase in the trevorite (or spinel) content with the increase in roasting temperature can be explained only partly. This has an effect on the quantities of the other phases. The reason presented for the increase in spinel phase is the formation of a mixed spinel that is refined as trevorite. An analysis of the a-cell constant of trevorite is also given in Table 16. This shows a gradual increase in the a-cell parameter, with a sudden decrease in the value being obtained in the 1 000 °C roast. The lattice constant of the trevorite spinel is affected by substitution of different elements on the octahedral and tetrahedral sites of the spinel solid solution. Any change in the substitution of

elements will be reflected in the a-cell parameter (Waychunas, 1991). This is to be expected, since many elements such as Ni, Cu, Fe, as well as Mg and Al (also Ru and Rh), can be incorporated in the structure, especially at higher temperatures under oxidising conditions.

The disappearance of the $PbSO_4$ peak is discussed in section 5.3.3.

Table 16: Quantification of phases by XRD in the BMR third stage leach residue roasted at different temperatures

	600 °C		700 °C		800 °C		900 °C		1 000 °C	
Phase	%	σ	%	σ	%	σ	%	Σ	%	σ
Anglesite ($PbSO_4$)	4.7	0.2	5.3	0.2	0.0	0.0	0.0	0.0	0.0	0.0
Platinum	18.5	0.3	20.7	0.2	28.9	0.2	34.1	0.3	21.2	0.6
Palladium	38.3	0.4	33.4	0.3	23.9	0.3	7.2	0.4	15.6	0.8
RhO_2 / RuO_2	17.9	0.3	14.8	0.2	15.3	0.2	15.7	0.2	13.6	0.2
PdO	10.0	0.2	6.7	0.2	0.0	0.0	0.0	0.0	0.0	0.0
Quartz	0.4	0.1	0.5	0.1	1.1	0.2	0.9	0.2	1.1	0.2
Trevorite/ Spinel	10.2	0.3	18.5	0.3	30.8	0.3	34.8	0.4	38.5	0.6
Cristobalite	0.0	0.0	0.0	0.0	0.0	0.0	7.5	0.6	10.0	0.5
Trevorite a-cell parameter	8.3456	Å	8.3458	Å	8.3477	Å	8.348	Å	8.3404	Å

SEM MLA characterisation of roasted product

Third stage leach residue that was roasted at 900 °C in air for four hours in a fluidised bed showed clear increase in the crystallinity of the feed product. Figure 13 shows a micrograph taken with the SEM. The presence of a bright alloy phase could be noticed in all the samples, indicated by point E in Figure 13 . This alloy phase consisted almost exclusively of Pt and Pd, with between 3% and 5% Rh also measured. Encapsulated within the bright alloy phase is very often a lighter phase, indicated by point D in Figure 13. This lighter phase most probably grew out of the PGM phase and is rich in Ir, Ru, and Rh. This secondary phase contains oxygen and small amounts of Fe and Cu. By far the majority of the PGM content in the sample was confined to the two phases described by points D and E.

Point C indicates a light grey phase that is present between the brighter alloy phases. The composition of this phase is not consistent, but it is mostly an oxidised As, Pb, Ni, Cu, Fe phase. Trace amounts of Te, Os, Ag, Ru and Pt were also found in the phase. The alloy phases (Points D and E) probably grew from the amorphous mixture and left behind the remaining oxide phase shown in Point C, leaving it mostly devoid of Pt, Pd, Ru, Rh and Ir.

Grain A is a Fe, Ni oxide (trevorite) and this grain is surrounded by a light grey matrix shown as Point B. This light grey phase could be seen surrounding most mineral inclusions such as quartz, trevorite, chromite, bronzite, etc. The light grey phase shown in Point B is also a varying oxidised As, Pb, Ni, Cu, Fe phase, similar to the phase described as Point C.

The remaining Te in the sample shows some association with Cu, as some areas were found to be simultaneously enriched in Te and Cu.

Grain F is large quartz inclusion and it originates from the silica that was added to the roast to stabilise the fluid bed.

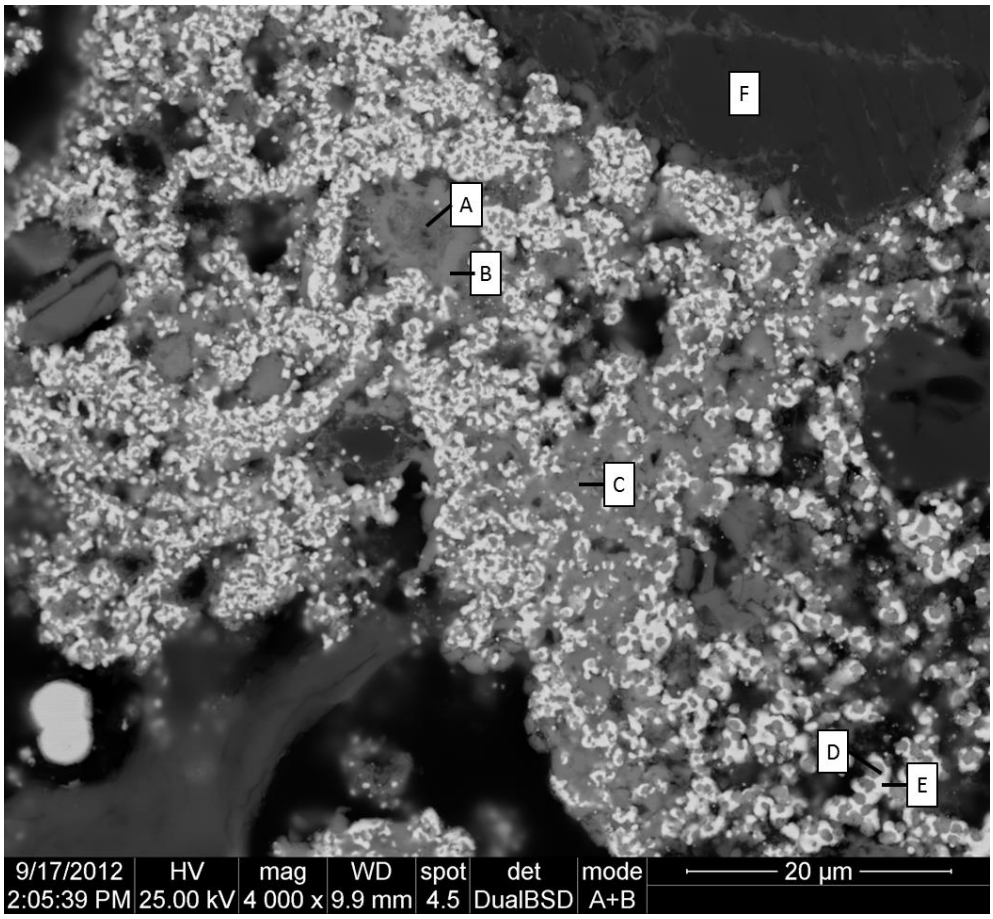

Figure 13: Photo micrograph of a particle from the roasted third stage leach residue

4.3 Characterising alloy

This section will describe the materials that were used and produced in the smelting test work.

4.3.1 Composition of feed materials and alloys produced

Three different feed materials were used for the smelting work to produce alloys. As the number of smelting tests continued to increase, new batches of third stage residue were requested from the BMR, with the result that the feed composition of the third stage residue differed between batches. The typical range of feed materials added in the smelting step is shown in Table 17. Note that the composition of the feed materials is expressed in an easily presentable form and the actual mineralogy and oxidation state may differ for different materials.

1. Third stage leach residue (taken directly from the BMR process).
2. Third stage leach residue that has been through a roasting step.

3. Third stage leach residue that has been through a base metal and Fe leaching step (Appendix A) and as well as a roasting step.

Table 17: Chemical composition of feed materials, with some of the oxides expressed in their typical oxidation state. The Min and Max values are provided from the three different feed material batches taken from the BMR process

Element/ Compound	Third Stage leach residue		Third Stage leach residue after roasting		Third Stage leach residue after base metal removal and roasting
	Min %	Max %	Min %	Max %	%
Au	0.6%	1.1%	0.7%	1.1%	0.5%
Ir	1.1%	1.4%	1.7%	2.0%	0.9%
Pd	11.2%	12.7%	11.8%	16.0%	14.4%
Pt	23.6%	32.8%	31.9%	35.3%	33.8%
Rh	3.3%	4.5%	4.3%	4.7%	4.9%
Ru	4.8%	7.0%	6.5%	9.2%	7.9%
Os	3.9%	5.9%	1.0%	2.8%	0.0%
Ag	0.7%	2.3%	0.3%	1.9%	1.7%
Al_2O_3	0.5%	0.6%	0.7%	0.8%	1.0%
CaO	0.0%	0.7%	0.3%	0.6%	0.7%
Fe_2O_3	7.3%	8.8%	10.6%	10.6%	1.8%
MgO	0.2%	0.3%	0.2%	0.3%	0.0%
S	0.3%	8.4%	0.0%	0.0%	0.1%
SiO_2	2.8%	6.1%	3.7%	5.3%	13.0%
As	1.2%	2.4%	1.0%	2.9%	2.2%
Bi	0.2%	0.3%	0.1%	0.3%	0.1%
Co	0.1%	0.2%	0.2%	0.2%	0.0%
Cr_2O_3	1.5%	2.4%	1.9%	4.0%	0.7%
Cu	1.2%	2.9%	1.5%	2.1%	1.4%
Ni	2.6%	6.0%	3.6%	7.2%	1.8%
Pb	1.5%	2.5%	0.5%	3.4%	0.4%
Se	0.0%	4.1%	0.0%	0.2%	0.0%
Te	0.1%	0.4%	0.1%	0.3%	0.1%

A fourth alloy was produced through the addition of Cu to modify the smelting behaviour of the roasted alloy. Representative samples of these alloys were chosen for performing phase quantification through XRD and SEM work. The chemical composition of the four alloys that were presented for phase quantification is summarised in Table 18. Note that Table 18 should not be used for direct comparison, since the final content of metals in the alloy could vary, both because of the processing route and variation in the original feed content between batches of material collected from the BMR.

Table 18: Chemical composition of the alloys produced during different processing routes

Element/ Compound	Direct Smelt	Roast-Smelt	Leach-Roast-Smelt	Roast-Smelt with Cu addition
Au	1.1%	1.2%	1.2%	0.4%
Ir	1.1%	2.3%	1.8%	0.6%
Pd	20.5%	18.1%	21.9%	6.5%
Pt	37.8%	39.2%	45.1%	13.9%
Rh	5.1%	5.7%	5.9%	1.9%
Ru	7.9%	8.5%	7.6%	2.3%
Total 6E	**73.5%**	**75.0%**	**83.5%**	**25.6%**
Al2O3	0.3%	0.3%	0.2%	0.1%
CaO	0.8%	0.2%	0.5%	1.3%
Si	0.3%	0.0%	0.9%	0.2%
Cr	0.6%	1.0%	0.5%	0.0%
S	3.2%	0.0%	0.3%	0.2%
As	2.9%	3.0%	3.9%	1.2%
Bi	0.1%	0.3%	0.2%	0.1%
Se	2.0%	0.0%	0.0%	0.1%
Te	0.4%	0.3%	0.2%	0.6%
Pb	0.3%	1.7%	0.7%	0.0%
Fe	4.4%	8.0%	2.3%	1.7%
Cu	1.8%	1.8%	2.4%	66.2%
Ni	4.6%	4.9%	3.1%	1.7%
Os	2.4%	0.6%	0.0%	0.0%
Ag	1.4%	2.0%	1.0%	0.8%
Total	**99.0%**	**99.1%**	**99.8%**	**99.8%**

4.3.2 Phase quantification of the alloys produced

In order to understand the mineralogy of the different alloys, phase quantification was done with XRD and SEM EDS. This investigation allows several aspects to be investigated:

- It is possible to investigate whether any primary or solid phases were left after the melt and included in the alloy.
- Solidification of different phases can be evaluated in these complex alloys.
- Association of minor elements in the phases can be evaluated.
- The presence of oxides and their form can be evaluated.
- The presence of the matte as a separate phase(s) can be confirmed and understood.

4.3.2.1 Alloy produced from direct smelting of third stage residue

An alloy that was produced in the test work at a temperature of 1 400 °C and ambient pressure is given in Table 18 under the Direct Smelt heading. A Total PGM content of 73.5% was achieved for this melt. The alloy was produced by directly melting third stage leach residue (with no preceding steps) and no reducing or oxidising agent addition. A CaO-SiO_2-Al_2O_3-Na_2O type slag addition of 50 g per 100 g third stage leach residue was used.

XRD was performed on the alloy. It is difficult to interpret the diffraction pattern, because of the presence of alloy phases that are similar and the fact that not many of the PGM phases encountered are in the database.

In spite of these difficulties, the following phases could be tentatively identified with XRD. The phase numbers refer to the corresponding number in Figure 14 and Table 19.

- Pt alloy which has diffraction characteristics of cubic PtFe alloy. This corresponds to Phase 1.
- A Pd alloy, corresponding to the (Pd, Ru, Pb) and (Pd, Rh, Pb, As) compounds of Phase 2 and Phase 3.
- A phase similar to heazlewoodite, $(Ni,Fe)_3S_2$, corresponding to Phase 4. The peaks of this phase are not well developed, so that its phase identification is tentative. According to the EDS analyses in Table 19, the composition of this phase calculates as M_6S_4 or $(Ni,Fe)_3S_2$, which is that of heazlewoodite. The XRD pattern is inconclusive in this regard, since the peaks of this phase are small in the XRD pattern.
- A phase with the characteristics of pentlandite, but with the composition of $(Ni,Cu)_9S_8$ given as Phase 5. Again the identification is tentative. The EDS analysis in Table 19 gives a composition approximating that of $(Cr, Cu)_9S_8$, which corresponds to the phase pentlandite $(Ni,Fe)_9S_8$ in the XRD pattern.
- A phase corresponding to NiSe; the corresponding phase was not encountered during SEM analysis. Perhaps Phase 3 could be a candidate.

SEM EDS investigation was done on the alloy. A backscattered electron image of the alloy sample is shown in Figure 14. At least five phases are present in the sample, as indicated by the differences in backscattered electron intensity. This intensity is proportional to the average atomic number of the phases. The phases that were analysed in Table 19 are labelled on the image.

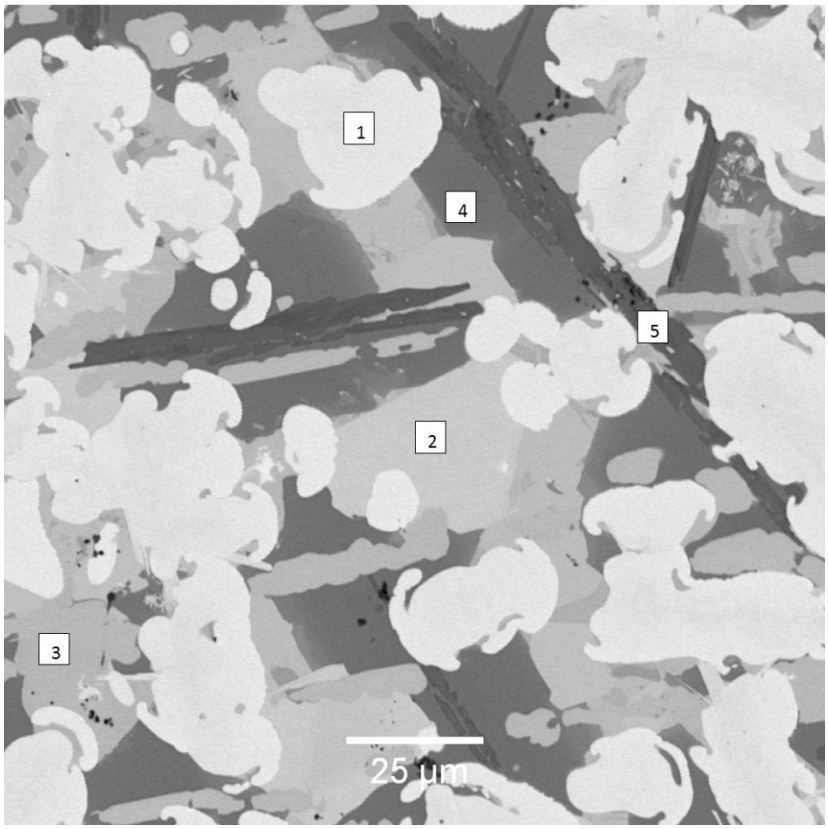

Figure 14: Backscatter electron image of the alloy (with some matte) that forms when third stage leach residue is melted directly

The phases that were identified are listed, starting with the highest backscattered intensity, in the order of decreasing intensity. It seems that many of these phases are alloys with a variable proportion of constituent elements.

Table 19: Elemental composition of phases identified with SEM-EDS in alloy produced by direct smelting third stage leach residue at 1400°C

Element	Phase 1 (wt%)	Phase 2 (wt%)	Phase 3 (wt%)	Phase 4 (wt%)	Phase 5 (wt%)
Cu-K	0.5	0.3	0.5	0.0	25.5
Ni-K	3.5	0.4	0.7	48.4	5.0
Ru-L	17.0	0.0	0.0	0.0	0.0
Rh-L	7.5	0.5	20.4	10.0	0.8
Pt-L	56.9	1.2	6.3	0.5	0.6
Fe-K	8.5	0.0	0.1	13.1	1.5
Cr-K	0.8	0.0	0.0	0.1	31.1
Pd-L	4.4	65.4	40.7	1.2	0.5
Ag-L	0.8	1.2	0.3	0.0	0.0
Au-L	0.0	0.0	0.0	0.0	0.0
S –K	0.0	0.0	0.0	23.4	30.0
Pb-L	0.0	13.2	16.6	0.5	0.4
Te-L	0.0	7.5	0.0	0.1	3.4
As-L	0.0	4.1	12.4	0.0	0.0
Se-L	0.4	0.5	1.6	2.7	1.5
Sb-L	0.0	6.1	0.7	0.0	0.0
Total	**100.0**	**100.0**	**100.0**	**100.0**	**100.0**

4.3.2.2 Alloy produced from Roast-Smelt of third stage residue

A typical alloy that was produced in the test work at a temperature of 1 500 °C and ambient pressure is given in Table 18 under the Roast-Smelt heading. A Total PGM content of 75.0% was achieved for this melt. The alloy was produced by first roasting third stage leach residue for 6 h at 850 °C. No reducing agent was added to the melt, but 10 g oxidising agent ($NaNO_3$) was added. An addition of CaO-SiO_2-Al_2O_3-Na_2O type slag at 50 g per 100 g feed material (roasted third stage leach residue) was used.

Both quenched and slow-cooled alloy samples from the smelting test work (at 1 500 °C) were analysed with XRD and examined with an SEM equipped with EDS in order to understand the phases present in the alloy after cooling. For both fast and slow cooling, three major phases could be found in the alloy sample. Figure 15 shows a photo micrograph of the slow-cooled sample and Figure 16 shows a photo micrograph of the quenched sample. The approximate compositions of the three phases are provided below:

- Phase 1: The major metal phase containing mainly Pt (49-53%), Fe (10-11%), Pd (7-8%) and Ru (13-18%)
- Phase 2: Minor palladium arsenide interstitial phase with composition including Pd (~55%), As (23-24%), Rh (10-12%), Ni (~4%), Cu (~3%) and Pb (0-2.5%). The Rh and Ni content seem to be inversely proportional to one another. The formula of this phase approximates that of

Pd_5As_2, with Rh, Ni and Cu substituting for Pd, and Pb substituting for As. Gervilla (1994) found that Pd_5As_2 could dissolve Ni up to 5.9 wt%.

- Phase 3: Minor Pd-Pb arsenide interstitial phase with composition Pd (65-67%), Pb (9-10%), As (11-12%) and Sb (~3%). Some Pt (2-3%) is also present in the latter sample. Matkovic (1993) studied the Pd-Pb-As system and found an intermetallic phase of Pd_3Pb_2As and a meta-stable phase of Pd_5PbAs_4. No other phases are currently known that approximate the composition of Phase 3. Instead, the composition of phase 3 could also approximate that of Pd_5As_2, with Pb and Sb substituting for As.

In addition to the major phases, an iron-chromium phase is present in small quantities with composition of Cr (60%-62%), Fe (~32%), Pd (~2.3%) and Ni (~1%). This, in all probability, is an iron chromium spinel phase, because of the fact that the atomic percentage of Cr is twice that of Fe. This phase was also confirmed to be an oxide by optical microscopy.

No primary crystalline phases could be found that had been in contact with the melt. The Ru and Rh content of the phases in the metal samples is highly variable and this could affect the crystallisation behaviour of the samples, ultimately affecting the crystallisation temperature of the metal.

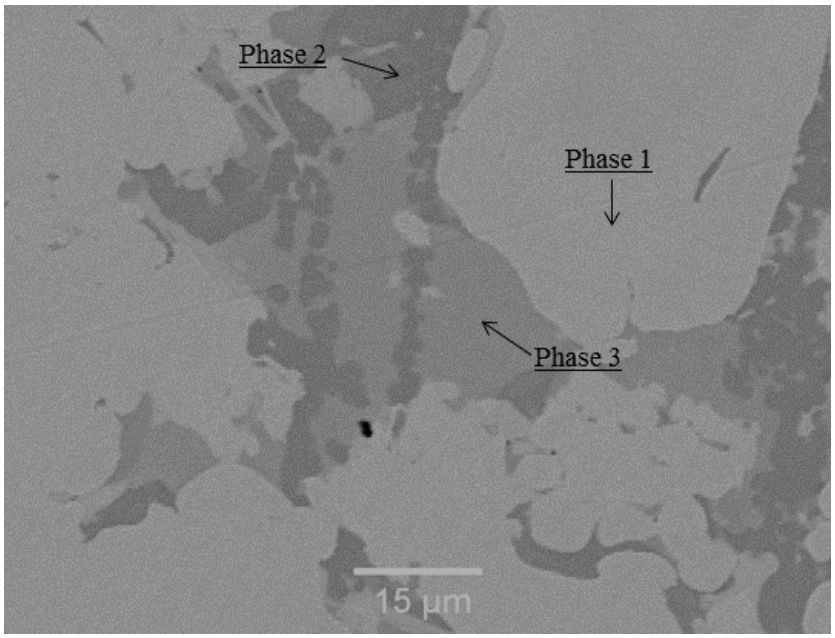

Figure 15: Photo micrograph of the phase structure in the slow-cooled alloy from a melt at 1 500 °C

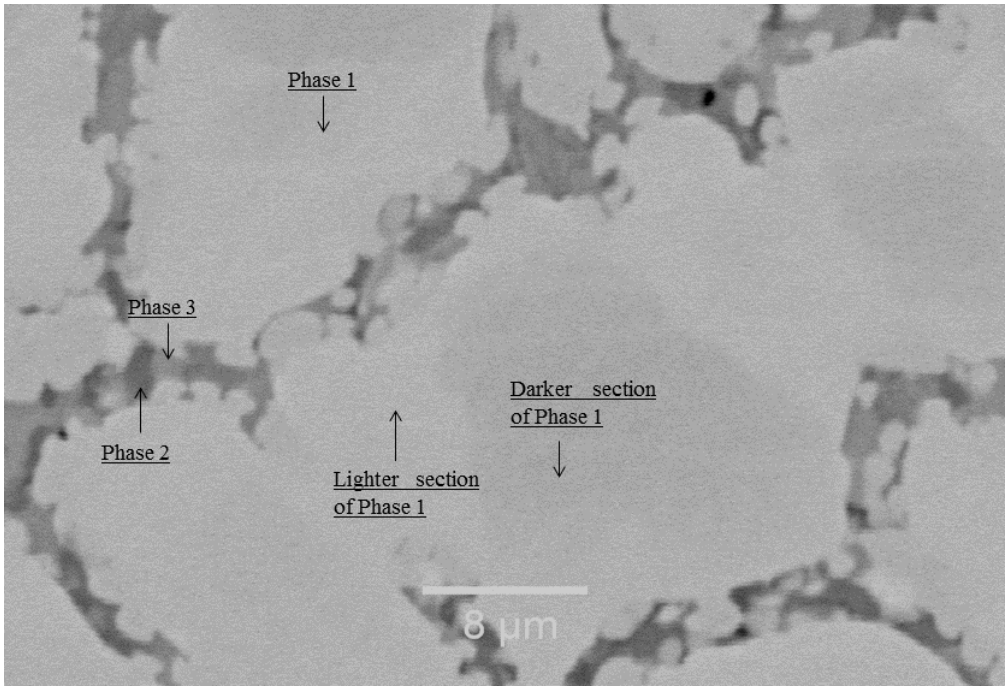

Figure 16: Photo micrograph of the phase structure in the quenched alloy from a melt at 1 500 °C

The alloy in Figure 16 was fast quenched to better preserve any phases that might have been present as primary solid phases in the melt (although it is clear that none was present). The lighter grains have a higher atomic number than the darker ones, indicating a higher PGE content, with the darker grains containing more Ni and Fe. The texture is typical of eutectic crystallisation, with the metal crystals having formed first, expelling the lower-melting phases to the grain boundaries, together with additional small crystallites of alloy. All metallic crystallites are not euhedral, but irregular in shape. They have similar crystal sizes, and are often surrounded by smaller metallic crystallites with interstitial arsenide phases.

XRD patterns of both the slow and fast cooled samples are very similar and only the peaks of the metallic phase (Phase 1) are present. This means that the identity or structure of the interstitial phases could not be established with certainty. There is the possibility that they could be amorphous.

Thermodynamic equilibrium modelling in FactSage® (with the solid solution phase active) was used to evaluate the phases that are predicted to form. If the system is heated, at approximately 1 050 °C Pd starts to form the first significant liquid phase comprising Pd (66%), As (17%) and Pb (11%). This finding correlates well with the last interstitial phase that solidifies. The last solid phase (FCC solid solution) that disappears at around 1 795 °C comprises a large array of metals, with the following approximate composition: Pt = 34%, Ir 11%, Os = 5%, Pd = 3%, Rh = 10%, Ru = 28%, Ni = 3% and Fe = 5%. SEM EDS work also found that the major phase was comprised of a large array of metals.

Both modelling and actual results suggest that a phase solidifies at high temperature and that this phase comprises the bulk of the PGMs, including Fe, Ni and Cu. The phase seems to reject some Pd

and most of the Pb and As. These metals solidify last, as an interstitial phase that could approximate a Pd_5As_2, with some metal substitution that takes place.

4.3.2.3 Alloy produced from leach-roast-smelt of third stage residue

No mineralogical quantification was performed on this sample. From the alloy assays in Table 18 it can be seen that the composition was very similar to the roast-smelt alloy, apart from the lower Cu, Ni and Fe content. The lower content of these elements lifted the observed melting temperature from 1 450 °C (for the roast-smelt test) to 1 510 °C (for the leach-roast-smelt test). It can be expected that the phase mineralogy would be affected. In the roast-melt alloy, the Fe reported in a Pt-Fe-Pd-Ru Phase 1 (from Table 19), making up around 10% by weight of this phase. With the lower Fe content and lower alloying effect, the melting temperature of this highest melting phase will be affected. The bulk of the Cu and Ni were contained in Phase 2 (from Table 19). Phase 2 contains a large array of metals, of which Cu and Ni made up around 7% of the content by weight. The reduction of the Cu and Ni might have a lower overall effect on Phase 2 than the reduction of Fe might have on Phase 1.

4.3.2.4 Alloy produced from roasting-smelting of third stage residue with Cu addition

An alloy that was produced in the test work, with addition of Cu at a temperature of 1 350 °C and ambient pressure, is given in Table 18 under the Roast-Smelt with Cu addition heading. A Total PGM content of 25.6 wt% was achieved for this melt. The alloy was produced by first roasting third stage leach residue, followed by smelting. An addition of 150 g Cu (as fine powder) was made per 100 g roasted product feed with no addition of a reducing or oxidising agent. An addition of CaO-SiO_2-Al_2O_3-Na_2O type slag, at 50 g per 100 g of third stage leach residue, was used.

Optical microscopy was performed on the sample. The metal sample was characterised by a very homogeneous quench surface on the upper side of the alloy disk, graduating into a multi-phase material towards the bottom. This can be seen in Figure 17(a), 17(b) and 17(c).

Figure 17: (a) shows the homogeneous chill margin on the top side of the metallic sample, (b) the appearance of a second phase in the mid section and (c) co-existing phases in the bottom section of the sample

The apparently homogeneous metal phase (Figure 17(a)) actually consists of a two phase assemblage (seen by the lighter and darker pattern in Figure 18 below). The darker phase contains more Cu and the bright phase has more Pt and Pd. It is not clear whether the darker phases in the image constitute two different phases or whether there is grain boundary migration of copper to

reflect an enrichment of copper along grain boundaries. The bright third phase is enriched in Ru and Ir. Table 20 shows the elemental composition of the three phases, as determined by SEM-EDS.

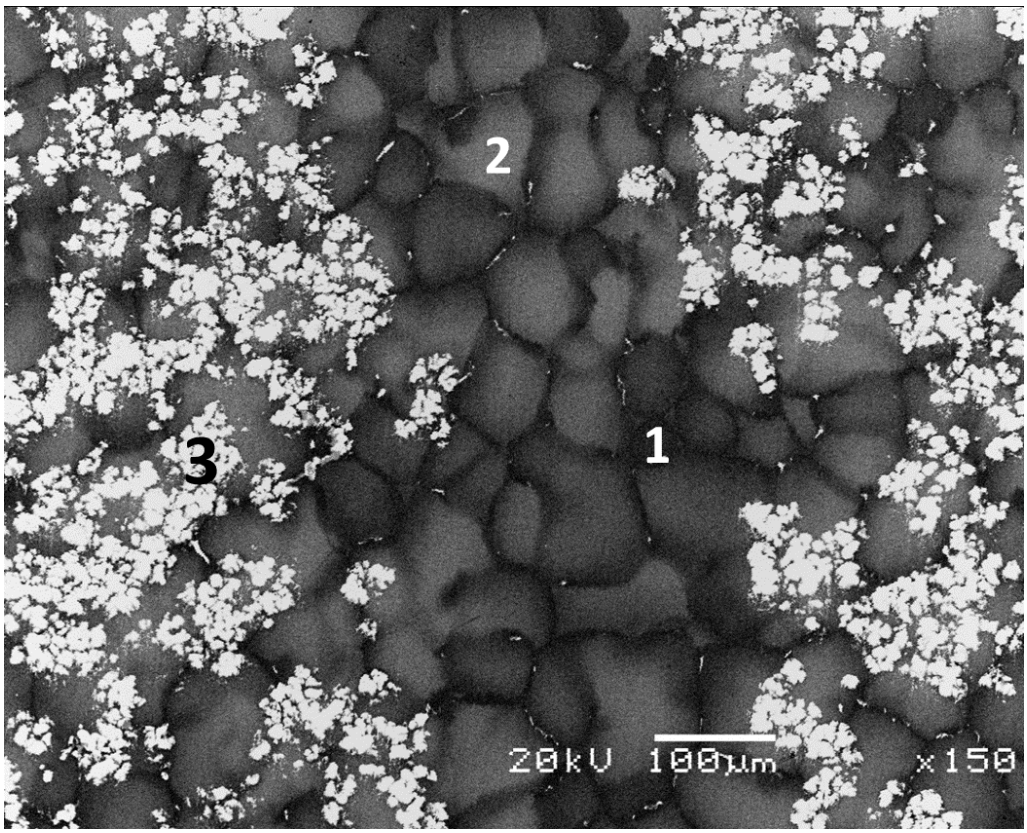

Figure 18: High resolution back scatter electron image of a lath containing a Cu rich phase or phases in an area containing the bright Ru-Ir phase

Table 20: SEM-EDS analysis (wt%) of the different regions shown in Figure 18

	Si	Fe	Ni	Cu	Ru	Rh	Pd	Ir	Pt
Point 1		1	2	77.6		1.3	6		12.2
Point 2	0.4	2.6	2.5	65.5		2.5	4.9		21.6
Point 3		1.7	0.6	6.5	74.1	4.5		12.6	

Bulk powder XRD was also performed on the sample. Three phases seemed to be present and were interpreted as those of a Cu-Pt-Pd alloy, a Cu_3Pt compound and a Ru compound. The observed pattern does not fit well with the calculated pattern, most probably because of a range of compositions that affect the peak positions and peak profiles. In addition there seems to be a prevalence of preferred orientation affecting the intensities. The interpretation is also difficult due to the scarcity of compounds in the database containing the above elements.

The XRD mineral phase quantification is given in Table 21.

Table 21: Phase quantification in the metallic sample

Phase	Weight %	Error (1 sigma)
Copper alloy	88.16	29
Ruthenium	7.82	28
Cu_3Pt	4.03	99

The separate Ru phase was present in the bottom section of the melt. It is possible that this phase crystallised first, due to the crucible side walls cooling more quickly than the rest of it. However, the small crystal size is not characteristic of a primary phase that cools from a melt. The FactSage® SGNoble and SGTE databases predicted that Ru would not be soluble in the Cu alloy and should form a separate phase during cooling. This is discussed in Section 6.2.5.

To test the hypothesis that the Ru (with some Ir) phase had remained solid during the melt (and therefore did not crystalise out first), the alloy phase was heated once more to the initial melt temperature of 1 350 °C in a vertical tube furnace, kept there for four hours and quenched in water. The separate phase enriched in Ru remained unchanged, pointing to the fact that it never melted, but possible stratified to the bottom of the crucible under the force of gravity.

This finding will have important implications where Cu is used as a collector in PGM recovery circuits. When Cu makes up the bulk of the alloy, Ru becomes insoluble and, depending on the Ru size and melt viscosities, might not be sufficiently recovered to the alloy phase.

4.4 Characterising slag

The first set of smelting tests used a borate based slag (B_2O_3-Na_2O-SiO_2), as it was hypothesised that the alloy phase would have a liquidus temperature (temperature where all solid material disappears and only molten material remains) below 1 400 °C, allowing the melt to proceed in a Silicon Carbide (SiC) crucible with a borate based slag, similar to what is used in gold refining (Marsden, 2006). However, during the test work it became clear that some solid material remained between 1 300 °C and 1 400 °C, preventing a clear separation between the slag and alloy phases. A decision was taken to use graphite crucibles and increase the temperature to 1 500 °C, but at this temperature clear evaporation of the slag was evident (primarily as $NaBO_2$, according to FactSage® modelling). The slag was changed from a borate based slag to a CaO-SiO_2-Al_2O_3-Na_2O type slag. Table 22 below provides the chemistry of the synthetic slag that was added to the melt (synthetic slag addition only, not the final slag achieved). A more detailed discussion on the final slag properties is provided in section 6.2.2.

Table 22: Summary of synthetic slag chemistry and viscosity at 1 400 °C

	B_2O_3-Na_2O-SiO_2 type slag	CaO-SiO_2-Al_2O_3-Na_2O type slag
SiO_2	39%	30%
Al_2O_3		10%
CaO		40%
Na_2O	24%	20%
B_2O_3	37%	
Addition range (g of slag added per 100 g roasted material feed)	28 to 56	25 to 100
Slag solidus temperature (°C)	589	807
Slag liquidus temperature (°C)	805	1 150
Slag viscosity at 1 400 °C (in poise) resulting from feed of CaO-SiO2-Al2O3-Na2O-B_2O_3	2.25	2.17

Liquidus and solidus temperatures were determined by FactSage®. The viscosities at 1 400 °C were calculated through the FactSage 'Viscosity' module. For the borate based slag the 'Glass database' was used and for the CaO based slag, the 'Melt database' was used.

The addition ratio in Table 22 is expressed as the total weight of synthetic slag added per 100 g of roasted third stage residue added to the melt. The synthetic slag components were mixed, first with each other and then with the roasted third leach residue, before the well mixed lot was added to the crucible.

4.5 Alloys used for high temperature treatment

Modelling showed that the volatile behaviour of different elements is closely related to the redox atmosphere in the melt (described in section 7.2.1), as well as to the content of minor elements. In order to test some of the modelling predictions and understand the behaviour better, three different alloy types were selected. When melting is performed directly on third stage residue in a slightly reducing environment, Se, Te, As and S would not be removed to any significant extent and the presence of these elements and their effect on Au and Ag losses was monitored. When roasting is performed prior to smelting, the alloy contains very little S and Se and less Te and As. When leaching is performed before roasting and smelting, Fe, Ni and Cu are partially removed. An alloy resulting from each of these three processing routes was subjected to the high temperature treatment step. The chemical content of the alloys is provided in Table 23.

Table 23: Elemental composition of three feed materials subjected to the step of high temperature treatment performed at 1 700 °C for 30 minutes

Element	As reported wt%			Normalised wt%		
	Direct Smelt	Roast-Smelt	Leach-Roast-Smelt	Direct Smelt	Roast-Smelt	Leach-Roast-Smelt
Au	1.0	1.3	1.1	1.1	1.4	1.3
Ir	1.0	1.7	1.5	1.2	1.9	1.8
Pd	18.6	19.1	18.8	21.7	21.2	22.4
Pt	34.3	39.4	38.7	40.0	43.9	46.2
Rh	4.6	4.9	5.1	5.4	5.4	6.0
Ru	7.2	6.2	6.5	8.4	6.9	7.7
Ag	1.3	0.4	0.9	1.5	0.5	1.0
S	2.9	0.3	0.3	3.4	0.3	0.3
As	2.6	2.9	3.3	3.0	3.2	4.0
Bi	0.1	0.3	0.1	0.1	0.3	0.2
Se	1.8	0.0	0.0	2.1	0.0	0.0
Te	0.4	0.1	0.1	0.5	0.1	0.2
Pb	0.3	1.1	0.6	0.3	1.2	0.7
Fe	4.0	6.3	2.0	4.7	7.0	2.4
Cu	1.6	1.7	2.1	1.9	1.9	2.5
Ni	4.2	4.2	2.7	4.8	4.6	3.2
Total	**85.8**	**89.8**	**83.9**	**100.0**	**100.0**	**100.0**

In most of the alloys produced, the alloy content (for a total of 23 metals) added up to 100%. A total of three laboratories (depending on availability) were used for the assaying work during the number of years over which the study was performed. Quite a significant difference was observed between the results from the laboratories at times, although this could not be statistically quantified. A single direct comparison was made on an alloy that showed a low total at one of the laboratories (93%). When re-analysed at another laboratory, the total came to 101%. Table 24 shows the direct comparison between the reported results of the two laboratories. A sample from two holes drilled directly adjacent to each other was submitted to the two laboratories. The variance between individual metals was also significant and might partly be explained by the sampling method and alloy heterogeneity. However, the low total of laboratory B cannot be explained. In an effort to keep the results free from analytical bias specific to a laboratory, as-reported values were always used to determine recoveries and the same laboratory was always used to assay the feed and product from any one given test.

Table 24: Assay comparison of the alloy drilled from adjacent holes between two different labs

Element/ Compound	Lab A	Lab B	Lab B normalised
Au	1.3%	1.3%	1.4%
Ir	2.3%	1.7%	1.8%
Pd	20.2%	19.1%	20.5%
Pt	40.7%	39.4%	42.4%
Rh	5.9%	4.9%	5.2%
Ru	8.5%	6.2%	6.7%
Ag	2.2%	0.4%	0.5%
Al2O3	0.5%	0.2%	0.2%
CaO	0.4%	1.8%	1.9%
Fe	7.5%	6.3%	6.8%
MgO	0.0%	0.0%	0.0%
MnO	0.0%	0.0%	0.0%
S	0.0%	0.3%	0.3%
SiO2	0.0%	0.9%	1.0%
As	2.9%	2.9%	3.1%
Bi	0.3%	0.3%	0.3%
Co	0.2%	0.0%	0.0%
Cr	0.7%	0.2%	0.3%
Cu	1.8%	1.7%	1.8%
Ni	4.4%	4.2%	4.5%
Pb	1.3%	1.1%	1.2%
Se	0.0%	0.0%	0.0%
Te	0.3%	0.1%	0.1%
Total	**101.4%**	**93.0%**	**100.0%**

4.6 Characterising atomised product

Two types of alloy were atomised: 1) alloy from directly smelting third stage leach residue, and 2) alloy from roasting and smelting third stage leach residue. The alloys were prepared from different third stage leach batches that were submitted to the high temperature treatment tests, therefore their chemical composition is shown in Table 25.

Table 25: Elemental composition in weight percentage of two alloys studied during the atomisation trials

Element	As reported wt%		Normalised wt%	
	Direct Smelt	Roast-Smelt	Direct Smelt	Roast-Smelt
Au	0.7	0.8	0.8	0.9
Ir	2.3	2.4	2.5	2.6
Pd	14.9	18.7	16.5	20.2
Pt	35	42.3	38.7	45.6
Rh	5.1	6.0	5.6	6.5
Ru	12.1	12.5	13.4	13.5
Ag	0.9	0.6	1.0	0.6
S	1.6	0.0	1.8	0.0
As	2.7	2.0	3.0	2.2
Bi	0.2	0.2	0.2	0.2
Se	3.4	0.0	3.8	0.0
Te	0.8	0.5	0.9	0.5
Pb	2.6	1.8	2.9	1.9
Fe	3.8	1.2	4.2	1.3
Cu	2.1	2.4	2.3	2.6
Ni	2.2	1.3	2.4	1.4
Total	90.4	92.7	100	100

Fourie (2011) made a study of the alloy that was produced from the atomisation tests as her final year project to complete the Bachelor's degree in Process Engineering at Stellenbosch University. Appendix B contains details and results of the test work. Figure 19 below shows an optical microscope photograph taken of the atomised alloy that was produced from roasting and smelting. The black dots visible in many of the bright alloy particles are openings, as the alloy particles were often hollow. This provides additional surface area for rapid dissolution and is beneficial from a dissolution perspective. The formation of hollow particles will be discussed under the discussion section (7.2.2).

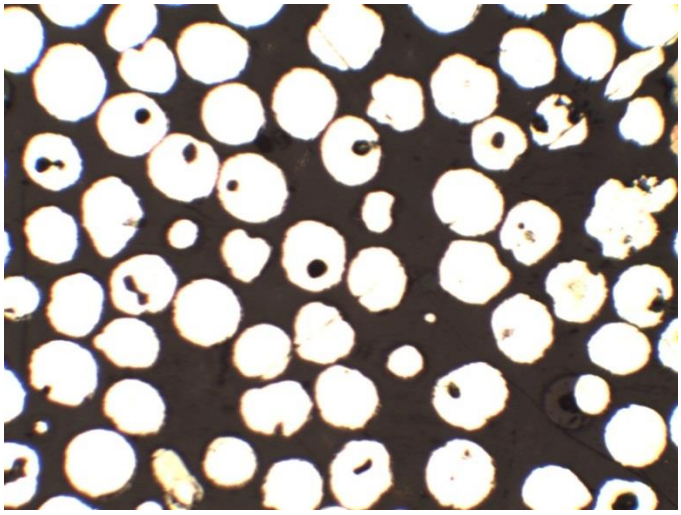

Figure 19: Optical microscope picture of atomised alloy particles. Image is taken at 10 x magnification and the sizing range is -125+75micron

SEM work on the alloy revealed two primary phases. This should be compared with the alloy in section 4.3.2.2 (Roast Smelt alloy). The phase distribution in the fast quenched (atomised) alloy is finer than the alloy obtained from the more slowly cooled smelt, with crystallite sizes in the micron and sub-micron range. Accurate phase analysis with EDS is complicated by the small phase size (due to beam interaction), but approximate analyses of the phases are provided in Table 26.

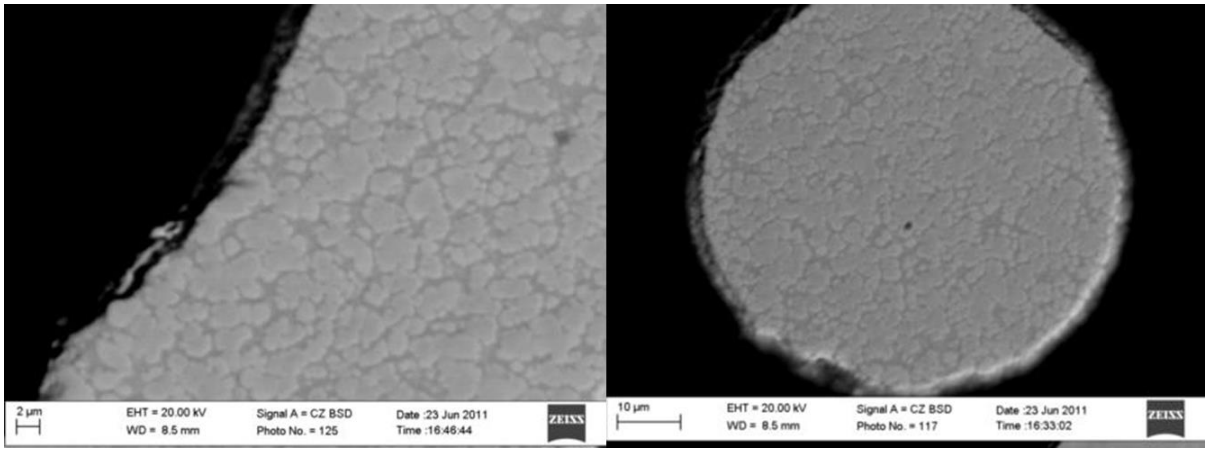

Figure 20: SEM picture of alloy produced, to show the distribution of the different phases

Table 26: Elemental composition of the lighter and darker phases in Figure 20, as determined with SEM-EDS

Phase	O	Cr	Fe	Ni	Cu	As	Pb	Sb	Te	Pt	Pd	Ru	Ir	Total
Dark phase	6.1	0.0	0.5	1.3	1.9	8.0	5.0	1.9	1.1	23.0	48.0	0.0	0.0	96.9
Light phase	2.7	0.4	2.5	0.9	0.3	0.2	0.0	0.0	0.0	46.8	7.2	34.9	4.1	99.9

The phase composition compares roughly with the more slowly cooled alloy from the smelt, forming a primary crystal phase high in Pt and Ru, while a secondary phase, which is rich in Pd, As and Pb, forms at a lower temperature. The oxygen content measured in the phases was not found in the SEM work of the slowly cooled alloy. The presence of oxygen in the alloy that was fast quenched could point to gas (including oxygen) solubility at high temperatures and insufficient time for the gas (oxygen) to diffuse out during rapid quenching. The porosity in the slowly cooled alloy (discussed in section 7.2.2.) supports the proposition of gas solubility at higher temperatures, while the poor dissolution of especially the OPMs in HCl/ Cl_2 (discussed in Appendix B) could suggest the possibility of the presence of some oxygen.

Chapter 5: Roasting

This chapter will discuss the results of the roasting modelling and test work.

5.1 Introduction and background

One of the objectives set for the study was to eliminate the caustic leaches from the BMR process. Since two distinct streams from the BMR undergo different caustic leaches, the two streams were studied independently. Results from the Se/Te precipitate modelling and test work are reported in Appendix C, while the results from the third stage leach residue (pressure leach residue) are reported in this chapter (Chapter 5). Figure 21 shows the Roasting step studied in this chapter, highlighted with a dashed yellow ellipse.

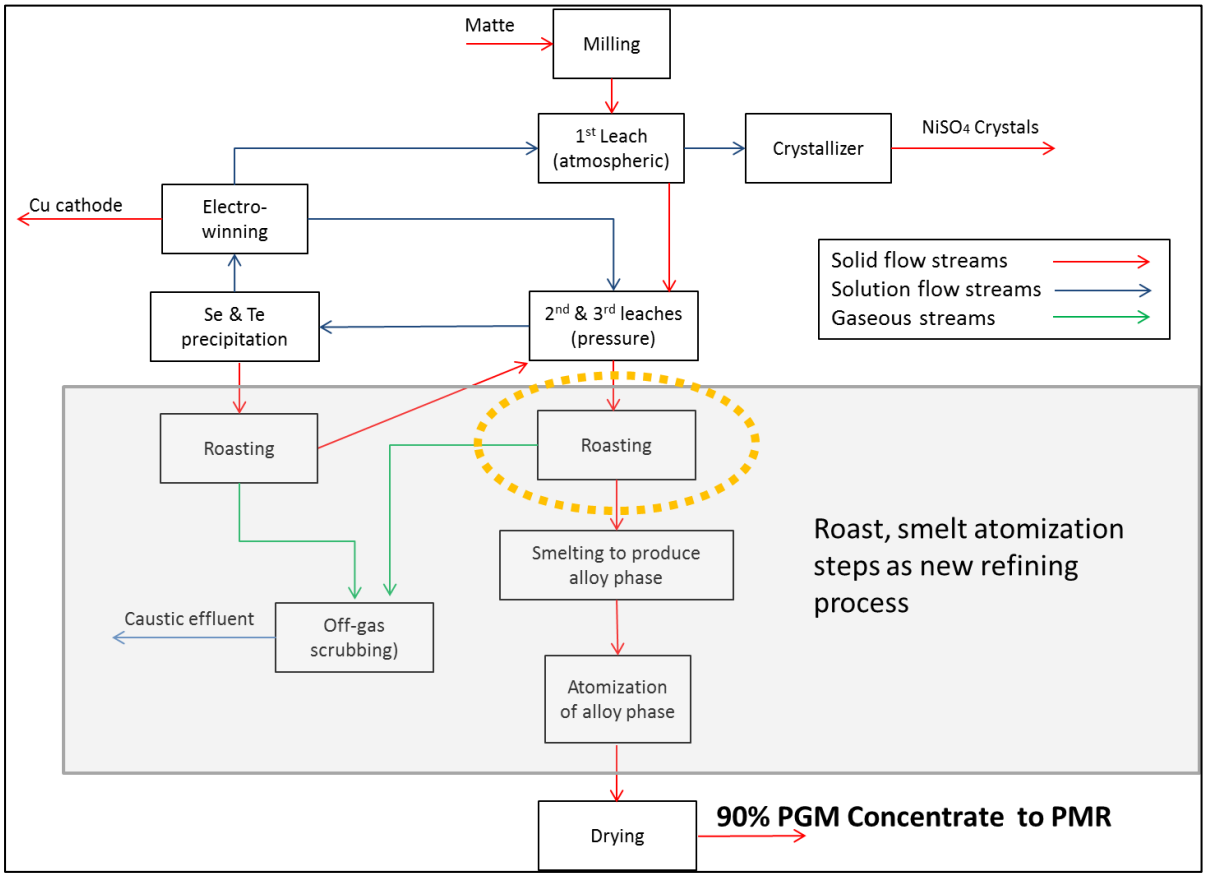

Figure 21: Block flow diagram of the proposed pyrometallurgical process that could be implemented between the BMR and PMR processes in order to remove contaminants from the PMR feed. The position of the roasting step discussed in this chapter is shown by the dashed yellow ellipse

In the Lonmin context, there are a number of amphoteric elements contained in the third stage leach residue that all show high volatility at moderate temperatures ranging from 600 °C to 1 000 °C. These amphoteric elements include Cr, Se, Te, As, Pb and S (Bi at 0.1 wt% and Sb at 0.01 wt% are very low). Additionally, Os can oxidise to OsO_4 and sublimate in the roasting environment. Os is not

recovered by Lonmin and is viewed as a nuisance element, requiring separation from Ru during distillation in the PMR process.

Roasting is ideally suited to the removal of a number of the contaminant elements (As, Se, Te, S and Os), since their volatile oxides will sublimate before any PGM losses to the gas phase will occur. These same elements are difficult to partition from an alloy or matte phase in a melt and require narrow partial oxygen pressure control in the melt, which is difficult to achieve. The stable oxides that are allowed to recrystallise during oxidative roasting will dissociate or be dissolved during the melt and will not create complexity for further processing.

Roasting as a technology is well developed and it is often economically viable to pre-treat materials for further pyrometallurgical or hydrometallurgical processing. However, it is conventionally applied to bulk flotation concentrates (in the case of sulphides) or sometime bulk ores (double refractory ores in gold processing). Roasting of a concentrated PGM leach residue poses unique challenges:

1. The PGM residue is exceedingly fine grained, allowing easy entrainment in fluids (gaseous or aqueous), so that even very little movement suspends the particles.
2. The extremely high value per unit mass ($/kg) creates a unique set of challenges.
    a. Entrainment losses of PGMs cannot be allowed.
    b. Rework, materials handling and transfer, and any handling that may suspend particles, should be minimised.
    c. In an engineered system theft and security remains a perpetual risk.
3. The thermodynamic and phase behaviour of PGMs and associated contaminants are poorly explored.
4. Phase and changes in the state of aggregation may occur for the individual mineral and amorphous phases present in the leach residue, leading to phase recrystallisation, potential vapour phase losses, etc.
5. Due to the poorly defined data on PGM minerals and their behaviour under various reduction-oxidation conditions at elevated temperatures, the reaction mechanisms, kinetics and mass transfer process are poorly understood or have never been studied at all, either for the pure components or for reacting mixtures.

Finding only thermodynamic solutions to this problem, without a proper understanding of the engineering constraints, would lead to a naive and impractical solution. The problem is inherently a convoluted one, where engineering know-how is as important to finding a solution as is an understanding of the thermochemical behaviour of mineral phases. High grade PGM-containing residues are treated in limited tonnage. The low throughput requirement through a roaster would therefore not lead to thermal efficiency being overweighed at the cost of chemical efficiency or recovery. Even if a roasting temperature of 900 °C were required, an expensive energy source such as electricity would still be favoured and show a low cost-sensitivity, when compared to the recovery of either the volatiles or precious metals.

Steenekamp (1999) reported that roasting in air was performed at the Lonmin BMR as a control step for Se and Te until 1996. Precipitated Cu_2Se and Cu_2Te were oxidised in a roast at 400 ˚C to $CuSeO_3$ and $CuTeO_3$. These copper selenites and tellurites were then leached with strong caustic soda to form soluble sodium selenites (Na_2SeO_3) and sodium tellurites (Na_2TeO_3). However, this roasting

step treated only the Se and Te that went into solution across the pressure leach (second and third stage leach). Poor control over total Se and Te passing to the PMR, and health considerations across the roasting step, led to the introduction of low and high pressure caustic leaches to the current BMR flow sheet to replace the roasting step. Steenekamp (2012) reported that Se and As removal were done by a high pressure leach and Te was removed by low pressure leach. Roasting is still employed by Northam as a control step for Se and Te (Bezuidenhout, 2013).

5.2 Results from roasting test work

As already described in Chapter 3 (Methods), two different test work campaigns were performed. The results (removal efficiencies) achieved during these test runs are summarised in section 5.2, while the interpretation of the results will be done in section 5.3. Elements will be grouped according to logical divisions, these being PGMs, volatile components, Pb and stable oxides.

Results of the extent of removal of elements/compounds during the roasting trials on third stage leach residue

Five stationary roasting tests were performed (30 g each) in a muffle furnace at 100 °C intervals from 600 °C to 1 000 °C. The material was left at temperature for two hours, in contact with excess air. Table 27 below contains the summary of the results for elements that can display volatile behaviour, as well as the PGMs. The results are expressed as elemental removal across the roast (removed weight of element expressed as a percentage of starting weight of an element).

Table 27: Percentage weight change achieved during the stationary bed roasting test work on third stage residue

Temperature	600 °C	700 °C	800 °C	900 °C	1 000 °C
Roast time	2h	2h	2h	2h	2h
Air flow	Convection	Convection	Convection	Convection	Convection
Ru	1%	1%	3%	3%	2%
Rh	0%	-5%	2%	0%	-1%
Pd	1%	2%	4%	2%	1%
Ag	0%	1%	-1%	-2%	-5%
Ir	1%	-2%	3%	2%	0%
Pt	0%	2%	5%	4%	8%
Au	0%	8%	5%	4%	5%
Pb	2%	-6%	-14%	6%	-10%
Se	-92%	-91%	-94%	-82%	-94%
Te	-23%	-17%	-20%	-28%	-40%
As	-60%	-64%	-55%	-37%	-32%
Bi	-6%	-9%	2%	8%	4%
Total S	-83%	-95%	-98%	-100%	-100%
Os	-3%	-13%	-33%	-54%	-71%

Sampling error and assaying errors are present where small variations can be seen in the results given in Table 27. Small weight changes of less than 5% can arguably be ignored and ascribed to sampling/assaying error. However, it is clear which elements are effectively removed and are temperature responsive. The low extent of removal of Te, Os and As is noteworthy.

FactSage® predictions indicated that efficient volatilisation of Te is sensitive to the gas volume in contact with the roast. A fluidised bed roaster was used to provide good gas/solid contact and should better illustrate the limits of removal that can be achieved by the roasting step. The stationary roasting tests showed insufficient removal of Te, Os and As, despite thermodynamic predictions. However, crucible-concentrate interactions, slow diffusion through the stationary bed and temperature variations throughout the stationary bed are expected to limit the diffusion and mass transfer rates. It was postulated that improved solid-gas contact would increase the removal of these elements (Te, Os and As). Table 28 below contains a summary of the test results that were achieved. The results of Table 28 are interpreted together with those in Table 29, where the results for stationary bed roasting, fluid bed roasting and modelling are presented together, and in Section 5.3 where interpretation is done per element. The summary in Table 28 is only for roast tests in oxidative environments, although a number of tests were done in inert environments (with N_2 gas) and reducing environments (a combination of CO and N_2 gas) to see whether there would be an improved removal of As (the results are discussed in section 5.3.2). The removal efficiencies were not calculated on a closed mass balance (weight in and weight out), as there was some carry-over of fines to the off-gas in the fluidised bed. It was decided rather to use Pt as a tie element (as Pt is inert throughout the roast and it is the most abundant element in the leach residue, which can be analysed with high accuracy). Removal efficiencies were therefore calculated as the difference between the elemental ratio to Platinum for the feed and the final product.

Table 28: Percentage weight change achieved during the fluidised bed roasting test work on third stage residue. Gas flow was 1.2Nm^3/hr for all tests reported

Parameter/ Element	700 °C	900 °C	900 °C	900 °C	900 °C	1 000 °C
Roast Time	6h	60 min	2h	6h	4h	4h
Gas atmosphere	Air	Air	Air	Air	40% Oxygen	40% Oxygen
Ru	2%	10%	7%	2%	5%	3%
Rh	2%	11%	9%	7%	4%	17%
Pd	0%	5%	4%	2%	-1%	11%
Ag	-9%	7%	-10%	-13%	-17%	15%
Ir	4%	10%	8%	5%	10%	-8%
Pt	0%	0%	0%	0%	0%	0%
Au	-4%	-5%	-4%	-4%	-9%	0%
Pb	7%	0%	6%	1%	0%	7%
Se	-95%	-94%	-95%	-96%	-96%	-96%
Te	4%	-65%	-77%	-77%	-71%	-99%
As	-42%	-45%	-49%	-52%	-36%	-62%
Bi	2%	20%	15%	10%	4%	24%
Total S	-99%	-100%	-100%	-100%	-100%	-100%
Os	-29%	-22%	-49%	-51%	-50%	-48%

Table 29 shows a comparison between the extent of removal achieved by stationary bed roasting, fluidised bed roasting and thermodynamic equilibrium modelling. The table shows a short roasting period and a long roasting period for the stationary bed and the fluidised bed respectively. With the short roasting time, the extent of removal in the fluid bed process is higher than that of the stationary bed. This is reflected in the results of Te removal, showing a difference between 28% and 65% removal. It is clear that better amphoteric removal can be obtained in the fluid bed, due to the good gas flow control and mixing in the heated chamber, which is not achievable in the stationary bed.

At six hour roasting times in the stationary bed, removal efficiencies of Se, Te and As are comparable to the fluid bed roasting at 1 hour. Comparing the fluid bed roasting time of 6 hours with 1 hour, Te removal improves from 65% to 77% and As removal from 45% to 52%. The marginal increase of removal achieved on volatile elements (especially Te, As and Os) at the 6 hour residence time might point to these elements being present in stable compounds that do not show volatile behaviour similar to that of the pure oxides. The quantitative removal of Se and S and the presence of Ru, Rh and Ir oxides occluded by alloy (from Figure 13) indicate that oxidation has progressed deep into the agglomerates. This supports the hypothesis that it is stable oxides that are limiting the volatile behaviour of the amphoteric elements, rather than a mass transfer limitation of oxygen during long residence times in a fluid bed reactor.

In the case of Os removal, there is a clear improvement from a 60 minute residence time to a two hour residence time. Residence times longer than two hours all seem to show removal efficiencies in

the 50% range, also indicating that Os volatile behaviour is probably not controlled by the formation of the pure oxide alone.

Thermodynamic modelling with FactSage® predicts a 100% removal of Se, Te, As, Bi and Os at 900 °C. This is based on the formation of pure oxides that have very high vapour pressures at this temperature. The test work in this paper show that Te, As and Os are not forming pure oxides, but rather complex oxide phases that are more stable at the 900 °C range.

Table 29: Comparison of percentage weight change achieved on third stage residue with stationary bed, fluidised bed and thermodynamic equilibrium modelling at 900 °C in air

Parameter/ Element	Stationary bed result	Fluid bed result	Stationary bed result	Fluid bed result	Thermodynamic modelling result
Temperature	900°C	900°C	900°C	900°C	900°C
Roast Time	2h	60 min	6h	6h	Equilibrium
Gas atmosphere	Air	Air	Air	Air	Air
Ru	3%	10%	1%	2%	0%
Rh	0%	11%	4%	7%	0%
Pd	2%	5%	1%	2%	0%
Ag	-2%	7%	-16%	-13%	0%
Ir	2%	10%	7%	5%	0%
Pt	4%	0%	0%	0%	0%
Au	4%	-5%	2%	-4%	0%
Pb	6%	0%	2%	1%	-39%
Se	-82%	-94%	-96%	-96%	-100%
Te	-28%	-65%	-59%	-77%	-100%
As	-37%	-45%	-45%	-52%	-100%
Bi	8%	20%	2%	10%	-100%
Total S	-100%	-100%	-100%	-100%	-100%
Os	-54%	-22%	-59%	-51%	-100%

5.3 Discussion of roasting test work results

5.3.1 Discussion of PGM behaviour

Some of the PGMs (Ru, Rh, Pd, Ir) have the tendency to oxidise at the lower temperatures investigated in this study (600 °C to 800 °C), while some can retain their oxide state to the 1 000 °C roasting temperature (Rh and Ru). Pt and Au do not oxidise in the roasting temperature range. However, due to the noble nature of PGMs, they all dissociate to their metallic form as temperatures continue to increase. At higher temperatures (900 °C to 1 700 °C), the vapour pressure of most PGM oxides becomes measurable and this may translate as Ru and Ir losses to the gas phase as oxide vapour during roasting (Jehn, H., 1984). Except for Pd, the vapour pressures of all PGM oxides are several orders of magnitude higher than their metallic states. During high temperature (800 °C to 1 700 °C) oxidation in air, Rh has the lowest mass loss to vapour, followed closely by Palladium and

Platinum. The mass loss to vapour of Ru and Ir is much higher, whereas Os oxidises and is lost to vapour most rapidly.

The specific behaviour of each PGM element will now be briefly discussed. The discussion is based on modelling results from FactSage® (SGNoble solution databases). Where the modelling behaviour was found to differ from the experimental work, this will be highlighted.

Platinum and gold do not oxidise at the lower temperatures (600 °C to 1 000 °C) in air. Their vapour pressures are so low at the roasting temperature range that no losses to the gas phase were predicted by modelling or measured in the test work. Thermodynamic modelling predicted that Pt and Au will always be present in the face centred cubic (FCC) solid solution phase that makes up the bulk of the solid mass. The SEM work (section 4.2) showed the presence of a metallic FCC Pt-Pd alloy phase at 900 °C. Bulk XRD measurements shown in Table 16 also confirmed the presence of the metallic FCC Pt-Pd alloy phase. Au was not measured in the alloy, but this might be due to the low content (0.6%) of Au in the original sample. The low Au content of the sample was also the cause of the large recovery variance reported in the roasting test work results.

Palladium is readily oxidised in the studied temperature range of 600 °C to 800 °C. PdO_2 is stable until about 773 °C, although FactSage® predicts that Pd already starts to join the FCC solid solution phase at 650 °C. Pure PdO_2 can theoretically dissociate to PdO between 773 °C and 804 °C, but in the complex residue this does not happen, as Pd instead joins the solid solution phase with Pt. Bulk XRD work reported in Table 16 confirms that Pd in the metallic form is measured across the entire temperature range of 600 °C to 1 000 °C. The XRD results in Table 16 further show the PdO phase present at 600 °C and 700 °C, but the peak disappears at 800 °C. Since this phase stoichiometry could not be verified, no conclusion can be drawn as to the oxidation state of Pd at the lower temperatures. SEM work on the 900 °C sample confirmed that almost all Pt and Pd was present as a solid solution alloy. No loss to the gas phase as vapour was predicted or measured over the roasting temperature range.

Thermodynamic modelling in FactSage® predicts that Iridium will fully oxidise to IrO_2 at the lower temperatures in air. In the complex residue matrix, IrO_2 starts to dissociate and Ir joins the FCC solid solution phase between 700 °C and 900 °C (although most of this dissociation to Ir in the solid solution phase happens close to 900 °C). Pure IrO_2 dissociates at about 1 030 °C and the solid solution matrix lowers the dissociation temperature by almost 150 °C. SEM analysis on the roasted sample at 900 °C showed that oxidised Ir, Rh and Ru was occluded as a separate phase from the Pt-Pd based alloy. It would appear that Ir does not dissociate to metal to join the FCC solid solution phase at 900 °C, as predicted by FactSage®.

FactSage® predicts small losses of Ir to the gas phase in the form of IrO_3, with a 0.3% vapour loss predicted to the gas phase between 900 °C and 1 000°C. The vapour losses of Ir happen through the further oxidation of IrO_2 to IrO_3 (gaseous phase). While the sensitivity of the experimental set-up does not allow measurement of Ir losses of less than a couple of per cent, Ir losses were measured in the single roasting test done at 1 000 °C in a 40% oxygen atmosphere for a four hour period (See Table 28). The accuracy of the measured 8% loss is questionable, as neither literature nor modelling supports this, while Ru losses did not accompany the Ir loss.

Ruthenium fully oxidises to RuO_2 at low temperatures and remains stable as this oxide through the temperature range to 1 000 °C. According to FactSage®, RuO_2 does not join the solid solution phase at all, but remains stable as a pure RuO_2 solid. Ru and Os are the only precious metals that have a hexagonal close packed (HCP) crystal structure, while the rest (Pt, Pd, Rh, Ir and Au) all have the face centered cubic (FCC) crystal structure. Despite this difference in the crystal structure of the metals, Vines *et al.* (1941) report that up to 68% Ru (the highest addition studied) will form solid solutions with Pt in the metallic state. The SEM work on the 900 °C roasting sample showed that the oxidised state of Ru does not join the Pt-Pd alloy phase, but is present as a separate solid solution phase. Although FactSage® accurately modelled the presence of the Ru oxide phase, the presence of Ir and Rh oxides in this solution phase was not predicted by FactSage®.

RuO_2 (as RuO_3 and RuO_4) and IrO_2 (as IrO_3) have the highest vapour pressure of the PGM oxides after Os as OsO_4. It is exactly the opposite for the metals, with Ru and Ir having the lowest vapour pressures compared to Os in a vacuum. Ru losses to the gas phase can become measurable around 1 000 °C, with 0.5% losses (as RuO_3 and RuO_4) predicted at thermodynamic equilibrium. As a pure RuO_2 solid, Ru will only dissociate from oxygen at about 1 470 °C. Losses of Ru to the vapour phase proceeds by the further oxidation of RuO_2 to RuO_3 and RuO_4, which are both only gaseous oxides.

Thermodynamic equilibrium predicts that Rh is present as an oxide in the full temperature range of roasting (600 °C to 1 000 °C), albeit in different oxidation states (4+, 3+ and 2+ respectively). The bulk mineralogical work results shown in Table 16 confirm the presence of Ru and Rh oxides across the entire roasting temperature range. However, at thermodynamic equilibrium it is predicted that Rh will increasingly dissociate from the pure oxide form and join the solid solution phase (Pt-Pd alloy phase from the SEM study) as the temperature increases. The thermodynamic equilibrium prediction of the solution of Rh into the Pt-Pd solid solution phase is shown in Table 30. SEM EDS analysis on the Pt-Pd alloy (FCC solid solution) phase confirmed the presence of some Rh in this phase, typically varying between 3% and 5% weight percentage content. This translates to between a 20% and a 30% distribution of Rh to the FCC Pt-Pd solid solution phase. This compares very favourably with the 27.1% distribution to the metallic FCC phase prediction by FactSage® at 900 °C.

Thermodynamic equilibrium does not predict any losses of Rh to the gas phase and no measureable losses could be seen during the experimental test work. Pure RhO_2 will change oxidation state to Rh_2O_3 at about 775 °C and Rh_2O_3 will change to Rh_2O at about 950 °C. Pure Rh_2O will only dissociate to Rh metal around 1 760 °C. Despite the higher dissociation temperature (compared to that of Ru), Rh tends to join solution phases (solid and liquid) more easily than Ru, due to the compatible FCC crystal structure.

Table 30: FactSage® prediction of Rh distribution between the FCC solid solution phase and the oxide phase, as well as the stable oxidation states in the residue, as a function of temperature

	600 °C	650 °C	700 °C	750 °C	800 °C	850 °C	900 °C	950 °C	1000 °C
% Distribution of Rh to FCC Pt-Pd solid solution	0.1%	0.4%	0.9%	2.3%	6.1%	11.5%	27.1%	49.3%	66.8%
% Distribution of Rh to pure solid oxide	99.9%	99.6%	99.1%	97.7%	93.9%	88.5%	72.9%	50.7%	33.2%
Dominant oxidation state as pure solid oxide	RhO_2	RhO_2	RhO_2	Rh_2O_3	Rh_2O_3	Rh_2O_3	Rh_2O_3	Rh_2O	Rh_2O

Oxidation of the OPMs at temperatures in the 800 °C to 900 °C range has been noted in the industry. This is in contrast to the PMs (Precious Metals – term used to describe the grouping of Pt, Pd and Au) that remain present as a metal in an oxidising environment at the same temperatures. Oxidised OPMs have a tendency to be poorly soluble in aqua regia (a mixture of nitric and hydrochloric acids) and also in a HCl/Cl_2 environment, though to a lesser degree. Historically, this difference between the behaviour of OPMs and PMs after roasting has been used industrially as a crude method to achieve separation between PMs and OPMs, thereby simplifying and optimising the respective refining circuits for each.

5.3.2 Discussion of volatile compound behaviour

This section will discuss the behaviour of the volatile components of the third stage leach residue. The roasting step is included in the new pyrometallurgical process specifically to remove the volatile elements. Os, Se, Te, S, and As are volatile at low temperatures from a solid state in their respective pure oxides and therefore a low temperature oxidative roast is ideally suited to remove these elements. The following elements are targeted as part of the roasting process and will be discussed individually: Os, Se, Te, S, and As. Although Ag is not recovered in the Lonmin PMR process, it will also be discussed.

The vapours resulting from the roasting process on third stage leach residue are toxic. Exposure to OsO_4 fumes is known to be harmful, resulting in irritation of the eyes and respiratory system. Chronic exposure will damage the liver, kidneys and skin. Exposure to SeO_2 fumes is known to be harmful, with symptoms including skin and eye irritation, stomach disorders, metallic taste and bad breath (amongst others). Short term exposure to SO_2 fumes may cause breathing difficulties, while long term exposure may cause chronic respiratory illness (US National Library of Medicine, Date). To avoid human contact with the fumes, good capture and adequate treatment is necessary.

Osmium is also classified as a PGM, while Au is typically not grouped with the six Platinum group metals, although it is a precious metal. In some refineries, Os is not recovered, while Au is recovered in all cases. For this reason Os is discussed under the volatiles and Au under PGMs. Os is the most volatile element of the PGM group as an oxide, and the least volatile as a metal. Pure Os can thermodynamically oxidise to OsO_4 at room temperature and will completely vaporise from around 50 °C (under equilibrium conditions), with the vapour pressure of OsO_4 increasing with temperature.

Os is difficult to analyse accurately, since it tends to oxidise during fusion. In this test work ICP-OES and XRF techniques were used for Os quantification. Although there may be a significant assaying error involved, the trends of Os removal can be viewed as indicative. Os removal increases proportionally from 3% at 600 °C to 71% at 1 000 °C. Thyse *et al.* (2010) reported that Osmium is often found as very small alloy inclusions together with Ru, which shares the HCP crystal structure, as secondary growth in a locked matrix in converter matte. The presence of small Os alloy inclusions was also found in the current SEM work on third stage leach residue material. Where Os could be analysed with the SEM EDS in the roasted product (section 4.2), oxygen was also present in the phase, together with Ru and Rh. Thermodynamic equilibrium modelling shows that Os forms several solid solutions with other precious metals in the absence of oxygen. The presence of Osmium in a solid solution phase could depress the activity of Osmium and correspondingly the fugacity/vapour pressure. No literature reference could be found for stable osmates that could form that would not display volatile behaviour.

Selenium is volatile as an oxide (SeO_2) and removal of Se would require Se to oxidise to SeO_2. Modelling shows that Se can be completely removed, and the experimental test work shows that Se removal in the mid ninety per cent range is achievable. It appears that Se removal happens very rapidly and across the full temperature range of roasting. Some of the first crystals that de-sublimated onto the cooler portion of the off-gas duct were collected and analysed during the roasting test work. They were shown to be almost pure SeO_2. Therefore, off-gas handling systems need to be designed to capture SeO_2 via condensation/de-sublimation.

Sulphur is present in the third stage leach residue in the form of sulphides (copper and PGM sulphides) and sulphates (lead, nickel and copper sulphates). S removal during roasting would include the oxidation of the sulphides, as well as the dissociation of the sulphates. Table 6 explains the Open system modelling as being more accurate by allowing only partial oxidation and loss of S as SO_2 from the system, instead of stabilising sulphates. Table 31 shows that the open system FactSage modelling predicts that S removal will proceed very similarly to the experimental results. Above 800 °C, complete S removal has already been achieved. The stability fields of transition metal sulphates decrease significantly with increasing temperature, as has been shown for numerous metals in Kellog ($\log[P_{O2}]$-$\log[P_{SO2}]$) diagrams.

Table 31: FactSage® prediction for sulphur weight change and sulphate decomposition from the leach residue compared to the actual sulphur removal

	600 °C	650 °C	700 °C	750 °C	800 °C	850 °C	900 °C	1000 °C	1 100 °C
S removal according to FactSage Open method	-90%	-91%	-95%	-97%	-98%	-100%	-100%	-100%	-100%
S removal from test work	-83%		-95%		-98%		-100%	-100%	
Metal sulphate species that decompose within the temperature interval		$Fe_2(SO_4)_3$	Ag_2SO_4	$MgSO_4$	(CuO) ($CuSO_4$)	$NiSO_4$		$CaSO_4$	(PbO) ($PbSO_4$)

Tellurium is only volatile in the roasting test work temperature range as tellurite (TeO_2). Te will oxidise at low temperatures (even at room temperature) to TeO_2, but the vapour pressure of TeO_2 only becomes appreciable above 700 °C. Based on thermodynamic modelling, TeO_2 shows a strong relationship between the extent of removal and the volume of the gas phase that is in contact with the sample, due to the relatively low vapour pressure of TeO_2. Of the different volatile species concerned in this residue, Te is the only one that displays such a strong correlation with gas volume and temperature. The modelled relationship between the extent of removal, temperature and gas volume can be seen in Figure 22. Actual results from the roasting test work testify to the improved extent of removal with longer retention times and better gas/solid contact, both leading to higher carrier gas volumes in contact with the solid phase. The fluid bed roasting could achieve around 80% removal of Te at 900 °C, while the poor gas flow conditions and short retention times of the first set of experiments could only achieve 40% removal at 1 000 °C. The experimental data show that 99% Te removal could be achieved at 1 000 °C in a 40% oxygen atmosphere for four hours. Four data points at 900 °C from the fluidised bed test work show low sensitivity of removal (between 70% and 77% achieved) with variable time and even variable oxygen potential. SEM-EDS work on the roasted sample at 900 °C showed that Te was often associated with high Cu and oxygen content.

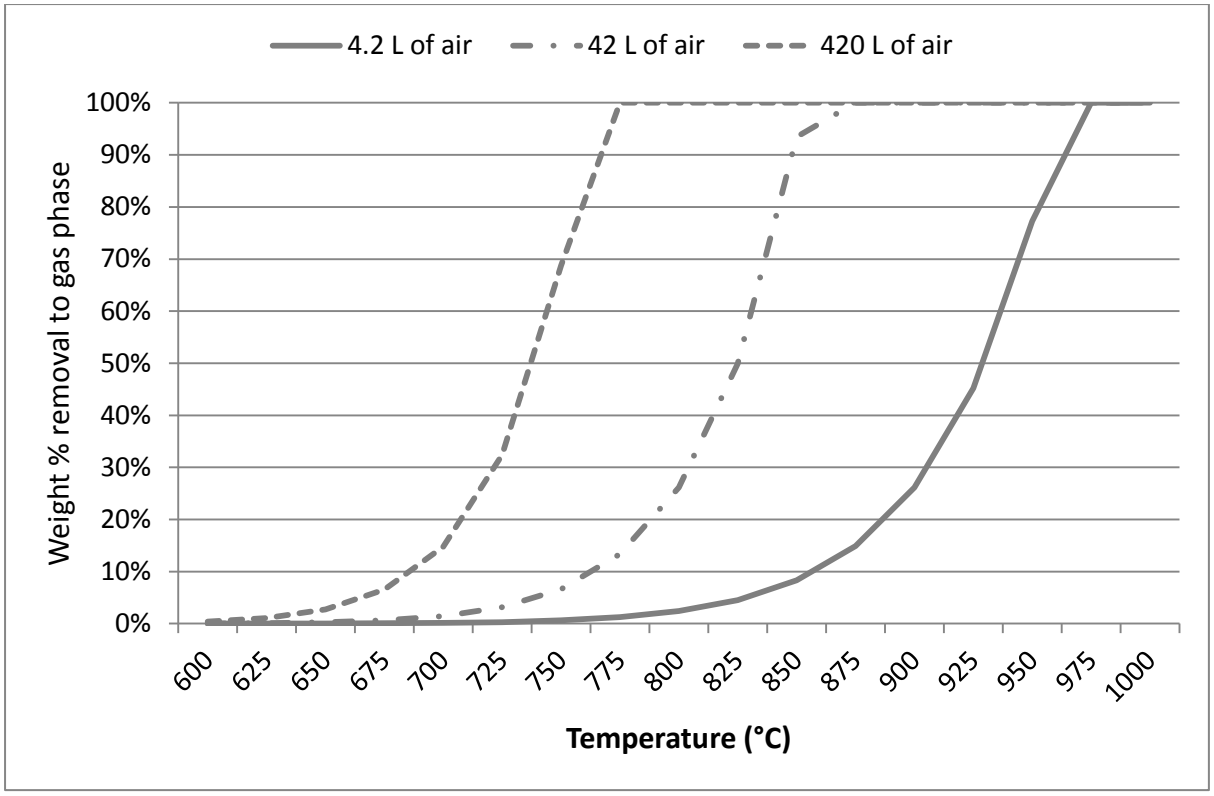

Figure 22: Effect of air volume on the removal of TeO_2 to the gas phase according to FactSage® prediction. Addition rate of air (Litre) is per 1g of Te

Table 32 below shows that Arsenic, of all the elements present in the residue, has the strongest thermodynamic driving force for oxidation (Gibbs free energy change) at the low temperature range up to around 800 °C.

Table 32: Gibbs free energy change for oxidation (Joule per mole of pure solid reactant) as a function of the temperature

Reaction	100 °C	300 °C	600 °C	800 °C	1 000 °C
$Os+2O_2 \rightarrow OsO_4$	-283 250	-250 719	-207 292	-178 700	-150 355
$Se+O_2 \rightarrow SeO_2$	-157 753	-121 275	-115 194	-113 015	-110 298
$Te+O_2 \rightarrow TeO2$	-256 266	-221 237	-166 563	-130 200	-99 105
$2As+1.5O_2 \rightarrow As_2O_3$	-278 555	-252 890	-222 135	-203 186	-181 032
$2As+2.5O_2 \rightarrow As_2O_5$	-371 345	-323 082	-249 657	-199 992	-145 785
$Pd+O_2 \rightarrow PdO_2$	-140 392	-103 625	-48 527	-11 850	24 778
$Pd+0.5O_2 \rightarrow PdO$	-74 904	-55 208	-26 363	-7 453	11 262
$Rh+O_2 \rightarrow RhO_2$	-205 821	-210 565	-216 950	-220 735	-224 130
$2Rh+1.5O_2 \rightarrow Rh_2O_3$	-139 500	-112 202	-72 327	-46 437	-21 118

Arsenic is volatile as an oxide, and has two oxide forms, being As_2O_5 and As_2O_3 (sometimes expressed as As_4O_6). Arsenic will oxidise at room temperature in oxidising environments. As_2O_5 is the most stable oxide at lower temperatures, up to about 790 °C, while As_2O_3 will be thermodynamically more stable above 790 °C. However, both these oxidation states will be present and FactSage® predictions show that primarily As_2O_3 will volatilise. As_2O_5 solid should be thermodynamically stable in the residue up to about 650 °C, after which all arsenic should have joined the gas phase. The formation and thermal stability of metal arsenates M_x $(AsO_4)^{3-}$ under oxidising atmospheres is well known in the gold, copper and iron industry. The best known of the arsenates are $FeAsO_4$, $Ca_3(AsO_4)_2$ and $Mg_3(AsO_4)_2$. The FactSage® Open system predicts the formation of $Ca_3(AsO_4)_2$ between 650 °C and 950 °C, thereby limiting the deportment of As to the gas phase to 94% (Table 6). Unfortunately the FactSage® databases available to the author did not include minerals like $FeAsO_4$ and $Mg_3(AsO_4)_2$, which are known to be non-volatile in gold ore roasting systems. The presence of the ferric (3+) ion stabilises iron arsenate as scorodite, and the third stage leach residue will have the biggest portion of Fe present in the ferric state after the strong oxidising conditions experienced in the preceding acidic pressure leaching.

The roasting results from the stationary bed tests support the viewpoint that a stable arsenic oxide species forms at higher temperature, since the extent of removal of As drops from about 60% at 800 °C to about 30% at 1 000 °C. The fluidised bed test work shows a consistent removal of around 45% to 50% in the temperature range of 700 °C to 900 °C. It seems that more residence time improves removal, but only marginally. The single data point in the fluid bed roast at 1 000 °C and 40% oxygen content shows the best extent of removal, at 62%. In order to test the hypothesis that a stable arsenate was limiting the volatile behaviour of arsenic oxide, reductive roasts were done by using a combination of N_2 and CO gas before and after the oxidative roast. However, no real improvement could be made on overall As removal compared to that achieved by an oxidative roast only. The presence of the remaining As in the roasted product was mostly in an oxidised phase associated with Pb, Ni, Fe and Cu.

An investigation was done to see if a stable PGM arsenide could be responsible for the refractory nature of arsenic in the roasting step. A list of known minerals was investigated and modelled in FactSage®, but none of the arsenides or sulpharsenides appears to be stable at the roasting temperatures in an oxidising environment. Although a mechanism for arsenic stability in the leach residue cannot be presented at this time, it seems that removal of around 50% could be achieved by roasting at temperatures of 850 °C to 900 °C.

Silver does not form stable oxides in the roasting temperature range. The vapour pressure of pure Ag can become sufficient at 1 000 °C to constitute some losses as Ag vapour to the gas phase, but the presence of the solid solution matrix seems to suppress this, so that no losses were predicted according to FactSage® modelling. If sulphur is present in an oxidising atmosphere, Ag_2SO_4 is present, but this decomposes between 650 °C and 700 °C and FactSage® predicted that all silver would join the FCC solid solution phase. The SEM-EDS work on the 900 °C sample found some Ag associated with the oxidised As, Pb, Ni, Fe, Cu phase. Results from the stationary bed roasting test work showed that some Ag losses might start to occur at the high temperature of around 1 000 °C. The fluidised bed roasting results are extremely variable, and it is not clear whether the results might be influenced by sampling or analytical errors.

5.3.3 Discussion of the behaviour of Pb compounds

The experimental results show that Pb is not volatile during the roasting process in the temperature range studied. Since Pb is a contaminant in the PMR feed, the subsequent smelting step needs to target the removal of lead.

Anglesite ($PbSO_4$) was detected in the feed sample with XRD (Table 16), but the Anglesite peak disappears at around 800 °C. The 'Normal' system Factsage® predicts that Pb will be stable only as a sulphate or an oxy-sulphate that will decompose at around 1 040 °C, which is higher than the roasting temperatures studied.

Thermodynamic modelling does not predict that the presence of a solid solution matrix will have any effect on the Pb decomposition, as Pb does not dissolve into the FCC solid solution. The SEM-EDS analyses on the sample roasted at 900 °C confirmed that Pb is present in an oxidised As, Cu, Ni, Fe phase.

Neither the near complete removal of S to the gas phase above 800 °C, nor the disappearance of the Anglesite peak at 800 °C, support a stable lead sulphate presence. In the absence of a heat stable sulphate phase, Pb will most probably be present as an oxide. Lead monoxide (PbO) is more stable at the roasting temperatures investigated, with PbO_2 decomposing to PbO.

5.3.4 Discussion of the behaviour of stable oxide compounds

Table 33 shows the stable oxides' weight percentage content as a function of temperature, according to FactSage® modelling.

Table 33: FactSage® prediction of stable oxide speciation in third stage residue as a function of temperature (wt%)

Compound	600 °C	650 °C	700 °C	750 °C	800 °C	850 °C	900 °C	950 °C	1 000 °C
$CuSO_4$	10.8	10.8	0.0	0.0	0.0	0.0	0.0	0.0	0.0
$NiSO_4$	8.0	8.0	8.0	8.0	8.0	0.9	0.0	0.0	0.0
Fe_2O_3	5.2	7.4	7.4	0.0	0.0	0.0	0.0	0.0	0.0
SiO_2	0.0	0.0	0.0	0.0	0.0	0.0	2.9	2.9	2.9
$MgSiO_3$	0.0	0.0	0.0	0.0	0.8	0.8	0.8	0.8	0.0
Ni_2SiO_4	0.0	0.0	0.0	0.0	0.0	0.0	0.6	0.6	0.6
$MgSiO_3$	0.0	0.0	0.0	0.0	0.0	0.0	0.0	0.0	0.8
$(NiO)(Fe_2O_3)$	0.0	0.0	0.0	0.0	0.0	10.8	10.8	10.8	10.8
$(CuO)(Fe_2O_3)$	0.0	0.0	0.0	11.0	11.0	0.0	0.0	0.0	0.0
$(CoO)(Cr_2O_3)$	0.0	0.3	0.3	0.3	0.3	0.3	0.3	0.3	0.3
$(MgO)(Cr_2O_3)$	0.0	0.0	0.0	0.3	0.3	0.3	0.3	0.3	0.3
$Mg_2Al_4Si_5O_{18}$	0.0	0.0	1.4	1.4	1.4	1.4	1.4	1.4	1.4

There are a number of stable oxides in the third stage leach residue, namely the oxides of Si, Cr, Fe, Ni, Cu, Ca, Al and Mg. Table 33 shows some of the major oxide species as they go through phase changes when the temperature increases. Firstly, the Cu and Ni sulphates decompose to leave Ni

and Cu free to form stable oxides. In the case of Ni, most Ni ends up as Trevorite in the spinel structure $NiO.Fe_2O_3$. The SEM EDS work on the sample roasted at 900 °C confirmed the presence of trevorite type spinels. However, Ni was found in an abundant oxidised phase of As, Pb, Ni, and Cu. In the case of Cu, the spinel structure $CuO.Fe_2O_3$ disappears and Cu joins the FCC solid solution phase between 800 °C and 900 °C, according to FactSage®. SEM EDS analysis on the sample roasted at 900 °C did not show any Cu in the metallic FCC solid solution phase, which primarily consisted of Pt, Pd and some Rh. SEM EDS showed that Cu was distributed consistently in the As, Pb, Fe and Ni rich phase.

The measurement in Table 16 of 38% trevorite spinel phase could be explained if another spinel type phase was refined (through the Rietveld refinement software) as trevorite. The oxidised As, Pb, Ni, Fe and Cu phase observed in the SEM work could potentially have been refined as trevorite, as it is rich in Fe, Ni and O. In the geoscience field, several studies have shown that both Ru and Rh are highly compatible and can be incorporated into spinel structures. For example, the phase $CuRh_2O_4$, $Mg(Rh,Ru)_2O_4$, $Cr(Rh, Ru)_2O_4$ has the spinel structure and can form when Rh and Ru is present under conditions where spinel type structures are allowed to crystallise (Capobianco *et al.*, 1990). These PGM containing spinels can be prepared by reacting Ru and Rh metal with an oxide phase, if left at temperature (1 000 °C to 1 450 °C) for sufficient time, normally some days. $CuRh_2O_4$ can be prepared by mixing cupric nitrate with solid Rh_2O_3, drying and annealing it between 700 °C and 900 °C (Ismunandar *et al.*, 1999). Spinel phases, especially chromite, are known to be concentrators of Ru and Rh (Jung-Woo Park *et al.*, 2012 and Righter *et al.*, 2004). The presence of the ferric ion (Fe^{3+}) improves the portioning of Ru to the spinel phase (Brenan *et al.*, 2012). SEM EDS work confirmed the presence of small amounts of Ru and Rh (between 1% and 3%) in the oxidised As, Pb, Ni, Fe and Cu phase. No Ru or Rh was measured in any of the inclusions that had a clear spinel form and stoichiometry.

If Ru or Rh is incorporated in the refractory spinel phase, it will affect the leachability in subsequent dissolution steps. The smelting step that is to follow the roasting step in the proposed pyrometallurgical process will decompose/dissolve spinels and collect the PGMs in an alloy phase.

Silica (SiO_2) will have the opportunity to recrystallise at roasting temperatures. The quartz phase is stable between room temperature and 867 °C, after which the phase transformation to tridymite will take place. The phase transformation to cristobalite will take place only at 1 465 °C and the measurement of cristobalite in Table 16 might be explained by the fact that cristobalite, although metastable, forms in preference to tridymite in high temperature experiments, even in the stability range of tridymite. The presence of silica is consistent with routine assaying of BMR concentrate and originates when slag is imperfectly separated from matte during converter matte granulation prior to BMR processing.

5.4 Conclusion

Roasting of PGM concentrate in air at temperatures between 800 °C and 900 °C is an effective way to remove volatile impurities, namely Se, Te, S, Os and As, with varying efficiency. Thermodynamic equilibrium modelling proved to be a useful tool to estimate the behaviour of most elements and minerals. Further investigation is merited into the poor extent of removal of Osmium and Arsenic from the BMR residue, the speciation of Pb and the potential inclusion of Ru and Rh in the spinel

phase. The multi-element complex nature of the pressure leach residue and the complex transitions that occur during heating and roasting make the analyses of results extremely complex, so that a combined approach of thermodynamic modelling, XRD, SEM-EDS and SDTA is required to de-convolute the complexity of the materials and the thermochemical transitions. The amorphous nature and very fine particulate sizes of a leach residue from an oxidative pressure leach step makes the identification of mineral speciation and association very difficult.

Iridium, Rhodium, Ruthenium and Palladium tend to oxidise at the lower temperatures. The dissociation temperature of Rh appears to be influenced by the presence of a metallic FCC solid solution phase that has time to crystallise at roasting temperatures. Although the vapour pressures of the PGM oxides are several orders of magnitude higher than those of the metal form (apart from Palladium), no losses of the PGMs to the vapour phase were measured. Further refining of the calcine from the roast would be possible during a smelting stage, as is discussed in the next chapter (chapter 6).

It is also possible to use air as the oxidation medium, which would be inexpensive and simpler to implement industrially. Stationary bed roasting can achieve volatilisation similar to that of fluidised bed roasting, though with slightly longer contact times required. Stationary bed roasting allows the use of simple equipment, such as multiple tray calciners, without the need for complex and expensive capture and recycling of particulate matter.

The advantage of a roasting step is that the PGMs will remain in the solid phase throughout the roast and their behaviour is relatively insensitive to control parameters (time, narrow temperature range and oxidising environment), unlike the current caustic leach used in the BMR process, where the process parameters such as pH, free caustic concentration and time require careful control.

Chapter 6: Smelting

This chapter will discuss the results of the smelting modelling and test work.

6.1 Introduction and background

For clarity, the flow sheet of the envisaged pyrometallurgical refining process is repeated. Figure 23 shows the position of the smelting step discussed in this chapter by a dashed yellow ellipse.

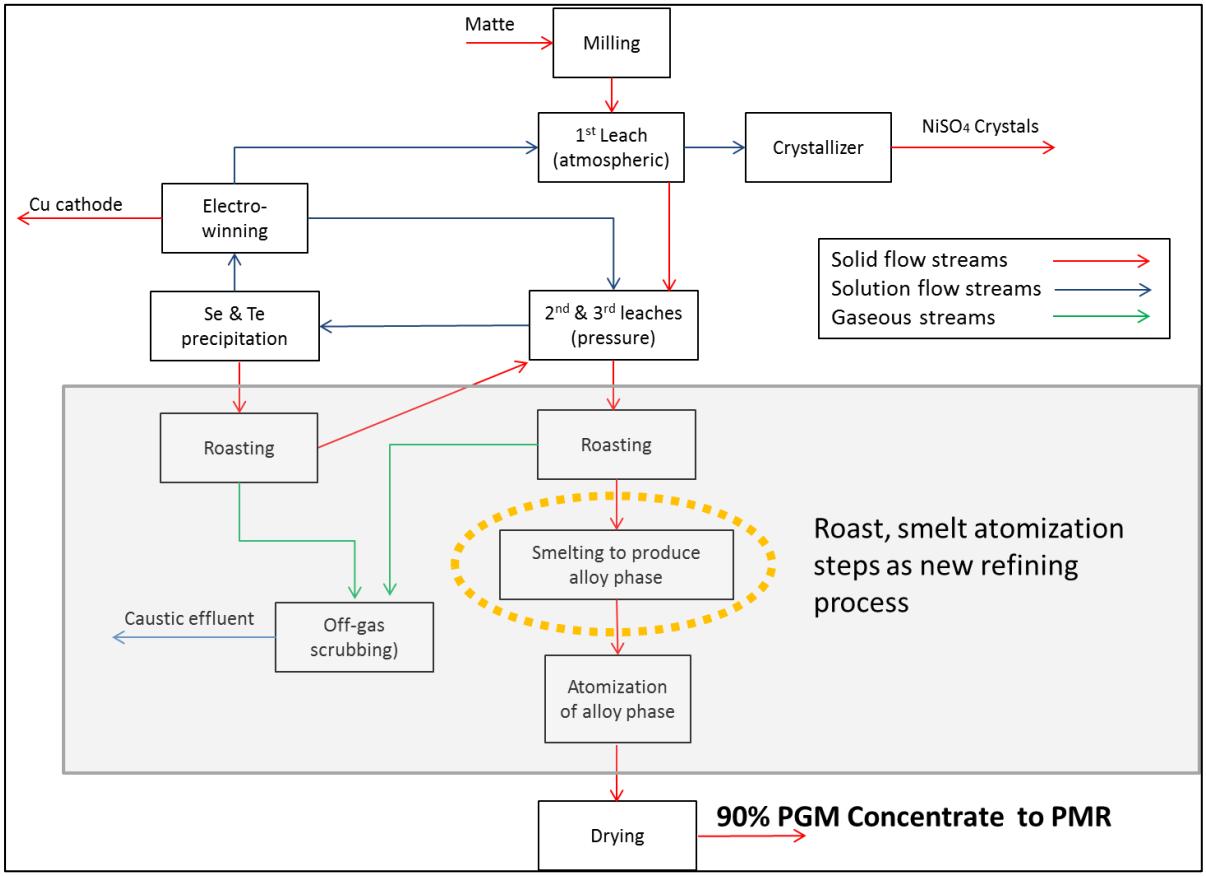

Figure 23: Block flow diagram of the proposed pyrometallurgical process that can be implemented between the BMR and PMR processes in order to remove contaminants from the PMR feed. The smelting step discussed in this chapter is shown by the dashed yellow ellipse

Smelting was envisaged as part of the flow sheet to remove contaminants, as it was perceived that a number of objectives could be met with a single step. These are listed below:

- A number of oxides are stable through the BMR process and therefore have poor control steps. Smelting provides the easiest method to control stable oxides in the third stage residue. SiO_2 content in third stage residue varies between 1% and 5% by mass, but can at times spike to 10%. SiO_2 hydrolyses in the PMR dissolution step and forms gels that complicate filtering in the PMR. SiO_2 originates from the smelter operation and is inert in the BMR process. Smelting to remove SiO_2 will act as a control step to stabilise PMR operation. Cr, Mg, Ca and Al oxides are present in third stage residue, typically amounting to between

1.5% and 2% of the weight content. Fe and Ni in the spinel phase are present in the third stage leach material and typically amount to 5% to 10% by weight. With proper slag design and redox control, it would be possible to absorb all the stable oxides in the slag phase and remove them from the PMR feed.

- Thermodynamically it is possible to stabilise almost all Fe and Ni and about half the Cu to the slag phase, without any associated PGM loss.
- Thermodynamically it is possible to remove most of the Pb to the slag/gas phase and about half of the As to the slag phase with a smelting step.
- The PGMs (especially the OPMs) need to be present in their metallic state to ensure rapid and complete dissolution in the HCl/Cl_2 step. PGMs that are partly oxidised or hydrolised show poor dissolution behaviour. The smelting step produces an alloy that contains all the PGMs in their metallic state.

Although the conceptual process (from Figure 23 above) was for smelting to follow roasting, a number of different processing routes were studied. This was done in order to test some of the hypotheses that were set for the smelting step in Chapter 2. The learning from the different systems proved insightful and complemented the conclusions drawn at the end of the chapter. Although the final recommendation is still for smelting to follow roasting (as in the original concept), the results are included in this chapter (and not an Appendix) since the results complement the understanding of the process and the conclusions drawn.

Figure 24 shows the four different smelting systems that were studied. The system names corresponding to the numbers shown in Figure 24 are given below:

1. Direct smelt of third stage residue.
2. Roast-Smelt of third stage residue.
3. Leach-Roast-Smelt of third stage residue.
4. Roast-Smelt of third stage residue with Cu addition.

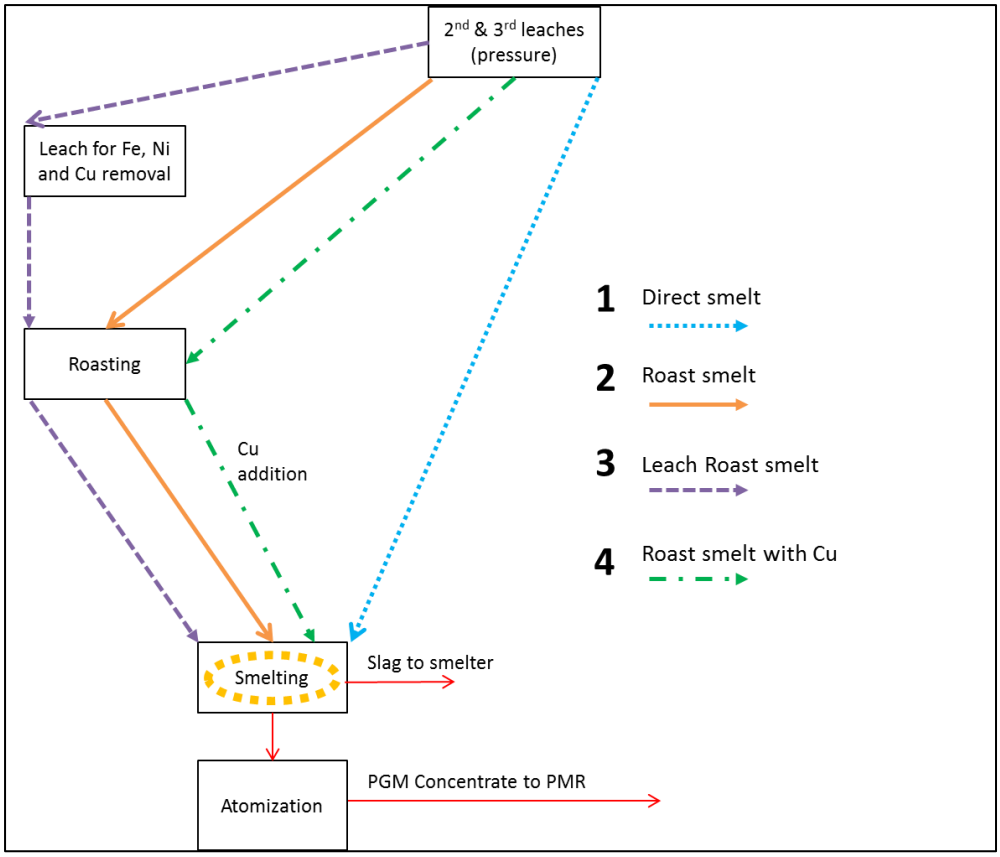

Figure 24: Block flow diagram to illustrate the four different types of smelting studied. The smelting step investigated is shown by the dashed yellow ellipse

1. It is possible to smelt third stage leach residue without any prior treatment. Some experiments were done to understand this option and the removal of Se, Te, As and S across a smelting step.
2. The roasting step (as discussed in Chapter 5) removes Se, S and partially removes As, Te and Os in a controlled environment, without any associated PGM losses. Smelting tests were performed on the roasted calcine to see if the contaminant removal would proceed to the extent predicted by modelling (as shown in Chapter 2). These tests are abbreviated to Roast-Smelt in the text.
3. Poor removal of Fe, Cu, Ni, As and Pb was found in the first experimental melts on roasted third stage leach residue (discussed in section 6.2). It was decided to see whether a leaching step could remove some of these contaminants prior to the smelting step. Leaching tests were performed on unroasted and roasted material. Leaching with formic acid and sulphuric acid on unroasted material showed good promise for the removal of Fe, Ni and Cu (discussed in Appendix A). It was decided to use this leach as a control step for Fe, Ni and Cu and thereafter to proceed with the roast to control S, Se, Te, As and Os. Smelting tests were performed on material prepared by leaching, followed by roasting. These tests are abbreviated to Leach-Roast-Smelt in the text.
4. A decision was taken to investigate whether Cu could be used to change the smelting behaviour of the system. These tests are abbreviated to Roast-Smelt with Cu addition in the text. Precious metals recovery from Waste Electrical and Electronic Equipment (WEEE) has

traditionally been done by refiners with Cu smelters (like Umicore), since Cu is often present in high quantities in WEEE, together with precious metals. Johnson (2012) reports that small and dedicated plasma arc furnaces are also used to collect precious metals in a Cu alloy (from sources like WEEE, spent auto catalytic converters and other secondary sources). The motivation for using Cu as collector was based on the following two reasons:

- The alloying effect of Cu should lower the liquidus temperature of the alloy system to a significant degree. It was envisaged that smelting could be performed at about 1 300 ˚C. Figure 25 shows the Cu-Pt and the Cu-Pd binary phase diagrams. Pt and Pd would be the biggest contributing elements in the alloy, therefore they are a good indication of the expected benefits as regards melting temperature. This lower temperature would allow the use of borate based slag, which is vastly superior to the SiO_2-Al_2O_3-CaO-Na_2O based slag used at higher temperatures, in its capacity to absorb spinel phases. The lower temperature also held the promise of less crucible interaction with the melt.

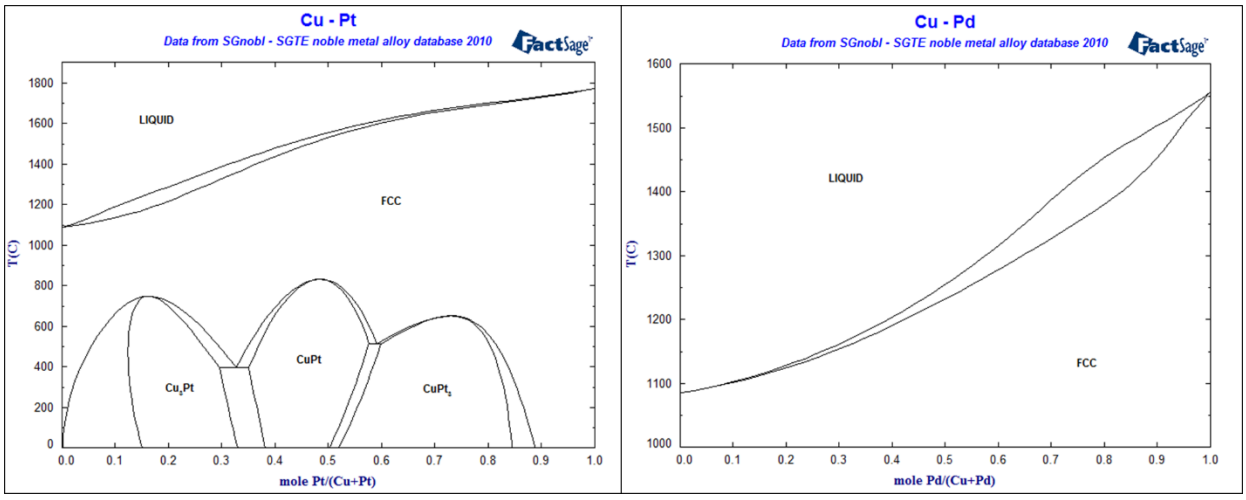

Figure 25: The binary phase diagram for Cu-Pt and Cu-Pd as generated by the FactSage® SGnoble (2010) database. The potential for Cu to lower the liquidus temperature of the alloy is clearly evident

- Cu could serve as a buffering element between the PGMs and Fe, Ni, As and Pb. It was envisaged that better redox control would be possible, in order to force Fe, Ni, As and Pb to the slag phase (discussed in section 6.2). Figure 26 shows the Ellingham diagram for the oxidation of the metals in their liquid state to their respective oxides. The Cu oxidation line lies between those of Fe, Ni, Pb, As and that of Ru (which is the first PGM that will oxidise). Cu would therefore be the best choice to allow for the near complete removal of Fe, Ni, As and Pb, without oxidising Ru.

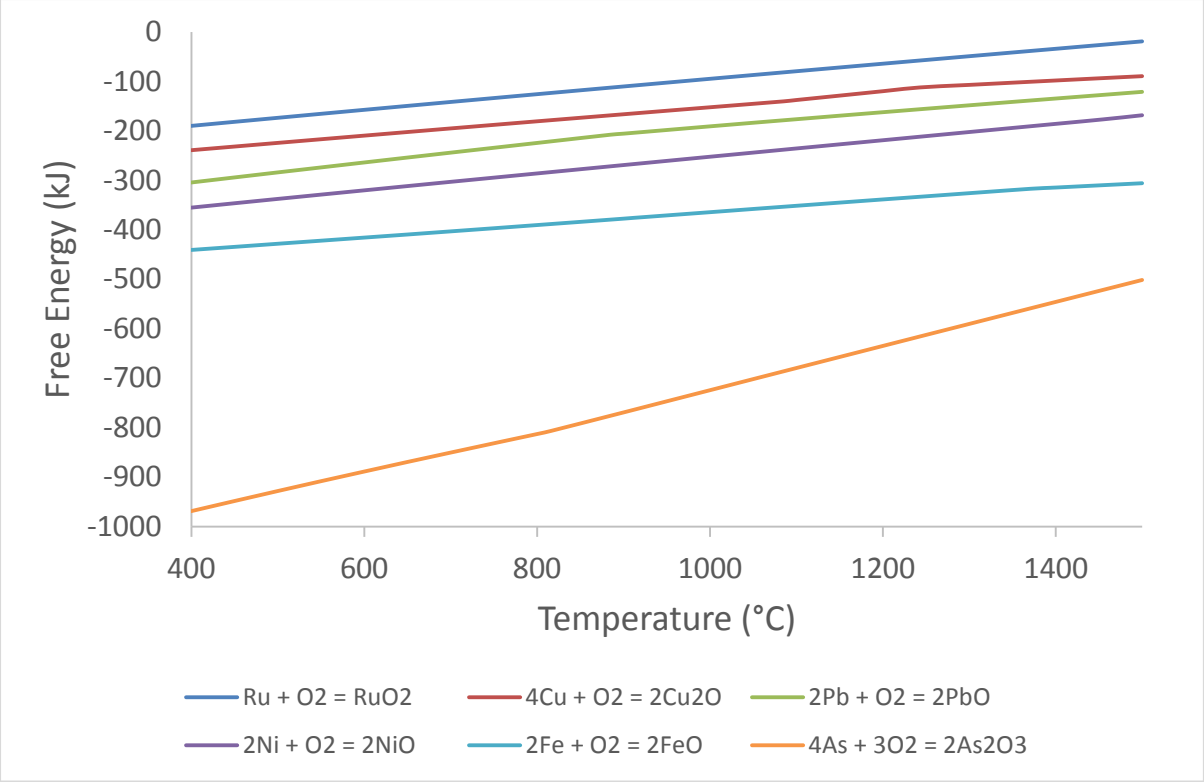

Figure 26: The Ellingham diagram showing the standard state oxidation of the following metals: Ru, Cu, Pb, Ni, Fe and As. The diagram shows that oxidation of Cu falls between the oxidation of Ru and that of the rest of the metals

6.2 Results and discussion of smelting test campaigns

This section will discuss the results obtained from the test work and interpret them based on modelling and literature. The first section will discuss the inability to control the redox potential (expressed as partial pressure of oxygen, or pO_2) in the experimental set-up, using the Roast-Smelt system as example. Thereafter a discussion will follow on the results for each of the four systems investigated.

6.2.1 General note on the ability to control smelting parameters

It is good to understand the sensitivity of the system to a number of drivers or variables. Unfortunately the experimental set-up was unable to clearly illustrate these sensitivities, so the following discussion will be theoretical, while comparing the actual results and thereby illustrating the shortcomings of the experimental work. In order to simplify the discussion, this section will focus only on the Roast-Smelt system, where third stage leach residue was roasted at 900 °C for six hours before proceeding to the melting step).

The main input variables, established through FactSage® modelling, are given below:

- Reduction/oxidation (redox) potential in the melt, normally expressed as partial oxygen pressure, pO_2 in atmosphere
- Temperature

- Pressure
- Slag composition and characteristics, which will influence the choice of flux addition for the make-up of the starting slag.

Effect of oxidising/ reducing atmosphere

The key to upgrading the third stage roasted residue to a maximum PGM content without experiencing associated PGM losses is to control the reducing or oxidising atmosphere in the melt. It is thermodynamically possible to preferentially oxidise most of the contaminants and thereby remove them to the slag and/or gas phases, without experiencing PGM losses.

Some oxygen is available in the feed material, as most of the reducible metals (Fe, Ni and Cu), stable oxides (Si, Ca and Al) and the OPMs (Ru, Rh, Ir) are associated with oxygen, especially after roasting. Thermodynamic modelling predicts that up to 1.4% losses of Ru can be experienced during heating to 1 500 °C if the roasted product is not mixed with a reducing agent. For this reason a carbohydrate (sugar) was mixed with the feed material to ensure that the initial conditions in the melt would allow Ru reduction to the metal state by reacting with excess oxygen during smelting. However, preventing Ru losses by adding the reducing agent will force most of the Cu, some Ni and limited Fe to the alloy phase. For this reason, an oxidation ($NaNO_3$) addition at the end of the melt was envisaged, which would oxidise some of the Cu and most of the Fe and Ni to the slag phase.

The restriction of having to use a receptive crucible material while maintaining temperatures of 1 500 °C in the melt, forced the use of graphite as a crucible material. It was clear from the recoveries of several metals that the crucible participated in the melt by introducing local reducing conditions at the crucible/melt surface. The addition of an oxidising agent did not prove to be an adequate method to limit recovery of Cu, Ni and Fe to the alloy phase. Control of the reducing or oxidising conditions could therefore not be achieved with the experimental set-up to the extent that had been hoped for.

Table 34: Metal recovery to the alloy phase at 1 500 °C as a function of initial reducing or oxidising environment

Element	7 g Reducing agent addition with cold feed. Addition of 5 g oxidising agent after 15 minutes at temperature	No initial addition. Addition of 15 g oxidising agent after 15 minutes at temperature:	Recoveries to alloy phase with thermodynamic modelling between 1 x 10^{-8} and 1 x 10^{-9} oxygen partial pressure
Ru	100%	100%	100%
As	88%	85%	99%
Pb	60%	54%	43%
Cr	23%	29%	3.8%–45%
Fe	88%	83%	90%–98%
Ni	100%	100%	100%

Table 34 shows that from the experimental results no distinguishable difference could be determined as being based on the addition of a reducing/oxidising agent. An experiment was run with the addition of an oxidising agent (instead of a reducing agent) to the cold feed material, but

not even this showed any distinguishable Ru loss. This finding indicates that Ru losses probably do not proceed as the RuO_2 is heated. It is possible that the heating rate allowed Ru dissociation from oxygen and dissolution into the alloy phase before there was sufficient time for the RuO_2 to oxidise to RuO_3. Table 34 also shows that no distinguishable difference could be measured for Fe and Ni, which both showed recoveries close to 100% to the alloy phase. This would only be possible if the reducing capacity of the crucible had participated in the melt. Even with high addition ratios of $NaNO_3$ (15 g $NaNO_3$ per 100 g feed material) and short melting times (10 minutes), the Fe and Ni recoveries to the alloy were close to 100%, pointing to the fact that the reducing environment created by the crucible interaction dominated recoveries. Arsenic and Pb will be discussed below, but their high recoveries also points to the crucible interaction creating reducing conditions. The extent of crucible interaction is largely scale dependant, with the small size of the melt in the relatively large crucible forcing high interaction. If larger scale tests could be done and the size of the batch increased, the contribution of the crucible material would decrease, as the bulk mass increases much faster than the mass of melt in contact with the crucible surface.

Fe, Ni and Cr recoveries to the alloy phase are a good indicator of the redox potential that was achieved in the system. Figure 27 below shows how reduction would proceed for Cu, Ni, Fe and Cr. Cr would start joining the alloy phase after the bulk of the Fe has already joined. Fe recovery to the alloy phase of between 83% and 88% was measured, while Cr recovery to the alloy phase of 23% to 29% was measured. Back-calculation of these recoveries with FactSage® puts the oxygen partial pressure (pO_2) of the system at between 1×10^{-10} atm and 1×10^{-8} atm. The consistent results in the same narrow band of recoveries (despite the addition ranges) indicate that the graphite crucible/melt interaction dominates and fixes the redox potential of the system. The net effect of the experimental set-up was that a 6E grade of 75% could be achieved in the alloy phase. The reason for this was primarily the presence of Fe, Ni and Cu that amounted to 15% of the alloy weight. Modelling showed that a theoretical 6E grade of 92% was possible, through perfect redox control without any associated PGM loss.

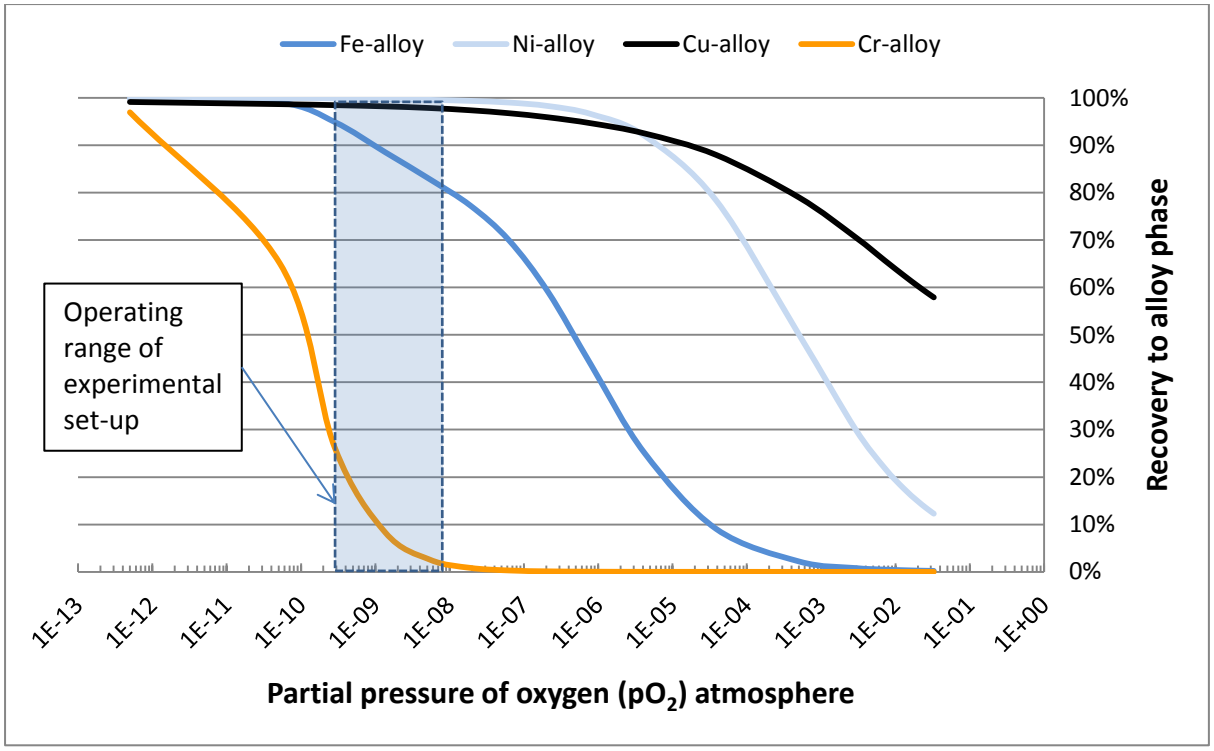

Figure 27: Cu, Ni, Fe and Cr recovery to the alloy phase at 1 500 °C as a function of partial oxygen pressure (pO_2), according to thermodynamic modelling

Pb and As are the major contaminant phases in the roasted product feed, apart from Fe, Ni and Cu. A more reducing atmosphere would increase the recovery of both As and Pb to the alloy phase, limiting partitioning to the slag phase as an oxide. Pb and As amounted to four weight per cent of the alloy content. The effect of the redox potential on these two elements will be discussed by using four modelled scenarios, which clearly show the sensitivity of partitioning to the redox potential.

Figure 28 shows the As partitioning to the alloy, slag and gas phases for the four modelled scenarios. When roasted material is smelted without any addition, 58% of the As will partition to the slag phase as As_2O_3. With a small addition (5 g $NaNO_3$ per 100 g feed material) of oxidising agent, the As partitioning to the slag phase can be increased to 71%. When the redox potential becomes slightly more reducing with carbohydrate addition (7 g carbohydrate per 100 g feed material), all the As partitions to the alloy phase. When the environment becomes very reducing (for instance, at the melt/ graphite crucible wall, simulated by 8 g C addition per 100 g feed material), As can volatilise as As or AsN gas species. This more reducing condition condition is represented as 'C crucible interact' in figures 28, 29 and 30. Actual As deportment to the alloy phase of 85% to 88% was measured for all the different scenarios, pointing to an insensitivity and lack of control over the redox environment. If, however, better control over the redox potential were possible, significant removal of As from the alloy phase to the slag phase should be possible.

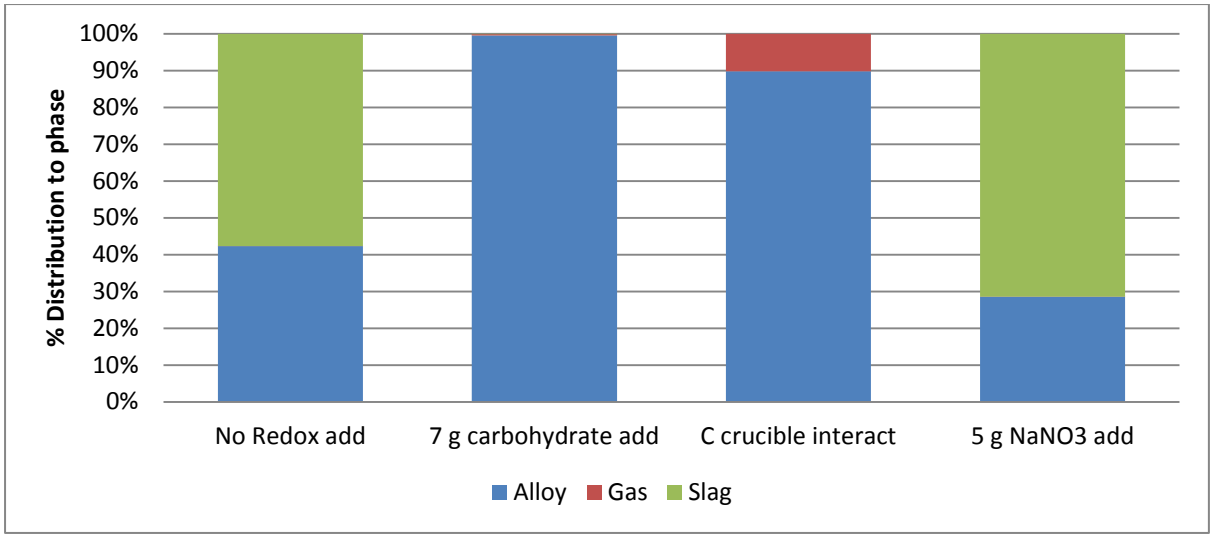

Figure 28: Arsenic partitioning to alloy, gas and slag phase at 1 500 °C for the different redox potential scenarios, according to thermodynamic modelling

The same approach as that described for As was followed to understand Pb partitioning. Figure 29 shows that 95% Pb partitioning to the slag and gas phases could be achieved if the roasted material were directly melted. Pb can partition to the slag phase as PbO or to the gas phase as both Pb and PbO, although the partitioning to the gas phase as PbO will dominate at 1 500 °C. Both PbO and Pb are volatile at high temperatures (1 500 °C) and the ratio of the volatile species of Pb will be determined by the redox potential. In a mildly reducing environment (7 g carbohydrate addition) Pb is stabilised in the melt, with around 43% recovery modelled to the alloy phase, compared to actual measured recoveries of 54% to 60%. At more reducing conditions (C crucible interaction) Pb vapour pressure dominates Pb removal to the gas phase. If the crucible did not interact and oxidising agent addition (in this case $NaNO_3$) were able to influence the redox potential, Pb recoveries to the alloy phase as low as 3% could be achieved, according to thermodynamic modelling.

Pb recovery to the alloy phase was found to be consistently higher than the modelled values, while the Pb content measured in the slag phase was always very low. This observation points to the fact that Pb vaporisation did not proceed to the extent predicted by modelling, forcing the Pb partitioning to the alloy phase. Pb vaporisation will be discussed under 'pressure control' later in this same section.

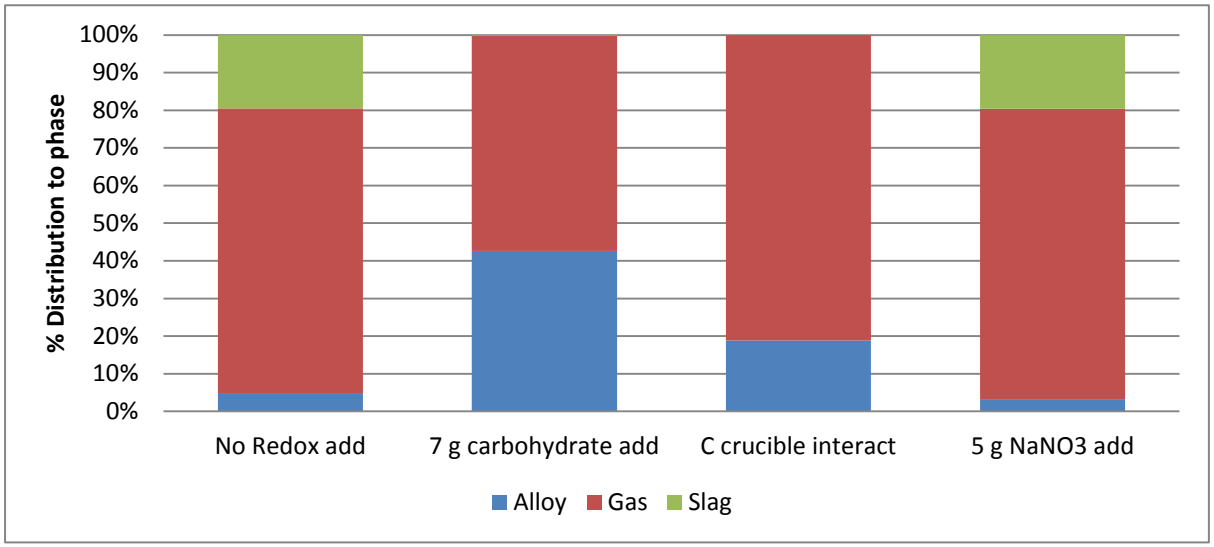

Figure 29: Lead partitioning to alloy, gas and slag phases at 1 500 °C, according to thermodynamic modelling of the different redox potential scenarios

Figure 30 shows that Ruthenium losses to the gas phase are driven by the oxidation potential of the system. Although no Ru losses were measured, modelling predicted that up to 1.4% losses could be expected to the gas phase during melting with no addition and 5% losses to the gas phase could be expected with the addition of an oxidising agent during melting. The melting profile in the experimental set-up took around 20 to 30 minutes to bring all the material to 1 500 °C. The fast heating rate probably allowed Ru dissociation from oxygen, which was achieved at 1 470 °C, and partial dissolution to the alloy phase before measureable losses of Ru to the gas phase occurred. Furthermore, during this time some interaction with the crucible wall would already have proceeded and loosely bound oxygen would have been partially removed from the system.

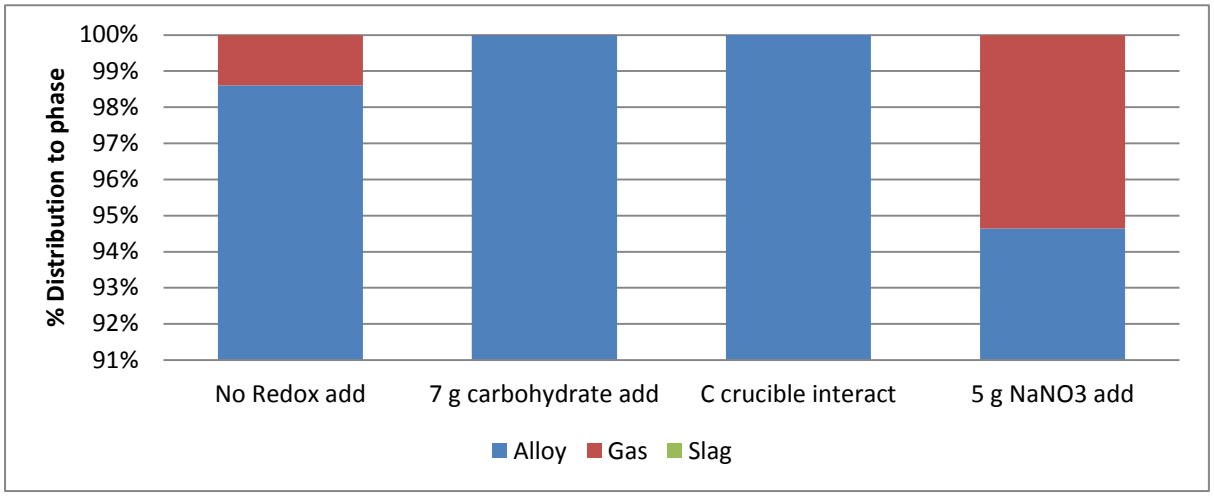

Figure 30: Ruthenium partitioning to alloy, gas and slag phases at 1 500 °C, according to thermodynamic modelling of the different redox potential scenarios

Effect of Temperature

Several melts were performed between 1 300 °C and 1 650 °C in an induction furnace on the Roast-Smelt system. The temperature at which the entire melt (slag and alloy phase) appeared molten was based only on visual observation. From visual observation, the melt appeared to be fully liquid in the temperature range 1 400 °C to 1 500 °C, but probably close to 1 450 °C. However, visual observation at high temperature can be misleading and inaccurate, as it is difficult to detect solid suspension in the molten phase.

Based on the findings of the redox potential results, modelling was done with a roasted product feed at a partial oxygen pressure of 2 x 10^{-8} atm. Thermodynamic equilibrium modelling predicted that the liquidus temperature of the alloy phase would be 1 230 °C if solid solution phases were not activated and 1 816 °C if solid solution phases (FCC structures) were allowed to form during slow melting in an inert environment. When the binary and ternary phase diagrams of the noble metals (Au-Pt-Pd-Rh-Ru-Ir) are studied, heat stable solid solution phases are found in all of them. Furthermore, binary noble metal phase diagrams do not display eutectic behaviour. Solid solution phases were noted in the SEM work performed on the BMR third stage residue that was roasted at 900 °C and this material served as feed to the melt. However, the solid solution phase observed in the roasted sample was mostly limited to a Pt-Pd-Au-Rh phase, while Table 35 shows that the last phase to melt at 1 816 °C would contain a large array of metals, especially Ir and Ru.

Table 35: Solid solution phase composition (wt%) for roasted product and final solid solution to join the melt

Element	Roast Product Solid Solution composition	Final Solid Solution composition to join melt
Ir	0%	11%
Os	0%	5%
Pd	35%	3%
Pt	45%	34%
Rh	5%	10%
Ru	5%	28%
Ni	0%	3%
Fe	0%	5%

As the heating profile during smelting is quite fast (30 minutes from ambient temperature to 1 500 °C), there would not be an opportunity for higher melting solid solution phases to recrystallise, and the observed liquidus temperature of 1 450 °C was between the modelled values of 1 230 °C and 1 795 °C. The formation of heat stable solid solution phases points to a temperature ramp-up profile sensitivity, with very slow heating not being favoured. SEM work done on the alloy produced from melts at 1 500 °C confirmed that no solid phases remained in the alloy.

The modelled and actual melting points were in a reducing environment of an oxygen partial pressure of approximately 2 x 10^{-8} atm. If the roasted product had to be smelted in an inert environment, resulting in a pO_2 of around 2 x 10^{-2} atm, modelling showed that the melting temperature would increase by a least 100 °C, but possibly by as much as 170 °C. The Solid Solution phase dissolves more easily into the liquid alloy phase at higher reducing potentials, probably due to the higher alloying content of particularly Fe and Ni.

Table 36 provides actual recovery results to the alloy phase for a number of tests performed with temperatures varying from 1 400 °C to 1 500 °C. Pd has the highest vapour pressure of the PGMs in its metallic state (Jehn, 1984), but no Pd losses could be detected up to 1 500 °C. Ru recoveries were not consistent and no trend was evident over the temperature range. Modelling did not predict Ru losses in the reducing atmosphere maintained in the melt.

Ag and Pb would display increased volatile behaviour as the temperature increased and this is consistent with the actual measurements. The effect of temperature on Fe and Ni partitioning to the alloy phase is limited, with partitioning already high to the alloy phase, driven primarily by the redox potential. The higher recovery of Cr to the alloy phase at the lower temperatures (1 400 °C and 1 450 °C) was not consistent with the modelling. At the temperatures lower than or close to the estimation of liquidus temperature (1 450 °C), some unmolten material might be left in the melt. The slag capacity for a stable chrome spinel and the reducing capacity of the crucible interaction will both be lower at the lower temperature, further limiting the absorption of the chrome spinel in the slag. It is suggested that the Cr partitioning is not true Cr reduction to the alloy phase, but rather an unmolten chrome spinel with sufficient density to be separated with the alloy button, thereby lifting the Cr content of the alloy. The presence of a Fe-Cr spinel phase was confirmed through SEM work.

The higher recovery of As to the alloy phase at lower temperatures is not consistent with the modelling, and no explanation can be offered for this behaviour.

Table 36: Experimental results of metal recovery (wt%) to the alloy phase as a function of temperature

Element	1 400 °C	1 450 °C	1 500 °C
Pd	100%	100%	100%
Ru	100%	94%	100%
Ag	95%	92%	87%
Fe	82%	90%	90%
Ni	100%	100%	100%
Cr	60%	66%	37%
As	100%	93%	85%
Pb	74%	62%	53%

Effect of pressure

From the first set of experiments it became clear that the recovery of Pb to the alloy phase was higher than the target values. A number of experiments were planned to test whether a partial vacuum would improve the removal of Pb to the gas phase. Thermodynamic modelling predicted that Pb recovery to the alloy phase could be decreased from 42% to 18% by applying a vacuum of 0.3 atmosphere pressure absolute to the melt system. The vacuum chamber was kept at an absolute pressure of 0.3 atmospheres for 30 minutes. Table 37 shows that the pressure chamber did not achieve Pb removal from the alloy. The actual Pb recovery to the alloy phase was higher in the lower pressure melts.

Table 37: Measured results of Pb recoveries to the alloy phase

Element/ Parameter	1 Atmosphere absolute	0.3 Atmosphere absolute
Pb	52%	62%
Cr	27%	75%
Fe	81%	98%
Total time at temperature	20 min	60 min

Pb removal at higher temperatures and reduced pressures was studied by Yoshida *et al.* (1999) from a Cu melt. They found that Pb evaporation follows the first order reaction rate and that the reaction constant is proportional to the reciprocal of the total pressure in the reactor and independent of the stirring condition. However, they found slow evaporation rates for Pb and concluded that mass transfer in the gas phase was the rate-limiting step. The reason for the insensitivity of Pb recovery to the pressure of the system is probably linked to the short time of only 30 minutes that the system was subjected to low pressure.

The total time that the melt was kept at temperature was increased from 20 minutes to 60 minutes by the introduction of the vacuum controlled step (a few minutes to draw a vacuum, 30 minutes at vacuum and some minutes to break the vacuum). From the higher Cr and Fe recoveries to the alloy phase at the longer melting times with the pressure control step, it is clear that the interaction of the crucible wall with the melt continued to reduce Fe and Cr to the alloy phase as time passed.

Slag viscosities

Slag viscosity is a function of temperature, with the viscosity decreasing as the temperature increases. A low viscosity in the slag phase is important to allow the alloy phase to drain and separate. The viscosity of the slag is made up of two parts: 1) the viscosity of the liquid portion of the slag, which was determined using the Viscosity module in FactSage® 6.2. and 2) the increased viscosity due to suspended solid particles in the slag, which was calculated by the Einstein-Roscoe equation as presented by Zhang *et al.* (2001) for up to 33 mass % solids (shown by equation 1).

The Viscosity module in FactSage® 6.2 uses a method to calculate the liquid viscosity of single phase slags and glasses. It is distinct from other viscosity models in that it directly relates the viscosity to the structure of the melt, and the structure, in turn, is calculated from the thermodynamic description of the melt using a Modified Quasichemical Model. The model has been checked against the experimental data available for Al_2O_3-B_2O_3-CaO-FeO-Fe_2O_3-K_2O-MgO-MnO-Na_2O-NiO-PbO-SiO_2-TiO_2-Ti_2O_3-ZnO-F melts and for Al_2O_3-B_2O_3-CaO-K_2O-MgO-Na_2O-PbO-SiO_2 glasses. In this study, the database for melts was used for the CaO-SiO_2-Al_2O_3-Na_2O slags, while the database for glasses was used for the B_2O_3- SiO_2-Al_2O_3-Na_2O type slags.

The roasted product feed contained a significant quantity of spinel phase (38% weight percentage measured by XRD). These spinel phases need to dissolve into the slag phase and higher temperature and reducing potential would improve the solubility. Thermodynamic modelling showed that the last of the spinel phase would only dissolve between 1 550 °C and 1 700 °C in inert to slightly reducing melting environments. The presence of solid spinel phase would increase the viscosity, according to equation 3.

$$\eta = \eta_0 (1-af)^{-n} \qquad (3)$$

where η and η_0 are the viscosity of the solid-containing and solid-free melt, respectively. The parameters a and n are constants, while ƒ is the mass fraction of solids in the melt. The value of the constants a and n is dependent on the particle size of the solids within the melt. The values of a=3.0 and n=2.5 were determined by Zhang *et al.* (2001) for spinel particles, which are the predominant solid particles in the studied slags.

The composition of the slag has a large effect on the viscosity, and the presence of Fe_xO, NiO, CuO and CrO will all serve to lower the viscosity. As the melt progresses and the slag comes into contact with the crucible wall, these easily reducible oxides are reduced and join the alloy phase, thereby removing them from the slag phase and increasing the viscosity. Visual observation indicated that the slag phase appeared to be quite liquid (like boiling water) at 1 500 °C, but the viscosity increased as the melt progressed, becoming like boiling syrup. A further contribution to the increased viscosity that was noted in the melt as time progressed was the loss of Na from the slag in a reducing

environment, primarily in the form of Na vapour. FactSage® predicted between 8% and 12% Na mass loss to the gas phase at an oxygen partial pressure of between 10^{-8} and 10^{-9} atm. During the experiments where a vacuum was drawn down to an absolute pressure of 0.3 bar, the slag appeared very sticky after the pressure step. This was probably related to the additional vaporisation of Na from the slag and the longer time at temperature necessary to reduce some of the oxides from the melt. FactSage® predicted Na losses of between 17% and 24% to the gas phase at 1 500 °C and an absolute system pressure of 0.3 atmosphere, as shown in Table 38 below: The partial evaporation of Na was confirmed by XRF analyses on the actual slags, with an Na_2O content of 17.5% measured for the samples open to atmosphere, and Na_2O levels of 15% measured for samples that were exposed to an absolute pressure of 0.3 bar.

Table 38: Comparison between FactSage® modelling and experimental results of slag composition

Parameter/ Compound	Modelling	Modelling	Measured composition	Modelling	Measured composition
Pressure (Atm)	1	1	1	0.3	0.3
Temperature	1 500 °C	1 500 °C	1 500 °C	1 500 °C	1 500 °C
Approximate Oxygen partial pressure	0.021	10^{-7}	10^{-7}	10^{-7}	10^{-7}
SiO2	27%	37%	36%	37%	40%
Al2O3	8%	10%	8%	11%	9%
CaO	28%	37%	33%	38%	30%
Na_2O	13%	17%	18%	15%	15%
NiO	5%	0%	0%	0%	0%
FeO	12%	1%	0%	1%	0%
Weight slag (g)	74	55	56	54	56
Weight spinel (g)	1.41	0	0	0	0
Liquid viscosity (poise)	1.00	2.00	1.96	2.31	4.77
Overall viscosity (poise)	1.15	2.00	1.96	2.31	4.77

Table 38 shows the calculated viscosity of the slag at the beginning of the melt to be 1.15 poise (with Fe, Ni, Cu and Cr still present as oxides), compared to the final slag viscosity of 2.0 poise (with the bulk of Fe, Ni, Cu and some Cr in the alloy phase). The effect of the presence of solid spinel type particles is also shown in the table. The low content of CaO in the partial vacuum slag drives the large viscosity variance between the modelled and measured slag compositions.

6.2.2 Smelting of third stage residue directly

Each system (or feed composition type) reacted differently in the smelting conditions. A summary of some important findings will be given for a system in which third stage residue was melted in an induction furnace at 1 400 °C. The melt was performed in a clay-graphite crucible at atmospheric pressure with an inert gas flushing inside the chamber.

Modelling was performed by varying the partial oxygen pressure by adding more O_2 gas to the otherwise inert gas atmosphere above the melt. Table 39 below shows the comparison of the actual recoveries to the modelled recoveries for a system with a partial oxygen pressure of 2.7 x 10^{-9} atm. The actual pO_2 of the system was not measured. Nell (2004) reported that the partial oxygen pressure in a typical PGM matte smelting furnace is between 10^{-8} to 10^{-9} atmospheres. The matte phase is interspersed in the alloy phase, as described in section 4.3.2, and recovery measurements to the alloy phase therefore include the recovery to the matte phase. The spinel phase would probably settle on top of the alloy phase and might be separated with it, influencing the assays of the alloy. This might be where the Cr content of the alloy comes from.

Table 39: Comparison between the modelled and measured recovery to the specified phases for the direct smelting of third stage leach residue (model predictions at $pO_2 = 2.7 \times 10^{-9}$atm)

Element	Measured	Modelled			
	Alloy	Total	Alloy	Matte	Spinel
Pt	100%	100%	100%	0%	0%
Pd	119%	100%	100%	0%	0%
Au	116%	32%	32%	0%	0%
Rh	97%	100%	100%	0%	0%
Ru	94%	100%	100%	0%	0%
Ir	91%	100%	100%	0%	0%
Ag	96%	78%	78%	0%	0%
As	113%	93%	93%	0%	0%
Cr	60%	73%	2%	0%	71%
Cu	107%	85%	63%	22%	0%
Fe	82%	80%	74%	5%	1%
Ni	106%	98%	92%	6%	0%
Pb	78%	9%	8%	0%	0%
S	40%	6%	0%	6%	0%
Se	61%	0%	0%	0%	0%
Te	114%	14%	14%	0%	0%

The modelled recovery of gold will not be discussed here – the high volatility is predicted as the AuS species. The modelling of Au in the presence of S is discussed in section 7.2.1 under the high temperature treatment step. However, it is worth noting that the modelling showed the same effect at 1 400 °C instead of 1 700 °C, with the effect even more pronounced at low temperatures.

The variable PGM content (between 119% and 91%) is difficult to interpret and it once again shows how difficult it is to make quantitative conclusions on such small scale work tests, coupled with sampling and analytical error. The system is not well described by modelling, since Pb, S, Se and Te were not removed to the extent predicted by FactSage®. FactSage® predicted that the deportment of Se, Te and Pb to the gas phase would not be influenced by the pO_2 of the system to a large extent, but rather by the formation of a large number of non-oxide volatile species. In the case of Se and Te, most of the volatile species (apart from PbSe and PbTe) were outside their temperature range and

could therefore not be used with confidence. PbSe and PbS account for almost all the predicted Pb vaporisation from the system. It would seem that the activity of the Pb, Se and Te (as well as S) in the matte and alloy phases is not accurately described by the FactSage® databases used.

In the case of S, the partitioning of S between the gas/slag/matte phases is very sensitive to oxygen partial pressures. FactSage® did not predict the stability of the matte phase accurately, by over-predicting partitioning to the gas phase and/or the slag phase. The reason for this is that CaS in the slag phase is stabilised in more reducing conditions, and SO_2 in the gas phase in more oxidising conditions. FactSage® predicts a maximum partitioning to the matte phase of 6%, while 40% was measured. Actual measurements of the slag showed 38.1 wt% partitioning of S to the slag phase, compared to the modelled value of only 18%. Actual S partitioning to the gas phase (by difference) was 21.9 wt%, while modelling predicted 76 wt%. Figure 31 shows the how the partitioning of S moves from the slag phase to the gas phase (with the matte phase having only a small contribution) when the system was modelled in FactSage®.

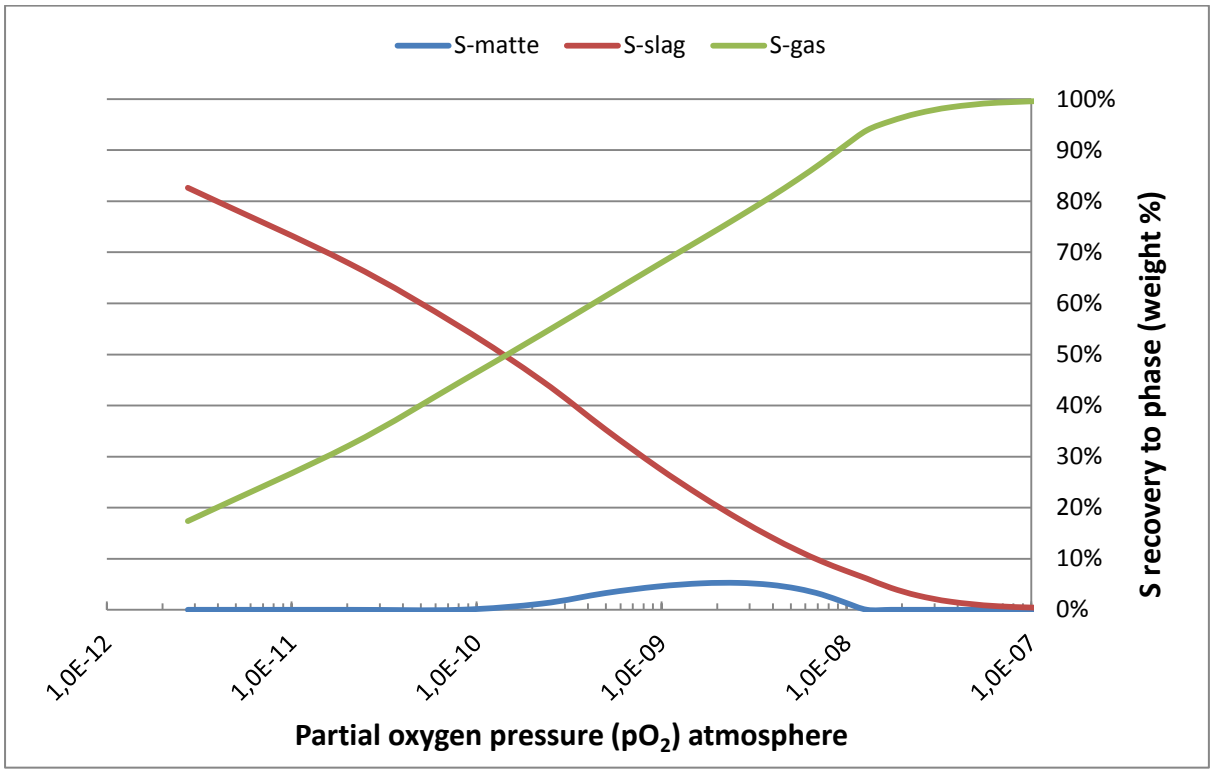

Figure 31: S recovery to the alloy, matte and gas phases at 1 400 °C according to thermodynamic modelling as a function of partial oxygen pressure (pO_2)

Actual smelting results show that the PGM content can be increased from a feed of around 44%-48% in third stage residue to around 72%-75% in the alloy. Basically all of the Os, Fe, Ni, Cu and As and most of the Cr, Se, Te, S, Pb and Ag would still be in the feed to the PMR process. It was mostly the oxides and hydroxides that were removed from the system, together with the partial removal of the elements Se, Te, S, Pb, Cr and Ag. Due to the poor description of the system through FactSage® modelling, it is unsure to what extent these contaminants would be removed if the pO_2 of the system were to be increased.

The visually observed melting point of the system was around 1 235 °C. Note that this is the temperature at which everything appeared molten. Solid particles in the slag phase (like spinel) and in the alloy phase could not be seen. FactSage® predictions for the system above showed the liquidus temperature of the melt (disregarding the spinel phase) to be 1 288 °C when the FCC solid solution phase was not activated. Ru is the last metal to join the alloy liquid phase at this temperature. However, a small quantity of Os is still a pure solid at this temperature. If Os is taken into account, the liquidus temperature becomes 1 469 °C. Modelling, therefore, predicts that the alloy would not have capacity to absorb the 4.5% Os in feed at temperatures below 1 469 °C. When the FCC solid solution phase was activated, the liquidus temperature of the system was predicted to be 1 883 °C.

The modelled temperature (ignoring Os and the FCC solid solution phase) of 1 288 °C is quite close to the observed temperature of 1 235 °C.

6.2.3 Smelting of third stage residue after roasting

The behaviour of the roasted third stage residue system has already been discussed in section 6.2.1. A comparison between the actual recoveries and the modelled recoveries at a partial oxygen pressure of 2 x 10^{-8} atm is provided in Table 40. It is difficult to judge whether low recoveries on Ru and Ir are actual, or due to sampling and analytical error. Fe, Cu and Ni are quite accurately predicted. Similar to the directly melted material, the presence of Cr in the alloy could be due to the spinel phase partly settling on the alloy and then being separated together with it. SEM work confirmed the presence of a Fe-Cr-O spinel in the alloy. The capacity of the slag to absorb chrome spinel is extremely limited under the conditions studied. Du Preez (2009) found that higher CaO content stabilises the spinel phase.

Table 40: Comparison between the modelled and measured recovery to the alloy phase for the roasted third stage smelt

Element	Measured Recovery	Modelled Recovery	
	Alloy	Alloy	Spinel
Pt	100%	100%	0%
Pd	109%	100%	0%
Au	96%	100%	0%
Rh	102%	100%	0%
Ru	91%	100%	0%
Ir	93%	100%	0%
Ag	92%	59%	0%
As	80%	100%	0%
Cr	22%	1%	93%
Cu	97%	97%	0%
Fe	81%	77%	15%
Ni	97%	99%	0.4%
Pb	46%	44%	0%
Te	77%	16%	0%

The visually observed melting point of the system was around 1 450 °C. FactSage® predictions for this system showed the liquidus temperature of the melt (discarding the spinel phase) to be 1 230 °C when the FCC solid solution phase was not activated. When the FCC solid solution phase was activated, the liquidus temperature of the system was predicted to be 1 816 °C. The remaining Os in the roasted product (around 1%) does not influence the liquidus temperature, as the alloy has sufficient capacity to absorb this lower Os content (compared to 4.5% Os content of the direct smelt test).

This processing route (roasting followed by smelting) has a higher upgrade factor on the alloy and a 6E grade of 79% could be achieved. The major difference between the direct smelting and roasting-smelting route is the more complete removal of volatile species during roasting (Os, S, Se and Te). Fe, Cu and Ni remain the biggest contaminants (amounting to 14%), followed by As and Pb, which are poorly removed, at around 4.5% by weight of the alloy.

6.2.4 Smelting of third stage residue after base metal leaching and roasting

A feed material was prepared by doing a combined formic acid/sulphuric acid leach on the third stage material. The leaching test work is described in Appendix A. The leach has the advantage that > 50% Fe and Ni and > 80% Cu can be leached out of third stage leach residue. It was found that the lower Fe, Ni and Cu content had an impact on the observed liquidus temperature of the system, lifting it to 1 510 °C. For the same system, FactSage® predicted the temperature at which the last solid disappeared as 1 324 °C if the FCC solid solution phase was ignored. When the FCC solid solution phase was activated, the liquidus temperature was predicted to be 1 907 °C.

Table 41 shows a comparison between the measured recoveries and the modelled recoveries at a partial oxygen pressure of 2 x 10^{-8} atm and 1 600 °C. The smelt was performed at 1 600 °C (due to the higher melting point of 1 510 °C) for 30 minutes at atmospheric pressure. The PGM recoveries to the alloy phase are very inconsistent, ranging from 186 wt% to 73 wt%. Given the high variabilities in recoveries measured in this test, no quantitative conclusions can be drawn. PGM recoveries to the slag phase were very low.

Table 41: Comparison between the modelled and measured recovery to the alloy phase for the leach-roast third stage smelt

Element	Measured Recovery		Modelled Recovery	
	Alloy	Slag	Alloy	Slag
Pt	102%	0.0%	100%	0.0%
Pd	116%	0.1%	100%	0.0%
Au	186%	1.3%	100%	0.0%
Rh	91%	0.1%	100%	0.0%
Ru	73%	0.1%	100%	0.0%
Ir	150%	0.7%	100%	0.0%
Ag	46%	1.6%	50%	0.0%
As	132%	0.6%	100%	0.0%
Cr	82%	30.1%	78%	21.9%
Cu	135%	1.0%	98%	0.6%
Fe	138%	12.8%	99%	1.0%
Ni	131%	1.5%	100%	0.0%
Pb	144%	1.8%	31%	0.0%
Te	136%	7.3%	13%	0.0%

The poor recoveries of Ru to the alloy phase of 73 wt% deserve some discussion. A repeat melt was performed and highly variable recoveries were once again measured. The Ru recovery was once again much lower than the other PGM recoveries, at 69 wt% to the alloy phase. In the experimental procedure discussion (section 3.4.2) it was mentioned that the melts at 1 600 °C required temperature measurements with a pyrometer, instead of the thermocouple used for the tests performed at lower temperatures (1 300 °C to 1 500 °C). Using the pyrometer meant that the melt was not enclosed within a sealing chamber. Nitrogen gas was simply flushed across the melt by purging. Thermodynamic modelling showed that a pO_2 of around 0.22 was required to oxidise and vaporise 27% of the Ru. It showed that air in contact with the melt at a temperature of 1 600 °C would have a significant impact on Ru losses. While Fe, Ni and Cu should have a stronger thermodynamic drive to oxidise than Ru would (shown in Figure 32), this was not observed. It is possible that the low concentrations of Fe, Ni and Cu in the Leach-Roast-Smelt alloy feed (6.8 wt% Fe+Ni+Cu, compared with 7.9 wt% Ru) meant that less Fe, Ni and Cu were present, favouring Ru contact with oxygen and a measureable Ru loss. Also, the higher temperature of 1 600 °C required for the melt would increase the vapour pressure of the Ru oxides.

Fe, Ni and Cu show complete recoveries to the alloy phase (with more than 100% measured), while Cr recoveries are 82%. Figure 32 shows the modelled recovery of Fe, Ni, Cu, Cr and Ru as a function

of the partial oxygen pressure. Ru recovery to the alloy phase remains at 100 wt%, even when Fe recoveries drop below 10 wt% to the alloy phase. High Ru losses to the vapour phase would not be expected, especially when Fe recoveries are still very high at more than 100 wt% measured. If the Ru losses are real, this would show non-equilibrium behaviour of the leach-roast-smelt system at the low Fe, Ni and Cu loadings and at 1 600 °C, with possible air ingress. If we compare Figure 32 with Figure 27, it is clear that the higher temperature allow higher Cr reducibility/solubility at the same pO_2.

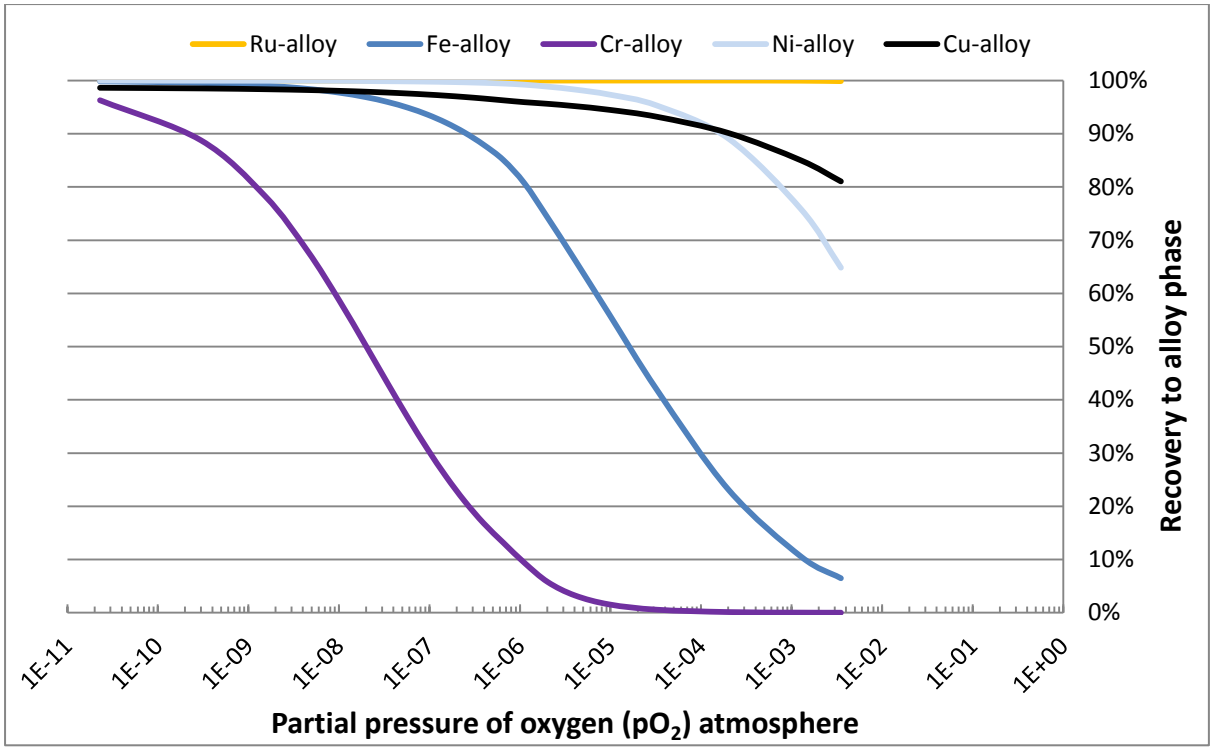

Figure 32: Cu, Ni, Fe, Cr and Ru recovery to the alloy phase at 1 600 °C according to thermodynamic modelling as a function of partial oxygen pressure (pO_2)

Table 41 also shows that Pb and Te did not volatilise to the extent modelled. It is interesting that Pb had such a poor removal in this melt at 1 600 °C, as almost complete removal was measured at 1 700 °C, with both melts at temperature for 30 minutes. The melt at 1 700 °C is described in section 7.2.1.

This processing route (leaching for Cu, Ni and Fe, followed by roasting and finally smelting) can achieve an alloy with a 6E grade of 83.5%. Apart from the Fe, Ni and Cu content that are removed before the melt, the remaining contaminants of As, Pb and Te do not behave differently in this melt at 1 600 °C when compared to the roast melt at 1 500 °C. Fe, Cu and Ni content in this alloy amounted to only 6.8%. Appendix A discusses the formic/ sulphuric leach and shows that Cu can be removed to a greater degree than was achieved in this batch. With better Cu removal, the Cu + Ni + Fe content can be as low as 4.5 wt% in the alloy. As and Pb remain the other significant contaminants left in this alloy at 3.9% As and around 0.7% Pb.

6.2.5 Smelting of third stage residue after roasting and with the addition of Cu

From the experimental work described above, it is clear that residues with a high PGM content can be smelted and that they are able to form an alloy phase without the addition of a collector. It is also clear from the experimental work that the key to removing the deleterious elements, As, Pb, Cu, Fe and Ni, would be the control of the redox potential of the melt. This can be achieved through proper furnace design (crucible interaction and integrity), gas atmosphere and addition of oxidising agent. This might require continuous AC or DC furnaces, which would bring its own complexities, for instance PGM lock-up and continuous operation. The other alternative option to manage the redox potential of the melt is to purposely add a buffering element, for instance Cu. Figure 26 shows that

the oxidation potential of Cu lies between that of the PGMs and the remaining contaminant elements, Ni, Fe, As and Pb. Using a buffering element like Cu would have the additional benefit of lowering the liquidus temperature of the alloy, which would lower the overall temperature requirement of the melt. The lower temperature requirement in the melt would allow the use of borate-based slags that have the advantage of good spinel solubility and good partitioning of As and Pb to the slag phase.

The perceived benefit is best described by means of two figures drawn up through FactSage® modelling. Figure 33 represents the Roast-melt system with Cu addition and Figure 34 represents the Roast-melt system without Cu addition. For the modelling with Cu addition, the following were added with the roasted third stage leach residue (expressed as g feed per 100 g roasted product feed) to a melt at 1 200 °C: 200 g N_2 gas, 100 g Borate based slag, 250 g CuO. The addition of sugar ($C_{12}H_{22}O_{11}$) was varied between 0 g and 100 g. Figure 33 shows that a large 'Ideal operating range' exists, where recoveries of Ni, Fe, As and Pb to the alloy phase are very low. The actual test work confirmed that temperatures as low as 1 200 °C can be used to achieve a fully liquid melt (apart from Ru, which will be discussed later) with a good viscosity. At these low temperatures, a silica-alumina crucible can be used. Using a ceramic crucible will ensure that the crucible does not influence the pO_2 of the melt directly. The concept of buffering can be explained by the wide range of partial oxygen pressures (pO_2) that will still fall within the ideal range (maximum impurity removal without Ru oxidation). The large Cu addition and the ability to use a ceramic crucible will stabilise the pO_2, while Cu oxidation will buffer the reaction of the other elements when small fluctuations of the pO_2 do occur. The recovery of Cu varies between 11% and 71% over the ideal operating range, while the recovery of other elements varies much less.

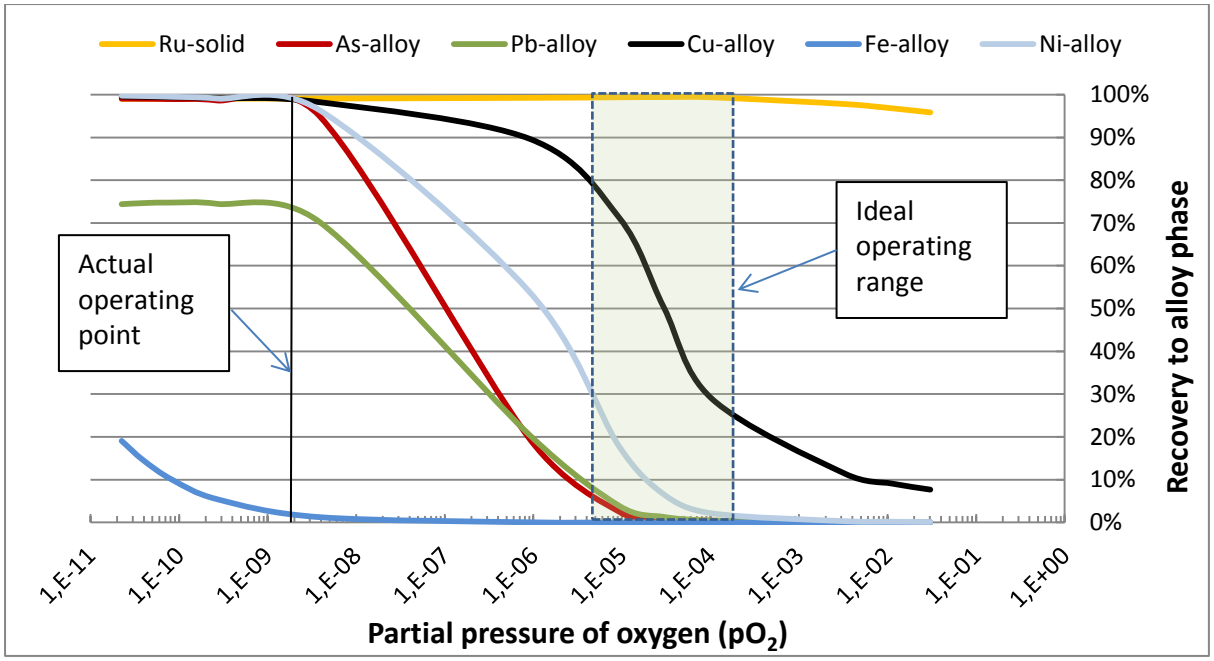

Figure 33: Elemental recoveries to the alloy phase (apart from Ru, which is recovered as a pure solid) as a function of partial oxygen pressure (pO_2) for the Roast-melt system with Cu addition. The ideal operating range for removal of contaminants is highlighted, as well as the actual operating point that was achieved in the experimental tests

For the modelling without Cu addition, the following were added with the roasted third stage leach residue (expressed as g feed per 100 g roasted product feed) to a melt at 1 500 °C: 200 g N_2 gas, 50 g CaO-SiO_2-Al_2O_3-Na_2O based slag, 8 g C. The addition of oxygen was varied between 0 g and 20 g. Figure 34 shows that a much smaller 'Ideal operating range' now exists, where recoveries of Ni, Fe and Pb to the alloy phase are low, while Ru losses to the vapour phase do not yet occur. Within this range, the recovery of As to the alloy phase remains high (above 50%), as does the recovery of Cu (above 63%). In the system without the addition of Cu, it would be more difficult to fix a pO_2 accurately (due to the high temperature requirement) and small changes in the pO_2 would directly result in recovery changes of several impurities. Better removal efficiency of impurities in the system with Cu addition is linked to a number of factors, including the better buffering potential, lower temperature requirement and slag type.

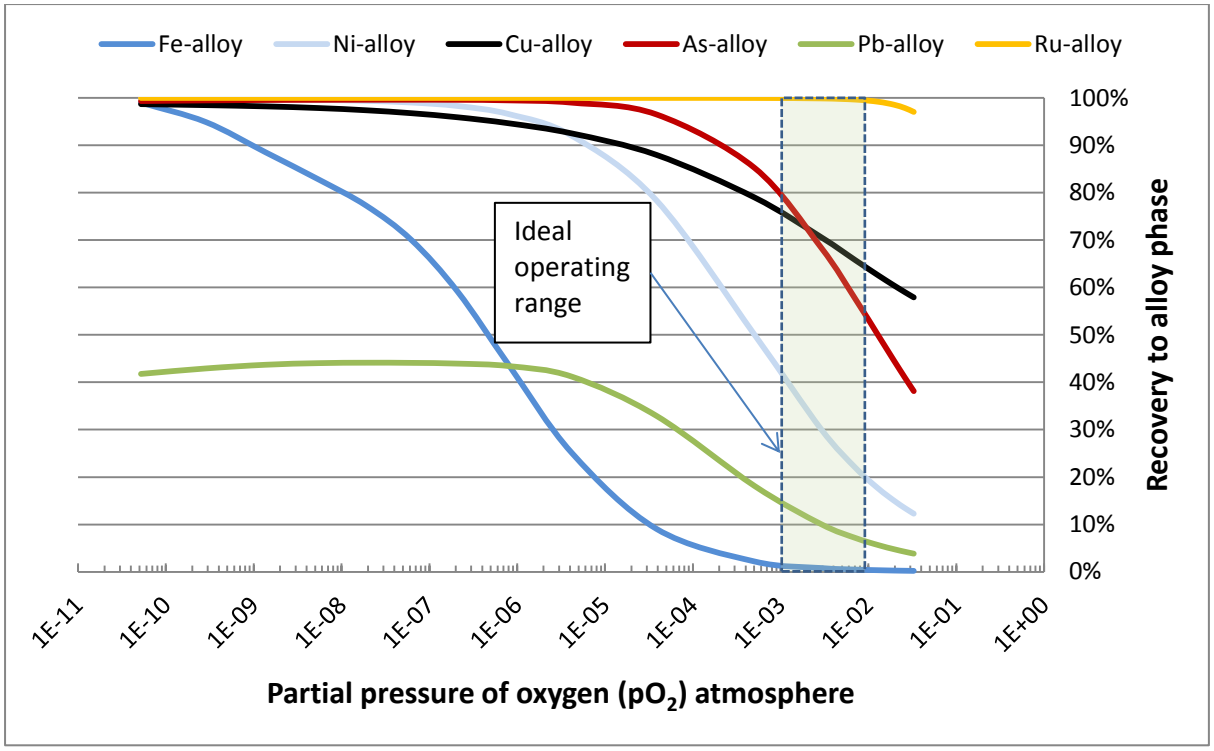

Figure 34: Elemental recoveries to the alloy phase as a function of partial oxygen pressure (pO_2) for the Roast-melt system without Cu addition. The ideal operating range for removal of contaminants is highlighted

The disadvantage of adding a buffering agent for redox control would be that an additional leaching step would be required, in this case a pressure leach to remove the Cu from the PGM matrix. However, since sulphuric based Cu leaching is already used by most PGM refiners, this additional leach can be incorporated into existing flow sheets quite easily. It is possible to achieve PGM concentrations of up to 95% after Cu leaching.

Raevskaya (1987) studied the Ru-Cu system and found insolubility over the full composition range. The Cu-Ru binary phase diagram (taken from the SGnoble database) is shown in Figure 35. The Cu-Ru system shows limited liquid solubility at mole % content of less than 0.02% and then also at temperatures > 1 500 °C.

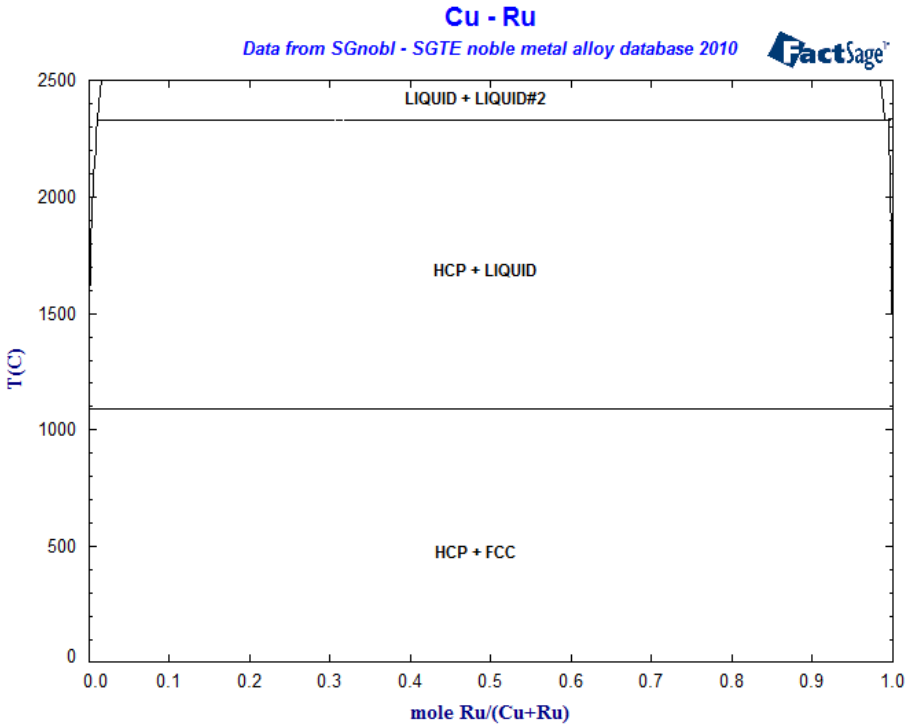

Figure 35: The binary phase diagram for Cu-Ru as generated by the FactSage® SGnoble (2010) database. The almost complete insolubility of Cu and Ru is clearly illustrated

The SGNoble database in FactSage predicted that Ru would be insoluble with the higher Cu alloys and be present as a Ru solid. To provide an indication of the required Cu content needed before Ru becomes insoluble in the alloy phase, modelling was done in which Cu was added to a typical alloy (as studied in this work) in increasing amounts. With Cu contents above 8.1% in the alloy, the first Ru solid started forming at 1 500 °C. The solubility is a function of temperature, with lower temperatures showing insolubility at lower Cu content (4.1% Cu at 1 400 °C) and higher temperatures showing insolubility at higher Cu contents (12.9% Cu at 1 600 °C). The insolubility of the Ru in the high Cu content alloy was confirmed with SEM work (as discussed in section 4.3.2.4). The SEM work confirmed that the Ru solid settled through the alloy and collected at the bottom, due to its higher density.

The impact of the insolubility on the actual recovery was studied in four experimental test runs. Table 42 shows the actual recoveries measured for the four tests. In all four tests, recovery of Ru to the alloy phase was the lowest of all the PGMs. This finding is of concern, and low recovery might be influenced by the very small size of the Ru particles that need to settle through the slag phase. However, assaying of the two slag samples from the muffle furnace melts showed a Ru recovery to the slag phase of less than 1% (expressed as weight % of feed). It is therefore not clear whether the low recovery to the alloy phase was an actual recovery loss, or simply a sampling error. If Ru was not evenly distributed throughout the button, the drilled sample might not have been representative.

Test number 2 contained a low addition of sugar to compensate for the interaction of the crucible with the melt. The full recovery of Cu to the alloy phase testifies that crucible interaction caused all CuO to revert from the slag to the alloy. The low Ru recovery is difficult to explain. Modelling of the system showed that Ru loss to the gas phase at 1 350 °C could be at most 12%, even with no sugar

addition, and should be zero with the sugar addition that was made, reducing RuO_2 to Ru. Unfortunately, this slag was not assayed and the alloy button was not investigated with SEM to provide a qualitative explanation for the low recovery. The inconclusive result of this test is testimony to the difficulty of predicting and managing Ru behaviour in the Cu system.

Table 42: Summary of the recoveries to the alloy phase obtained from the Roast-Smelt tests with addition of Cu

Parameter/ Element	Test 1	Test 2	Test 3	Test 4
Type of furnace	Induction	Induction	Muffle	Muffle
Temperature	1 350 °C	1 350 °C	1 200 °C	1 200 °C
Approach followed	Cu oxidation	CuO reduction	CuO reduction	CuO reduction
Pt	95%	91%	92%	100%
Pd	115%	85%	114%	124%
Au	89%	105%	95%	97%
Rh	97%	72%	87%	88%
Ru	74%	7%	86%	75%
Ir	118%	36%	94%	91%
Ag	75%	371%	277%	141%
As	109%	111%	97%	101%
Cr	2%	22%	3%	2%
Cu	74%	104%	91%	94%
Fe	62%	84%	3%	2%
Ni	124%	120%	75%	100%
Pb	89%	255%	150%	187%

The two tests in the induction furnace showed high Fe recoveries (62 wt% and 84 wt%), while the lower temperature tests in the ceramic crucible in the muffle furnace showed low Fe recovery (3 wt% and 2 wt%). This once again pointed to the melt interacting with the crucible, resulting in poor control of the pO_2. Discussion of the system will therefore focus on the two muffle furnace tests performed at 1 200 °C. Figure 33 shows modelled recovery of the system, as well as the point at which the two tests ended up, as the 'Actual operating point'.

In this case, the system was too reducing, not because of crucible interaction, but due to over-addition of reducing agent (sugar). The calculation to determine sugar addition over-accounted for the oxygen in the roasted alloy (associated with the OPMs and stable oxides). Due to time and budget constraints, no additional work was performed on the system. However, it is suggested that better control over the pO_2 would yield better removal of Ni, As and Pb to the slag phase. In theory, Cu should buffer Ru oxidation and therefore losses to the gas phase. Also, at 1 200 °C, the vapour pressure of RuO_3 and RuO_4 is low and losses of only 2% Ru to the gas phase are modelled, even at the point where 90% of the Cu is oxidised to the slag phase.

Table 43 compares the actual results obtained with the modelled results of the system. Back-calculating the pO_2 from Fe recovery puts the pO_2 at 4×10^{-9} atm. The actual results compare very

favourably with the modelled results at this point. One exception is Pb, which shows no volatile behaviour, even at a long melt time of 90 minutes, while modelling predicted 24 wt% to report to the gas phase. At 1 200 °C, Cr solubility in the borate based slag remained a problem, with modelling having predicted that 76% of the Cr would be in the spinel phase.

Table 43: Comparison between the actual recoveries and the modelled recovery for the Roast-Smelt test with CuO and addition of reducing agent in a muffle furnace at 1 200 °C

Element	Measured	Modelled				
	Alloy	Alloy	Solid	Gas	Spinel	Slag
Pt	100%	100%	0%	0%	0%	0%
Pd	124%	100%	0%	0%	0%	0%
Au	97%	100%	0%	0%	0%	0%
Rh	88%	100%	0%	0%	0%	0%
Ru	75%	1%	99%	0%	0%	0%
Ir	91%	100%	0%	0%	0%	0%
Ag	141%	100%	0%	0%	0%	0%
As	101%	95%	0%	1%	0%	4%
Cr	2%	0%	0%	0%	76%	24%
Cu	94%	98%	0%	0%	0%	2%
Fe	2%	1%	0%	0%	14%	85%
Ni	100%	96%	0%	0%	0%	3%
Pb	187%	70%	0%	24%	0%	6%
Te	141%	86%	0%	14%	0%	0%

Producing an alloy with around 70% Cu content produces its own challenges. These are shortly listed below:

- Cu removal. A high-pressure leach with sulphuric acid (to most easily integrate into the BMR circuit) will be required. During this highly oxidising leach, it is possible that some of the PGMs (especially the OPMs) might either go into solution, or oxidise, and this will affect their ability to dissolve in the HCl/ Cl_2 environment in the PMR.
- Increasing costs by producing CuO powder and then having to use a suitable reducing agent.
- Ru recovery, due to insolubility in the alloy phase. The test results showed low Ru recovery, although an actual loss mechanism was not established and the low recovery might simply be sampling error. Even if Ru is recovered with the alloy as a separate phase, it is unsure how the Ru will behave in a highly oxidising pressure leach to remove Cu.

The potential benefits of the system are also listed below:

- More precise pO_2 control by addition of both the oxidation and reducing agent. This, in turn, might remove Fe, Ni, Pb and As almost completely to the slag phase. This was unfortunately not proved in the experimental work.
- Lower temperatures are required in the melt, allowing simpler refractory materials and longer life.

6.3 Conclusion

The smelting of PGM-rich residue can create a PGM-rich alloy that separates from the slag phase. No addition of a collector is necessary to achieve PGM collection in the alloy and the PGMs will drain from the slag phase efficiently. When the smelting step is properly managed, recovery of PGMs to the alloy phase of greater than 99% can be achieved. No loss of Ru due to volatilisation could be measured during the initial heat-up phase, despite the presence of oxygen in the matrix, indicating that a sufficiently high heating rate would allow Ru-oxygen dissociation before measureable losses of Ru oxide could be experienced.

The redox environment is the most critical aspect of the melt. Although the current experimental set-up was not ideal, due to the graphite crucible interaction, sufficient evidence is presented to illustrate that very high PGM content (>80%) can be achieved through melting, without experiencing PGM losses. From the combined evaluation of experimental and modelled data, it would appear that a partial oxygen pressure (pO_2) in the range of 10^{-3} to 10^{-5} atm would allow the best separation of PGMs from contaminants such as Fe, Ni, As and Pb.

The removal of Pb to the gas phase was lower than the modelled values in all four of the systems studied. No additional Pb could be volatilised by the introduction of a partial vacuum above the melt. It would appear that Pb removal from the high PGM matrix either does not proceed according to thermodynamic predictions, or proceeds only slowly at ambient pressure or in a partial vacuum at 1 500 °C.

FactSage® modelling poorly describes the system in which pressure leach residue is smelted without prior roasting. The presence of the matte phase is under-predicted and the recovery of Se, Te, Pb and S to the gas phase is over-predicted.

The temperature required to achieve a fully liquid alloy phase was found to be sensitive to the presence of elements such as Fe, Ni, Cu, S, Pb, and possibly As, Se and Te. When third stage residue was melted directly, the fully molten temperature was observed to be 1 235 °C. When the material was roasted, this observed fully molten temperature increased to 1 450 °C. When additional Fe, Ni and Cu are removed prior to roasting, the observed fully molten temperature increased further to 1 510 °C. The addition of Cu to produce an alloy with Cu content between 60% and 70% brought the temperature to below 1 200 °C.

When Cu was added to the alloy phase and made up more than about 8% of the alloy by weight at 1 500 °C, Ru insolubility might start to appear. Ru that is insoluble in the alloy could still drain from the slag and settle at the bottom of the alloy pool (depending on the density difference between the alloy and Ru). Low Ru recovery was noted in the Cu alloys studied, but no mechanism for this low recovery could be established.

The type of slag used does not seem to have a significant impact on the recovery of PGMs. However, Cr presence in the alloy phase can be partially explained by the settling of chrome spinel from the slag, which was then separated with the alloy phase. Engineering of a slag with a high capacity for spinel (after roasting) and a low viscosity, allowing alloy to drain through the slag during casting, is required.

Lower loadings of Fe, Ni and Cu in the Leach-Roast-Smelt alloy showed that Ru losses to oxidation and volatilisation might be impacted at higher temperatures (1 600 °C), without proper control over the gaseous atmosphere in the melt.

Chapter 7: Atomisation and high temperature treatment

This chapter will discuss the atomisation process and the high temperature treatment that can be done during the heating stage in order to atomise the alloy.

7.1 Introduction and background

For ease of reference, the flow sheet of the envisaged pyrometallurgical refining process is repeated. Figure 36 shows the position of the atomisation step in the flow sheet as a dashed yellow ellipse. Although the atomisation step is shown as a single block, it comprises smelting, casting, quenching and de-watering steps, as discussed in section 3.4.3.

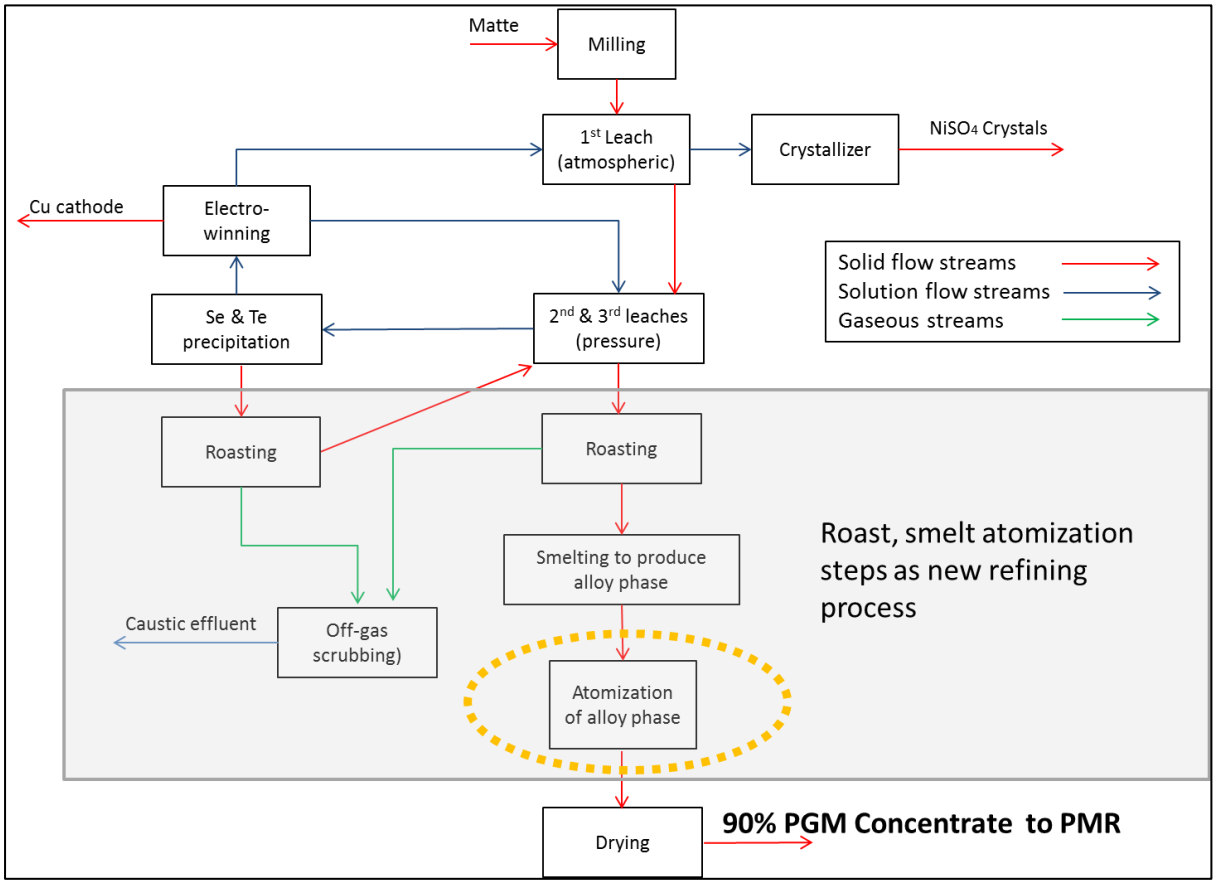

Figure 36: Block flow diagram of the proposed pyrometallurgical process to be implemented between the BMR and PMR processes in order to remove contaminants from the PMR feed. The atomisation step discussed in this chapter is shown in the dashed yellow ellipse

The necessity of re-smelting the alloy after solidification and slag/alloy separation, to facilitate atomisation, presented the opportunity to vaporise selected metals at high temperatures and in a controlled environment. This concept was explored and was termed the high temperature treatment step. The results from this step will be discussed separately, although the high temperature treatment step forms part of the atomisation sequence.

The end goal of the process investigated was to make the improved alloy phase available for dissolution in the PMR process in a hydrochloric acid/chlorine dissolve. The alloy needed to have a high surface area in order to allow the dissolution to proceed rapidly. Finer particles were also important, to ensure that the particles could suspend easily, thereby keeping the required agitator speed, and the energy requirement, low.

The alloy is extremely hard, but not brittle (i.e. it is tough). This makes crushing and milling of the alloy difficult. It was decided to focus the work on atomisation, as this can achieve very small particle sizes with a narrow particle size distribution range. Dunkley *et al.* (2008) performed atomisation test work on Fe-Ni-Co-Cu alloy that contained PGMs. They found that alloy particles of 20 micron could readily be achieved with atomisation. The test work on atomisation was done in order to confirm that atomisation could achieve this goal, as well as to study the phases that were formed in the rapid-quenching environment of atomisation.

Atomisation requires that the alloy phase (physically separated from the slag phase after the smelting step) be re-melted. The liquidus temperature of the alloy phase is quite high (a typical range of 1 235 °C to 1 510 °C for the alloy studied). It is also necessary to superheat the alloy phase with typical superheat values of between 50 °C and 120 °C above the liquidus temperature. The superheating ensures that the alloy remains fluid during the casting into the tundish and the subsequent funnelling into the water jet stream.

Both Pb and Bi show significant volatile behaviour at the temperatures and conditions that were required for the atomisation heat. A number of experiments were performed to monitor volatile behaviour during this high temperature treatment step. The high temperature treatment step could be designed and controlled as a distinct process, although smelting would effectively be an implicit part of the atomisation sequence.

7.2 Results and discussion

7.2.1 High temperature treatment

The FactSage® modelling parameters that were used to model the high temperature treatment step are discussed in Section 3.3.3.

Table 44 shows the measured recovery of elements to the alloy phase for all three alloy types studied. The table reports the recovery across the high temperature treatment step (starting with the alloy product after the smelting step reported in Table 18). The recoveries are determined with Pt as tie element. The use of this method provided more consistent results for the small scale on which the tests were carried out. The high value for S recovery for the Roast-melt alloy is due to the very low starting value of S (0.0% from Table 18), which amplified any analytical and sampling error.

Table 44: Summary of the wt% recovery to the alloy phase for the three alloys measured in the experimental runs

Element	Direct Melt	Roast-Melt	Leach-Roast-Melt
Au	79%	88%	99%
Ir	98%	95%	94%
Pd	88%	105%	101%
Pt	100%	100%	100%
Rh	116%	104%	95%
Ru	118%	97%	88%
Ag	1%	25%	6%
S	2%	119%	9%
As	108%	113%	102%
Bi	6%	2%	4%
Se	0%	0%	0%
Te	1%	4%	15%
Pb	14%	3%	9%
Fe	126%	107%	102%
Cu	83%	59%	83%
Ni	128%	106%	105%

Marsden *et al.* (2006) reported that Te would cause Au volatilisation, presumably through a species such as AuTe. They report that an alloy containing 5% Te will lose between 2% and 4% of the contained Au in one hour at 1 245 °C and that alloys containing 5% Hg or Sb lose approximately 0.2% of the gold under similar conditions. The volatile gold species of Au tellurides and antimonides are not included in the FactSage® databases.

A number of studies have been done in the geo-science field on the fugacity of Au in the presence of S, mostly as a method to explain vapour transport of metals like Ag, Au and Cu. Zezin (2010) completed his thesis on the fugacity of gold in the presence of H_2S and H_2O, but studied only systems with lower temperatures (300 °C to 400 °C) and higher pressure (230 bar). He found that the fugacity of Au increases with the fugacity of H_2S, and that reactions involving the formation of volatile sulphide species control the solubility of Au in the gas phase. Most of the studies in the geo-science field focused on water vapour systems, with reduced sulphur species forming H_2S gas. Pokrovski *et al.* (2008) estimated the vapour-liquid partitioning of gold and other metals at temperatures up to 500 °C for water-salt (±sulphur) systems. They found that the addition of 1-3 wt% of S to the system increased the equilibrium distribution coefficient (Km = mvapour/mliquid) for gold by a factor of 100, allowing for its preferential partitioning into the vapour by up to 10 times. These studies confirm that the presesence of S have a strong influence on the fugacity of gold at elevated temperatures.

The FactSage® database includes the gaseous species of AuS, and the formation of this species led to over-prediction of Au losses to the gas phase to a large extent. When the Open system was run with FactSage®, and a Nitrogen gas with 1 000 ppm O_2 was allowed to be in contact with the alloy (by

addition of 20 g gas per 100 g feed for 10 steps), Au losses (as AuS) to the gas phase of ~ 70 wt% were predicted. Actual Au losses were measured to be approximately 12% for the roast-smelt product. FactSage® modelling for Au recovery can therefore not be done accurately, due to the lack of species such as gold telluride, sellenide and antimonide in the database, and the over-prediction of AuS.

The extent of Ag losses to vapour across the high temperature treatment step would restrict the use of this process step where Ag is recovered. In the case of Lonmin, Ag is not recovered.

Volatile behaviour of alloy from direct smelting of third stage leach residue

The directly smelted alloy had the highest content of S, Se and Te of the three alloy types studied. Modelling predicted that all these elements would be removed in the high temperature treatment process and the actual measurements confirmed this, as can be seen in Table 45.

Table 45: Recovery (wt%) to the alloy phase across the high temperature treatment step, of alloy that was produced by directly smelting third stage leach residue. The measured recoveries from experimental work and the modelled recoveries are shown

Element	Actual recoveries	Modelled recoveries
Au	79%	2%*
Ir	98%	100%
Pd	88%	100%
Pt	100%	100%
Rh	116%	100%
Ru	118%	100%
Ag	1%	2%
S	2%	0%
As	108%	96%
Bi	6%	4%
Se	0%	0%
Te	1%	0%
Pb	14%	0%
Fe	126%	100%
Cu	83%	92%
Ni	128%	100%

* Values of Au recoveries cannot be accurately modelled

Overall there is good correlation between the measured and actual results, apart from Au that has already been discussed. Pb removal did not proceed to the extent modelled, with 14 wt% recovery measured and 0 wt% recovery modelled to the alloy phase. Section 6.2.2 describes the direct smelting of third stage leach residue and also found that FactSage did not accurately predict Pb removal, over-predicting the formation of volatile species like PbSe and PbS. With the bulk of S, Se and Te absent from the system, FactSage predicts the Pb recovery closely (as can be seen from the results for the Roast-melt alloy in Table 46).

Pd has the highest vapour pressure of the PGMs in the metallic state, and the vapour pressure of the metal is higher than that of the oxide (Jehn, 1984). For all the other PGMs, the vapour pressure of the oxide is several orders of magnitude higher than that of the metal. Loss of Pd to the gas phase was modelled to be only 0.1 wt%. The low measured Pd recovery in this test was not consistent with the recoveries of Pt, Rh and Ru shown in Table 44, which showed more than 100% recovery. It is therefore interpreted as a sampling/assaying error.

Figure 37 shows the modelled recovery of certain elements to the gas phase per step (from the Open system in FactSage®). Each step shows a 20 g gas addition per 100 g feed alloy. It is important to maintain a good gas flow across the system in order to achieve good Bi, Ag and S removal. Au is simply included to show that Au losses are incorrectly attributed to high AuS vaporisation in the presence of S in the melt (S removal is slow, according to the modelling).

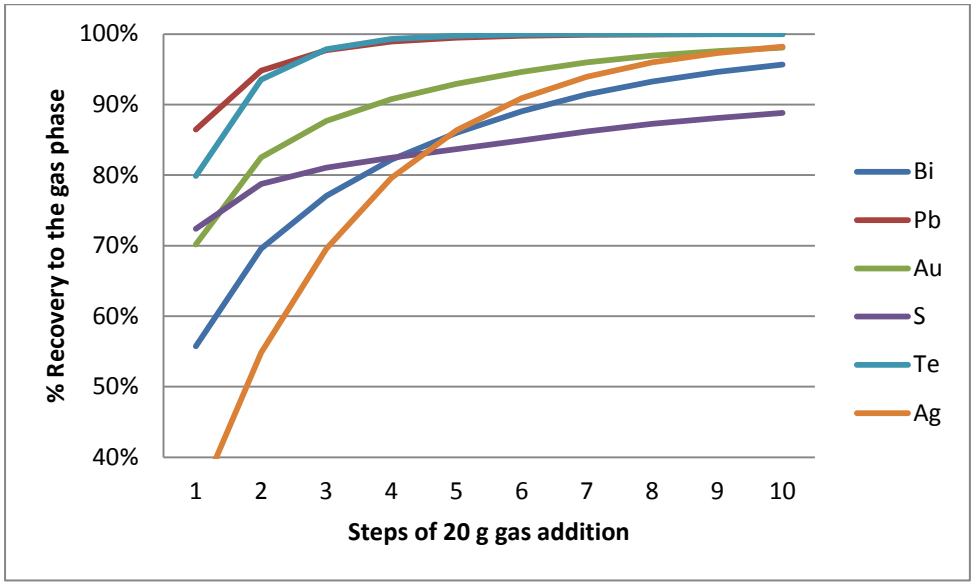

Figure 37: Cumulative recovery to the gas phase for certain elements, as predicted by modelling for the direct alloy

Ni and Fe showed over a 100 wt% recovery, while a Cu recovery in the alloy of 83 wt% was measured in the test work. FactSage® had predicted around 7 wt% Cu losses to the gas phase (as Cu, CuS, CuSe and CuTe).

Volatile behaviour of alloy from Roast-Smelt process

The alloy produced from roasting and smelting contain less S, Se, Te and As than the alloy produced from direct smelting of third stage leach residue. The comparison between the elemental measured recoveries and the modelled recoveries for the roast-smelt alloy across the high temperature treatment step is shown in Table 46.

Table 46: Recovery to the alloy phase (wt%) across the high temperature treatment step of alloy that was produced by roasting and smelting third stage leach residue. The measured recoveries from experimental work and the modelled recoveries are shown

Element	Actual recoveries	Modelled recoveries
Au	88%	66%
Ir	95%	100%
Pd	105%	100%
Pt	100%	100%
Rh	104%	100%
Ru	97%	100%
Ag	25%	1%
S	119%	0%
As	113%	96%
Bi	2%	14%
Se	0%	0%
Te	4%	0%
Pb	3%	0%
Fe	107%	100%
Cu	59%	94%
Ni	106%	100%

The measured recoveries once again compare quite favourably with the modelled recoveries. Bi removal proceeded better than the modelled values, while Ag removal proceeded worse. It must once again be pointed out that some deviations occurred in single tests that were not consistent when all three tests were viewed together (Table 44). The measured Ag recovery to the alloy phase was high for this measurement, while the Ag recoveries were low in the other two alloys, a result which is more consistent with the modelling predictions. S recovery is another example of an assay that might not be correct, with S recoveries measured as 119% in this test, while modelling and the measurements from the assays of the other 2 alloys show values between 0% and 9%. Figure 38 shows low S recoveries to the gas phase, and consequently lower Au loss (as AuS) to the gas phase. This is an artefact of a relatively high Ca content that was assayed in the feed material (probably incorrectly so, potentially due to a small piece of slag inclusion). FactSage® predicted the formation of CaS that is stable in the slag phase and therefore the S reports sparingly to the gas phase.

Figure 38 shows the predicted removal per step for this alloy. Bi removal proceeds more slowly than with the directly melted alloy, as the contribution of vapour species like BiS, BiSe and BiTe is less. It should, however, be noted that Bi recoveries were measured at between 4% and 6% for all the tests, indicating that the contribution of these species (BiTe, etc.) is not significant. It is also possible that the total flow volume is not accurate for the model, as flow during heat-up and cool down periods might have contributed to the available time at a particular temperature and therefore to the vaporisation. The heat-up and cool down periods were not included in the modelling.

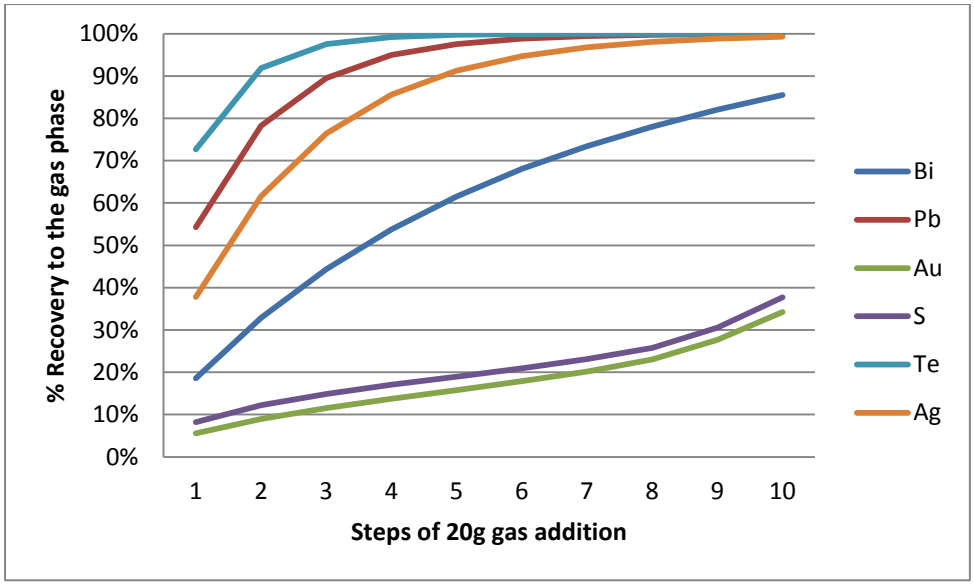

Figure 38: Cumulative recovery to the gas phase for certain elements as predicted by modelling for the roast-melt alloy

Volatile behaviour for alloy from Leach-Roast-Smelt process

The behaviour of this alloy is very similar to the roast-smelt alloy, apart from the lower Fe and Ni content. The comparison between the measured recoveries and the modelled recoveries is given in Table 47.

Table 47: Recovery to the alloy phase (wt%) across the high temperature treatment step of alloy that was produced by leaching, roasting and smelting third stage leach residue. The measured recoveries from experimental work and the modelled recoveries are shown

Element	Actual recoveries	Modelled recoveries
Au	99%	42%
Ir	94%	100%
Pd	101%	100%
Pt	100%	100%
Rh	95%	100%
Ru	88%	100%
Ag	6%	3%
S	9%	0%
As	102%	98%
Bi	4%	21%
Se	0%	0%
Te	15%	0%
Pb	9%	0%
Fe	102%	100%
Cu	83%	95%
Ni	105%	100%

The low recovery value of 88% for Ru is not consistent with the Ru recoveries of the other two alloys (118% and 97%). In order to test whether Ru oxidation, and therefore volatilisation as RuO_4 or RuO_4, could happen thermodynamically, some modelling runs were performed on the system with 20 steps of gas addition (instead of ten) and an O_2 content of 10 000 ppm (instead of 1 000 ppm). In this scenario, pO_2 values reached 0.008 atmospheres at the end of the melt and the small slag phase comprised all the Fe and most of the Ni. Only 0.54% Ru losses were predicted at this point. With the slag phase not activated, the Ru loss to the gas phase was predicted to be 0.86%. However, the smelting step of the Leach-Roast-Smelt also measured low Ru recoveries of 73% to the alloy. The discussion on the smelting step suggests that the lower base metal loadings might affect the Ru losses. It might be possible that air in contact with the melt could oxidise Ru, without oxidising Fe, Ni and Cu (due to their lower prevalence) and that the system is not properly described by equilibrium modelling.

7.2.2 Atomisation

The primary objective of atomisation was to achieve a small particle size, preferably within a narrow size range. The discussion of results will focus on the achieved particle size and the parameters that determine the particle size. Two types of alloy (direct smelt and the roast smelt alloys) were experimentally atomised at 30 bar pressure. Sieve analyses were performed on the atomised alloy, and the weight percentage falling within a sizing interval is provided in Table 48 below. Figure 39 shows the same data set represented as a histogram. The particle size achieved in the experimental set-up is relatively large compared to the current feed material to the PMR, which has a D_{50} around 20 micron.

Table 48: Particle size distribution achieved from atomisation trials on two different alloy types. The wt% falling within a size range is shown per alloy type

Size (micron)	Melt directly alloy	Roast-Melt alloy
+2800	2%	2%
-2800+1000	2%	8%
-1000+500	3%	19%
-500+250	12%	29%
-250+125	29%	26%
-125+75	24%	10%
-75	29%	7%
Total	100%	100%
D_{50}	~125 micron	~275 micron

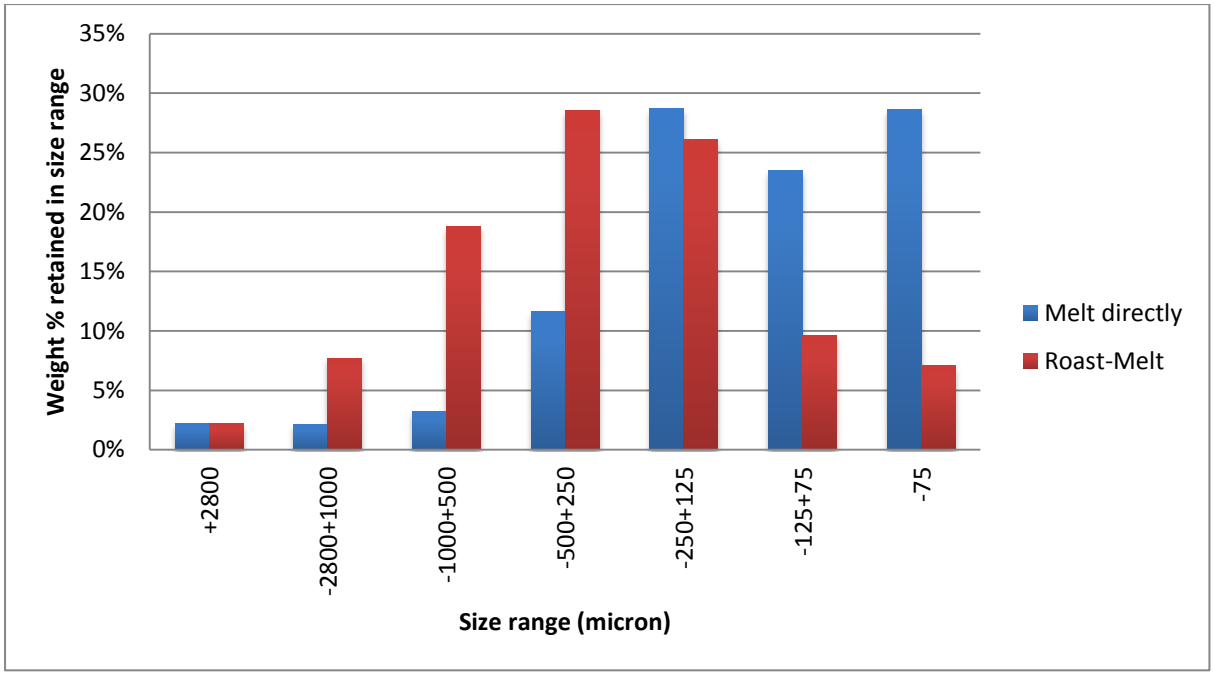

Figure 39: Histogram of sieve analyses shown as weight % retained on sieve size interval

Persson (2012) studied several factors that can influence the particle size (expressed for convenience as D_{50}) of water atomised metal powders. He studied all the major variables, including surface tension, viscosity, melt stream diameter, water pressure, water jet angle and water to metal ratio. The two variables with the highest impact were found to be viscosity and surface tension. The relative importance of viscous and surface tension forces in resisting atomisation is determined by the ratio between the viscous energy dissipation and the surface energy of an atomised alloy droplet. Any change in the composition and temperature will most probably influence both the surface tension and the viscosity of the melt, and unless very good fundamental data and models are available for the studied system, it will be difficult to single out an effect. No data or models for the viscosity or interfacial tension could be found for an alloy that resembled the current system (80% PGMs with a complex mixture of metals that made up the remaining 20%) and it was outside the scope of this study to develop such a model. Only general comments will be made on the trends.

Surface tension has a large impact on the particle size that is achieved through atomisation, with a lower melt surface tension reducing the mean particle size (Dubberstein *et al.*, 2013). In the current work, two different alloys were subjected to the same atomisation conditions (same pressure, water flow and superheat). The alloy resulting from direct smelting had more impurities (in the form of S, Se, Te and As) than the alloy produced by roasting before smelting. S, Se and Te are well known to reduce surface tension (Sahoo *et al.*, 1988) and it was therefore expected that the alloy from direct smelting would have a smaller mean particle size. Table 48 shows that the D_{50} of the directly melted alloy was less than half (125 micron vs. 275 micron) of that of the roast-smelt alloy. Liebermann (1984) showed that Se and Te have a very strong effect on lowering the melt surface tension of a Fe-Ni alloy, even at small rates of addition. Se was shown to reduce the surface tension (N/m) of the melt from 1.3 to 0.9 at an addition rate of 1 atomic per cent. The effect of Te was found to be even greater than the effect of Se. It is suggested that the combined content of S, Se and Te in the directly melted alloy decreased the surface tension and contributed significantly to the smaller particle size.

Dunkley *et al.* (2008) studied Fe-Ni-Cu alloys containing PGMs as well as some of the other elements in the current alloy, such as Cr and S, and found that the relationship between the pressure of the water jets and the resulting particle size is such that the mean particle size can be halved by doubling the pressure. They studied pressures ranging from 20 bar to 200 bar. The pressure of 30 bar in this experiment, being at the lower end of this range, makes the relationship applicable to the current work. They calculated that the pressure (in bar) multiplied by the D_{50} size (in mm) provides a constant (c) for an alloy, and that this can be used to determine the pressure requirement to achieve a particular size requirement. Equation 4 shows this relationship with D_{50} being the median particle size in microns, P being the atomisation pressure in bars and c the constant.

$$D_{50} \times P = c \qquad (4)$$

The constant values were calculated to be around 4.5 for their alloy with 6 wt% S, 5.28 for an alloy with around 1 wt% S and they expected an alloy with no S to have a constant value greater than 6. If we had to apply this same logic to the current experimental work (by utilising the D_{50} obtained from the test done at 30 bar to determine a constant), the alloy generated by direct melting of third stage residue would give a constant (c) of 3.75 and the alloy generated from roast melt would give a constant (c) of 8.25. Using the calculated constants, it was found from Eq. (4) that to achieve a D_{50} of 20 microns would require a pressure of 187.5 bar to atomise the alloy from the direct melting of third stage residue and 412.5 bar to atomise the alloy from roasting and melting third stage residue.

Wang *et al.* (1989) studied the effect of a number of parameters on the particle size of shot that was achieved by atomising Cu in a water jet. They found that the particle size was insensitive to the superheat, but this was probably because of the narrow temperature range that they investigated (with ranges of 50 °C to 120 °C superheat studied). For most melts, melt surface tension becomes lower with increasing temperature, while the viscosity of the melt will also reduce with increased temperature (superheat). Liebermann (1984) studied the effect of superheat on the surface tension of a Fe-Ni alloy. The reduction in surface tension with an increase in temperature was shown to be linear, but the slope was not steep. Surface tension reduced from 1.3 N/m to 1.1 N/m as the temperature increased from 1 100 °C to 1 600 °C. Ankus *et al.* (1992) also studied the effect of superheat on the particle size in the atomisation of silver (Ag). They investigated superheats of 75 °C to 430 °C and found a decrease of particle size to superheat of about 5%-10% per 100 °C of superheat. The effect of superheat is considerably smaller than the effect of pressure, and is therefore of secondary importance.

The hollow particles that were noted in the atomised alloy were not consistent. Some of the alloys had a large proportion of particles with a hollow opening (see Figure 19) and some had nearly all solid particles. Even the particles within a single alloy varied in the amount of porosity that was noticed. Figure 40 shows two particles of the same size and from a single atomisation run that displayed, respectively, significant porosity and no porosity. Stereological effects could partially explain the observed difference in porosity of the particles.

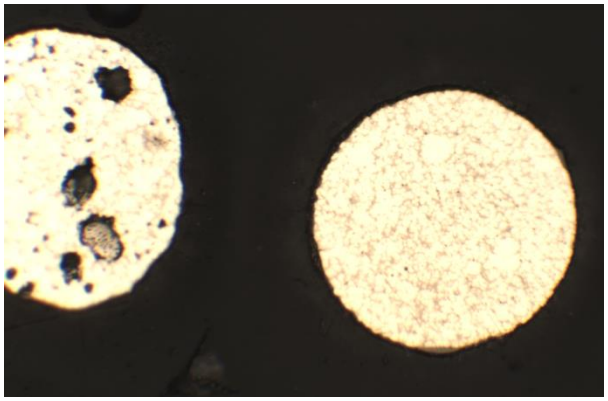

Figure 40: Photo of two particles from the same atomised batch showing very high porosity and no porosity, respectively

Porosity of varying degree was noticed in most of the alloys produced in the smelting test work during slow cooling in the crucible with the slag on top. The porosity was, at times, of such an extent that the alloy appeared like 'swiss cheese', as shown in Figure 41. The rounded edges of the porosity hollows support the idea that the porosity was caused by gas formation (and pressure) and not solidification shrinkage.

Figure 41: Photo of an alloy button that has been sawed in half. The alloy button was left to cool slowly in a graphite crucible with slag on top of the alloy

However, if the same alloy was separated from the slag, re-melted in the graphite crucible and fast quenched, a solid metallic button was formed with no apparent porosity. Figure 42 shows a photo of the same alloy a) allowed to cool slowly in the crucible with slag and b) separated from slag, re-melted and fast cooled. Assaying of the two samples (with and without porosity) and even SEM work did not reveal a difference in the alloy composition or phases. Given the detection of oxygen in the phases from the atomised product (Table 26 in section 4.6), it is possible that the solution of gas happened in the alloy phase. When the metal is slow cooled, sufficient time is allowed for the gas (which has significantly reduced solubility in the solid phase) to nucleate bubbles. In the case of quicker cooling (quenching), sufficient time is not allowed for the gas to diffuse out of the alloy. Although no porosity is then apparent, the gas (eg oxygen) content of the alloy should be measurable.

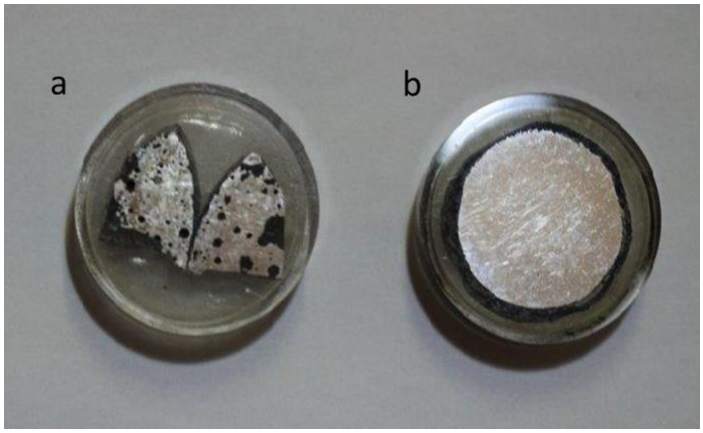

Figure 42: Photo of the same alloy: a) alloy allowed to cool slowly in the crucible with slag and b) alloy separated from slag, re-melted in a crucible and fast cooled

Gas related porosity in metals forms due to changing in gas solubility during cooling. At high temperatures, some gases might dissolve in the molten metal. When the metal cools, the dissolved gas is rejected from the solidifying metal, due to its dramatically reduced solubility in the solid state. At some point this rejected gas will nucleate a bubble in the supersaturated liquid remaining in the droplet, and additional gas will rapidly diffuse to this bubble to expand it. During atomisation, with sufficient initial gas content and sufficient cooling rate, the bubble will grow to the point that it bursts.

A literature search for gas solubility in PGMs provided only a single reference to oxygen solubility in platinum. Velho (1972) studied the diffusivity and solubility of oxygen in platinum and Pt-Ni alloys. The study was done at high temperatures (1 400 °C to 1 550 °C), but in the solid state. Velho found low solubility, only 19 ppm, for oxygen at 1 450 °C and 1 atm oxygen pressure. This low solubility in the solid state suggests that, if any oxygen were dissolved in the molten alloy, gas evolution would result during solidification. This could lead to porosity during slow cooling and atomisation, or to gas species (like oxygen) being trapped in the solidified matrix. Small changes in the conditions that two particles experience (such as the cooling rate) might explain the difference in observed porosity between the two particles in Figure 40.

Several studies have also been done on the solubility of carbon in platinum. Hecq (1981) reported C concentrations of around 1.2% close to the melting temperature of Pt. Siller *et al.* (1968) found that C concentration in Pd at melting point is even higher, at 2.4%. Given the even higher solubility of C in Fe and Ni, it might be safe to assume that some C from the graphite crucible wall might have gone into solution in the metal bath. Yokoyama *et al.* (1998) also found that C diffusion is three to six times faster in Pd, compared to C diffusion in Fe and Ni. However, the solubility of C in Pt and Pd at room temperature is close to zero and the C normally forms graphite inclusions in the metal upon cooling. The presence of oxygen dissolved in the molten metal phase might force CO formation within the alloy, forming CO gas.

The solubility of C in pure molten Cu is very low (0.0004% at 1 475 °C), which is negligible compared to the other metals. The opposite is true for oxygen solubility, with the oxygen solubility in molten Cu >> Fe, Ni, Pt. No porosity was noted in the alloys to which large Cu additions had been made

(alloy Cu content ~ 60% mass), but this observation could also be due to the lower temperature and the different slag type concerned.

7.3 Conclusion

The necessity to atomise the alloy to produce a fine particle for rapid dissolution provided an opportunity to remove two contaminants, Pb and Bi, which were not removed in prior processing. This removal step could be linked to atomisation as a single processing step, which would limit both capital and operational expenditure.

High temperature treatment was shown to be effective in the removal of Pb and Bi, achieving removal efficiencies of > 85% in all the alloys studied (direct melt, roast-melt and leach-roast-melt). The loss of Au as volatile species of AuS, AuSe and AuTe is a concern and Au losses were measured in an alloy that contained S, Se and Te. The actual extent of these losses cannot be quantified from the work done, but it is clear that thermodynamic modelling over-predicted the losses of AuS, while AuSe and AuTe were not available in the database. When S, Se and Te were removed in roasting, Au losses could not be shown to be within the bounds of experimental/sampling/analytical error. Pd losses due to Pd vaporisation could also not be shown with certainty. Ru showed a low recovery (88%) across the high temperature treatment test with low Fe, Ni and Cu content. This finding corresponds to possible Ru losses measured across the smelting step of alloys with low Fe, Ni and Cu content (see Chapter 6).

Observed porosity in the alloys studied (1 400 °C to 1 700 °C), suggest that differential gas solubiliy at temperature leads to porosity during slow cooling and atomisation. Carbon solubility could contribute to this gas formation during solidification, as the solubility of both the gas and C are considerably less in the solid phase. When the cooling conditions are sufficiently rapid, gas entrainment into the solidified phases is possible.

Atomisation was shown to be possible for the high PGM alloys. The presence of contaminants that lower the surface tension (such as S, Se and Te) produces a finer particle. For a certain alloy composition, pressure is the single biggest factor influencing the particle size achieved. For the Roast-Smelt alloy, an estimated pressure of 412 bar bar would be needed to achieve a D_{50} of 20 micron.

Chapter 8: Evaluation of the full pyrometallurgical refining process

This chapter will evaluate the combined pyrometallurgical refining process flow sheet in order to compare the alloy with a typical PMR feed material. Shortcomings of the process studied will be discussed and a more optimal flow sheet will be proposed.

8.1 Performance of the full pyrometallurgical refining process

The flow sheet that was proposed originally (Figure 3) achieved low removal of Fe, Ni and Cu across the smelting step, due to poor pO_2 control in the experimental set-up. This led to the investigation of the possibility of introducing a leaching step prior to smelting to remove these three elements, together with As and Pb, as reported in Appendix A. Figure 43 shows the flow sheet that provided the highest grade of PGM alloy. This flow sheet was studied in consecutive steps and in duplicate to produce a final product that could be compared to a typical PMR feed material. Note that the flow sheet studied differs from the original concept flow sheet (Figure 3) by the addition of the Formic/sulphuric acid leach step, in order to remove Fe, Ni and Cu prior to roasting.

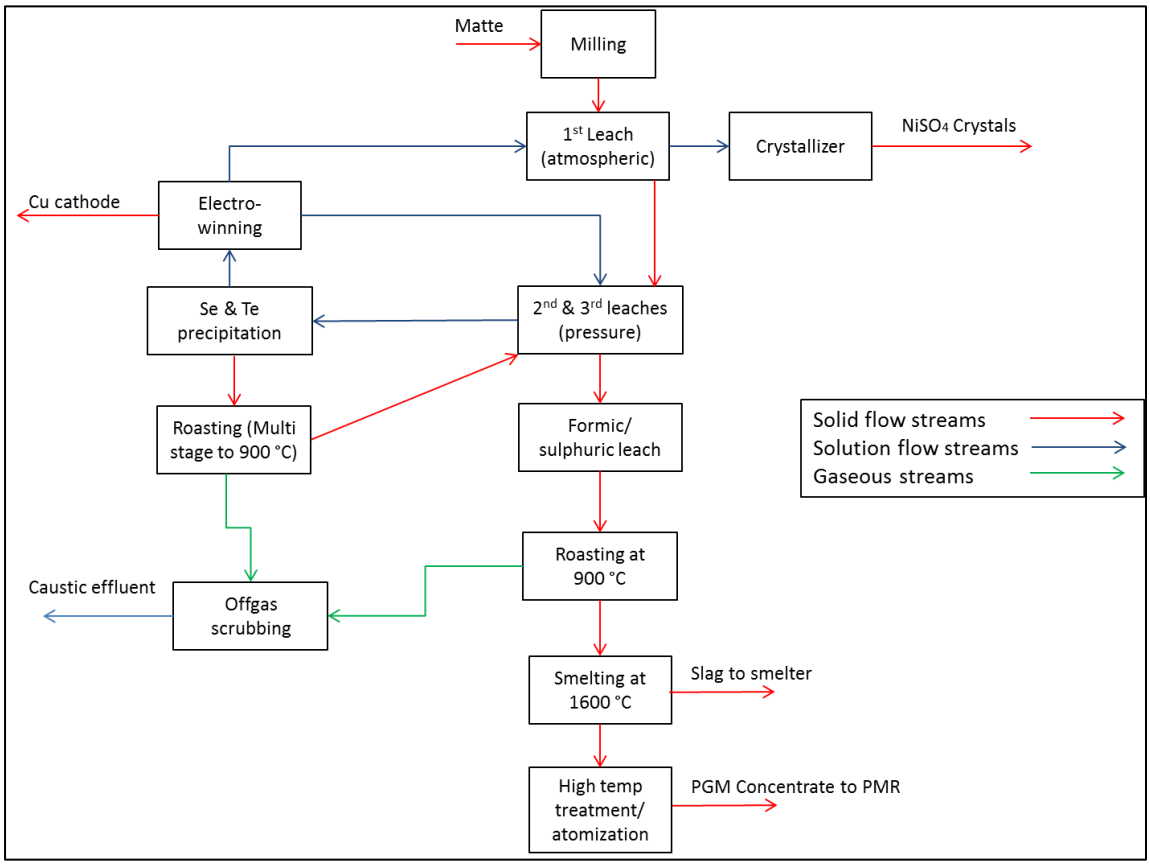

Figure 43: Block flow diagram of the flow sheet that was studied to determine overall rate of recovery and grade of the result of the pyrometallurgical refining process

Below is a summary of the conditions used in the experiments to study consecutive steps in the full flow sheet:

- Leaching of Fe, Ni and Cu from third stage residue:
  - 10:1 liquid to solid ratio.
  - 1:1 Formic to Sulphuric acid ratio.
  - 10% v/v H_2SO_4 concentration.
  - 900 °C for four hours.
- Roasting
  - for 6 hours at 900 °C
  - in muffle furnace with excess oxygen.
- Smelting
  - at 1 600 °C in graphite crucible.
  - No addition of oxidising agent/reduction agents;
  - Addition of only CaO-SiO_2-Al_2O_3-Na_2O slag.
  - Inert gas flushing was done above the crucible.
- High temperature treatment
  - at 1 700 °C for 30 minutes.
  - A graphite crucible was used
  - Inert gas flushing was maintained above the melt.

Table 49 shows the elemental recoveries that were achieved, in each processing step and for the total process. The recoveries are reported as they were calculated in the mass balance for each step. Several data points in the smelting and high temperature treatment step show recoveries substantially more than 100%, which is impossible for a system that cannot release inventory. These data points can be ascribed to sampling error beause of heterogeneity in the alloy and analytical error, sometimes compounded by a very low concentration of the element. Some of the highlights of measured recovery are discussed below:

- The ability to partially remove Fe (70%), Ni (54%) and Cu (80%) with the formic/sulphuric acid leach was confirmed. Partial leaching of Ir (7%) was noted and is described in Appendix A.
- Recovery of the volatile elements of S, Se, Te and Os behaved similarly to the results described in Chapter 5. No As removal was achieved across the roast. This does not correspond with the partial removal results obtained in the roasting test work (see Chapter 5).
- Smelting recovery confirmed the results obtained from the smelting investigation (see Chapter 6).
- High temperature recovery confirmed the results obtained from the atomisation investigation (see Chapter 7).

Table 49: Recoveries achieved per processing step when the recommended flow sheet was experimentally applied on a batch of third stage leach residue

Element	Leaching	Roasting	Smelting	High temp	Total	Slag
Pt	100%	99%	102%	101%	102%	0.0%
Pd	100%	101%	116%	102%	120%	0.1%
Au	100%	101%	126%	100%	127%	0.9%
Rh	100%	107%	91%	96%	94%	0.1%
Ru	100%	94%	73%	89%	61%	0.1%
Ir	93%	100%	150%	95%	133%	0.7%
Sum	100%	99%	102%	100%	101%	0.1%
Ag	100%	105%	46%	6%	3%	1.6%
Os	84%	23%	99%	98%	18%	0.7%
As	100%	104%	132%	104%	143%	0.6%
Bi	100%	98%	181%	4%	7%	9.4%
Cr	83%	79%	82%	97%	53%	30.1%
Cu	20%	102%	135%	84%	23%	4.8%
Fe	30%	95%	138%	103%	40%	12.8%
Ni	46%	111%	131%	106%	71%	1.5%
Pb	100%	118%	144%	10%	16%	1.8%
S	66%	1%	91%	50%	0%	92.4%
Se	100%	0%	257%	59%	1%	66.0%
Si	87%	136%	11%	106%	14%	
Te	100%	29%	136%	15%	6%	7.3%
Al	97%	119%	12%	97%	13%	
Ca	94%	74%	56%	98%	39%	
% Mass loss	**21%**	**12%**	**24%**	**2%**	**58%**	

The elemental composition achieved for the residue/calcine/alloy/slag is provided in Table 50. A final alloy composition of 85.14% 6E could be achieved, with a starting 6E composition of 43.97% in third stage leach residue.

Table 50: Elemental composition in weight percentage of the residue/calcine/alloy/slag generated per processing step when the recommended flow sheet was experimentally applied on a batch of third stage residue

Element	Third stage residue	Formic/sulphuric residue	Roasting calcine	Smelt alloy	High temp alloy	Slag
Pt	23.80	29.95	33.80	45.11	46.59	0.02
Pd	9.91	12.47	14.40	21.91	22.88	0.03
Au	0.52	0.65	0.75	1.24	1.27	0.01
Rh	3.22	4.05	4.94	5.89	5.80	0.01
Ru	5.84	7.35	7.87	7.57	6.87	0.01
Ir	0.68	0.80	0.91	1.79	1.74	0.01
Sum 6E	**43.97**	**55.28**	**62.43**	**83.50**	**85.14**	**0.09**
Ag	1.11	1.40	1.67	1.00	0.06	0.04
Os	3.70	3.90	1.00	1.30	1.30	0.01
As	1.50	1.89	2.24	3.88	4.10	0.02
Bi	0.05	0.06	0.07	0.17	0.01	0.01
Cr	0.49	0.51	0.46	0.50	0.49	0.21
Cu	0.95	0.24	0.28	0.49	0.42	0.02
Fe	3.18	1.20	1.29	2.34	2.47	0.25
Ni	2.49	1.44	1.82	3.13	3.38	0.04
Pb	0.22	0.28	0.37	0.70	0.07	0.01
S	10.10	8.35	0.05	0.06	0.03	0.07
Se	1.92	2.42	0.01	0.03	0.02	0.01
Si	3.58	3.94	6.08	0.88	0.95	22.30
Te	0.22	0.28	0.09	0.16	0.02	0.01
Al	0.31	0.38	0.51	0.08	0.08	5.70
Ca	0.50	0.59	0.50	0.37	0.37	21.80
TOTAL:	**74.29**	**82.14**	**79.11**	**98.58**	**98.92**	**50.59**

** Os assays were not performed in this test. The composition of Os was manually inserted (based on other test results) to have the composition as complete as possible.

A comparison was done between the final concentrate that is currently produced by the BMR and the product of the pyrometallurgical refining process proposed in this thesis. The comparison is shown in Table 51. The total of the current BMR concentrate adds up to only 87.5% and the remainder would probably be a mixture of oxides, hydroxi-oxides and sulphates. The standard deviation of the BMR concentrate (expressed as % of feed composition) is also shown in the table. From the table it can be seen that the PGM content of feed to the PMR could improve from 65.8% to 85.1%. Percentages of all the contaminants are lower, apart from As and Ni. It should be noted that the As content in the test batch was very high and no removal was measured in the roasting step, which is not consistent with the test work done on roasting in the rest of the study. The largest benefits are seen in the low levels of Ag, Bi, Pb, S, Se, Si and Te.

Table 51: Comparison between the current BMR concentrate fed to the Lonmin PMR and the alloy that could be produced if the proposed pyrometallurgical refining flow sheet were applied

Element	Current BMR concentrate (%)	Standard deviation of current BMR concentrate (%)	Alloy from pyrometallurgical refining process (%)
Pt	34.2	8%	46.6
Pd	15.9	8%	22.9
Au	0.8	10%	1.3
Rh	5.0	12%	5.8
Ru	8.2	17%	6.9
Ir	1.8	14%	1.7
Sum	**65.8**		**85.1**
Ag	1.1	12%	0.1
Os	1.5	22%	1.3
As	2.4	17%	4.1
Bi	0.2	0%	0.0
Cr	1.0	62%	0.5
Cu	2.1	62%	0.4
Fe	2.6	58%	2.5
Ni	1.5	33%	3.4
Pb	3.5	36%	0.1
S	1.1	50%	0.0
Se	0.5	121%	0.0
Si	2.1	60%	0.9
Te	1.0	61%	0.0
Al	0.8	65%	0.1
Ca	0.3	68%	0.4
TOTAL:	**87.5**		**98.9**

8.2 Process limitations

The flow sheet that was investigated showed some deviations from the initial modelling that was performed. Some of these deviations can be explained by poor or uncertain control over parameters such as redox potential in the melt, while others can be explained by uncertain mineralogy, as with As removal across the roast. These limitations would diminish the feasibility of implementing the process, as PGM losses could be costly and contaminant concentrations problematic. It is possible that some of the limitations, such as better atmosphere control in the melt and the atomisation step, could be engineered out, while others could potentially be optimised by additional test work. The most important concerns regarding the flow sheet will be discussed from a scientific, engineering and business perspective:

1. Poor As removal across the roasting step. The roasting test work performed at 9 00 °C (presented in Chapter 5) showed that As removal of around 40% could be achieved (in all six of the tests

done at this temperature in air). The poor removal efficiency achieved in the repeat test (reported in this chapter) raises a flag of caution. Arsenic did not react according to the modelling in either the roasting or leaching steps, and the speciation change of As during the roasting step is not properly understood. A number of residue samples were taken from the pressure leach process during the investigation. It appears that As could sometimes be present in refractory minerals and that As behaviour across the roast could be variable. A lower roasting temperature might show improved As removal, with Table 27 showing the best As removal at between 600 °C and 700 °C. A two-step roasting approach could be followed, controlling for three hours at 600 °C and three hours at 900 °C, to more effectively target As. No solution to the problem of near quantitative removal of As could be presented in this work, and there is good reason to believe that As removal might vary from batch to batch.

2. Ru losses were measured across the smelting step at 1 600 °C on an alloy with low Fe, Ni and Cu content and with poor gaseous atmosphere control. Ru would be the PGM with the highest probability of loss across the smelting step, due to oxidation and volatilisation. Oxidation could proceed by the oxygen already contained in the feed material during heating, or by the gas atmosphere in contact with the melt. The fact that 100% recovery of Fe and Ni was measured across the smelting step, means that the system either did not achieve equilibrium, or that Ru losses occurred early in the melt. This can potentially be addressed by one or more of the following corrective steps: 1) mixing a mild reductant with the melt to reduce oxygen content during the heating phase, 2) allowing more Fe, Ni and Cu into the melt (to buffer Ru oxidation), 3) lower temperature requirements, or 4) better control over the pO_2 achieved in the melt. High Ru losses might be a fatal flaw associated with the flow sheet.
3. Ru loss across the high temperature treatment step on an alloy with low Fe, Ni and Cu content. The high temperature treatment step was once again performed without a sealed chamber, and some air ingress might have occurred. Remedial actions could include better gas atmosphere control and a higher Fe, Ni and Cu content.
4. If satisfactory removal of Fe, Ni and Cu cannot be achieved across the smelting step, it would be possible to introduce a leach prior to roasting or after atomisation. Test work in Appendix A shows that about 7% Ir goes into solution across a formic/sulphuric acid leach on the pressure leach residue. Solution from the formic/sulphuric acid leach could be integrated into the BMR process, where partial cementation in contact with fresh matte will limit overall losses, but some Ir losses might still occur.
5. The calcine from the Leach-Roast step appears completely molten only at 1 510 °C. The smelting temperature requirement is therefore around 1 600 °C. At this temperature, refractory wear will be higher, in the form of graphite oxidation with any oxygen in the atmosphere, as well as crucible interaction with the melt.
6. The use of a smelting step will produce an alloy and a slag phase. It is envisaged that these phases will be separated by cooling and mechanical separation. It is also envisaged that cooling will be done through a casting process (potentially a gravity feed in multiple moulds displacing slag). However, casting would mix the alloy and slag phases, dispersing alloy droplets into the slag. The alloy needs to settle through the slag before it solidifies and, invariably, some alloy might be lost to the slag. This alloy can be recovered by either remelting the slag, or by crushing and gravity separation. It is also possible to simply send the slag to the smelter complex and allow the alloy to be recovered across the current smelting step (performed on flotation concentrate). It is also possible to make use of tapholes set at different elevations in order to tap the phases separately.

7. The slag composition used in this test work showed low chrome solubility and the stability of a spinel phase. The spinel could contribute to chrome settling on top of the alloy phase, not allowing clear separation to the slag phase. A slag composition with a higher capacity for chrome spinel should be investigated.
8. The test work on dissolution of alloy in the HCl/Cl_2 environment (Appendix B) showed poor and variable dissolution. This remains a concern and more work is needed to establish the conditions needed to bring the alloy into solution. It needs to be established whether near full dissolution of the alloy can be achieved, and what the conditions for this would be.
9. Poor understanding of the commercial benefit associated with removing contaminants from the PMR. The impact on recovery, the rate of residue formation and the rate of effluent production is not quantified nor has it been studied in detail.
10. Manhandling of material during the roasting, smelting and atomisation steps. Any required manhandling of high PGM materials introduces a security risk. These risks can be managed, either by security systems, or by complicated materials-handling equipment, to avoid manhandling.
11. Safety and health concerns around exposure to vapours and high temperatures of the new process.
12. First-of-a-kind implementation in the PGM industry.
13. Introduction of complexity and a process that will have no existing skill-base in the existing BMR and PMR.

8.3 Proposed optimal process route

Based on the shortcomings of the process that has been described in the above sections (8.1 and 8.2), a slightly different process route is proposed. The leach to remove Fe and Ni can be moved to the final step of the process, after atomisation, as can be seen in Figure 44.

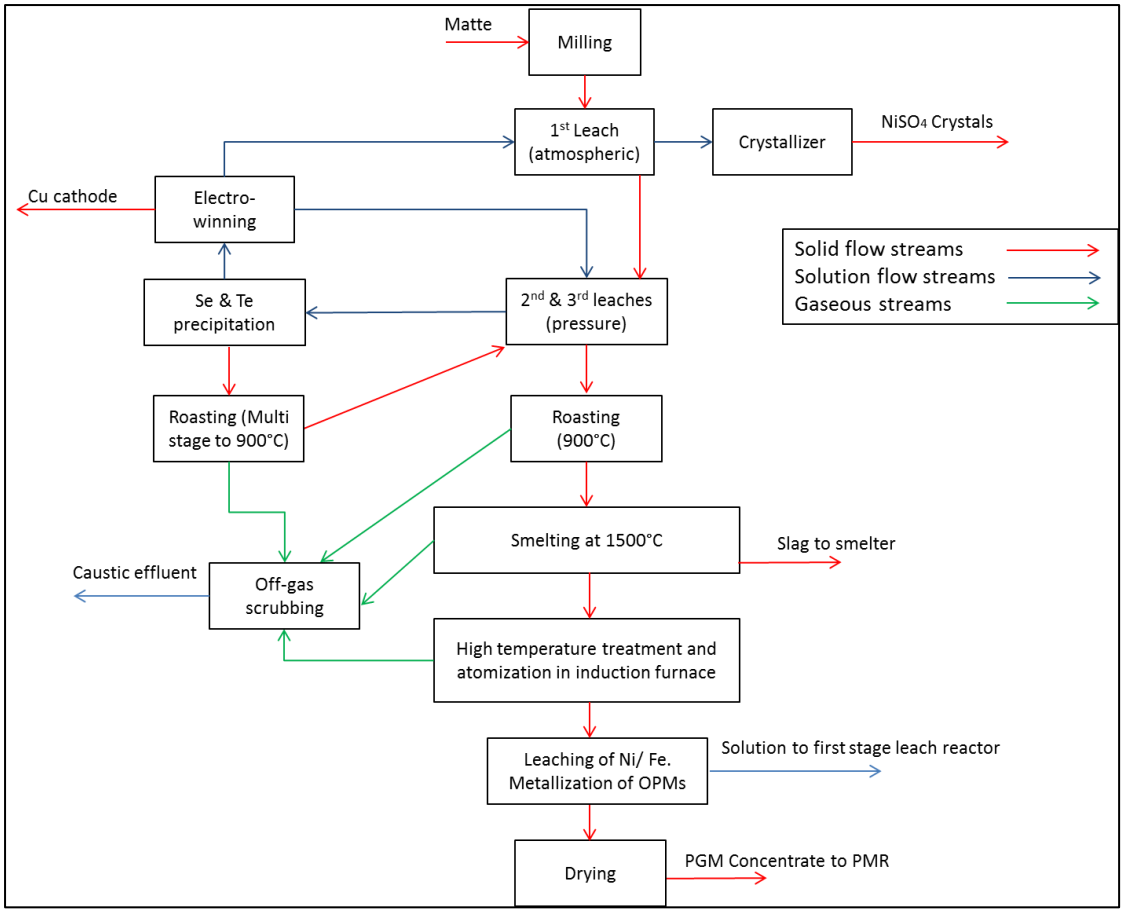

Figure 44: Proposed optimal flow sheet for pyrometallurgical refining of high grade PGM containing residues

Moving the leach to the final position will have the following benefits:

1. Ru losses were shown to be lower during both the smelting and the high temperature treatment steps with a higher Fe, Ni and Cu content in the alloy.
2. The temperature requirement in the smelting step could be lowered by almost 100 °C, simplifying furnace operation, integrity, cost and maintenance.
3. Improved leachability: Final metallisation of the OPMs can occur during the reducing formic acid/sulphuric acid leach (as is currently the case with the formic leach following on the caustic leach in the Lonmin BMR). Partial removal of Fe, Ni and Cu might leave the alloy more porous, further improving leachability.

Since metallisation of the OPMs will be a criterion for the final leach after atomisation, the ORP might have to be maintained as negative, thereby restricting Cu from going into solution. This is discussed in Appendix A.

General note on furnace/crucible choice

In order to allow more control over the oxygen partial pressure achieved in the melt, interaction of the crucible with the melt will need to be limited. This can be achieved by using either a refractory lined crucible or a cooled graphite lined crucible (that should support a freeze lining). These types of

crucible could be fitted into an AC or DC or plasma arc furnace. Plasma arc furnaces often make use of cooled graphite crucibles and are used extensively to recover PGMs from scrap and autocatalytic converters. Induction heating is not ideal for limiting crucible interaction, due to the requirement to transfer heat into the melt via a receptor crucible.

Induction furnace heating through direct coupling is mostly used to melt alloys for atomisation. It is recommended that a ceramic (such as Alumina or Zirconia) crucible be used for heating, instead of a graphite crucible. The wear rates on the graphite crucible at 1 700 °C (when maintained at temperature during the high temperature treatment step) would probably render it not be cost effective.

Chapter 9: Conclusion

Although every chapter that has presented results already contains its own conclusions with the major findings from that specific investigation, a combined conclusion in this chapter will endeavour to tie the process together, focussing on the interlinks and the practical aspects. It will also conclude on the objectives and hypotheses that were set in Chapter 2.

Hydrometallurgy is used almost exclusively in the PGM industry to refine material with a PGM content of more than a couple of percent. This study has fundamentally and practically illustrated that it is possible to use pyrometallurgy to separate PGMs from a large number of metals, oxides and amphoterics by making use of their noble nature (low vapour pressures and resistance to oxidation at high temperatures). By effectively using a combination of roasting and smelting, it is possible to upgrade the PGM content of a pressure leach residue from a low forty per cent to a high eighty per cent, with low PGM losses.

Ru losses (between 9 wt% and 39 wt%) were shown to be sensitive to the combined Fe, Ni and Cu content of the feed to the smelting step, to the temperature, and to the contact of air with the melt. The use of Cu as an alloy modifier was also shown to be a concern in Ru recovery, because of the insolubility of Ru in a Cu alloy. Au losses were also shown to be a concern, because the presence of Se, Te and S at high temperatures increased the vapour pressure of species such as AuSe, AuTe and AuS.

Almost no literature exists on the high temperature behaviour of high grade PGM residues or alloys with > 50% PGM content. Thermodynamic equilibrium modelling was shown to be a very useful tool to interpret and understand elemental behaviour across the roasting and smelting steps. However, FactSage® modelling did not accurately predict the following scenarios:

- The behaviour of As, S, Os and Te during the roasting step. This is most probably due to the complex speciation, association and distribution of metals in the amorphous residue coming from a BMR process.
- The volatility of Au in the presence of S, Se and Te in the alloy phase.
- The extent and composition of the matte phase in melts where a matte phase was stable, including the deportment of S, Se, Te and Pb.
- Melting temperatures of the alloy phase were not accurately predicted, as there was under-prediction of the melting temperature without solid solution phases activated and over-prediction of the melting temperature with solid solution phases activated, although it was fully understood that the actual melting temperature would fall somewhere in between the two.
- Ru losses were measured during the smelting and high temperature treatment step with low Fe, Ni and Cu loadings and poor pO_2 control. The measured Ru losses ments were not predicted by modelling.

Roasting was shown to be a convenient processing step by which to remove volatile elements in a controlled environment without any PGM losses. The quantitative removal of S, Se and Te prevents possible Au losses in the subsequent smelting step. The removal of S, Se, Te, As and Os across the smelting step was shown to be more difficult and risky than their removal across the roasting step.

Special attention would be required when designing the roasting step for the off-gas, materials handling and particulate suspension/reticulation in the gas. However, air could be used as an oxidising medium in the roast and a stationary bed roaster could achieve similar results to those of a fluid bed roaster, albeit at longer times (four to six hours being required instead of two hours). Below follows a summary of the most important conclusions from the roasting step:

- S removal proceeded better than modelling had predicted, with limited heat stable sulphate formation, and almost complete S removal is possible at temperatures as low as 700 °C. Also, Se removal is almost complete at 600 °C.
- Arsenic removal proved difficult, with neither temperature nor the reducing/oxidising environment showing clear clues to the reason for the poor removal efficiency. Arsenic might be associated with certain metals or minerals that is controlling the mass transfer in the residue.
- Te removal proceeded slowly and improved with both time and temperature in an oxidising environment.
- The incomplete removal of Os cannot be satisfactorily explained. It was suggested that Os could have associated with other PGMs (such as Ru) in a solid solution phase that might depress the activity and, correspondingly, the fugacity/vapour pressure.
- PGM oxidation (Pd, Rh, Ir and Ru) was confirmed, and it seems that thermodynamic modelling predicts the behaviour of these elements during roasting quite well.
- Extensive solid solution formation encompassing Pt, Pd and some Rh was observed, as well as spinel phase formation. However, re-crystallisation to the spinel phase proceeds slowly and clear distinction of minerals was not easy. Many metals were noted to be still in a blended mix with oxygen (no clear minerals emerging) at the end of a six hour roast.
- It is possible to replace both the high pressure and low pressure caustic leaches from the BMR process with two roasting steps.

Further investigation is merited into the poor extent of removal of Osmium and Arsenic from the BMR residue, the speciation of Pb and the potential inclusion of Ru and Rh in the spinel phase.

Smelting was shown to be effective in forming an alloy phase and a slag phase that separated without the addition of a collecting agent. After solidification, separation of alloy and slag proceeded easily through mechanical impact. Special attention will be required when designing the smelting step for the off-gas, materials handling, furnace type, slag type and the casting arrangement to allow for slag/alloy separation. The furnace type and design should minimise interaction of the crucible, electrodes, etc. in order to allow for good redox control. A summary of the major conclusions from the smelting step is provided below:

- The smelting step effectively removed the stable oxides of SiO_2, Al_2O_3, CaO and MgO to the slag phase.
- The experimental set-up did not allow proper redox control and the graphite crucible interaction reduced Fe, Ni, Cu, As and Pb to the alloy phase. Sufficient evidence was presented that good deportment of Fe, Ni, Cu, As and Pb to the slag phase could be achieved if the melt redox potential were controlled better than was achieved in the experimental set-up.

- Ru losses were not observed during heating, despite Ru entering the feed in the oxidised state, and even with the addition of an oxidising agent. This was probably due to the high heating rate and dissociation of RuO_2 before further oxidation could take place (possibly assisted by the graphite crucible interaction). However, Ru losses were shown to be possible at low Fe, Ni and Cu content (6.8 wt%), high temperature (1 600 °C) and with poor gaseous atmosphere control, as when some air was allowed to come into contact with the melt. Final removal of Fe, Ni and Cu should rather be done from atomised alloy, although this option was not experimentally explored in this thesis.
- Prior removal of S, Se and Te would be necessary if high temperatures (> 1 600 °C) were planned for the melt, due to vaporisation of Au species such as AuS, AuSe and AuTe. No clear Au losses could be shown during the melt at 1 400 °C in the presence of Se, Te and S. However, a recovery of 79% at 1 700 °C was recorded in the presence of 6% Se, Te and S.
- The melting temperature (all-molten temperature or liquidus temperature) is influenced by the presence of contaminants. Removal of S, Se, Te and As through roasting lifts the observed melting temperature from 1 230 °C to 1 450 °C. Partial removal of Fe, Ni and Cu further lifts the observed melting temperature to 1 510 °C.
- Cu can be used as an alloy modifier. With addition of Cu to achieve a Cu content in the alloy phase of > 60% by weight, melting temperatures as low as 1 200 °C are sufficient to collect PGMs and separate them from the slag phase. However, Ru is insoluble in the Cu-rich alloy, and settled through the Cu alloy. Varying Ru recoveries were measured, pointing to a possible loss mechanism whereby Ru is not properly collected and drained to the alloy phase.
- The removal of Pb was shown to be consistently lower than modelling predictions at 1 400 °C, 1 500 °C and 1 600 °C, even with the application of a partial vacuum of 0.3 bar absolute. Rapid and near complete Pb removal proceeded at 1 700 °C and atmospheric pressure.
- Cr recovery to the alloy phase was influenced by the presence of spinel originating from the roasting step possibly settling through the slag and being separated with the alloy phase. The slag chemistry should be optimised to allow for greater spinel absorptive capacity.

Atomisation was shown to be an effective method to produce fine particulate from the alloy phase. Due to the experimental set-up limitations of 30 bar pressure, particulate of the required sizing, D_{50} of 20 micron, could not be produced. Using equations from literature, the pressure requirement to achieve the required size was calculated as 412 bar. Porosity in the alloy particles and in the alloy buttons testified to the solubility of gases in the alloy phase. The cooling rate was shown to influence the porosity. Greater than 2 wt% oxygen was measured in the atomised alloy, indicating that some gas could be locked in the solidification structure. With very low solubilities of oxygen in the alloy, the oxygen could be present as oxides with the OPMs. Atomisation will probably have to be implemented in an inert gaseous environment, adding to the required cost and complexity. Pb removal was not achieved across the roasting, which is a fundamental limitation or the smelting, an experimental limitation, steps. It was shown that a high temperature treatment step could be used for Pb and Bi vaporisation when the alloy is melted for atomisation. Short times (30 minutes) at 1 700 °C showed near quantitative removal of Pb, Bi and Ag. If Ag is recovered as a pay metal, the use of the high temperature treatment step would not be viable. This high temperature treatment

step would require that S, Se and Te have already been removed, to avoid Au losses, and that oxygen is not allowed to come into contact with the melt, to avoid Ru losses.

Dissolution behaviour of the atomised alloy in a HCl/Cl_2 environment showed that dissolution proceeded at similar ORP values, temperatures and rates as with the current BMR concentrate. However, applying similar dissolution conditions to those used on BMR concentrate to the alloy, showed varying and poor results, with only 45% to 92% of the alloy going into solution. The remaining residue was a mixture of many metals, but the poor dissolution behaviour of the OPMs made the largest contribution. Different leaching conditions might improve the dissolution behaviour, but different atomisation conditions might also be required, avoiding oxygen contact during atomisation. It would also be possible to do a reducing leach on the atomised alloy in order to metallise any OPM oxides that might have formed during atomisation. More work would be necessary to show that the high PGM alloys can achieve near complete dissolution in HCl/ Cl_2.

Partial removal of Fe and Ni (about 50 wt%) and Cu (about 80 wt%) from pressure leach residue was shown to be possible through the use of a combined formic acid/sulphuric acid leach. However, about 7 wt% Ir went into solution across this leach. The lower content of Fe, Ni and Cu also raised concern about Ru losses across the smelting and high temperature treatment steps. It was recommended instead to perform the combined formic/sulphuric acid leach on the alloy after atomisation, although this was not studied experimentally. The advantages of doing the leach on the alloy is that Fe and Ni would still be available during smelting for alloy modification, the atomised particles could be left porous after leaching and a reducing leach could improve OPM dissolution in the PMR.

References

Ankus, A.T. & Venter, R.D. 1992. The water atomization of silver: effect of pressure and superheat, *Powder Technology*, **73**(2): 169-179.

Baboian, R. 2005. *Corrosion Tests and Standards: Application and Interpretation*. West Conshohocken, PA: ASTM International.

Bale C.W., Chartrand P, Decterov S.A., Ben Mahfoud R., Melançon J., Pelton A.D., Eriksson G., Hack K. & Petersen S. 2001. *FactSage®*: *Thermochemical Software and Databases*. Montreal: Ecole Polytechnique de Montreal, CRCT.

Bale, C.W., Bélisle, E., Chartrand P., Decterov S.A., Eriksson, G., Hack, G., Jung, I-H., Kang, Y-B., Melançon, J., Pelton, A.D., Robelin, C., Petersen, S. & Bale, P. 2008. FactSage® Thermochemical Software and Databases – Recent Developments, *CalPhad J*., **32**(2): 189-228.

Bezuidenhout, G.A., Eksteen, J.J., Akdogan, G., Bradshaw, S.M. & De Villiers, J.P.R. 2013. Pyrometallurgical upgrading of PGM-rich leach residues from the Western Platinum Base Metals Refinery through roasting, *Minerals Engineering*, **53**, November: 228‑240.

Bezuidenhout, G.A. & Eksteen, J.J. 2012. Refining of platinum group metals concentrates, Patent publication number WO 2012/104806 A1, Publication date 9 August 2012.

Bezuidenhout, G.A. 2013. Personal visit to Northam smelter and BMR, April 2013.

Brenan J.M., Finnigan G.F., McDonough W.F. & Homolova V. 2012. Experimental constraints on the partitioning of Ru, Rh, Ir, Pt and Pd between chromite and silicate melt: The importance of ferric iron, *Chemical Geology*, **302-303**, April: 16-32.

Capobianco C.J. & Drake M.J. 1990. Partitioning of ruthenium, rhodium, and palladium between spinel and silicate melt and implications for platinum group element fractionation trends, Geo*chimica et Cosmochimica Acta*, **54**(3), March: 869-874.

Crundwell, F., Moats, M.S., Ramachandran, V., Robinson, T.G. & Davenport, W.G. 2011. *Extractive metallurgy of Nickel, Cobalt and Platinum-group metals.* Amsterdam: Elsevier.

Dorfling, C., Akdogan, G., Bradshaw, S.M. & Eksteen, J.J. 2011. Determination of the relative leaching kinetics of Cu, Rh, Ru and Ir during the sulphuric acid pressure leaching of leach residue derived from Ni-Cu converter matte enriched in platinum group metals, *Minerals Engineering*, **24**(6): 583-589.

Dorfling, C., Akdogan, G., Bradshaw, S.M. & Eksteen, J.J. 2013. Estimation of Rh, Ru, and Ir leaching kinetics during the sulfuric acid pressure leaching of Ni–Cu matte as a function of temperature, pressure, and acid concentration, *Hydrometallurgy*, **138**: 21–32.

Du Preez, R. C. 2007. *Investigating the effect of slag chemistry on the chrome deportment between slag and matte phase*, Thesis presented in partial fulfilment of the requirements for the degree MScEng, in the Faculty of Engineering, University of Stellenbosch.

Dubberstein, T. & Heller, H. 2013. Effect of surface tension on gas atomization of a CrMnNi steel alloy. *Steel Research International*, **84**(9): 845-851.

Dunkley, J.J., Norval, D., Jones, R.T. & Chennels, P. 2008. *Water atomization of PGM-containing intermediate alloys*. Third International Platinum Conference, 'Platinum in Transformation'. The Southern African Institute of Mining and Metallurgy: 155-159.

Fourie, M.A. 2011. *Material characterization and dissolution properties of various Lonmin PMR feed materials*. Final year BEng project, Department of Process Engineering, Stellenbosch University.

Frosta, R.L., Waina, D., Martensa, W.N., Ashley C. Lockea, A.C., Martinez-Friasa, J., Rulla, F., Thermal decomposition and X-ray diffraction of sulphate efflorescent minerals from El Jaroso Ravine, Sierra Almagrera, Spain, 2007, Thermochimica Acta, **460** (1–2): 9–14.

Gervilla, F., Makoviky, E., Makovicky, M. & Rose-Hansen, J. 1994. The system Pd-Ni-As at 790 °C and 450 °C, *Economic Geology*, **89**(7): 1630-1639.

Hecq, A., Robert, T. & Hecq, M. 1981. On the study of sputtered C-Pt compounds and their behaviour in the CO oxidation reaction, *Journal of Less Common Metals*, **80**(2): 83-89.

Heshmatpour, B. & Heestand, R.L. 1985. Recovery of Ir from scrap and residues, *Journal of Less Common Metals*, **105**(1): 119-128.

Ismunandar, I., Kennedy, J.B. & Hunter, B.A. 1999. Phase transformation in the $CuRh_2O_4$: A powder neutron diffraction study, *Materials Research Bulletin*, **34**(1): 135-143.

Jehn, H. 1984. High temperature behaviour of platinum group metals in oxidizing atmospheres, *Journal of Less-Common Metals*, **100**: 321-339.

Jones, R.T. 2005. *An overview of Southern African PGM Smelting*. Nickel and Cobalt 2005: Challenges in Extraction and Production, 44th Annual Conference of Metallurgists, Calgary, Alberta, Canada, 21-24 August: 147-178.

Johnson, R.T. 2012. Plasma smelting technology that can be used to recover precious metals from electronic scrap, *Recycling Today*, April. Online: https://www.recyclingtoday.com/rt0412-plasma-smelting-technology-electronics.aspx Accessed: January 2014

Jung-Woo Park, J.W., Campbell, I.H. & Eggins, S.M. 2012. Enrichment of Rh, Ru, Ir and Os in Cr spinels from oxidized magmas: Evidence from the Ambae volcano, Vanuatu, *Geochimica et Cosmochimica Acta*, **78**: 28-50.

Kleeberg, R. & Bergmann, J. 2002. *Quantitative phase analysis using the Rietveld method and a fundamental parameter approach*. Powder Diffraction: Proceedings of the Second International School on Powder Diffraction, Kolkata, Eds: S.P. Sengupta and P. Chatterjee. 63-67.

Lakefield Research. 2000. *Internal investigation for Lonmin: Report on the pressure caustic leach of BMR third stage concentrate and attempted inerting of the leachate*. Johannesburg: Lakefield Research.

Langmuir, D., Mahoney, J. & Rowson, J. 2006. Solubility products of amorphous ferric arsenate and crystalline scorodite (FeAsO4. 2H2O) and their application to arsenic behaviour in buried mine tailings, *Geochimica et Cosmochimica Acta,* **70**(12):2942-2956.

Latti, D. & Adair, B.J.I. 2001. An assessment of stereological assessment procedures, *Minerals Engineering*, **14**(12): 1579-1587.

Liebermann, H. 1984. Effect of elemental additions and superheat on Fe-Ni base metal surface tension and metallic glass embrittlement, *Journal of Non-crystalline Solids*, **61 & 62**: 719-724.

Lloyd, G.E. 1985. Review of instrumentation, techniques and applications of SEM in mineralogy. In White, J.C. Ed. *Short course in applications of electron microscopy in the earth sciences*. Québec: Mineralogical Association of Canada.

Marsden, J.O. & House, I. 2006. *Chemistry of Gold Extraction*, 2nd edition, Englewood, CO: Society of Mining, Metallurgy, and Exploration.

Matkovic, P. & Matkovic, T. 1993. A new intermetallic phase in the Pd-Pb-As system, *Journal of Alloys and Compounds*, **202**(1-2): 107-112.

McCulloch, N. 2012. *Internal report to Lonmin: Minor element deportment study across the BMR process*.

Mitov, I., Paneva, D., Boris, K., Comparative study of the thermal decomposition of iron oxyhydroxides, 2002, Original Research Article, Thermochimica Acta, **386** (2): 179-188.

Neikov, O.D., Naboychenko, S., Mourachova, I.B., Gopienko V.G., Frishberg, I.V. & Lotsko, D.V. 2009. *Handbook of non-ferrous metal powders: Technologies and applications.* Amsterdam: Elsevier Science.

Nell, J. 2004. Melting of platinum group metal concentrates in South Africa, *The Journal of the South African Institute of Mining and Metallurgy*, **104**(9): 423-428.

Outotec. 2011. *HSC Chemistry: thermochemical software with a versatile flowsheet simulation module, version 7.1*. Espoo, Finland: Outotec.

Overbeek, G. 2013. *Investigation into the upgrading of PGMs from the Lonmin Base Metal Refinery third stage leach residue*. Internal report on work conducted for Lonmin, August 2013.

Persson, F. 2012. *A study of factors affecting the particle size of water atomized metal powders*, PhD Thesis. School of Industrial Engineering and Management, Royal Institute of Technology, Stockholm.

Pokrovski, G.S., Borisova, A.Y. & Harrichoury, J. 2008. The effect of sulphur on vapour–liquid fractionation of metals in hydrothermal systems, *Earth and Planetary Science Letters*, **266**: 345-362.

Raevskaya, M.V., Yanson, I.E., Tatarkina, A.L. & Sokolova I.G. 1987. The effect of nickel on interaction in the copper-ruthenium system, *Journal of the Less Common Metals*, **132**(2): 237-241.

Righter, K., Campbell A.J., Humayun, M. & Hervig, R.L. 2004. Partitioning of Ru, Rh, Pd, Re, Ir, and Au between Cr-bearing spinel, olivine, pyroxene and silicate melts, *Geochimica et Cosmochimica Acta*, **68**(4): 867-880.

Ritchie, S. & Eksteen, J.J. 2011. Investigating the effect of slag bath conditions on the existence of multiphase emulsion zones in PGM smelting furnaces using computation fluid dynamics, *Minerals Engineering*, **24**(7): 661-675.

Sahoo, P., Debroy, T. & McNallan, M.J. 1988. Surface tension of binary metal- Surface active solution systems under conditions relevant to welding metallurgy, *Metal Transactions B*, **19**(B): 483-491.

Siller, R.H., Oates, W.H. & McLellan, R.B. 1968. The solubility of Carbon in Palladium and Platinum, *Journal of the Less Common Metals*, **16**:71-73.

Smith, S. 2012. *Mineralogical analyses of BMR residues*. Internal report by ALS Chemex, to Lonmin, 7 September 2012.

Steenekamp, N. & Dunn, G.M. 1999. *Operation of and improvements to the Lohnro base metal refinery*, Proceedings of EPD Congress, Minerals and Metals Society 1999, San Diego: 365–378.

Steenekamp, N.J. & Turner-Jones, M.T.J. 2012. *The Lonmin Base Metal Refinery: Operation and continual improvements 1985 to 2012*, MetSoc Conference, Toronto, 2012.

Thyse, E., Akdogan, G. & Eksteen, J.J. 2010. The effect of changes in iron-endpoint during Peirce-Smith converting on PGE-containing nickel converter matte mineralization, *Minerals Engineering*, **24**(7): 688-697.

U.S National Library of Medicine: Toxicology and Environmental Health Information Program. Online: http://www.nlm.nih.gov/pubs/factsheets/sis.html Accessed: November 2012

Van Schalkwyk, R.F., Eksteen, J.J., Petersen, J., Thyse E.L. & Akdogan, G. 2011. An experimental evaluation of the leaching kinetics of PGM-containing Ni-Cu-Fe-S Peirce Smith converter matte, under atmospheric leach conditions, *Minerals Engineering*, **24**(6): 524-534.

Velho, L.R. & Bartlett, R.W. 1972. Diffusivity and solubility of oxygen in Platinum and Pt-Ni alloys, *Metallurgical Transactions*, **3**(1): 65-72.

Vines, R.F. &, Wise, E.M. 1941. *The Platinum Metals and Their Alloys*. Toronto: International Nickel Company.

Wang, X.S. & Latto, B. 1989. Shot production by water atomization, *Powder Technology*, **59**(3): 209-216.

Waychunas, G.A. 1991. Crystal chemistry of oxides and oxyhydroxides, *Reviews in Mineralogy*, *Vol. 25*: *Oxide Minerals: Petrologic and magnetic significance*. Lindslay, D.H. Ed. Chantilly, VA: Mineralogical Society of America.

Yokoyama, H., Namakura, H. & Koiwa, M. 1998. Solubility and diffusion of Carbon in Palladium, *Acta Mater*, **46**(8): 2823-2830.

Yoshida, T., Nagasaka, T. & Hino, M. 1999. Evaporation rate of Zn and Pb in copper melt under reduced pressure, *J. Japanese inst. Metals*, **63**(2): 167-173.

Zhang, S., Jahanshahi, S., Sun, M., Lim, B., Bourke, S., Wright, S. & Somerville, M. 2001. *Development and applications of models for pyrometallurgical processes*. Materials Forum, 25. 136-153.

Zezin, D. 2010. *The solubility of gold in water-hydrogen sulphide vapours: An experimental study*. PhD Thesis submitted to the Department of Earth Sciences, McGill University, Canada.

Appendix A.1: Leaching of Fe, Ni and Cu before roasting step

A.1 Introduction and background

Due to the poor control over the redox environment in the melt, base metals, iron, arsenic and lead could not be removed from the alloy phase to the extent predicted. In order to compensate for this poor removal across the smelting step, it was decided to investigate a number of leaching steps to see whether some of these elements could be leached out of the feed prior to or after the roasting step. Figure 45 shows a block flow diagram illustrating the point in the flow sheet at which the leach step was investigated. This step was not included in the original concept flowsheet shown in Chapter 1 (Figure 3).

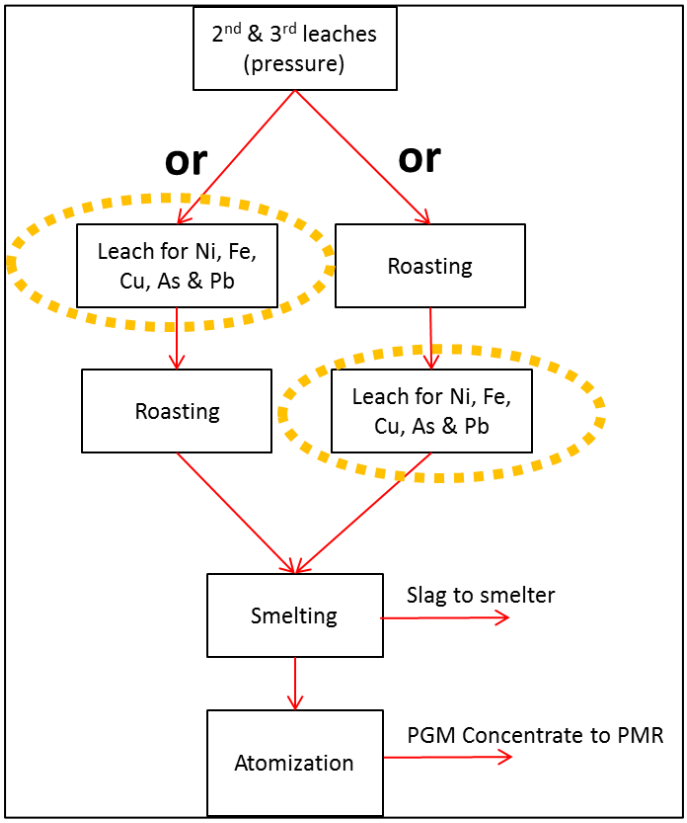

Figure 45: Block flow diagram to illustrate where the leaching step was investigated. The leaching step investigated is shown by the dashed yellow ellipse

However, what had been learned from the test work results led to a recommendation on the flow sheet that is different from the original concept flow sheet. The final recommended flow sheet is shown in Chapter 8, Figure 44. Although the final recommended flow sheet process was not proved experimentally, moving the base metal leaching to the final step, after atomisation, should have advantages; 1) allowing final metallisation of PGMs, thereby improving leaching of especially the OPMs in the PMR, 2) leaving some porosity in the alloy matrix for improved leaching kinetics and 3) leaving Fe, Ni and Cu across the smelting and high temperature treatment steps to prevent Ru losses. For purposes of comparison with the leach position studied, Figure 46 illustrates the point at which the leaching step is recommended.

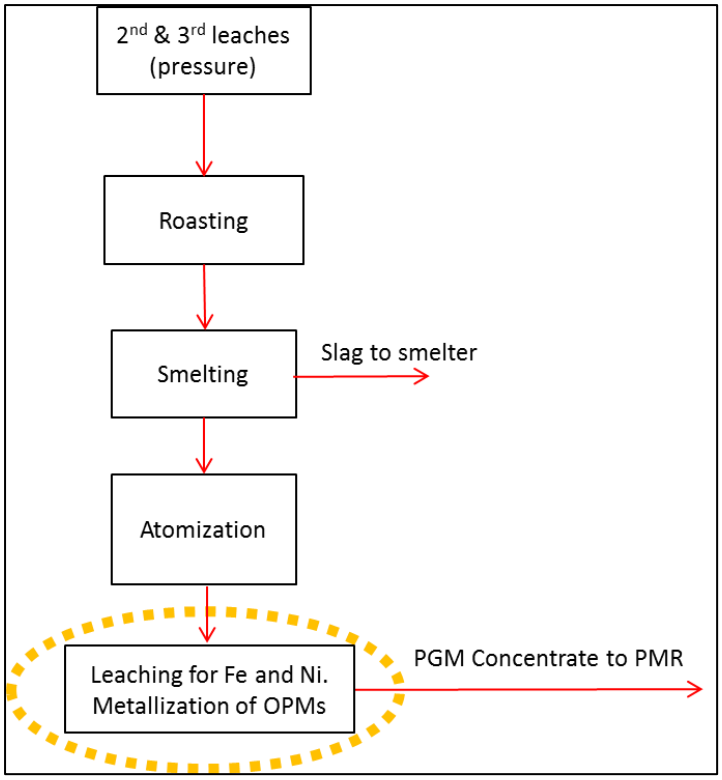

Figure 46: Block flow diagram to illustrate where the leaching step was finally recommended. The leaching step is shown by the dashed yellow ellipse

A.2: Methodology and materials

This section will briefly describe the thermodynamic modelling approach, the experimental set-up and the materials that were used.

Thermodynamic equilibrium modelling

Thermodynamic equilibrium modelling was used to evaluate the leaching of Fe, Ni, Cu, As and Pb from third stage residue and roasted third stage residue material. Modelling of the leaching process was performed with HSC Chemistry version 7.1 as supplied by Outotec (2011). The 'Eh-pH-Diagrams' and 'Reaction Equations' modules were used in the modelling work. The approach of using the Eh/pH diagrams was intended to mimic the actual leach conditions through using the same temperature and molalities as had been used in the experimental work. Table 52 shows the molality values that were calculated for the current system (third stage residue and roasted third stage residue) and these values were used in the Eh/pH graphs, unless otherwise stated.

Table 52: Approximate molalities calculated for the test work (on third stage residue and roasted third stage residue) and used in the Eh/pH diagrams

Element	Molality
Na	2.500
N	1.270
C	2.652
S	0.156
As	0.027
Fe	0.057
Ni	0.034
Cu	0.031
Pt	0.128
Pb	0.005

Experimental procedure and set-up

Leaching of third stage residue and roasted third stage residue

A number of leaching trials were performed on different feed materials. The leaching trials are summarised in Table 53.

Table 53: Summary of leach trials performed on different feed materials (to the smelt step) to understand As, Pb, Fe, Cu and Ni removal

	Test #	Weight	First leach	Second leach	Third leach
Third stage leach residue	7	50g	Caustic 10:1 (liquid:solid) 10% m/v NaOH 15ml H_2O_2 (30%)	Formic & Sulphuric acid 10:1 (liquid:solid) 10% v/v H_2SO_4 1:1 Formic: Sulphuric	
	11	45g	Formic & Sulphuric acid 10:1 (liquid:solid) 10g HCOOH and 10g H_2SO_4 1:1 Formic: Sulphuric		
Roast 650 °C on third stage	8	45g	Nitric acid 10:1 (liquid:solid) 8% v/v HNO_3	Formic & Sulphuric acid 10:1 (liquid:solid) 10% v/v H_2SO_4 1:1 Formic: Sulphuric	
	9	45g	Formic & Sulphuric acid 10:1 (liquid:solid) 10g HCOOH and 10g H_2SO_4 1:1 Formic: Sulphuric		
	10	49.3g	Caustic 10:1 (liquid:solid) 10% m/v NaOH	Formic & Sulphuric acid 10:1 (liquid:solid) 10% v/v H_2SO_4 1:1 Formic: Sulphuric	
Roast 900 °C on third stage	1	50g	Acetic acid 10:1 (liquid:solid) 10% v/v CH_3COOH	Sulphuric acid 10:1 (liquid:solid) 10% v/v H_2SO_4	
	2	50g	Sulphuric acid 10:1 (liquid:solid) 10% v/v H_2SO_4	Caustic 10:1 (liquid:solid) 10% m/v NaOH	
	3	45g	Formic acid 10:1 (liquid:solid) 10% v/v HCOOH	Sulphuric acid 10:1 (liquid:solid) 10% v/v H_2SO_4	Caustic 10:1 (liquid:solid) 10% m/v NaOH
	4	50g	Nitric acid 10:1 (liquid:solid) 8% v/v HNO_3	Formic & Sulphuric acid 10:1 (liquid:solid) 10% v/v H_2SO_4 1:1 Formic: Sulphuric	
	5	43g	Formic & Sulphuric acid 10:1 (liquid:solid) 10g HCOOH and 10g H_2SO_4 1:1 Formic: Sulphuric		
	6	50g	Caustic 10:1 (liquid:solid) 10% m/v NaOH	Formic & Sulphuric acid 10:1 (liquid:solid) 10g HCOOH and 10g H_2SO_4 1:1 Formic: Sulphuric	

Each leaching step was followed by a liquid/solid separation step through filtering. Only the solids proceeded to the following leach. All leaches were performed at atmospheric pressure. Leaches numbers one through three were allowed to proceed at room temperature for 24 hours. Leaches numbers four to eleven (and the repeats of some of the leaches thereafter) were performed at 90 °C for a period of between four and eight hours. Samples were taken during certain leaches, at different time intervals, to investigate the effectiveness of the leach procedure over time.

Different lixiviates were used. These are listed below:

- Acetic acid (CH_3COOH)
- Formic acid (CHOOH)
- Nitric acid (HNO_3)
- Sulphuric acid (H_2SO_4)
- Caustic (NaOH)
- Hydrogen Peroxide (H_2O_2) was used as oxidising agent in the caustic leach in test 1.

Materials used

Third stage leach residue was used in the experiments. In some of the experiments roasting in a muffle furnace with excess air at 900 °C or 650 °C for 6 hours was done to prepare roasted product feed for the leaching experiments. The chemical composition of the third stage leach residue and the roasted product is given in Table 54 below:

Table 54: Elemental composition (given in weight %) of the materials used in the leaching work to remove As, Pb, Fe, Cu and Ni

Element	Third stage residue	Roast 650°C	Roast 900°C
Pt	21.3	32.1	34.0
Pd	9.8	13.4	15.0
Au	0.6	0.8	0.9
Rh	3.0	3.9	4.4
Ru	6.3	7.5	9.5
Ir	0.6	1.8	0.9
Sum 6E	**41.6**	**59.6**	**64.6**
Ag	0.6	1.0	0.8
Os	5.1	7.6	1.6
As	0.9	1.9	2.0
Bi	0.1	0.1	0.2
Cr	0.6	1.0	1.0
Cu	1.9	2.4	2.7
Fe	3.1	4.4	5.0
Ni	1.7	2.8	3.2
Pb	0.4	0.7	0.7
S	4.1	1.1	0.0
Sb	0.1	0.3	0.0
Se	4.5	0.0	0.0
Si	0.2	2.1	2.4
Te	1.4	2.8	0.7
Al	0.3	0.4	0.5
Ca	0.5	0.5	0.5
TOTAL:	**67.1**	**88.7**	**85.7**

A.3: Results and discussion

The results of the leaching work are provided in full at the end of Appendix A. Only important abstracts of the data will be discussed in this section. A short rationale will be given for the types of lixiviate investigated, as well as the expected leaching reactions.

Acetic acid (CH_3COOH)

Organic acids (acetic and formic) were used to target the removal of Cu and Pb. The reaction with CuO is shown in reaction 5. The reaction of PbO with acetic acid is shown in reaction 6.

$$CuO + CH3COOH \rightarrow Cu(CH3COO)_2(a) + H_2O \quad (5)$$

$$PbO + 4CH3COOH \rightarrow Pb(CH3COO)_4 + H_2O + 2H^+ \quad (6)$$

A single test of acetic acid was done on roasted material at 900 °C. Limited Cu could be removed and only around 18% of the Pb. Pb removal with formic acid performed better at 44% in similar conditions. A decision was taken to focus on the use of formic acid as lixiviant, rather than acetic acid.

Formic acid (CHOOH)

A formic acid/Sulphuric acid leach is currently used in the BMR process as a final leach before the concentrate is dispatched to the PMR (Steenekamp, 2012). Spinel phases such as magnetite (Fe_3O_4) and trevorite ($NiO.Fe_2O_3$) are normally very stable, and therefore inert, in the typical oxidising environment in the BMR. The reducing ability of the medium is used to reduce Fe from the Fe^{3+} to the Fe^{2+} state, thereby allowing Fe and Ni in the spinel structure to go into solution. Reactions 7 and 8 show the typical reactions that are expected and employed by Lonmin to bring Fe and Ni into solution:

$$Fe_3O_4(s) + HCOOH(aq) + 3H_2SO_4(aq) \rightarrow 3FeSO_4(aq) + 4H_2O\,(l) + CO_2(g) \quad (7)$$

$$NiFe_2O_4(s) + HCOOH(aq) + 3H_2SO_4(aq) \rightarrow 2FeSO_4(aq) + NiSO_4(aq) + 4H_2O(l) + CO_2(g) \quad (8)$$

The formic/sulphuric leach in the Lonmin BMR has the added responsibility of reducing any oxidised PGMs to the metallic state (Lakefield Research, 2000). PGMs (especially OPMs) that are in the oxidised state will not dissolve in the hydrochloric/chlorine dissolution step in the PMR. An example of the reduction of Rh to the metallic state is shown in reaction 9:

$$Rh_2O_3xH_2O\,(s) + 3HCOOH\,(aq) \rightarrow 2Rh\,(s) + (3+x)H_2O\,(aq) + 3CO_2\,(g) \quad (9)$$

Nitric acid (HNO_3)

The optimum concentration of the nitric acid leach selected for the test is 8% (m/v). The nitric acid dissociates, according to reaction 10, to allow the following species to exist:

$$HNO_3 + H_2O \rightarrow H^+(aq) + NO_3^-(aq) \quad (10)$$

Once the concentration of HNO_3 increases to greater than 1M the unwanted reaction 11 is promoted:

$$4HNO_3 + 2H_2O \rightarrow 4NO_2(g) + 4H_2O\,(aq) + O_2(g) \quad (11)$$

Nitric acid is capable of bringing Pb, PbO and PbO_2 into solution. The reaction with PbO is shown as an example in reaction 13. The process of leaching CuO with nitric acid would proceed according to reaction 12.

$$CuO + 2HNO_3 \rightarrow Cu(NO_3)_2 + H_2O \quad (12)$$

$$PbO + 2HNO_3 \rightarrow Pb^{2+} + 2NO_3^- + H_2O \quad (13)$$

Sulphuric acid (H_2SO_4)

Sulphuric acid was used alone, but also in combination with formic acid. Sulphuric acid should be able to bring Fe, Ni and Cu into solution under atmospheric conditions. Oxidising conditions are necessary for Cu and Ni leaching, but strongly oxidising conditions will promote Fe^{3+} formation and therefore re-precipitation of Fe as a number of species. The leaching process with sulphuric acid would proceed according to reaction 14:

$$(Fe, Ni, Cu)O + H_2SO_4 \rightarrow (Fe, Ni, Cu)SO_4 + H_2O \quad (14)$$

Caustic Soda (NaOH)

Caustic soda is currently used in the BMR process as the second last leach (prior to the formic/sulphuric acid leach). The caustic leach is a control step for the following elements: Se, Te, As, S and Os. The existing high pressure caustic leach is performed at 20 bar pressure at a temperature of 170 °C to 180 °C, resulting in an oxygen overpressure of 7 bar. As the experimental tests were only performed at atmospheric pressure, hydrogen peroxide (H_2O_2) was used as oxidising agent in the caustic leach in test 1. The oxidising agent (H_2O_2) was used to oxidise the elements As, Pb and, to a degree, Se:

$$As \rightarrow As^{+3};\ Pb \rightarrow Pb^{+2};\ Se \rightarrow Se^{+4}$$

In the case of selenium, for example, the reaction equation proceeds according to reaction 15:

$$Se + 4H_2O_2 + NaOH \rightarrow Na_2OSeO_4 + 5H_2O \quad (15)$$

Being amphoteric, Pb is susceptible to corrosion by both acids and alkalis under certain conditions. Abdul *et al.* (1972) investigated the leaching of lead in an alkaline environment. They reported the leaching of PbO to plumbite ions in a caustic environment as proceeding according to reaction 16. However, this reaction is reversible, and significant passivation of the surface by PbO takes place. Abdul *et al.* found that passivation would be affected more readily the higher the alkali concentration, provided a critical concentration of > 2 M is exceeded. A concentration of approximately 2.5 M was used in the current study. Baboian (2005) mentions that Pb can be used to containerise caustic solutions up to 10% at 90 °C, with corrosion proceeding sufficiently slowly due to the passivation effect of PbO.

$$PbO + OH^- \rightarrow HPbO2^- \quad (16)$$

No Pb leaching is currently experienced at the Lonmin BMR during the high pressure caustic leach on third stage residue. This will be discussed under the Pb removal heading.

A discussion will now follow to summarise the behaviour of the different elements during the leaching test campaign.

Removal of As

The dissolution of As does not proceed by complexation with the ligands investigated. Arsenic is an amphoteric element and it is possible to bring As into solution in either an alkaline medium (as species like AsO_4^{2-} or AsO_3^-) or in an acidic medium (as species like $HAsO_4^{2-}$, $H_2AsO_4^-$, $HAsO_3^{2-}$ and $H_2AsO_3^-$). Figure 47 below shows the Eh/pH diagram (Pourbaix diagram) for the Pt-As system in water. Pt was chosen, as some As could be in the anionic state and associated with the PGMs. Dissolution of As will proceed only if oxidising conditions exist in the leach. If N is added to evaluate HNO_3, the figure remains basically unchanged, since no complexation takes place, and this is therefore not shown.

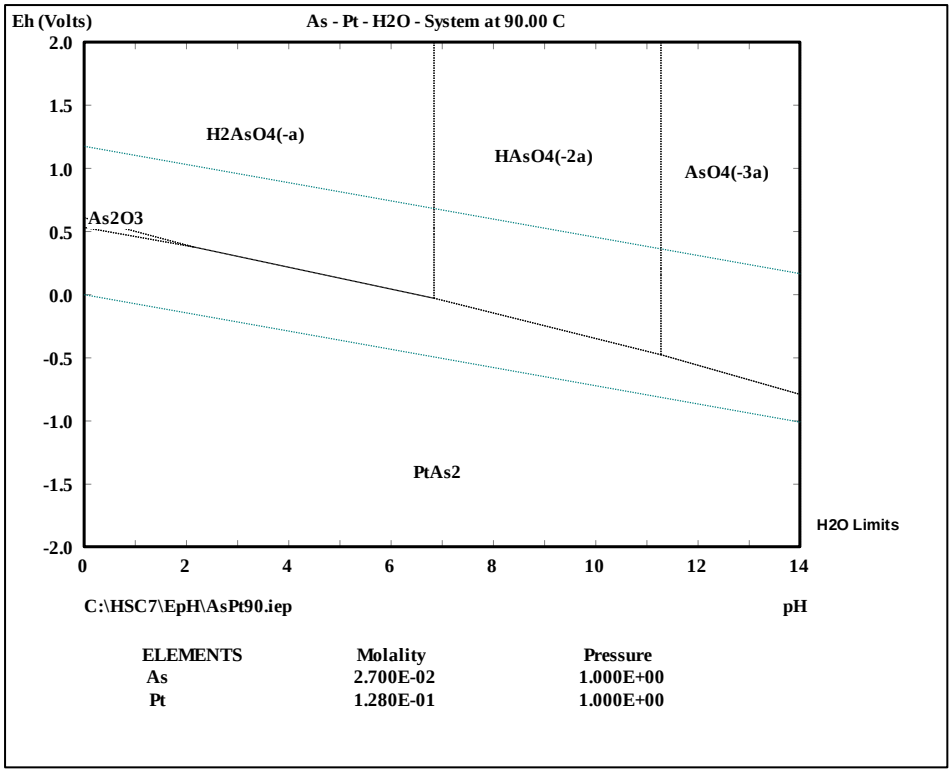

Figure 47: Eh/pH diagram of the As-Pt system in water

McCulloch (2012) found that approximately 40% of the feed As leaches during the oxidative acid pressure leaching step (second and third stage leach) in the Lonmin BMR. This fact attests to the creation and solubility of species in an oxidising acid environment. An additional 30% (expressed as % of overall feed to BMR process) of the As is leached in the high pressure caustic leach currently used in the BMR. This, once again, attests to the ability of As to be leached in the caustic and oxidising environment. However, the remaining 30% (% of feed to BMR) of the As passes, with the final concentrate, to the PMR. The incomplete leaching in both the acidic and alkaline environments shows that the reaction is kinetically constrained, probably through a mass transfer limitation. Arsenic showed poor vaporisation in the roasting test work, despite thermodynamic modelling predicting full volatilisation. No single mineral or species could be identified from this work, but it is concluded that As removal is complicated and is retarded by the interaction of As within the mix of metals.

After roasting, some As could be associated with minerals such as ferric arsenate ($FeAsO_4$). The Eh/pH diagram for the As-Fe system in water is shown in Figure 48. Once again, As should go into dissolution in both the acidic and alkaline environments, as long as the conditions remain oxidising (Langmuir, 2006).

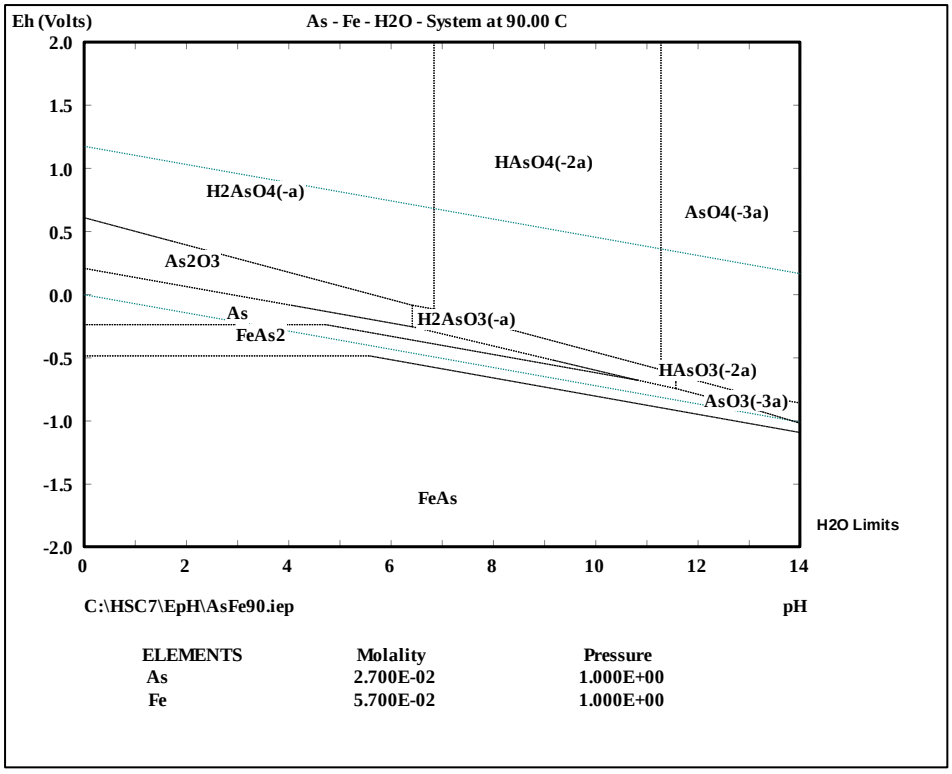

Figure 48: Eh/pH diagram of the As-Fe system in water

Table 55 shows the removal of As to solution for the different feed types in a caustic environment. The leach conditions were always at 90 °C for 8 hours and with a concentration of 10% mass NaOH per volume, with a total solid to liquid ratio of 1:10.

Table 55: Summary of the removal of As (weight % leaching into solution) in an alkaline environment

Lixiviate	Third stage leach	Roast 650 °C	Roast 900 °C
Caustic	44*	12	6

* In this trial hydrogen peroxide was added as an oxidising agent, while the roasting trials did not receive peroxide.

Third stage leach residue is currently treated with a high pressure caustic leach and removal efficiencies of around 50% (expressed as % leached across this step) are routinely achieved. Similar removal efficiencies were achieved on third stage leach residue by the use of peroxide and caustic soda (44%) at atmospheric temperature and pressure. The use of peroxide seems to allow the oxidation of As to the As^{3+} state that facilitates the removal of As by the formation of sodium arsenite (Na_3AsO_3), according to reaction (17). The arsenite can oxidise further to arsenate (Na_3AsO_4). Both the arsenite and arsenate are soluble in the alkaline environment.

$$Pt_3As_4 + NaOH + O_2 \rightarrow PtO_2.\ xH_2O + Na_3AsO_3 \qquad (17)$$

The poor leaching efficiency achieved for the roasted product could be due to a combination of factors. No peroxide was added as an oxidising agent in the leach tests of the roasted material, and

this could potentially skew the results. Arsenic is a small constituent of the mass of the system. During roasting, many of the metals in the matrix oxidise, forming very stable oxides that will not be amenable to leaching in a caustic environment. This could seal off some of the As, and contribute to the poor removal results.

Table 56 shows the removal of As to solution for the different feed types in an acidic environment. The leach conditions were all at 90 °C for 8 hours and with the respective concentrations of 10% volume H_2SO_4, 10% volume CHOOH, and 8% mass per volume, with a total solid to liquid ratio of 1:10.

Table 56: Summary of the removal of As (weight % leaching into solution) in an acidic environment from a feed sample that was roasted at 900 °C. Each value represents a separate leach

Lixiviate	Roast 900 °C
Nitric	52
Sulphuric	37
Formic followed by sulphuric	55

The poor removal efficiency of only 2% (not shown in a table) that was measured for the formic/sulphuric leach on third stage residue, once again points to the requirement of an oxidising environment. The formic/sulphuric acid leach currently employed by the BMR after the high pressure caustic leach, also shows no As removal.

The Eh/pH diagram of Fe-As system in water shows that As should be soluble in both an acidic and an alkaline environment. However, the caustic solution failed to remove As from the roasted sample, while the leaches in Table 56 showed removal efficiency of between 37% and 55% in an acidic environment. This behaviour must be linked to a change in the oxidation state of As during roasting. It is not clear what As species forms during roasting, but its behaviour is not predicted with the species included in the HSC modelling package.

Removal of Pb

The ability of Pb to be leached by different ligands depends on the speciation and oxidation state of the Pb. However, to pinpoint a speciation in either the third stage residue or the roasted product is not straightforward. XRD analyses of the third stage leach residue shows a peak at the anglesite ($PbSO_4$) position, but the peak is flat and broadened, due to the amorphous nature of the residue. Given the stability and poor solubility of $PbSO_4$ in the BMR environment, it is probably correct to assume that Pb would be partly speciated as $PbSO_4$ in the third stage leach residue. Although thermodynamic modelling of the roasting step shows that $PbSO_4$ should remain stable up to 1 040 °C, and some $PbO.PbSO_4$ complexes will form, a lot more S was removed experimentally than predicted by FactSage (refer section 5.3.2). Around 90% S removal was measured at 650 °C while 0% was predicted by FactSage (due to predicted stable sulphate formation of Ni, etc.) and >99% removal was achieved at 900 °C vs. the 38% removal predicted by FactSage. XRD analyses showed that the anglesite peak disappeared at 800 °C. The disappearance of the anglesite peak and the good removal

of S, despite the thermal stability of $PbSO_4$ show that Pb is not distinctly speciated as sulphate, but could instead be present in a complex mix of metals as a mixed oxide/sulphate/metal.

The Eh/pH diagrams of the Pb-N and Pb-N-S systems in water are shown in Figure 49 and Figure 50 respectively. HNO_3 would be able to bring Pb^{2+} into solution in the acidic and oxidising environment created by the dissociation of HNO_3. However, the moment S is added to the system, $PbSO_4$ becomes stable. The solubility of $PbSO_4$ is extremely low.

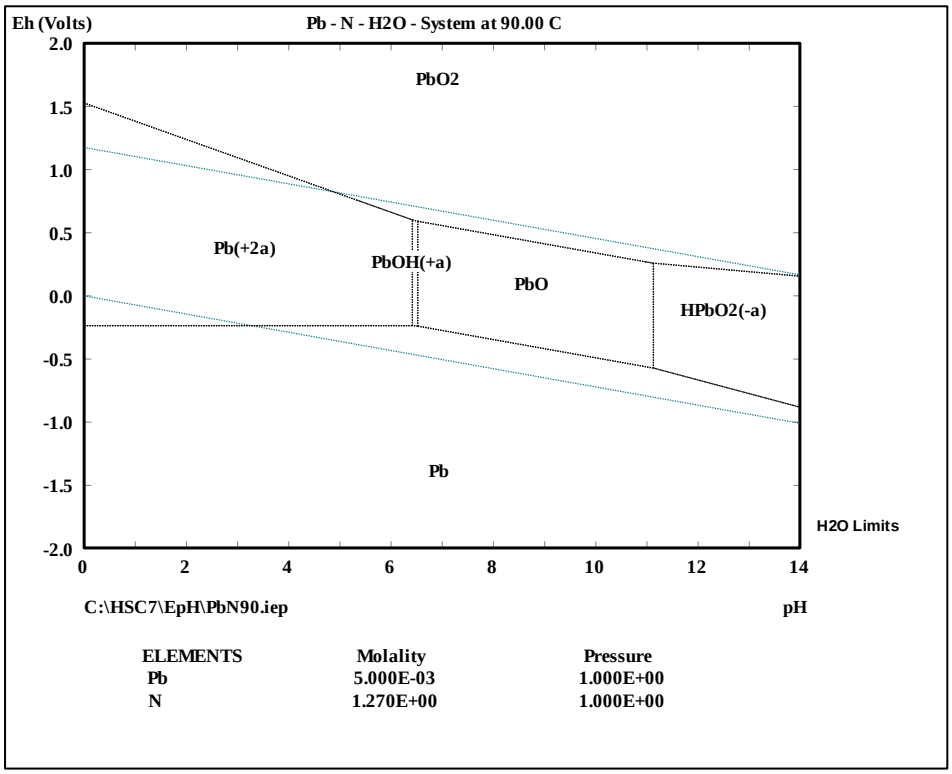

Figure 49: Eh/ pH diagram of the Pb-N system in water

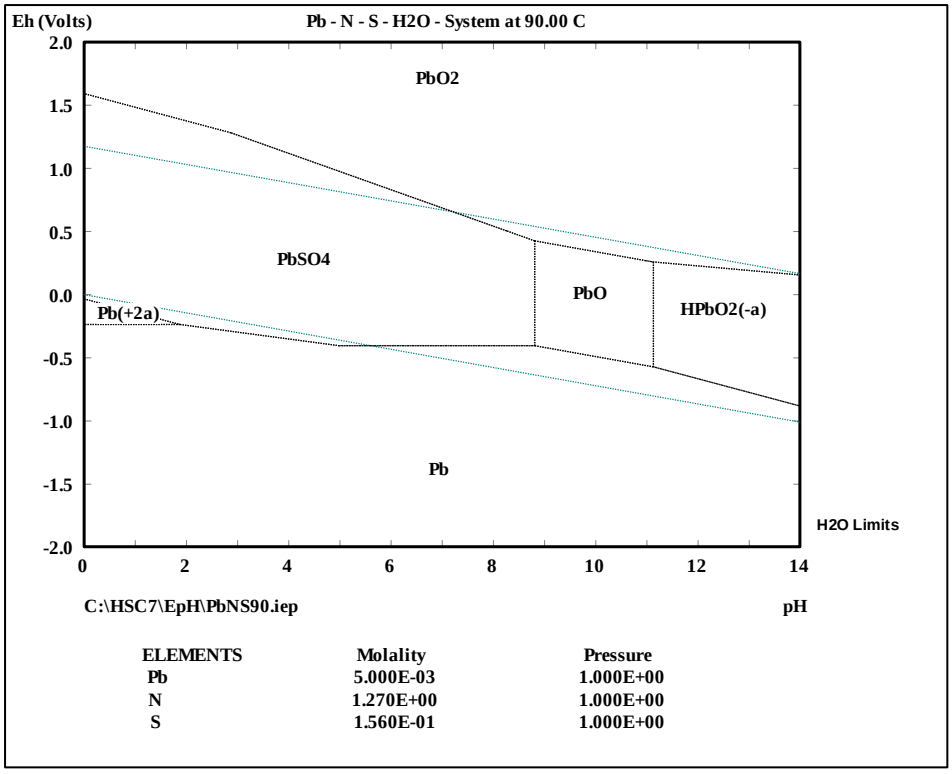

Figure 50: Eh/ pH diagram of the Pb-N-S system in water

If we look at the Pb-C system in water (Figure 51) to evaluate acetic acid and formic acid leaching, it is clear that Pb can be leached in a strongly acidic environment (as Pb^{2+}), although some complexation (formation of acetate species, if acetic acid is used) is possible in more reducing environments. $PbCO_3$ is stable over a wide pH range of about 2 to 11.5 and has very low solubility in water, providing another species that could keep Pb from going into solution. When S is added to the Pb-C system in water, the diagram looks essentially the same as with the Pb-N-S system in water, with the $PbSO_4$ stability zone not allowing any dissolution in the range investigated.

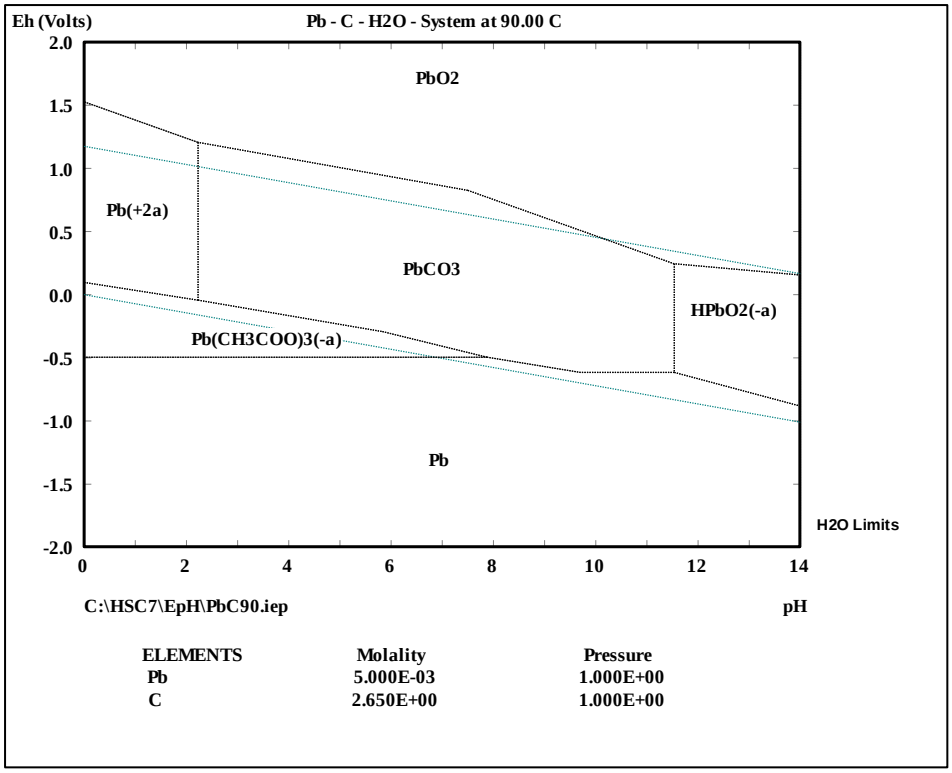

Figure 51: Eh/ pH diagram of the Pb-C system in water

To evaluate the use of caustic soda, the Eh/ pH diagram of the Pb-Na system was drawn up (Figure 52). When S is added to the Pb-Na system (Figure 53), the Pb^{2+} range (in the acidic pH range) is once again replaced by $PbSO_4$ stability. However, in the alkali pH range, the stability of the $HPbO_2^-$ remains unchanged as in Figure 52 and it would thermodynamically speaking be possible to still bring Pb into solution.

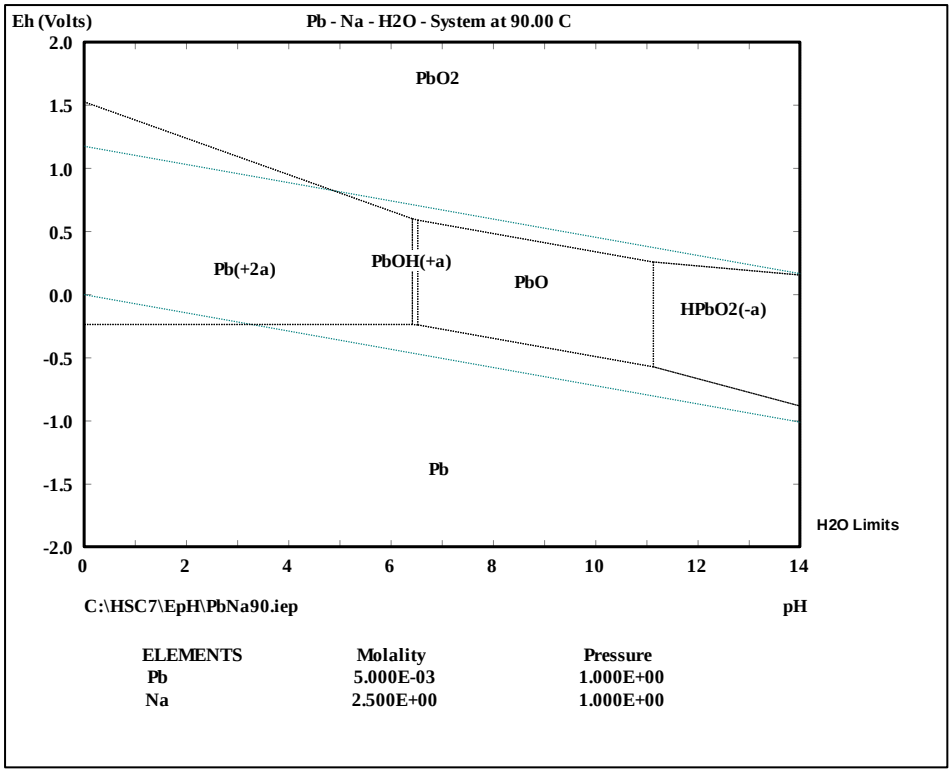

Figure 52: Eh/pH diagram of the Pb-Na system in water

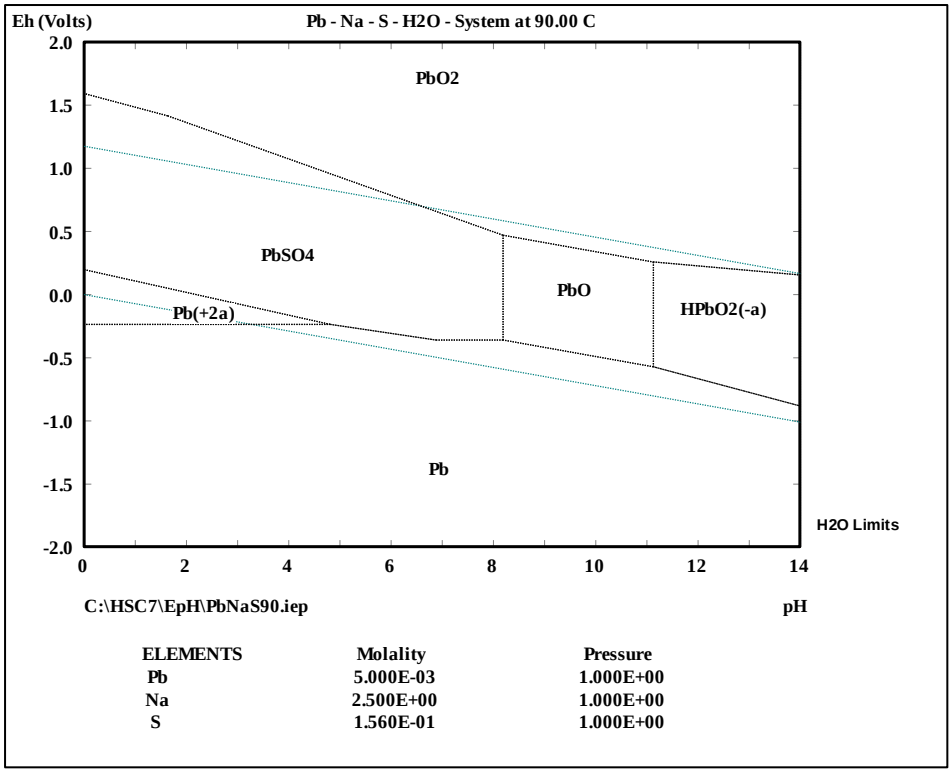

Figure 53: Eh/pH diagram of the Pb-Na-S system in water

The experimental results of Pb going into solution are shown in Table 57. Each block represents a separate leach that was performed and the values are the % that went into solution across that leach.

Table 57: Summary of the removal of Pb (weight % leaching into solution) for the different leaches on different feed types

Lixiviate	Third stage leach	Roast 650 °C	Roast 900 °C
Nitric	52	66	73
Formic/ Sulphuric	2	0	1
Formic only	N/A	N/A	44
Caustic	0	26	31

The use of a formic/sulphuric leach shows almost no leach behaviour for all feed types. This can be explained by the presence of S and the stability of $PbSO_4$. Even in the roasted product, the S contained in the sulphuric leach will not allow Pb^{2+} into solution. However, when only formic acid was used on the roasted product at 900 °C, with S removed from the matrix, 44% of the Pb went into solution.

The use of nitric acid is clearly a good method to leach Pb. No PGM losses were measured during the nitric acid leach of third stage or roasted material, as long as the nitric leach was not preceeded by another leach. In a single leach experiment where a nitric acid leach followed a formic/sulphuric acid leach, leaching of between 40% and 50% was reported for Pd, Rh, Ru and Ir. The leaching behaviour of Pb from the roasted samples was expected, based on the Eh/pH diagrams. However, the leaching behaviour of Pb from the third stage residue was not expected, due to the presence of S. No explanation can be provided for this, but it needs to be remembered that the interaction of the ligand, S and Pb will be influenced by the mixture of other elements in the matrix.

A high pressure caustic leach is currently employed by Lonmin on the third stage leach residue. No Pb removal is reported from this current process, and this corresponds with the finding of 0% Pb removal in a caustic leach on third stage residue. The Eh/pH diagram predicts that Pb would be soluble as $HPbO_2^-$ in an alkaline environment. Passivation of the surface, either by $PbSO_4$ (although this would not be stable at high pH), or more likely by the dissociation of $HPbO_2^-$ to PbO, is probably preventing Pb from going into solution. The removal of Pb in a caustic lixiviate improves when the material has been roasted, with 26% removal into solution reported for roasting at 650 °C and 31% removal for roasting at 900 °C. This might partly be explained by the removal of S from the system through roasting. It is also possible that the oxidation state of Pb changes in the roasting step, contributing to removal efficiency.

Removal of Fe and Ni

As explained earlier, a formic/sulphuric leach is currently employed by the Lonmin BMR after the high pressure caustic leach. The formic/sulphuric leach is performed in order to metallise PGMs and to reduce and remove some of the more stable Fe and Ni phases, such as magnetite and trevorite. Removal efficiencies of between 40% and 60% are achieved for both Fe and Ni. This result ties in

with the removal achieved in doing a formic leach directly on third stage residue, when Fe removal of 62% and Ni removal of 48% was measured. Table 58 show the removal efficiency of Fe in different media and for different feed types and Table 59 shows the removal efficiency of Ni.

Table 58: Summary of the removal of Fe (weight % leaching into solution) for the different leaches on different feed types

Lixiviate	Third stage leach	Roast 650 °C	Roast 900 °C
Nitric	N/A	1	0
Formic/ Sulphuric	62	99	2
Caustic	1	0	0

Table 59: Summary of the removal of Ni (weight % leaching into solution) for the different leaches on different feed types

Lixiviate	Third stage leach	Roast 650 °C	Roast 900 °C
Nitric	N/A	26	7
Formic/ Sulphuric	48	79	11
Caustic	0	0	0

The efficiency of Fe leaching across the formic/sulphuric leach varies a great deal,according to the feed material, with low temperature roasting showing an improvement in leaching efficiency (99% leached, instead of 62% leached, in third stage residue), while almost no leaching is seen in the 900 °C roasted feed. The same trend is true for Ni, with 79% leaching with feed roasted at 650 °C and only 11% leaching with feed roasted at 900 °C.

For the roasting at 650 °C, formation of the spinel type oxides in which Fe would be tied up is not thermodynamically stable; instead this is in the temperature range of stable sulphates for both the Fe and Ni. One would expect, and one can see, that roasting at 650 °C allows the sulphate phases and the simple oxides of Fe and Ni to go into solution almost completely.

For the roasted material at 900 °C, S has been eliminated from the matrix. Highly oxidised phases such as Fe_2O_3 and Fe_3O_4 are stable, as are complex phases like trevorite (Fe_2O_3. NiO). The Eh/pH diagram in Figure 54 shows that reducing and acidic conditions can bring Fe into solution, as is the case with a formic/sulphuric leach. The low leaching behaviour of Fe at 900 °C can be explained only by either a kinetic limitation on the reduction and removal of Fe from the complex metal mix within which it lies, or potentially, by the formic reducing capacity having been spent on reducing other species (like the PGMs) and not being available to reduce Fe.

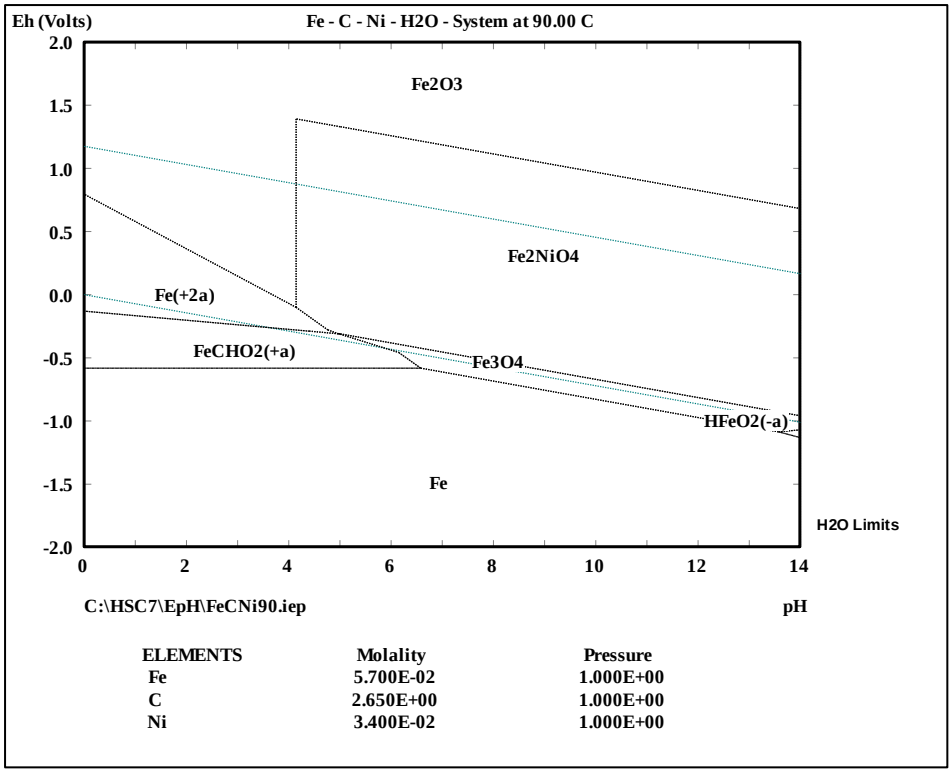

Figure 54: Eh/pH diagram of the Fe-C-Ni system in water

From Table 58 it can be seen that Fe did not leach in a caustic or nitric media, regardless of whether it had been roasted or not. These results are in line with thermodynamic predictions. No leaching was found for Ni in the caustic leach, but limited leaching of Ni took place in a nitric medium for roasted feed. 26% of Ni can be leached with nitric for a feed material roasted at 650 °C, while only 7% can be leached for a feed roasted at 900 °C. Examining the Eh/pH diagrams for Fe-N (Figure 55) and Ni-N and Fe-Ni-N, shows that Ni can be brought into solution in acidic and oxidising conditions (as is the case in a nitric acid leach), while Fe can only be brought into solution when conditions are more reducing (which was not the case with the nitric acid leach in this study). The higher leaching of Ni with nitric acid in the feed roasted at 650 °C once again confirms the presence of simpler Ni species.

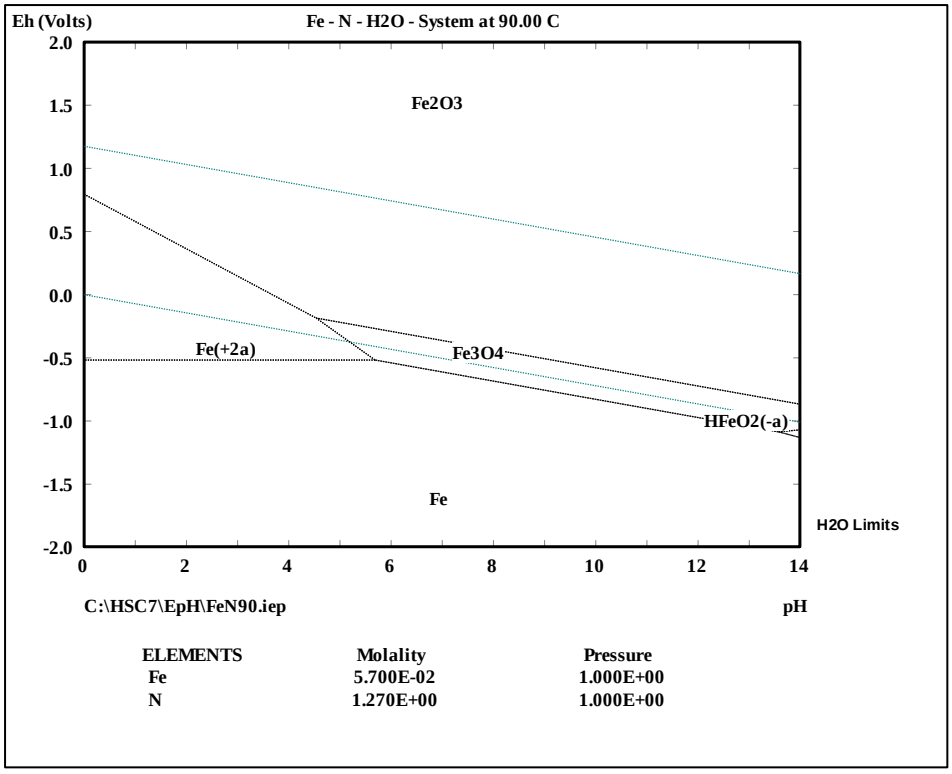

Figure 55: Eh/pH diagram of the Fe-N system in water

Removal of Cu

The dissolution behaviour of the Cu from different feed materials and with different lixiviates is shown in Table 60.

Table 60: Summary of the removal of Cu (weight % leaching into solution) for the different leaches on different feed types

Lixiviate	Third stage leach	Roast 650 °C	Roast 900 °C
Nitric	N/A	37	15
Formic/ Sulphuric	78	0	25
Caustic	1	1	0

It is clear that Cu does not dissolve in a caustic medium, regardless of feed condition. The ability of a nitric medium to bring Cu into solution is very similar to its behaviour with Ni, with the efficacy of removal being higher after a 650 °C roast (at 37%) than after a 900 °C roast (at 15%). Figure 56 shows the Cu-C-S system in water, but it looks almost exactly the same as the Cu-N-S system would, if it were to be drawn as in water. The behaviour of Cu in a nitric environment is therefore also described by Figure 56. Cu will go into solution at low pH and under highly oxidising conditions. The discussion below shows the importance of creating an oxidising environment in the formic/sulphuric leach in order to bring Cu into solution also.

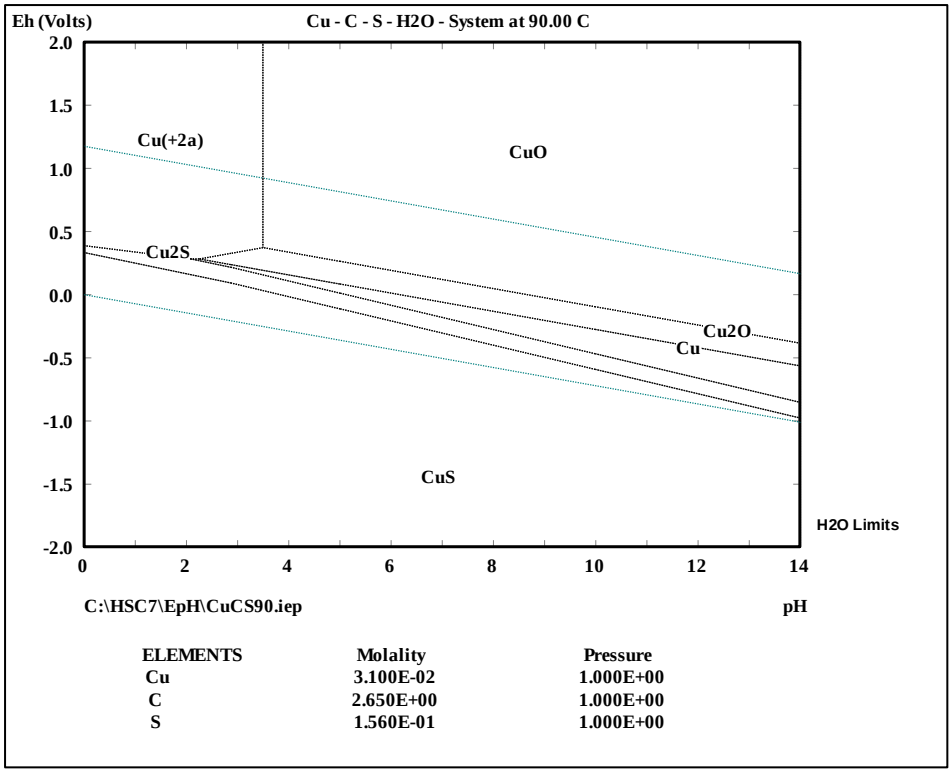

Figure 56: Eh/pH diagram of the Cu-C-S system in water

A total of four repeats were performed on third stage leach material in the formic/sulphuric medium to understand the leaching behaviour of Cu. Table 61 shows some extent of Cu leaching, as well as the important parameters that explain the varying behaviour. When the final oxidation-reduction potential (ORP) is positive, Cu leaches to a large extent (around 67% to 81%). Cu starts leaching only when the solution turns oxidising, while Fe and Ni remain in solution. Formic acid will create a reducing environment (negative ORP) and, unless the ORP is turned positive, Cu will not go into solution. Figure 57 shows the concentration of Fe, Ni and Cu in solution as a time series. At about 180 minutes Cu starts going into solution, when the ORP turns positive. In the experimental setup, air was simply bubbled through the solution after three hours (180 minutes).

Table 61: The extent of dissolution (wt%) of Cu, Fe and Ni as a function of some leaching parameters

Parameter/ Element	Third stage	Third stage	Third stage	Third stage
Lixiviant	Formic: Sulphuric (1:1)	Formic: Sulphuric (1:1)	Formic: Sulphuric (1:1)	Formic: Sulphuric (1:1)
Concentration	10% v/v	10% v/v	10% v/v	10% v/v
Temperature	90 °C	90 °C	90 °C	90 °C
Time	6 hours	6 hours	8 hours	7 hours
Final ORP (mV)	-235	-245	343	410
Initial pH	1.25	1.25	1.2	1.3
Final pH	1.3	1.25	1.5	1.7
Ir	6.2	6.6	9.1	5.4
Cu	0.0	0.3	67.2	81.1
Fe	52.5	87.1	50.9	58.5
Ni	71.1	54.1	42.6	52.7

Figure 57 shows that Cu starts going into solution soon as this starts, while Fe and Ni remain in solution.

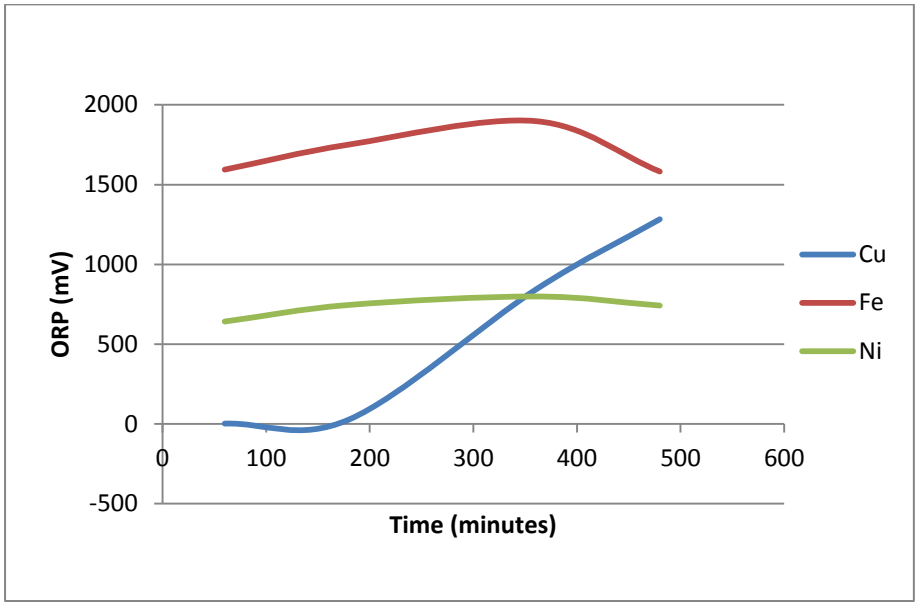

Figure 57: Time series graph showing the concentration of Cu, Fe and Ni in solution

The current operating procedure finishes the leach soon as the ORP turns positive. Air sparging for an hour or two after the ORP turns positive could act as a final polish to bring Cu into solution, thereby upgrading the PGM content in the PMR feed. However, it is not certain whether the oxidising conditions at the end of the leach would partly oxidise OPMs, thereby adversely affecting their dissolution in the HCl/ Cl_2 leach in the PMR. Further work is necessary in order to understand

OPM oxidation. If roasting follows the leach, there will be no effect on OPM recovery, and the improved Cu removal could be used.

Leaching of Ir

Iridium is the only PGM that displayed leaching behaviour in the leaching trials performed. Iridium displayed leaching behaviour only in the formic/sulphuric medium, as can be seen in Table 62.

Table 62: Leaching behaviour of Ir for different feed materials, in a formic/sulphuric medium. The values are shown as mass % that went into solution

Lixiviate	Third stage leach	Roast 650°C	Roast 900°C
Formic/ Sulphuric	7.4	2.7	0.0

McCulloch (2012) found that Lonmin experienced Ir leaching in the formic/sulphuric leach performed on high pressure caustic leach residue, but that Ru and Rh did not show leaching behaviour. The current test work found leaching to a similar extent (7.4 mass %) for the third stage leach material. It would appear that the formic/sulphuric combination selectively brings Ir into solution in both the caustic residue and the third stage leach material. It is interesting to note that the leaching behaviour of Ir reduces when the material is roasted, with that roasted at a temperature of 900 °C showing no leaching behaviour.

Table 61 (Cu leaching behaviour) shows that Ir goes into solution, regardless of the sequence of formic/sulphuric addition (either going from positive to negative ORP, or vice-versa). It is not sure as to what species the Ir goes into solution as, and no literature could be found on this behaviour in a formic/sulphuric environment. Heshmatpour *et al.* (1985) studied the recovery of Ir from scrap by first producing an alloy and then selectively leaching the carrier metal from the alloy to leave the Ir. They reported partial Ir leaching with the use of oxidising acids like HNO_3 and H_2SO_4. The Lonmin BMR process also sees Ir leaching within the autoclave sulphuric leaching. Dorfling *et al.* (2013) studied the leaching of OPMs from a Lonmin matte and found that Ir^{3+} went into solution in the oxidising sulphuric acid leach. In the oxidising pressure leaching with sulphuric acid they found co-dissolution of Ru and Rh together with the Ir, which was not seen in the current work. The leaching rate of the OPM sulphides (Ir_3S_2) was the fastest, followed by the metallic phase (Ir) and finally the oxide phase (IrO_2).

No explanation can be given for the preferential leaching behaviour of Ir in the formic/sulphuric acid leach and it was outside the scope of the current work to investigate it in more detail.

A.4: Conclusion

The use of a leaching step on third stage residue holds good promise for partial removal of Fe, Ni and Cu. Removal of Fe, Ni and Cu needs to be done prior to roasting, since roasting at the preferred process temperature of 900 °C does not leave Fe, Ni and Cu amenable to leaching (despite it being thermodynamically possible). The use of a formic/sulphuric leach provides the best results for Fe (65%), Ni (48%) and Cu (81%) removal. Formic acid needs to be added first (to reduce Fe^{3+} to Fe^{2+}), after which sulphuric acid can be added. The ORP needs to be positive, to provide an oxidising

environment at the end of the leach in order to ensure good Cu removal. About 7% Ir leaching can be expected and the liquor from the leach will have to be integrated into the existing BMR process.

Pb removal can only be done when there is very little S present; in other words, after roasting. Sulphuric acid cannot be used, as this would stabilise $PbSO_4$. After roasting, both formic acid (44%) and caustic (31%) show some leaching ability of Pb. Nitric acid was able to leach Pb for unroasted and roasted product, although the leaching ability improved with the roasting temperature.

The removal of As in third stage material is only possible by the use of caustic (44%), provided that an oxidising environment can be provided. When the material is roasted, caustic leaching becomes less effective. No fundamental explanation for this can be provided. Leaching in an acidic environment proved ineffective on third stage leach material, while the efficiency improved on roasted material. Up to 55% As could be leached on roasted material at 900 °C with a formic/sulphuric leach. It would appear that As did change its oxidation state during roasting, but the species and its thermodynamic behaviour is not properly predicted by either HSC or FactSage, from the roasting test work that was done.

A.5: Full leach results for Fe, Ni, Cu, As and Pb removal: roasted and unroasted product

Table 63: Test results of leach tests 1 to 3. All values are reported in weight % of element remaining in the solid phase

Parameter	Test 1	Test 1	Test 2	Test 2	Test 2	Test 3	Test 3
Leach number	1	2	1	2	3	1	2
Feed type	Roast 900 °C	Roast 900 °C	Roast 900 °C	Roast 900 °C	Roast 900 °C	Roast 900 °C	Roast 900 °C
Lixiviant	Acetic	Sulphuric	Formic	Sulphuric	Caustic	Sulphuric	Caustic
Concentration	10% v/v	10% v/v	10% v/v	10% v/v	10% m/v	10% v/v	10% m/v
Temperature	25 °C	25 °C	25 °C	25 °C	25 °C	25 °C	25 °C
Time	24 h	24 h	24 h	24 h	24 h	24 h	24 h
Oxidising agent	None	None	None	None	None	None	None
Element							
Pt	100.0	100.0	100.0	100.0	100.0	100.0	100.0
Pd	100.0	99.9	100.0	100.0	100.0	100.0	100.0
Au	100.0	100.0	100.0	100.0	100.0	100.0	100.0
Rh	100.0	100.0	99.9	99.8	99.8	100.0	100.0
Ru	100.0	100.0	100.0	100.0	100.0	100.0	100.0
Ir	100.0	99.9	100.0	100.0	100.0	100.0	100.0
Ag	90.9	75.4	100.0	72.8	72.8	71.8	71.8
Os	99.9	99.9	100.0	100.0	99.9	100.0	100.0
As	95.8	67.1	75.9	45.3	43.0	63.3	62.2
Bi	94.5	43.3	99.9	21.4	21.4	43.6	43.1
Cr	99.9	99.6	99.1	98.9	98.8	99.6	99.5
Cu	98.6	92.3	90.2	82.6	82.6	91.0	91.0
Fe	100.0	99.5	94.5	94.2	94.2	99.3	99.3
Ni	99.8	96.4	92.8	90.1	90.0	96.3	96.3
Pb	82.2	81.1	55.9	54.9	35.8	98.8	43.8
S	79.4	347.3	96.6	31.6	36.4	353.3	133.5
Sb	98.7	93.9	98.9	97.9	92.2	98.8	97.4
Se	84.7	66.2	98.9	88.2	87.0	71.6	64.8
Si	100.0	99.6	96.8	96.7	3.6	100.0	91.0
Te	98.2	83.0	96.3	74.4	65.9	82.3	81.5
Al	99.3	98.5	92.7	91.9	89.5	98.2	95.5
Ca	94.2	85.7	91.3	85.7	85.4	90.5	90.2

Table 64: Test results of leach tests 4 to 6. All values are reported in weight % of element remaining in the solid phase

Parameter	Test 4	Test 4	Test 5	Test 6	Test 6
Leach number	1	2	1	1	2
Feed type	Roast 900 °C	Roast 900 °C	Roast 900 °C	Roast 900 °C	Roast 900 °C
Lixiviant	Nitric	Formic: Sulphuric (1:1)	Formic: Sulphuric (1:1)	Caustic	Formic: Sulphuric (1:1)
Concentration	8% m/v	10% v/v	10% v/v	10% m/v	10% v/v
Temperature	90 °C	90 °C	90 °C	90 °C	90 °C
Time	8 h	8 h	8 h	8 h	8 h
Oxidising agent	None	None	None	None	None
Element					
Pt	100.0	100.0	100.0	100.0	100.0
Pd	99.9	99.9	100.0	100.0	100.0
Au	100.0	100.0	100.0	100.0	100.0
Rh	100.0	100.0	99.7	100.0	100.0
Ru	100.0	100.0	100.0	100.0	100.0
Ir	100.0	99.7	100.0	100.0	99.8
Ag	81.2	81.1	98.9	98.7	98.7
Os	100.0	99.9	99.3	100.0	100.0
As	47.7	45.0	34.0	93.7	40.6
Bi	88.9	88.9	99.6	98.5	98.4
Cr	99.6	94.5	98.3	99.9	96.8
Cu	85.4	84.7	75.2	99.8	74.6
Fe	99.5	87.8	97.5	99.9	95.3
Ni	93.4	84.9	89.3	99.9	88.5
Pb	26.9	26.4	98.5	69.1	68.2
S	6394.0	4579.2	46.5	470.0	6360.0
Sb	99.0	97.4	98.5	99.0	95.0
Se	98.8	98.0	93.0	98.5	96.3
Si	98.3	97.4	99.5	69.5	68.0
Te	90.4	90.4	78.0	99.8	91.1
Al	96.0	89.4	94.8	94.8	88.6
Ca	89.7	84.6	85.1	99.7	82.6

Table 65: Test results of leach tests 8 to 10. All values are reported in weight % of element remaining in the solid phase

Parameter	Test 8	Test 8	Test 9	Test 10	Test 10
Leach number	1	2	1	1	2
Feed type	Roast 650 °C	Roast 650 °C	Roast 650 °C	Roast 650 °C	Roast 650 °C
Lixiviant	Nitric	Formic: Sulphuric (1:1)	Formic: Sulphuric (1:1)	Caustic	Formic: Sulphuric (1:1)
Concentration	8% m/v	10% v/v	10% v/v	10% m/v	10% v/v
Temperature	90 °C	90 °C	90 °C	90 °C	90 °C
Time	8 h	8 h	8 h	8 h	8 h
Oxidising agent	None	None	None	None	None
Element					
Pt	100.0	100.0	100.0	100.0	100.0
Pd	99.7	99.7	100.0	100.0	99.9
Au	100.0	100.0	100.0	100.0	100.0
Rh	100.0	99.4	100.0	100.0	100.0
Ru	100.0	96.9	100.0	100.0	99.9
Ir	100.0	99.5	97.3	100.0	99.2
Ag	82.2	82.2	100.0	100.0	99.9
Os	100.0	100.0	99.9	100.0	100.0
As	84.3	84.2	100.0	87.7	59.6
Bi	98.1	98.1	100.0	99.7	99.6
Cr	99.4	68.9	61.4	99.5	93.1
Cu	62.8	45.8	99.9	99.3	73.8
Fe	98.7	29.1	0.7	100.0	84.3
Ni	73.6	42.7	21.4	100.0	80.8
Pb	33.6	32.3	99.5	74.0	72.7
S	23.6	80.4	0.9	24.7	119.4
Sb	100.0	91.7	99.2	93.3	95.0
Se	99.1	57.0	99.7	943.2	85.2
Si	98.3	99.7	97.1	13.0	1.2
Te	97.9	99.8	100.0	100.0	98.7
Al	96.1	96.0	94.2	91.3	82.2
Ca	93.5	95.0	93.0	99.7	88.3

Table 66: Test results of leach tests 7 and 11. All values are reported in weight % of element remaining in the solid phase

Parameter	Test 7	Test 7	Test 11
Leach number	1	2	1
Feed type	Third stage leach	Third stage leach	Third stage leach
Lixiviant	Caustic (15 ml H2O2 30%)	Formic: Sulphuric (1:1)	Formic: Sulphuric (1:1)
Concentration	10% m/v	10% v/v	10% v/v
Temperature	90 °C	90 °C	90 °C
Time	8 h	8 h	8 h
Oxidising agent	H_2O_2	None	None
Element			
Pt	97.9	97.9	100.0
Pd	99.9	99.9	100.0
Au	99.8	99.8	100.0
Rh	99.8	99.8	100.0
Ru	97.6	97.6	99.9
Ir	98.0	93.3	92.6
Ag	97.8	94.1	99.6
Os	99.4	99.3	100.0
As	55.6	55.6	98.2
Bi	99.9	99.8	69.2
Cr	92.9	87.7	86.5
Cu	99.3	84.5	21.6
Fe	99.5	36.2	37.7
Ni	100.0	25.4	52.1
Pb	99.7	98.3	97.9
S	79.1	42.6	146.4
Sb	47.9	47.7	88.8
Se	23.6	23.6	100.0
Si	178.0	119.7	81.1
Te	82.7	82.7	97.3
Al	87.4	83.3	98.6
Ca	99.6	89.1	94.8

Appendix B: Leaching of atomised alloy in HCl/ Cl_2

B.1: Introduction and background

An integral part of the new process studied in this thesis was to produce an alloy that could be fed into the existing PMR circuit. This implies that the alloy be fed to a hydrochloric acid/ chlorine dissolution step in PMR. The alloy would need to dissolve virtually completely (+98% by mass, as is currently the case with BMR concentrate) and the dissolution reaction would need to be predictable and controllable from both a temperature and a redox perspective. In order to compare the dissolution of the alloy to that of the existing concentrate fed to the PMR, a study was performed to monitor the dissolution process. The experimental work for the alloy dissolution in HCl/Cl_2 was performed by Yolande Fourie as a final year BEng project necessary to complete the requirements for her engineering degree at Stellenbosch University (Fourie, 2011).

B.2: Methodology and materials

This section will briefly describe the experimental set-up and the materials that were used.

Leaching of alloys

A small scale experimental set-up was designed in order to compare the dissolution behaviour of the current PMR concentrate feed with that of the alloy. The experimental set-up and conditions replicated the actual plant conditions as far as possible.

A Cole Parmer handheld infrared temperature measuring device was employed to measure the temperature of the process fluid present in the reactor vessel. These temperature devices make use of 635 nm wavelengths to measure the temperature. A Hamilton Oxytrobe Platinum type probe was employed to measure the mV of the dissolution reactions.

Feed Material: The amount of feed material was very limited, due to the small amount of alloy available. The amount of feed material fed into the dissolution reactor was 40 g of the alloy material, while the minimum amount of concentrate feed material was 50 g.

Solvent Addition: The solvent addition for the dissolution reaction was a 1:1 ratio of water and hydrochloric acid (6 M). The solvent that was added to the dissolution reactor was in a 6:1 ratio of liquid:solid, based on the weight of the solid sample fed to the reactor.

Chlorine Addition: Chlorine gas was sparged into the dissolution reactor vessel to improve the dissolution properties of the reaction. The amount of chlorine sparged was dependent on the reactor volume (1 200 ml) and the solid sample weight that was fed, which ranged between 30 and 60 g. These feed conditions required a chlorine gas flow rate of between 3 and 5 L/hr.

Thermal Addition: Energy was supplied to the reactor by means of a heater at the bottom of the reactor. Temperature control was set at a point between 60 °C and 75 °C for each of the different experimental runs.

Suspension of the solids in the liquid phase was achieved through a magnetic stirrer. Rotation of the stirrer was set at 300 to 500 revolutions per minute in order to achieve suspension. In some of the alloy runs the stirrer speed had to be increased even further in order to maintain suspension during the leach.

The experiments were performed within an enclosed extraction system. A picture of the experimental set-up is shown in Figure 58.

Figure 58: Picture of the experimental set-up used to compare normal concentrate dissolution and alloy dissolution

A total of 12 tests was done: six on concentrate and six on alloy. A summary of the test conditions is provided in Table 67.

Materials used

The atomised alloy that was used for the dissolution tests in hydrochloric acid/chlorine is described in section 4.6. The elemental composition is provided in Table 25, while the particle size is provided in section 7.2.2, in Table 48. Note that only the size fraction of -250 micron was used in the dissolution test work.

B.3: Results and discussion

A summary of the different test runs and some important measurements taken during the test are provided in Table 67.

Table 67: Summary of test runs that were done to compare the dissolution of the current PMR concentrate feed to that of the the alloy, in a hydrochloric acid/chlorine environment

Test number	Feed material	Size screen range (micron)	Maximum temperature (°C)	Reading of mV stability region	Temperature stability (°C)
1	Concentrate	-125	74	946	70
2	Concentrate	-125	78	947	66
3	Concentrate	-125	78.2	947	67
4	Concentrate	-125	83.2	955	71
5	Alloy	-125	83.6	928	70.5
6	Concentrate	-125	85	963	61
7	Alloy	-125	83.2	954	60
8	Alloy	-125	88.1	810	61
9	Concentrate	-125	82.5	846	62
10	Alloy	-125	84.3	950	63
11	Alloy	+125-250	81.2	936	61
12	Alloy	+125-250	83	959	63

The two main variables that were monitored during the leaching tests were the temperature and the oxidation reduction potential of the solution (measured in milli Volts–mV). A time series graph of each test was constructed for these two important variables. Figure 59 shows a graph of the temperature and the ORP respectively for a test run with current PMR concentrate feed. Chlorine gas purging is started when the temperature reaches 70 °C through heating of the bottom pad. A short while after this the ORP starts rising and stabilises at around 950 mV. The temperature rises due to the initial rapid exothermic reaction, but then stabilised at the control temperature of 70 °C.

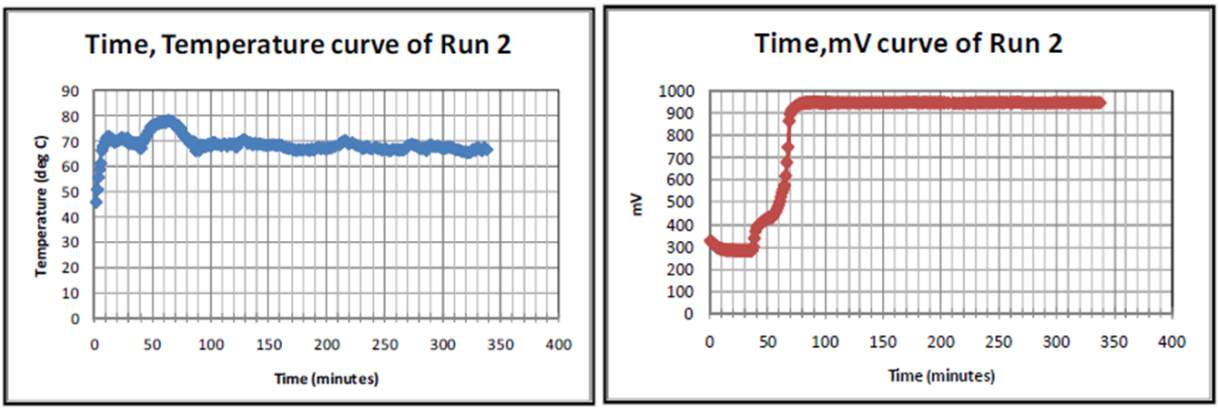

Figure 59: Time series graph of the temperature and ORP (mV) readings during the reaction of current PMR feed material in a hydrochloric acid/chlorine environment

Figure 60 shows the equivalent time series graph of temperature and ORP for alloy.

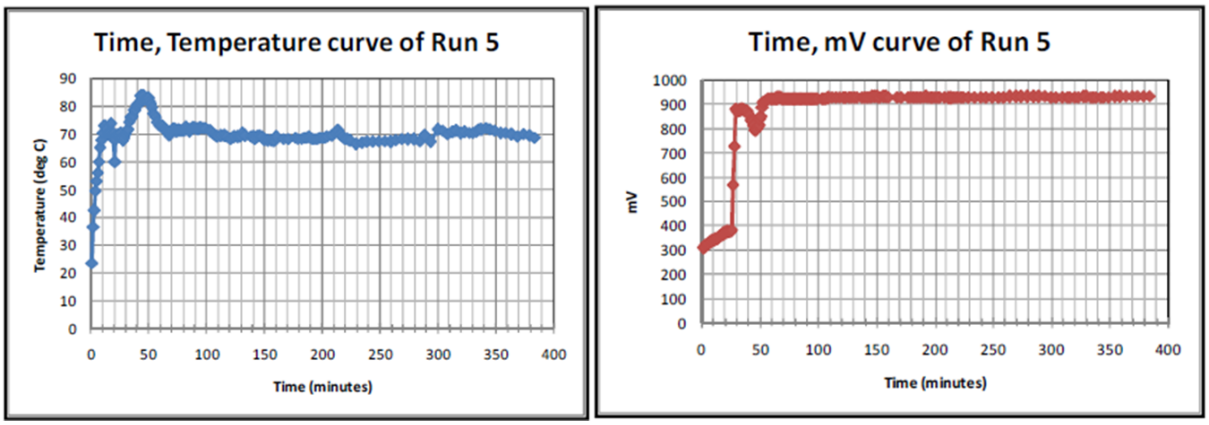

Figure 60: Time series graph of the temperature and ORP (mV) readings during the reaction of PGM alloy in a hydrochloric acid/chlorine environment

Comparing all the graphs for alloy and concentrate, it was found that both alloy and concentrate reacted very similarly to the leach conditions. No distinguishable difference could be noticed between the rate at which the temperature rose, nor the point at which it stabilised, for either alloy or concentrate.

The same is true for the oxidation reduction potential (ORP) mV readings. The ORP readings obtained in the test runs compare favourably with the ORP reading of 950mV achieved in the dissolution vessels of the PMR. There is a drop in the ORP mV readings after the chlorine gas is added in the alloy, but this then recovers and stabilises at similar values to those of the concentrate. This temporary dip in ORP values after the chlorine addition had started was noted in all the test runs performed with alloy.

In all the runs with concentrate, the initial colour of the leach was orange and this changed to a dark red-brown after the chlorine sparging started. In all the runs with alloy, the initial colour of the leach was green and this changed to an orange colour after the chlorine sparging started.

Table 68 below summarises the weight of solids that remained after each leach, as well as the dissolution time allowed for each test run.

Table 68: Summary of test runs that were done to compare the dissolution of the current PMR concentrate feed to that of the alloy in a hydrochloric acid/chlorine environment

Test number	Feed material	Feed mass (g)	Solid mass remaining (g)	% Solids into solution	Dissolution time (min)
1	Concentrate	50.0	-	100.0	270.0
2	Concentrate	50.1	-	100.0	340.0
3	Concentrate	50.9	-	100.0	340.0
4	Concentrate	50.3	-	100.0	380.0
5	Alloy	40.0	4.6	88.4	380.0
6	Concentrate	50.2	3.8	92.4	540.0
7	Alloy	40.0	12.7	68.4	540.0
8	Alloy	40.0	21.7	45.7	540.0
9	Concentrate	50.8	4.5	91.2	570.0
10	Alloy	40.2	13.3	66.8	540.0
11	Alloy	40.0	15.2	62.0	540.0
12	Alloy	40.0	16.3	59.2	600.0

Alloys are normally quite chemically reactive, if sufficient surface area is available for a reaction to proceed. The poor extent of leaching of the alloy is difficult to explain. There does not seem to be great sensitivity to the dissolution time. Most of the concentrates achieved 100% dissolution at low reaction times (as low as 270 minutes). Even the longer reaction times of the alloys (up to 600 minutes) did not promote higher dissolution. The poor extent of dissolution of the alloys could be linked to some stable phase that is present, or that forms on the surface and passivates the reaction, or to poor mixing, as this is a solid/liquid interaction, or to the low surface area available for the reaction, or to a combination of these causes.

Chemical analyses of the solids that were fed in for each test run, and the solid weight that was removed after the leach was complete, allows an evaluation of the metals that were responsible for the poor extent of leaching. The percentage of each metal that was leached, based on the solids mass calculation, is given in Table 69.

Table 69: The weight % of each element that went into solution in a hydrochloric acid/chlorine dissolve. Tests 5,7,8,10,11 and 12 are alloy dissolves, denoted by 'A'. Tests 6 and 9 are BMR concentrate dissolves, denoted by 'C'

Test #	Pt	Pd	Au	Rh	Ru	Ir	Ag	Cu	Pb	Ni	Fe	Se	As	Te
5 'A'	89	97	99	84	70	70	94	98	99	99	88	95	83	99
6 'C'	100	100	100	100	99	97	85	100	100	99	86	100	95	100
7 'A'	66	95	97	63	14	2	78	95	99	98	82	73	65	97
8 'A'	99	99	79	98	95	94	95	96	100	100	62	100	97	100
9 'C'	100	100	100	100	99	97	64	100	100	99	80	100	94	100
10 'A'	68	94	97	62	4	0	61	95	99	99	85	67	98	92
11 'A'	70	93	97	59	0	0	91	94	99	98	75	62	97	90
12 'A'	75	95	98	64	0	0	90	95	99	99	79	59	98	95

The concentrate provides almost complete solubility for the PGMs, with only 1% Ru not going into solution and 3% Ir. The existing BMR process ends with a reducing leach (formic acid), in order to metallise any PGMs that might be in an oxidised form. When the final leach in the BMR process is an oxidising leach, Rh, Ru and Ir (the OPMs) could partially oxidise. Oxidised OPMs dissolve poorly in a hydrochloric acid/chlorine environment and will remain as part of the residue. In the case of the alloys, the OPMs did not go into solution, with the following average values being leached out: Rh = 72%, Ru = 31%, Ir = 27%. Little effort was made during atomisation to control oxygen coming into contact with the melt. The smelt step had nitrogen gas flushing across the crucible, but the casting and quenching steps were done open to the atmosphere. The measurement of oxygen by the SEM EDS in Table 26 confirms the presence of oxygen and this would contribute to the poor OPM dissolution. This observation might thus require atomisation to proceed in an inert or reducing atmosphere, which would increase the cost and complexity of the atomisation step.

Pt solubility was also not very good, at an average of 78% for the alloys. The poor solubility of Pt is not consistent in the alloy tests, as 99% of the Pt went into solution in test 8. The solubility of the base metals (Ni and Cu), Fe, Ag, Pb and As is comparable between the alloy and the concentrate. Dissolution of the amphoterics (Se and Te) proceeds better in the concentrate than in the alloy.

There are some important physical differences between the two samples, and these will contribute to the poor leaching behaviour of the alloys. However, there are probably chemical differences (in speciation of the PGMs), or the formation of a passivation layer, that might be contributing heavily towards to the poor leaching behaviour. This was not studied in further detail during this research and could be the subject of future work. The physical differences in dissolution behaviour could partially be explained by the points below.

- Typical concentrate feed to the PMR is very fine, as 80% of the mass will pass 20 micron. Table 48 in section 7.2.2 gives the particle size distribution of the alloy. Although only the -125 micron and -250 micron size ranges were used in the dissolution tests, the distribution would be biased towards the greater size.

- In order to maintain suspension of the alloy during the leach, the speed of the magnetic stirrer was increased. As the rpm increased, the splattering of slurry increased and large amounts of solid material were noted on the sides of the vessel. If solid material is dispersed on the sides of the vessel the possibility of dissolution of that material is lost, due to poor or no contact between it and the liquid. This physical effect would skew the data, although the extent was not quantified.

Solution samples were taken from the vessel at set time intervals during the dissolution test. It is interesting to examine the difference in behaviour between the alloy and the concentrate, as this will provide an indication of whether the dissolution is proceeding as time proceeds, or whether the dissolution rate has already flattened out. Pt should proceed into solution in the tested leaching environment as $PtCl_6^{2-}$. Figure 61 shows the Pt concentration in solution as a time series for a concentrate dissolution test and for two alloy dissolution tests.

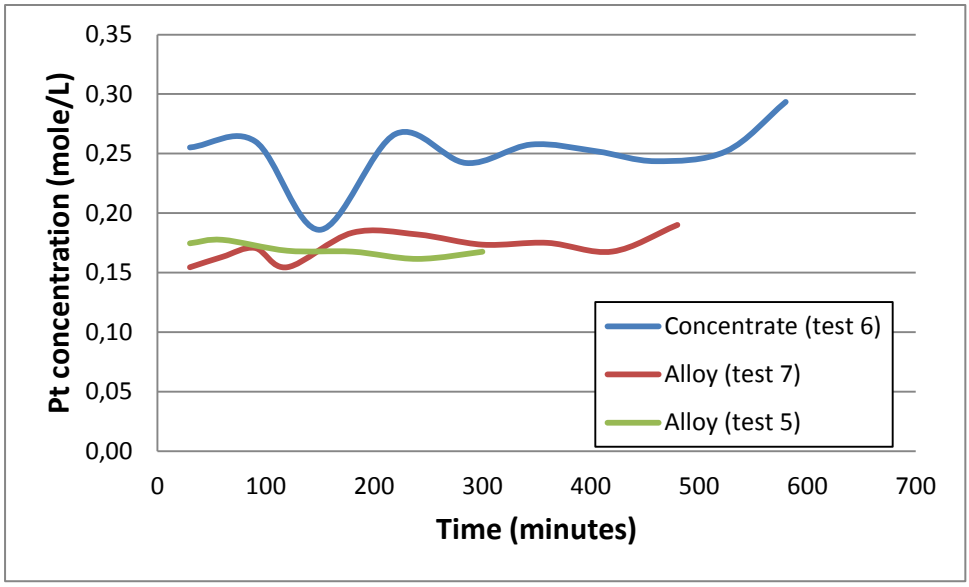

Figure 61: Time series graph of the Pt concentration in solution for a concentrate (test 6) and two alloy dissolution tests (tests 5 & 7)

The concentrate test shows that Pt concentration is already high in the first sample (taken at 30 minutes). The concentration of Pt in solution remains more or less constant throughout the entire leach at a value of approximately 0.25 mole/L). The low value at time 159 min and the high value at the end could simply be sampling/analytical error.

The concentrations of two alloy tests are provided (a high Pt leaching in test 5 at 89% and the lowest Pt leaching in test 7 at 66%) in order to get a better representation of the behaviour of Pt. The Pt concentration in solution of the alloy also seems to be high at the first sampling interval (at 30 minutes) and appears to remain more or less constant throughout the entire leaching period. This corresponds to the observation that the longer leaching times (for the later test runs) did not show an improvement in the percentage of material that is leached. The poor dissolution was not studied further, and it is therefore still uncertain what limits the reaction. Different conditions in the leach might be required to dissolve the alloy more completely. This should be studied further.

B.4: Conclusion

Dissolution of the alloy proceeds very similarly to the way it does with the current concentrate, if one compares the ORP and the temperature. Colour differences in the final solution and considerably more residue left over from the alloy leaches (between 12% and 55%) testifies that there are differences in the dissolution behaviour. It appears that metals proceed into solution quite rapidly and that additional time does not bring more metal into solution. The reason for the poor dissolution behaviour was not studied in more detail. Different leaching conditions might be required in order to bring 98%+ alloy into solution. The poor leaching of Ru and Ir in some of the alloys is particularly concerning. If the OPMs are partly oxidised, this would influence their dissolution behaviour in a chlorine environment. The use of an inert or reducing environment during atomisation (both across the melt and in the spray chamber) is necessary to ensure that oxygen cannot react with or be locked into the structure. This should be investigated further.

Appendix C: Roasting results of treating the Se and Te precipitate

C.1: Introduction and background

One of the objectives set for the study was to remove the caustic leaches from the BMR process. In order to confirm that a roasting step could achieve sufficient Se and Te removal from this precipitate before it was fed back to the BMR process, roasting test work was performed on this material. This appendix will contain the discussion around this investigation. For clarity, Figure 62 shows the specific roasting step that was investigated as part of the proposed flow sheet, in the form of a yellow dashed ellipse.

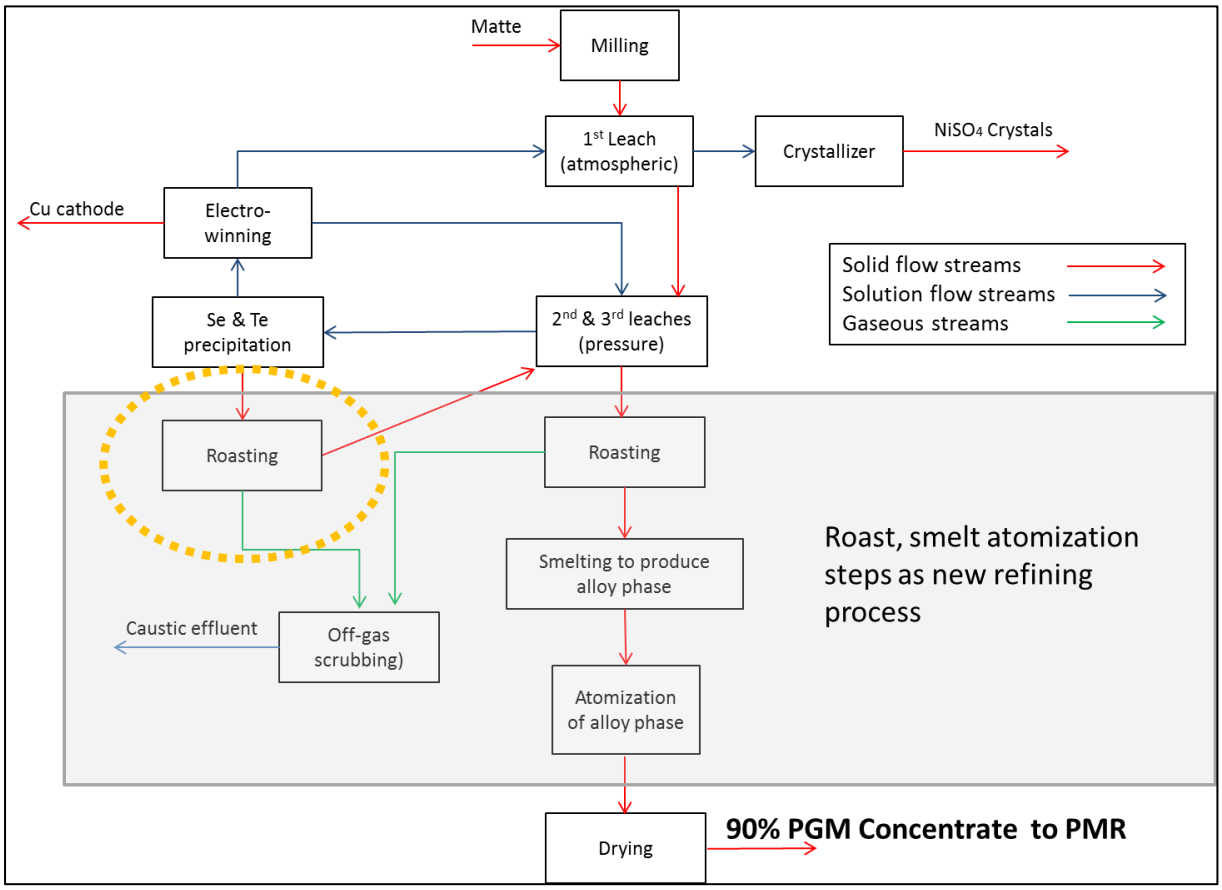

Figure 62: Block flow diagram of the proposed pyrometallurgical process that could be implemented between the BMR and PMR processes in order to remove contaminants from the PMR feed. The roasting processing step investigated in this appendix is shown by the dashed yellow ellipse

C.2: Chemical Composition

A typical composition of the Se/Te precipitate that is currently treated by a low pressure caustic leach for Te removal is shown in Table 70. A set of roasting tests was performed on this product. The PGM content of this precipitate is quite low at 2.6%, which could be due to both coprecipitation of PGMs and carry over of solids after filtering.

Table 70: Typical chemical composition of Se/Te precipitate, filtered after sulphurous acid reduction of second stage liquor, expressed as species that were used for thermodynamic modelling

Species	Pt	Pd	Au	Rh	Ru	Ir	6E	Ag	FeSO4	NiSO4	SiO2	CaO
Weight %	0.4	0.2	0.1	0.4	1.4	0.2	2.6	0.1	0.3	6.1	0.2	0.1

Species	Cu2Se	Cu	Cu2Te	CuS	PbSO4	As	Bi	Total
Weight %	38.6	6.6	21.4	9.0	0.1	0.1	0.2	85.3

C.3: Experimental set-up

The Se/Te precipitate roasting investigation was done together with the third stage leach residue. The experimental set-up was therefore similar to that in the description in section 3.4.1.

A single set of roasts was also performed on the Se/Te precipitate that is produced by sulphurous acid reduction to Cu_2Te and Cu_2Se. This set of roasting tests was done in a silica tray in a muffle furnace, with excess air, in temperature steps of 100 ˚C from 600 ˚C to 800 ˚C. However, severe sintering/partial melting was observed at 800 ˚C.

The circulating fluidised bed set-up described in section 3.4.1 was used for roasting tests on the Se/Te precipitate.

C.4: Results giving the extent of removal of elements/compounds during the roasting trials on Se/Te precipitate

A single set of roasting tests was performed on the Se/Te precipitate that is produced by sulphurous acid reduction of second stage liquor. The material showed sintering behaviour at 800 ˚C and formed a molten pool at 900 ˚C, when the sample in the silica tray was placed directly into a muffle furnace controlled at the set roasting temperature. The results of the first roasting test work, in a muffle furnace for 2 hours at set temperature intervals, are given in Table 71.

Another set of roasting tests was done in both a muffle furnace and a fluidised bed. When the temperature was slowly increased from 400 ˚C up to 900 ˚C, no sintering or melting of the sample was noted. The slow heating rate allows low melting species (like sellenides and tellurides) to oxidise at low temperatures, thereby changing the speciation when temperature is reached. No sintering or melting behaviour was noted when the Se/Te precipitate was added to a hot pre-established

fluidised bed with silica. Although the fast heating rate could still form low melting phase (similar to inserting the tray into a hot muffle furnace), the intensive mixing probably suspends the particles and allows good air contact for oxide formation and vaporisation. Both of these observations point to the fact that sintering to temperatures up to 900 ˚C can be achieved, as long as the heating rate or mixing is controlled.

The low PGM content of the feed material could explain the varying recovery that was measured for the different roast tests. No actual loss mechanism is known or suspected to explain the low and varying PGM recovery measurements.

Table 71: Percentage weight change achieved at temperature increments during the stationary bed roasting test work of Se/Te precipitate. Temperature of the roast increased in 100 °C steps from 600 °C to 800 °C

Temperature	600 °C	700 °C	800 °C
Roast time	2 h	2 h	2 h
Air flow	Convection	Convection	Convection
Ru	-24%	-15%	0%
Rh	-25%	-15%	-16%
Pd	-16%	-27%	-31%
Ag	-16%	-27%	-31%
Ir	-20%	-10%	0%
Pt	0%	-1%	0%
Au	-16%	-27%	-31%
Pb	0%	0%	0%
Se	-99%	-100%	-100%
Te	0%	0%	-96%
As	0%	0%	0%
Bi	-7%	-15%	-78%
Total S	-26%	-92%	-98%

A second set of roasting experiments was done, in both a fluidised bed and a stationary bed at different temperatures and oxidation environments. These tests are summarised in Table 72. The results from Table 72 show that higher temperatures can be used as long as slow heating or an established fluid bed is used for roasting. It is interesting to note that a similar degree of Te removal was achieved here as with third stage leach residue roasting. The single value of 98% removal at 800 ˚C measured in the first set of set of experiments (Table 71) is not consistent with the results of the second round of test work, and could be incorrect. It would appear that up to 71% Te can be removed if roasting of Se/Te precipitate is done in air at 900 ˚C. Te removal as TeO_2 is similar in the Se/Te precipitate to what it was in the third stage residue, from a modelling perspective. Modelled Te removal is discussed under section 5.3.2.

The important role of gas flow dynamics and gas particle interaction (fluid bed versus static bed) is therefore clear, showing that the selection and design of the process are crucial in obtaining the preferred level of oxidation with minimal losses.

Table 72: Percentage weight change achieved during the fluidised bed roasting test work, as well as in a single muffle furnace test, on Se/Te precipitate. Gas flow was 1.2 Nm^3/hr for all tests reported

Temperature	800 °C	850 °C	800 °C	900 °C	850 °C	900 °C
Roast Time	60 min	4 h	2 h	6 h	4 h	4 h
Gas atmosphere	Air	Air	Air	Air	40 % O2	20 % CO, 80 % N2
Furnace type	Fluid bed with SiO2	Stationary bed	Fluid bed with SiO2	Fluid bed with SiO2	Fluid bed with SiO2	Fluid bed with SiO2
Ru	-9%	-16%	-9%	-30%	-25%	2%
Rh	-4%	-10%	-1%	-10%	-15%	17%
Pd	-5%	-11%	0%	-9%	-13%	17%
Ag	-100%	-100%	-100%	-100%	-100%	-12%
Ir	-16%	-17%	-11%	-20%	-22%	-3%
Pt	-19%	-22%	-8%	-12%	-26%	-16%
Au	-16%	-22%	-3%	-15%	-25%	-2%
Pb	-5%	-49%	-12%	-40%	-41%	-90%
Se	-97%	-100%	-100%	-92%	-99%	-100%
Te	-8%	-23%	-22%	-71%	-41%	23%
As	-1%	-11%	1%	-9%	-18%	8%
Bi	-6%	-19%	-11%	-20%	-32%	-87%
Sb	-1%	-5%	39%	16%	14%	35%
Total S	-99%	-100%	-100%	-100%	-100%	-99%
Os	-100%	-100%	-100%	-100%	-100%	-75%

A roasting step performed on the Se/Te precipitate would bleed Se and Te from the BMR circuit. However, the calcine (roasted residue) from this roast would not contain much PGM, with the bulk of the content being Cu. It is suggested that the calcine be added back to the pressure leach step to remove the Cu and allow the PGMs to join up with the main residue stream. However, to see whether a dedicated leach could be used to remove the bulk of the Cu, and thereby achieve the blending of the Se/Te stream to the pressure leaching residue stream as a feed for the proposed pyrometallugical process, a single leaching test was performed in 35 g/l H_2SO_4 at 80 ˚C for six hours.

The leach was performed on the calcine from Se/Te precipitation product roasted at 700˚C. Seventy two per cent of the Cu was leached from the calcine, while only 14% of the Te leached. This acid leach after low temperature roasting (600 ˚C to 700 ˚C) would serve as a crude method to leach the bulk of the Cu from the calcine, thereby preventing too much Cu from being blended with the third stage leach residue. The residue from the acid wash could then be blended with the third stage leach residue to proceed through the third stage residue treatment, provided that Te were removed in the third stage leach treatment step. The elemental composition is provided in order to understand the calcine/residue from a process where Se and S have been removed during low temperature leaching and most of the Cu has been leached from this calcine with H_2SO_4. Seventy seven per cent of the

mass of the original Se/Te precipitate was removed and a residue was left that primarily contains base metals, Te and PGMs. If high temperature roasting and smelting were to be applied to third stage residue (and Te thus effectively removed), the product of roasting and leaching the Se/Te precipitate could be blended with third stage leach to proceed through roasting and smelting. Table 73 shows the compositional change that was measured across a 700 ˚C roast on Se/Te precipitate, followed by a H_2SO_4 leaching step.

Table 73: Elemental composition in weight percentage of Se/Te precipitate, calcine from roasting Se/Te precipitate at 700 ˚C, and the residue after H_2SO_4 leaching of the calcine

Element/ Compound	Se/Te precipitate	Calcine from roast at 700 ˚C	H_2SO_4 leach residue
Ni	3.1	4.3	8.4
Cu	36.3	51.3	32.2
Co	0.0	0.0	0.0
Fe	0.1	0.2	0.4
Se	12.6	0.2	0.3
Te	4.9	6.7	13.2
As	0.4	0.4	0.6
Pb	0.1	0.3	0.4
SiO2	1.1	1.7	3.5
S	8.0	0.0	0.2
Pt	1.8	2.6	5.7
Pd	1.1	1.5	3.1
Au	0.1	0.1	0.2
Rh	0.6	0.8	1.7
Ru	1.8	2.5	5.2
Ir	0.0	0.0	0.3
Os	0.0	0.0	0.0
Ag	0.2	0.2	0.4
Mass reduction		27%	50.3%

C.5: Discussion of Se/Te precipitate roasting over the 600 ˚C to 800 ˚C temperature range

Cu_2Se decomposes at 425 ˚C to CuO and SeO_2. The vapour pressure of SeO_2 at the decomposition temperature is sufficient to effectively evaporate the Se and leave CuO behind. Roasting at 600 ˚C for 2 hours in air shows complete removal of Se. Cu_2Te can decompose at room temperature to CuO and TeO_2. However, the vapour pressure of TeO_2 becomes significant only at temperatures greater than 700 ˚C. Section 5.3 discussed Te volatilisation in more detail. No removal of Te was shown at roasting temperatures of 600 ˚C and 700 ˚C, while 71% was shown at 900 ˚C.

CuS can oxidise to $CuSO_4$ at room temperature. Gradual oxidation to $CuO.CuSO_4$ is then possible, until the sulphate phase becomes unstable and only oxide remains at 734 ˚C (for the modelled

system). The gradual oxidation of CuS to $CuO.CuSO_4$ explains the S removal achieved between 600 ˚C and 700 ˚C (26% to 92% removal) and the basic disappearance of S measured at 800 ˚C.

Roasting of the Se/Te precipitate can achieve full Se removal at temperatures as low as 600 ˚C. Te removal will proceed only at temperatures closer to 800 ˚C, but sintering behaviour was noted at 800 ˚C, due to low melting phases. It would be possible to eliminate the current low pressure caustic leaching of the Se/Te precipitate performed to remove Te by either:

1. Roasting at temperature increments in order to allow full oxidation of the system and prevent sintering/melting during quick heating. The sintering/melting behaviour is caused by rapid heating, which does not allow oxidation to phases with either high volatility or a high melting temperature. A final roasting temperature of at least 900 ˚C would be necessary for partial Te and complete Se and S removal. The calcine from this roast could then be added to the third stage leach for Cu removal and PGM recovery.
2. Roasting at a low temperature (600 ˚C or 700 ˚C), to remove Se and oxidise Cu to CuO and $CuSO_4$. The roasting could be followed by atmospheric sulphuric acid leaching of the Cu and blending of the remaining Te/PGM residue to the third stage leach treatment step. However, this leach is only a crude method to separate most of the Cu from the Te rich residue. Where a low temperature roast (650 ˚C) is done on the third stage leach residue stream, Te will not be removed and this option cannot be used, as no Te bleed would then exist from the BMR circuit and more Te would end up in the PMR feed.

C.6: Conclusion on the roasting of Se/ Te precipitate

Full Se removal can be achieved by roasting the Se/Te precipitate at temperatures as low as 600 ˚C. Te removal will proceed only at temperatures closer to 800 ˚C, but sintering behaviour was noted at 800 ˚C, due to phases with a lower melting point. It would be possible to eliminate caustic leaching of the Se/Te precipitate to remove Te by either:

- Roasting in stages with incremental temperatures, in order to allow full oxidation of the system and prevent melting during quick heating. A final roasting temperature of at least 800 ˚C would be necessary for near complete Te and complete Se removal. The calcine from this roast could then be added to the second stage leach for Cu removal.
- Roasting at a low temperature (600 ˚C or 700 ˚C) to remove Se and oxidise Cu to CuO and $CuSO_4$, followed by sulphuric acid leaching of the Cu and blending of the remaining Te/PGM residue to the third stage leach treatment step.

Appendix D: Summary of roasting and smelting test conditions

This appendix contains details of the roasting and smelting test conditions that was used in the experimental work. The last section of the appendix more information of the smelting test campaigns that were done, which include the melts of the high temperature treatment step.

D.1: Roasting test work

Two different experimental test sets were performed for roasting. The first set of roasts were performed at the University of Pretoria. This test set was aimed to understand the extent to which actual volatilization results compared to modelled results at the temperature range 600 °C to 1000 °C. Based on the lower-than-modelled results obtained for As, Os and Te, a decision was taken to perform roasting test work in a fluid bed at Outotec Frankfurt.Table 74 Table 74 shows a summary of the conditions of all the test work performed on PGM residue. In some of the fluid bed tests, a start bed of either SiO_2 or a small amount of calcine (with known composition) was used.

Table 74: Summary of test conditions for roasting test work performed on PGM residue.

#	Laboratory used	Type furnace	Start Bed	Temperature (°C)	Gaseous atmosphere	Gas flow rate (L/h)	Time	Feed weight (g)
1	University of Pretoria	Muffle	N/A	600	Air	No forced air flow. Door 10 mm open and suction on off-gas	2 h	30
2	University of Pretoria	Muffle	N/A	700	Air		2 h	30
3	University of Pretoria	Muffle	N/A	800	Air		2 h	30
4	University of Pretoria	Muffle	N/A	900	Air		2 h	30
5	University of Pretoria	Muffle	N/A	1000	Air		2 h	30
1	Outotec Frankfurt	Fluid bed	None	900	Air	1,2 Nm3/hr	60 min	80
2	Outotec Frankfurt	Fluid bed	Calcine	900	Air	1,2 Nm3/hr	60 min	80
3	Outotec Frankfurt	Fluid bed	Calcine	900	90%N2 + 10%CO	1,2 Nm3/hr	60 min	80
4	Outotec Frankfurt	Fluid bed	SiO_2	900	N2	1,2 Nm3/hr	60 min	80
5	Outotec Frankfurt	Fluid bed	SiO_2	900	Air	1,2 Nm3/hr	2 h	80
6	Outotec Frankfurt	Fluid bed	None	650	N2	1,2 Nm3/hr	90 min	80
7	Outotec Frankfurt	Muffle	N/A	850	Air	200 L/h	4 h	80
8	Outotec Frankfurt	Fluid bed	None	650	N2/ Air = 5% O2	1,2 Nm3/hr	90 min	80
9	Outotec Frankfurt	Fluid bed	None	650	N2/ Air = 10% O2	1,2 Nm3/hr	90 min	80
10	Outotec Frankfurt	Fluid bed	SiO_2	900	Air	1,2 Nm3/hr	6 h	80
11	Outotec Frankfurt	Fluid bed	None	800	90%N2 + 10%CO	1,2 Nm3/hr	90 min	80
12	Outotec Frankfurt	Fluid bed	None	700	Air	1,2 Nm3/hr	6 h	80
13	Outotec Frankfurt	Fluid bed	None	600	90%N2 + 10%CO	1,2 Nm3/hr	90 min	80
14	Outotec Frankfurt	Muffle	N/A	850	Air	200 L/h	6 h	80
15	Outotec Frankfurt	Fluid bed	None	900	40 % O2	1,2 Nm3/hr	4 h	80
16	Outotec Frankfurt	Fluid bed	None	900	20 % CO, 80 % N2	1,2 Nm3/hr	4 h	80
17	Outotec Frankfurt	Fluid bed	None	1000	40 % O2	1,2 Nm3/hr	4 h	80

Table 75 shows a summary of the roasting test work that was performed on Se/ Te precipitate.

Table 75: Summary of test conditions for roasting test work performed on Se/ Te precipitate.

#	Laboratory used	Type furnace	Start Bed	Temperature (°C)	Gaseous atmosphere	Gas flow rate (L/h)	Time	Feed weight (g)
1	University of Pretoria	Muffle	N/A	600	Air	No forced air flow. Door 10 mm open and suction on off-gas	2 h	30
2	University of Pretoria	Muffle	N/A	700	Air		2 h	30
3	University of Pretoria	Muffle	N/A	800	Air		2 h	30
4	University of Pretoria	Muffle	N/A	900	Air		2 h	30
1	Outotec Frankfurt	Fluid bed	Calcine	800	Air	0,8 Nm3/hr	60 min	80
2	Outotec Frankfurt	Fluid bed	Calcine	800 - 1000	Air	0,8 Nm3/hr	6 h	80
3	Outotec Frankfurt	Muffle	N/A	850	Air	200 L/h	4 h	80
4	Outotec Frankfurt	Fluid bed	SiO2	800	Air	0,8 Nm3/hr	2 h	80
5	Outotec Frankfurt	Fluid bed	Calcine	900	Air	0,8 Nm3/hr	6 h	80
6	Outotec Frankfurt	Fluid bed	Calcine	850	40 % O2	0,8 Nm3/hr	4 h	80
7	Outotec Frankfurt	Fluid bed	Calcine	900	20 % CO, 80 % N2	0,8 Nm3/hr	4 h	80

D.2: Details of smelting campaigns in the induction furnace

Four different systems were investigated to produce an alloy. They have already been described in the Introduction section and comprisethe Direct Smelt, Roast-Smelt, Leach-Roast-Smelt and Roast-Smelt with Cu addition systems. In order to study the different systems, a specific set of variables was compiled for each system. The major variables are summarised in Table 76 for easy comparison. The time at temperature and the specific ranges of things like total weight or slag per weight of feed addition) is specified in Table 77.

Table 76: Summary of important control variables used for the different smelting campaigns to study the four different feed systems

Type of furnace	Type of feed	Weight of feed	Temperature range	Type of slag	Redox modifier	Pressure range	Alloy modifier
Induction	Third stage residue/Roasted third stage	500 g	1 300 °C to 1 500 °C	(B_2O_3-SiO_2-Na_2O)	$NaNO_3$	Atm	None
Induction	Third stage residue/ Roasted third stage	130 g to 170 g	1 400 °C to 1 500 °C	(SiO_2-Al_2O_3-CaO-Na_2O)	$NaNO_3$/ $C_{12}H_{11}O_{22}$	0.3 bar to 1 bar absolute	None
Induction	Leach-Roast third stage	130 g to 170 g	1 600 °C	(SiO_2-Al_2O_3-CaO-Na_2O)	None	Atm	None
Induction/ Muffle	Roasted third stage	150 g	1 250 °C to 1 350 °C	(B_2O_3-SiO_2-Na_2O)/ (SiO_2-Al_2O_3-CaO-Na_2O)	CuO/ $CuSO_4$/ $C_{12}H_{11}O_{22}$ / $NaNO_3$	Atm	Cu as Cu, CuO and $CuSO_4$

The first round of smelting test work, comprising 18 melts, was performed in an induction furnace under normal atmospheric pressure conditions using 500 g of material feed for each test. The smelting temperature was varied between 1 300 °C and 1 500 °C. A Borate based slag (described in section 4.4) was used in this test work campaign, due to the perception that a lower temperature that would be required in the melt. SiC crucibles were used for melts below 1 400 ˚C. Above 1 400 ˚C SiC crucibles show high wear rates, start breaking down and their electrical conductivity changes (making it difficult to control heat input to the melt through the receptor crucible receiving the electro-magnetic field of the induction furnace). Graphite crucibles were used for melts at 1 400 ˚C and higher, since graphite shows very stable electrical and thermal conductivities for a high temperature range (1 000 ˚C to 2 500 ˚C). It became clear during this campaign that temperatures higher than 1 400 ˚C would be required for the Roast-Smelt feed. As the temperature of a fully molten pool had been observed to be 1 450 ˚C, the temperature of the Roast-Smelt feed was then controlled to 1 500 °C. At these temperatures the borate based slag showed significant evaporative losses. Pb removal was also not achieved at the expected levels, pointing to the possible necessity to lower the pressure of the atmosphere above the melt to favour Pb/PbO volatilisation. At the lower temperatures, and especially in the SiC crucible rather than the graphite crucible, it was noted that redox control was better than at higher temperatures. The borate based slag also absorbed chrome spinel with less Cr reporting to the alloy phase. This is discussed in section 6.2. After the realisation that the crucible was participating in the melt, an effort was made to find a ceramic crucible that would be inert and would not react with the melt. This effort was unsuccessful and all the crucibles dissolved into the slag/ alloy penetrated into the crucible.

A second smelting test campaign comprising 13 melts was run with smaller melts of 130 g to 175 g feed material, in the temperature range between 1 400 °C and 1 500 °C with a CaO-SiO_2-Al_2O_3-Na_2O based slag. The experimental set-up was designed in such a manner that the pressure above the melt could be controlled under vacuum atmospheres as low as -70 kPa for increased Pb vaporisation. The experimental set-up worked very well, but the results were disappointing, with no

Pb removal improvement noticed. SiC crucibles were used for the melts at 1 400 °C as clay graphite was used for all temperatures above 1 400 °C. Several combinations of reducing ($C_{12}H_{22}O_{11}$) and oxidising ($NaNO_3$) agent additions were done to see whether the redox potential of the system could be influenced. It was found that the additions had very little effect on the final partial oxygen pressure (pO_2) achieved and that it was the crucible/melt interaction that was probably fixing the pO_2 of the system.

A third round of smelting tests (comprising just 2 melts) was done to study the Leach-Roast-Smelt system. The observed temperature at which the entire system was molten was only 1 510 °C and a decision was taken to run the tests at 1 600 °C at atmospheric pressure. No variable testing of the system was done, simply two repeats of a smelt at 1 600 °C for 30 minutes, at the set temperature and at atmospheric pressure.

Table 77 shows a summary of the smelting tests that were performed. Unsuccessful tests and repeats are not listed in the table. Unsuccessful tests experienced some form of experimental set-up problem, for instance where different crucible types dissolved into the slag, temperature control was not problematic, electrical problems were experienced, etc.

Table 77: Summary of smelting tests performed in induction furnace on unroasted, roasted and leach-roast feed material.

#	Feed type	Feed weight (g)	Temperature (°C)	Crucible type	Oxidation agent ($NaNO_3$	Reduction agent ($C_{12}H_{22}O_{11}$)	Time at temperature (min)	Slag addition rate (per 100g feed)	Absolute Pressure	Slag type
P1M1	Unroasted	500	1300	SiC	0	0	20	50	Atm	(B_2O_3-SiO_2-Na_2O)
P1M3	Roasted	500	1300	SiC	0	0	20	25	Atm	(B_2O_3-SiO_2-Na_2O)
P1M4	Roasted	500	1350	SiC	0	0	20	50	Atm	(B_2O_3-SiO_2-Na_2O)
P1M7	Unroasted	500	1350	SiC	50	0	20	50	Atm	(B_2O_3-SiO_2-Na_2O)
P1M9	Unroasted	500	1350	SiC	0	0	20	50	Atm	(B_2O_3-SiO_2-Na_2O)
P1M14	Roasted	500	1400	Graphite	0	0	20	25	Atm	(B_2O_3-SiO_2-Na_2O)
P1M15	Roasted	500	1400	Graphite	0	0	20	50	Atm	(B_2O_3-SiO_2-Na_2O)
P1M18	Unroasted	500	1350	Graphite	50	0	20	50	Atm	(B_2O_3-SiO_2-Na_2O)
P2M2	Roasted	175	1400	SiC	5	7	60	50	0,3	(SiO_2-Al_2O_3-CaO-Na_2O)
P2M3	Roasted	175	1450	SiC	5	7	60	50	0,3	(SiO_2-Al_2O_3-CaO-Na_2O)
P2M4	Roasted	175	1500	Clay Graphite	5	7	60	50	0,3	(SiO_2-Al_2O_3-CaO-Na_2O)
P2M5	Roasted	175	1500	Clay Graphite	5	7	60	50	Atm	(SiO_2-Al_2O_3-CaO-Na_2O)
P2M6	Roasted	175	1500	Clay Graphite	10	0	60	50	Atm	(SiO_2-Al_2O_3-CaO-Na_2O)
P2M7	Roasted	175	1500	Clay Graphite	10	5	20	50	Atm	(SiO_2-Al_2O_3-CaO-Na_2O)
P2M8	Roasted	175	1500	Clay Graphite	5 + 10	0	60	50	Atm	(SiO_2-Al_2O_3-CaO-Na_2O)
P2M9	Roasted	175	1500	Clay Graphite	5 + 10	0	20	50	Atm	(SiO_2-Al_2O_3-CaO-Na_2O)
P2M10	Roasted	175	1500	Clay Graphite	5 + 10	0	20	25	Atm	(SiO_2-Al_2O_3-CaO-Na_2O)
P2M13	Unroasted	130	1500	Clay Graphite	0	0	20	50	Atm	(SiO_2-Al_2O_3-CaO-Na_2O)
P3M2	Leach-Roast	175	1600	Clay Graphite	0	0	20	50	Atm	(SiO_2-Al_2O_3-CaO-Na_2O)

D.3: Details of melts with addition of Cu

To study the Roast-Smelt system with addition of Cu, four tests were performed. Two of these tests were done in an induction furnace with a SiC crucible at 1 350 °C and a SiO_2-Al_2O_3-CaO-Na_2O type slag. The first test had a large Cu addition (in the form of Cu powder) together with an oxidising agent ($NaNO_3$) to oxidise the Fe and Ni from the alloy. The observed temperature at which everything was molten for this system was around 1 236 °C. The second test started with a large CuO addition, together with a reducing agent (sucrose sugar as $C_{12}H_{22}O_{11}$) to reduce most of the Cu to the alloy phase, but leave enough free oxygen to oxidise Fe and Ni to the slag phase. These trials were not successful to the extent that had been hoped for. Two tests were done in a muffle furnace in an alumina-silica crucible, with the addition of a B_2O_3-SiO_2-Na_2O type slag, at 1 200 °C. The trials were based on the idea of a controlled reduction of Cu from CuO and sugar. A summary of the test parameters is provided in Table 78.

Table 78: Summary of the test parameters used to study the Roast-Smelt system with addition of Cu

Parameter	Test 1	Test 2	Test 3	Test 4
Roasted feed addition (gram)	75	112	20	20
Cu addition (gram)	150			
CuO addition (gram)		150	55	55
$CuSO_4$ addition (gram)				
Sugar addition (gram)		18	19	19
$NaNO_3$ addition (gram)	10			
Total slag addition (gram)	37	56	58	58
Slag addition composition SiO_2	30%	30%		55%
Slag addition composition CaO	40%	40%		
Slag addition composition Na_2O	20%	20%	40%	45%
Slag addition composition Al_2O_3	10%	10%		
Slag addition composition B_2O_3			60%	
Temperature (C)	1 350	1 350	1 200	1 200
Time (minutes)	30	30	90	90

D.4: High temperature treatment test work

A total of 4 tests was performed - a single test was done on each of three different alloy systems, these being the Direct Melt, Roast-Smelt and Leach-Roast-Smelt of third stage residue. A repeat of the Leach-Roast-Smelt system was done, but the Roast-Smelt with Cu addition was not studied. It was decided to use a single temperature and time (being 30 minutes at 1 700 °C) in order to prove the concept only. The results of these single tests per alloy type were compared to the modelling results. Table 79 provides a summary of the test work campaign on the high temperature treatment of alloy to selectively volatilise Pb and Bi.

Table 79: High temperature treatment tests performed on different alloys to understand volatile behaviour

Test number	Alloy preparation route	Temperature (°C)	Time at temperature (min)	Crucible	Gas atmosphere
1	Direct smelting of third stage residue	1 700	30	Graphite	Inert (N2)
2	Roasting, smelting of third stage residue	1 700	30	Graphite	Inert (N2)
3*	Leaching, roasting, smelting of third stage residue	1 700	30	Graphite	Inert (N2)

***** A repeat was performed on this this test to determine repeatability of the results.

D.5: Melt in vertical tube furnace

A single melt was attempted in a vertical tube furnace where good redox control could be achieved by controlling the crucible type and the gaseous atmosphere above the melt. Roasted calcine with a CaO-SiO_2-Al_2O_3-Na_2O based slag were subject to 1 500 °C for six hours in a high magnesia crucible. After 6 hours, it was clear that melting had been achieved. However, the alloy did not collect and settle, with the effect that very fine alloy prills were scattered in the slag. It was decided to abandon this type of test work. The test does show that good convection and movement are necessary in the furnace in order to effectively collect the alloy. This is exactly what was happening in the large scale furnaces employed in the PGM industry. Ritchie *et al.* (2010) studied the effect of electrode immersion with CFD and showed mean slag velocities of around 0.05 m/s. In the induction furnace, movement of the slag/ alloy phase could be visually observed.

Appendix E: Additional flow sheet suggestion for the Lonmin process

E.1: Introduction and background

The evaluation of the new pyrometallurgical refining process was done within the Lonmin context, but is applicable to most of the refiners that use the smelting-BMR-PMR route. Within the Lonmin context, some findings from the process studied could be used to propose flow sheets besides the full pyrometallurgical process proposed in Figure 44. Two flow sheets are proposed: 1) A flow sheet is suggested where only roasting is done, to replace the caustic leaches currently performed in the BMR. 2) The basic steps, of roasting, smelting and atomisation, could be applied to many PGM-containing residues. A flow sheet is suggested for Lonmin to handle their internally generated residues.

Development of a full new process to handle the main-stream product from the Lonmin BMR would take significant time and expenditure and would initially add significant risk to the process. It would be possible to implement the new process in stages. Roasting, for instance, could be implemented on its own merits as a stand-alone process to replace the existing caustic leaches.

It is also possible to develop the pyrometallurgical processing route of roasting, smelting and atomisation on a side-stream of the Lonmin process, i.e. on the residues that are currently generated in the BMR and PMR circuits. This would lower the risk of implementation compared to implementing a complete new process on the main-stream product (BMR leach residue). The equipment set-up, skill set and key findings could then be expanded to handle the main-stream.

E.2: Proposal to replace caustic leaches in the BMR with a roasting step.

Roasting could be implemented to replace the caustic leaches and optimise the current process. The main objective would not be to eliminate additional contaminants from the PMR feed, but to improve recovery in the BMR, eg no losses in the caustic leaches, and to optimise the formic/sulphuric acid leach to remove Cu and less Ir. Zero PGM loss could be achieved through a roasting step instead of the current PGM loss to caustic effluent. It is recommended to limit the temperature of the roast to 650 °C or 700 °C. This would remove most of the Se and S, while partially removing As, Os and Te. The use of the lower temperature range is outside the temperature range for formation of spinels, thus locking in Cu, Fe and Ni. The use of a formic/sulpuric acid leach showed that maximum Fe and Ni removal can be achieved on a roasted calcine at 650 °C (99% Fe leaching and 79% Ni leaching). Ir leaching on the roasted calcine was also lower at 2.7%, instead of the 7.4% measured on third stage residue. Although the measurement of Cu removal by this test showed no Cu removal, this was because the ORP was not controlled so as to be positive at the end of the leach (this being one of the first tests, this important variable was not properly understood). There is a concern that, although finishing the formic/sulphuric leach at a positive ORP would bring Cu into solution, it might also partly oxidise OPMs, thereby negatively affecting their dissolution in HCl/Cl_2. If the formic/sulphuric acid leach were followed by roasting, finishing with a positive ORP would have no effect on OPM dissolution and Cu could be leached. However, when residue from the formic/sulphuric leach needs to be fed to the PMR, additional work should first be done on whether ending the leach on a positive ORP (to bring Cu into solution) would adversely affect OPM leaching.

The low pressure caustic leach on the Se/Te precipitate could also be replaced by a roast (potentially in the same equipment, if roasting is done in batches). The roasting of this leach should start out at low temperatures (around 500 °C to 600 °C) to oxidise CuS, Cu_2Te and Cu_2Se to their respective oxides. Actual roasting test work on this precipitate showed that exposure to roasting temperatures > 700 °C allowed low-melting phases to sinter through partial melting. After an hour at the low temperature, the temperature can be lifted to 900 °C for five hours to ensure that Te is vaporised. Test work showed that Te removal of 71% by weight can be achieved. Scrubbing of roasting gases (from both the third stage residue and the Se/Te precipitate) should be done with caustic to form soluble selenates/tellurates/osmates/sulphates. The proposed flow sheet for implementing the roasting step to replace the two caustic leaches in the BMR is shown in Figure 63 below.

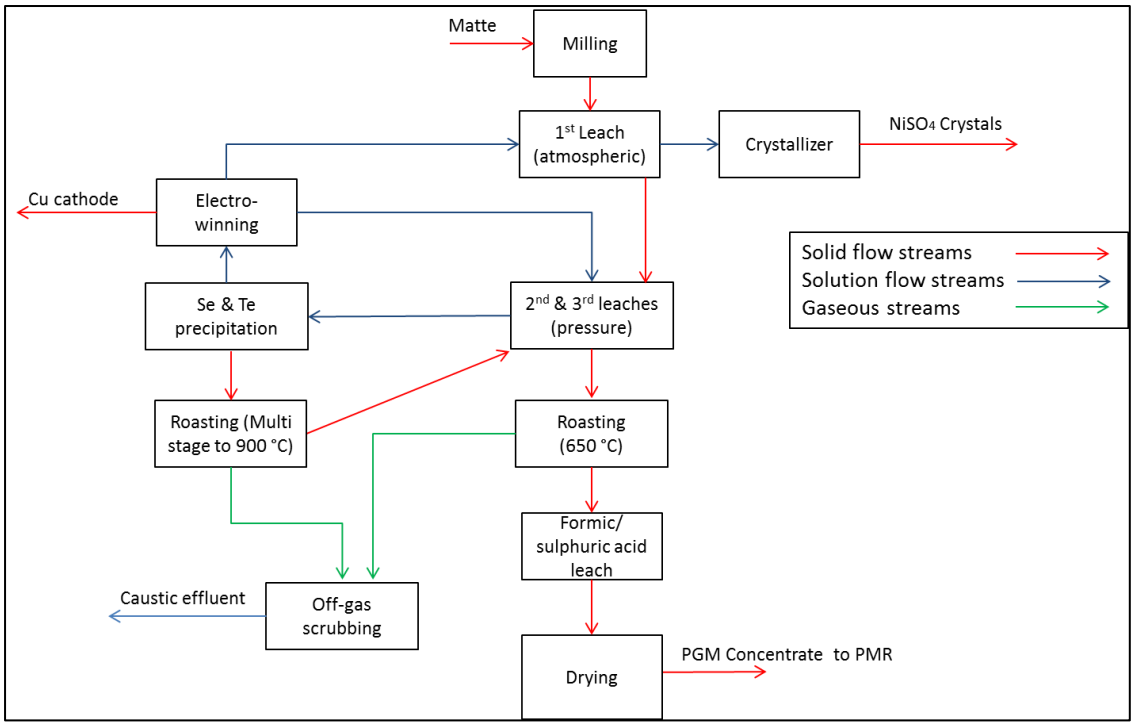

Figure 63: Recommended flow sheet showing the early implementation of roasting to replace caustic leaching

Implementation of the roasting step to replace the caustic leaches will only happen after sufficient pilot plant work. A summary of the risks and opportunities presented by pursuing roasting to replace the caustic leaches is listed below:

Opportunities:

- Eliminate caustic leaches from BMR process; saving PGM losses and effluent disposal costs.
- Improved leaching of Ni and Fe in the formic leach after roasting at 650°°C.
- Lower Ir leaching during the formic leach after roasting at 650°°C.
- Test work should be done to see whether improved formic/sulphuric leach operation to remove Cu would have an effect on OPM dissolution in the PMR.

- Possibility to fast-track the roasting step. The roasting step could be implemented independently of the smelting and atomisation steps, but would fit into the flow sheet, if these steps were shown to be viable during pilot plant test work.
- Spreading the risk of implementing a full new flow sheet. The technical risk of implementing the roasting step is small, compared to the smelt and atomisation steps.
- Lower initial capital cost and learning regarding the roasting step that could be applied to the Roast-Smelt-Atomisation flow sheet.
- Higher overall S and Se removal from PMR feed.
- The use of a high temperature roasting step would allow the use of combustible filter aid (or the use of papers) to assist with filtering in the BMR process.

Risks:

- Materials handling during roasting (man handling).
- Using the same roasting equipment for different feed streams (for example contamination, or applying the incorrect operating procedure to a feed stream).
- Safety and health aspects associated with vapours from roasting and its products at high temperatures. .
- Caustic scrubbing of roasting the off-gas stream and subsequent generation of effluent.
- Roasted calcine would have to be milled fine before it was fed to the formic/sulphuric acid leach. Roasting test work showed that agglomorates form during normal drying or roasting and these agglomorates would probably slow leaching reactions down. If the roasted calcine is fed to a smelting step, the formation of agglomorates becomes an advantage, because fewer dust losses during feeding to the furnace would occur. The current drying step is done under vacuum (to prevent oxidation), mixes the concentrate continually with rabblers and is only done when the residue has been properly washed. It was noticed that agglomorates only formed when the residue was not properly washed and mixed during drying. If the dried product is milled and then subjected to roasting, the product would remain fine. It might therefore be possible to avoid milling by doing drying in a way that is similar to what is currently done after the formic/sulphuric acid leach.
- Potential lower overall Os removal across the BMR. This risk is not properly quantified, as Os is not measured in BMR concentrate, so the final levels that are currently achieved are uncertain.
- Potential lower overall As removal across the BMR. The current high pressure caustic leach removes roughly 50% of the As contained in third stage residue. Roasting at 650°°C might not allow As removal to the same level.
- Brown fields implementation, by fitting a roasting circuit into existing available space, while new infrastructure (in the form of a building) could be built for the full Roast-Smelt-Atomisation flow sheet.

E.3: Proposal to treat internally generated BMR and PMR residues by means of a pyrometallurgical refining process

Lonmin is currently toll treating residues from the PMR circuit. A pyrometallurgical process similar to the one described in this thesis could be used to recover PGMs from the residues. The one big

difference between the process described in this thesis and the recovery of PGMs from residues would be the need for a collector during smelting of the residue feed. The PGM content of the third stage leach material is sufficient that PGMs would effectively alloy, melt and collect themselves in the alloy phase. The use of Fe and Ni could be considered as candidates for the collection of PGMs from PMR residues during the melting step. Cu might not the best choice, due to the insolubility of Ru in the Cu and, therefore, potential Ru losses.

NiO can be produced by simply roasting the $NiSO_4.6H_2O$ produced by the Lonmin PMR. It is recommended to simply mix the nickel sulphate crystals in the correct ratio with the residue prior to roasting. The same roasting process would decompose the nickel sulphate to oxide and volatilise the necessary elements from the residue. Ni oxide would therefore not have to be procured. Several reductants can be used in the melt and procured cheaply. A dedicated Ni leach would have to be done on the atomised alloy. It is unsure whether some the PGMs would go into solution across this leach or whether they would partially oxidise, influencing their dissolution behaviour in the HCl/Cl_2 environment. A Ni based collection step and a sulphate based leaching step is recommended in order to re-integrate the solution from the Ni leach to the BMR circuit, for Ni and PGM recovery. It would even be possible to pump the atomised alloy directly to the first stage leach reactor, where Ni and Fe would be leached as part of the normal BMR circuit.

The Lonmin BMR does not have sufficient Fe removal to absorb an Fe rich solution from a Fe collection residue circuit. If PGM losses across the Fe leach could be kept sufficiently low could , it would be possible to use Fe as a collector and create an effluent for disposal. However, the Ni collection route seems a lot simpler than the Fe collection route.

The basic processing steps–roasting, smelting, high temperature treatment, atomisation and leaching of base metals and Fe–would all be applicable to the treatment of residues. Figure 64 shows a typical flow sheet that could be applied for recovery of PGMs from residues. Note the similarity of the processing steps. Solution from the Fe/ Ni leach would be sent to the BMR first stage, caustic effluent would also be generated in a similar scrubbing circuit, slag would also be sent to the smelter, etc. Synergies between the two projects are tremendous.

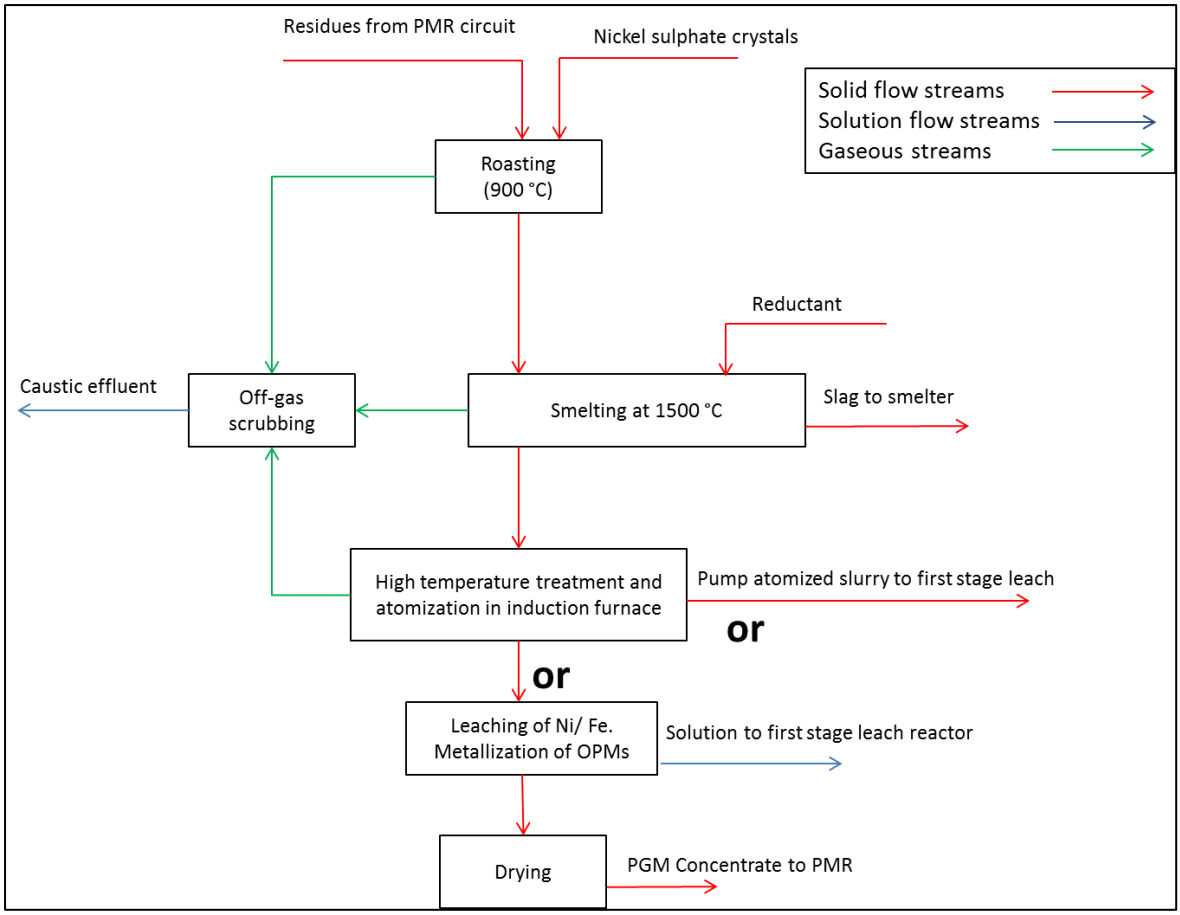

Figure 64: Recommended flow sheet showing the envisaged flow sheet for treating residues generated in the PMR process

Funding capital is difficult to procure in the current market environment, but it would be possible for Lonmin to share equipment/infrastructure/overhead cost between the two projects for removing contaminants from the PMR feed and to internally recycle the reduced residues produced by the PMR. It is recommended that these projects be studied and piloted at the same time and with the same pieces of equipment.

Opportunities:

- Development of a skill set to treat residues and various other materials that might be available in the market (typically generated from recycling of PGMs or by PGM recoveries as a by product, such as Cu production).
- Synergies with the removal of contaminants to the PMR feed project.
- Less dependency on toll treating.
- Very good integration into the BMR flow sheet.

Risks:

- Adds complexity to an existing simple flow sheet for treating residue materials from the PMR.
- NiO has carcinogenic properties.

- High SO_2 loadings to the roaster off-gas from nickel sulphate decomposition.
- Possible As and Pb build-up in the circuit.